

# Maillard reactions in spray dryers

A thesis submitted in fulfilment of the requirements for the degree of Doctor of Philosophy.

By

Zelin Zhou

Supervisor: Timothy Langrish

February 2023

School of Chemical and Biomolecular Engineering

The University of Sydney

*For My family, friends, and myself.*

## Statement of originality

This is to certify that, to the best of my knowledge, the content of this thesis is my own work. This thesis has not been submitted for any degree or other purposes.

I certify that the intellectual content of this thesis is the product of my own work and that all the assistance received in preparing this thesis and sources has been acknowledged.

Zelin Zhou

## Acknowledgements

Words could not express my gratitude to my thesis supervisor, Prof. Timothy A.G. Langrish. He has kindly guided and provided constant support throughout my journey of exploring the unknown. Aside from being the guiding light for my journey into the unknown, he also acted as a moral standard for me to learn from. His constant support in my academic work and life is essential to my journey.

I am most grateful to all my committee members and anonymous reviewers for their valuable and constructive feedback. Their comments and feedback have helped me see my work from perspectives that I would not have otherwise. Their valuable inputs have greatly improved the quality and impact of my research works and have become an essential part of this thesis.

I would also thank members of our research group, particularly (in alphabetical order) Sining Cai, Jingying Cheng, Shu Cheng, Zexin Lei, Yongmei Sun, Songwen Tan, and Chao Zhong, for providing a supportive environment, constructive comments, coffee, and gossip.

I am grateful to the School of Chemical and Biomolecular Engineering, University of Sydney, for providing a friendly working environment. I am also grateful to the CBE technical support team members, particularly (in alphabetical order) Dr. Bogumil Eichstaedt, Dr. Tino Kausmann, Dr. Jeffery Shi, Ms. Nancy Xie, and Dr. Xia Zhong, for their technical support, which has been a critical part of this thesis.

My sincere thanks to all the people I met before, during and after the journey, friends or not.

In the end, a special thanks to Manly beach, NSW, Australia, a place that has brought me back from the edge of depression multiple times.

This research is supported by an Australian Government Research Training Program (RTP) Scholarship.

Sincerely,

Zelin

This section of the acknowledgement contains non-English materials. Permissions have been granted from the Higher Degree by the Research Administration Centre of the University of Sydney and the supervisor of this thesis, given that a translation is provided.

## 致谢

在此，我想先感谢在我十八岁时先我一步而去的生父，周书磊。感谢他从小开始培养我的各种兴趣爱好，孜孜不倦地将他毕生所学教给我，让我知道世间万物的基本法则。即使我现在知道其中很多并不完全正确，但是确实是为我的之后的学习以及博士研究奠定了扎实的基础。泽林不孝，未能参加您的葬礼。愿您在另一边一切安好。

我也同样地对我生母，劳敏柔，心怀感激。感谢她多年来对我生活和学习上的支持。我知道"单亲家庭"很难，但是她做到了。如果说我的老师是我探索人类知识边界旅途中的指路明灯，生父是千里之行的第一步，那她就是允许我勇往直前的安全网。人们总说寒门出贵子，希望泽林也能成为那个贵子。

然后我也想感谢我的继父，黄汉光。感谢他成为我生母的支持并成为她的安全网。

最后，我由衷的感谢生命中遇到过或将要遇到的每个人。

顺颂文祺

周泽林

Translation:

### Acknowledgement

First, I would like to express my gratitude to my biological father, Shulei Zhou, who left the world when I was 18. Thank him for teaching me all he knew when I was a child and showing me how everything works. Although now I know some of them are wrong, the knowledge he taught me has provided a sound foundation for my studies, which I am forever grateful for. Zelin is not a devoted son and could not attend your funeral. I hope everything is fine on the other side of the world.

I am also grateful to my mother, Mingrou Lao. Many thanks for her constant support of my living and study. Raising a child like me is hard, especially in a single-parent family. But she made it. Suppose my supervisor is the "lighthouse" of my journey into the unknown, my father (Shulei) is the first step of the thousand-mile journey, and then she is the "safety net" that lets me push the boundary of human knowledge fearlessly. People always say a child from a poor family is more likely to be successful; Zelin hopes he can be that person.

I would also like to thank my stepfather, Hanguang Huang, for supporting my mum and becoming her "safety net".

In the end, I am forever grateful to all the people I have met or to be met in my life.

Best regards,

Zelin

## Abstract

Spray drying has been widely used to extend the shelf life of perishable goods and reduce the cost of transportation, and one of the typical applications of spray drying processes is milk powder production or the production of other spray-dried dairy products. The combination of high protein and reducing sugars makes milk particularly subject to Maillard reactions during thermal processing, including spray drying. Given the importance of food safety and the complex nature of Maillard reactions, it is important to study the kinetics of Maillard reactions that occur during the spray drying processes. In this thesis, the kinetics of Maillard reactions in spray dryers were investigated more systematically from an engineering point of view.

This work has started with investigating the kinetics of Maillard reactions in spray dryers with different feed compositions under different operating conditions. The impact of different feed compositions and operating conditions, including inlet gas temperature and dimensions of dryers, were investigated. The extent of the Maillard reactions in the spray-dried products was evaluated based on fluorometric and colourimetric methods. In general, a significant increase in reaction rates was specifically observed when the inlet gas temperature increased from 180 °C to 190 °C ( $T_{out} = 136 - 141$  °C), suggesting that proteins (protein unfolding) in the feed could play an important role in the reaction kinetics. Results from experiments with model systems with different component lactose-WPI ratios (1:2, 1:1, 2:1) further emphasised this point. A null result obtained from experiments with the laboratory-scale spray dryer suggested that the kinetic of Maillard reactions could also be significantly affected by the particle residence time distribution, which leads to the next research topic of this thesis.

Particle residence time distribution (RTD), an important performance indicator for spray dryers, determines the reaction time for Maillard reactions within spray dryers. Particle residence time distributions for four different designs of a newly-designed pilot-scale spray dryer were investigated here. A laser-based non-intrusive RTD measurement system has been developed for this purpose and validated against data available in the literature. The RTD measurements result showed a significant difference in mean particle residence time due to

different dimensions and designs. The mean particle residence time for a smaller spray dryer is significantly shorter than those for larger spray dryers (3.3 seconds vs. 6.8 - 27.2 seconds). This observation explained the null results observed for the laboratory-scale dryer in the earlier section of this thesis. In addition to explaining previous experimental observations, the RTD measurement results also showed that the later designs of spray dryers have clear advantages over earlier designs, mainly in terms of the particle-to-gas residence ratios (Design 1: 1.5 - 2.7 s/s, Design 2: 1.5 - 2.6 s/s, Design 3: 1.5 - 2.5 s/s, and Design 4: 1.0 - 1.7 s/s). Furthermore, fluctuations observed in the measured system response curves also demonstrated the potential connection between drying chamber geometry and the wall deposition and re-entrainment processes.

Apart from experimental works, this thesis has also developed a mathematical model for predicting the Maillard reactions kinetics in spray dryers. Two different modelling approaches, lumped and distributed-parameter modelling approaches, have been used, and prediction results have been compared. In general, prediction results from both approaches are comparable to the experimental data measured earlier in this thesis, which is a significant improvement over similar models developed in other studies. The performance of the distributed-parameter model is 17.7% better compared with the lumped-parameter model, though the fact that the effects of component segregation were only approximated.

In summary, this thesis used a more systematic approach to the question of Maillard reactions in spray dryers from an engineering point of view. The methods and findings in this thesis could be further developed and refined in future studies. The correlations between colour intensity and the extent of Maillard reactions can be further developed as a rapid online quality evaluation method. The RTD measurement system developed in this thesis can also be easily adapted for measuring the RTD of other spray dryers and used to validate computational fluid dynamics (CFD) simulation results. Last but not least, the preliminary mathematical model developed in the last part of the thesis has clearly demonstrated the advantages of the distributed-parameter modelling approach over the lumped-parameter model for multi-component reactions. The distributed-parameter modelling approach can also be adapted



for reactions in many other processes. Its applications are not limited to multi-component reactions (e.g., Maillard reactions) as it provides potentially more realistic temperatures and moisture contents profile within the system than lumped-parameter approaches.

## List of publications:

The following works have been published for submission in international refereed journals at the time this thesis was written. I designed the study, analysed the data and wrote the majority of the draft with the guidance of the supervisor of this thesis, Professor Timothy Langrish. Other co-contributors of the works have assisted with the design of the experiment, data acquisition, or editing of the manuscript. Unless stated otherwise, I am the first author and the corresponding author of the following works.

The order of the publications is based on the date of the manuscripts published.

**Zhou, Z.**, Langrish, T.A.G., 2021a. A review of Maillard reactions in spray dryers. *J. Food Eng.* 305, 110615. <https://doi.org/10.1016/j.jfoodeng.2021.110615>

**Zhou, Z.**, Langrish, T.A.G., 2021b. Color formation and Maillard reactions during the spray drying process of skim milk and model systems. *J. Food Process Eng.* <https://doi.org/10.1111/jfpe.13936>

**Zhou, Z.**, Langrish, T.A.G., Cai, S., 2022. Using particle residence time distributions as an experimental approach for evaluating the performance of different designs for a pilot-scale spray dryer. *Processes* 11, 40. <https://doi.org/10.3390/pr11010040>

I also co-authored the following works, which were published in international refereed journals when this thesis was written.

Cheng, S., Zhong, C., Langrish, T.A.G., Sun, Y., **Zhou, Z.**, Lei, Z., 2022. The relative importance of internal and external physical resistances to mass transfer for caffeine release from apple pectin tablets. *Curr Res Food Sci* 5, 634–641. <https://doi.org/10.1016/j.crfs.2022.03.014>

Sun, Y., Zhong, C., **Zhou, Z.**, Lei, Z., Langrish, T.A.G., 2022. A review of in vitro methods for measuring the Glycemic Index of single foods: Understanding the interaction of mass transfer and reaction engineering by dimensional analysis. *Processes (Basel)* 10, 759. <https://doi.org/10.3390/pr10040759>

Zhong, C., Tan, S., **Zhou, Z.**, Zhong, X., Langrish, T.A.G., 2023. Applications of aged powders of spray-dried whey protein isolate and ascorbic acid in the field of food safety. *Drying Technol.* 1–11. <https://doi.org/10.1080/07373937.2023.2175214>

Zelin Zhou

As supervisor for the candidature upon which this thesis is based, I can confirm that the authorship attribution statements above are correct.

Timothy Langrish

## Abbreviations

| <b>Abbreviations</b> | <b>Full name</b>   |
|----------------------|--|
| AMP                  | Advanced Maillard reactions products                                 |
| BI                   | Browning index   |
| CFD                  | Computational fluid dynamics   |
| CPS                  | Count per second   |
| CSTR                 | Continuous stirred tank reactor                                      |
| DG                   | Deoxyosone   |
| FAST                 | Fluorescence of advanced Maillard products<br>and soluble tryptophan |
| FTIR                 | Fourier transform infrared spectroscopy                              |
| FVM                  | Finite volume method   |
| Lac                  | Lactose  |
| NEB                  | Non-enzymatic browning   |
| OD                   | Optical density  |
| RTD                  | Residence time distribution  |
| SEM                  | Scanning electron microscopy   |
| SNR                  | Signal-to-noise ratio  |
| Trp                  | Tryptophan   |
| UV-Vis               | Ultraviolet-visible spectroscopy                                     |
| WPI                  | Whey protein isolate   |

## Table of contents

|  |     |
|--|-----|
| Maillard reactions in spray dryers.....            | 1   |
| Statement of originality.....                      | III |
| Acknowledgements.....                              | IV  |
| 致谢   | V   |
| Abstract   | VII |
| List of publications: .....                        | X   |
| Abbreviations                                      | XI  |
| Table of contents.....                             | XII |
| Chapter 1. Introduction .....                      | 1   |
| 1.1. Spray drying.....                             | 2   |
| 1.2. Milk powder production .....                  | 3   |
| 1.2.1. Physical properties.....                    | 4   |
| 1.2.2. Thermal degradation.....                    | 4   |
| 1.2.3. Maillard reactions .....                    | 5   |
| 1.3. Importance of spray dryer designs.....        | 7   |
| 1.4. Segregation during spray drying.....          | 8   |
| 1.5. Thesis Aim.....                               | 9   |
| 1.6. Thesis structure .....                        | 10  |
| Chapter 2. Literature review.....                  | 12  |
| 2.1. Introduction.....                             | 14  |
| 2.2. Maillard reactions .....                      | 18  |
| 2.2.1. The early stage of Maillard reactions ..... | 19  |

|            |  |    |
|------------|--|----|
| 2.2.2.     | The intermediate stage of Maillard reactions .....                         | 22 |
| 2.2.3.     | The final stage of Maillard reactions .....                                | 24 |
| 2.2.4.     | Application of Maillard reactions in spray drying.....                     | 25 |
| 2.3.       | Kinetic studies of Maillard reactions .....                                | 25 |
| 2.3.1.     | Kinetic studies of Maillard reactions in liquid systems.....               | 25 |
| 2.3.2.     | Kinetic studies of Maillard reactions applicable to spray drying .....     | 27 |
| 2.3.3.     | Studies on Maillard reactions in spray-dried powders during storage .....  | 31 |
| 2.4.       | Factors affecting the kinetics of Maillard reactions in spray dryers ..... | 31 |
| 2.4.1.     | Effect of feed composition .....   | 32 |
| 2.4.2.     | Effect of oxygen .....   | 34 |
| 2.4.3.     | Effect of pH .....   | 34 |
| 2.4.4.     | The role of water.....   | 35 |
| 2.4.5.     | Glass transition temperature ( $T_g$ ).....                                | 36 |
| 2.4.6.     | Segregation .....  | 37 |
| 2.4.7.     | Wall deposition and re-entrainment .....                                   | 39 |
| 2.4.8.     | Particle residence time distribution in spray dryers.....                  | 40 |
| 2.4.9.     | Drying kinetics in spray dryers.....                                       | 42 |
| 2.4.10.    | Artificial neural networks (ANN) models .....                              | 46 |
| 2.5.       | Conclusions.....   | 47 |
| Chapter 3. | Methods and materials.....   | 49 |
| 3.1.       | Materials .....  | 51 |
| 3.2.       | Spray dryers .....   | 52 |
| 3.2.1.     | Laboratory-scale spray dryer .....   | 52 |
| 3.2.2.     | Pilot-scale spray dryer .....  | 53 |

|            |   |    |
|------------|---|----|
| 3.3.       | Spray drying.....   | 56 |
| 3.3.1.     | Effect of different operating conditions and feed compositions on the kinetics of Maillard reactions in spray dryers..... | 56 |
| 3.3.2.     | Effect of different designs and sizes of the spray dryer on particle residence time distribution.....                     | 57 |
| 3.4.       | Particle residence time distribution measurement .....  | 58 |
| 3.4.1.     | Particle residence time distribution .....  | 58 |
| 3.4.1.     | Spray drying conditions used for particle residence time distribution measurement   | 59 |
| 3.4.2.     | Particle residence time measurement devices for laboratory-scale spray dryer  | 60 |
| 3.4.3.     | Particle residence time measurement device for pilot-scale spray dryer....  | 64 |
| 3.4.4.     | Analysis of the fluctuations in the signal.....   | 69 |
| 3.5.       | Product quality assessments.....  | 69 |
| 3.5.1.     | Colour measurement.....   | 69 |
| 3.5.2.     | Fluorescence of Advanced Maillard products and Soluble Tryptophan (FAST)  | 71 |
| 3.5.3.     | Particle size distribution .....  | 72 |
| 3.5.4.     | Scanning electron microscopy (SEM).....   | 72 |
| 3.5.5.     | Moisture content measurement.....   | 72 |
| 3.6.       | Heating model systems under isothermal conditions.....  | 72 |
| 3.7.       | Conclusions.....  | 73 |
| Chapter 4. | Maillard reactions with different inlet gas temperatures and feed compositions  | 74 |
| 4.1.       | Introduction.....   | 76 |

|   |   |     |
|---|---|-----|
| 4.2.  | Fluorometric measurement results – Fresh skim milk & reconstituted skim milk                          |     |
|   |   | 77  |
| 4.3.  | Fluorometric measurement results – lactose-WPI model systems .....                                    | 80  |
| 4.4.  | Colour analysis of the samples .....  | 82  |
| 4.5.  | Maillard reactions occur during the spray drying process within the laboratory-scale spray dryer..... | 86  |
| 4.6.  | Conclusions.....  | 87  |
| Chapter 5. Effect of different designs of the spray dryer on the particle residence time distribution and the quality of the final product..... |   |     |
|   |   | 88  |
| 5.1.  | Introduction.....   | 90  |
| 5.2.  | Method validation .....   | 90  |
| 5.2.1.  | Validation against published data.....  | 90  |
| 5.2.2.  | Difference between the automated injection system and manual dye injection                            | 93  |
| 5.2.3.  | Effect of different dye injection volumes .....   | 94  |
| 5.3.  | Particle residence time distribution for pilot-scale spray dryer .....                                | 94  |
| 5.3.1.  | Mean particle residence time – $\tau$ .....   | 94  |
| 5.3.1.  | The ratios between mean particle residence times and gas residence times                              | 98  |
| 5.4.  | Spread of particle residence time – $n$ .....   | 101 |
| 5.5.  | Fluctuations in measured signals .....  | 103 |
| 5.5.1.  | Flow related factors .....  | 105 |
| 5.5.2.  | Wall deposition and wall deposit re-entrainment related factors .....                                 | 108 |
| 5.6.  | Effect of feed stickiness .....   | 116 |

|            |  |     |
|------------|--|-----|
| 5.7.       | Other performance parameters.....  | 118 |
| 5.7.1.     | Solid recovery rates .....   | 118 |
| 5.7.2.     | Morphology of the particles .....  | 120 |
| 5.8.       | Conclusion .....   | 121 |
| Chapter 6. | Modelling Maillard reactions under different spray drying conditions....   | 122 |
| 6.1.       | Introduction.....  | 124 |
| 6.2.       | Modelling the drying kinetics .....  | 125 |
| 6.2.1.     | Lumped-parameter modelling approach.....                                   | 126 |
| 6.2.2.     | Distributed-parameter modelling approach .....                             | 130 |
| 6.3.       | Kinetic model for Maillard reactions in spray drying.....                  | 138 |
| 6.3.1.     | Effect of temperature on the kinetics of Maillard reactions .....          | 139 |
| 6.3.1.     | Effect of moisture content on the kinetics of Maillard reactions .....     | 140 |
| 6.3.2.     | Effect of reactant ratio on the kinetics of Maillard reactions .....       | 140 |
| 6.3.3.     | Fitting of the kinetic parameters .....                                    | 143 |
| 6.3.4.     | Sensitivity analysis for different factors .....                           | 145 |
| 6.4.       | Prediction model for kinetics constants .....                              | 146 |
| 6.4.1.     | Temperature dependency of the kinetics constant.....                       | 147 |
| 6.4.2.     | Combined effects of temperature and moisture content.....                  | 149 |
| 6.4.3.     | Modelling Maillard reactions kinetics with different drying kinetic models |     |
|            | 152  |     |
| 6.5.       | Simulation results from different modelling approaches.....                | 153 |
| 6.5.1.     | Drying kinetics predicted by different modelling approaches.....           | 153 |
| 6.5.2.     | Predicted internal particle temperature, moisture content and component    |     |
|            | distribution   | 158 |



|            |   |     |
|------------|---|-----|
| 6.5.3.     | Effect of the number of sublayers on prediction results.....  | 159 |
| 6.5.4.     | Prediction results from the lumped-parameter model .....  | 161 |
| 6.5.1.     | Prediction results from the distributed-parameter model .....   | 162 |
| 6.6.       | Limitations of the simulation models developed.....   | 165 |
| 6.6.1.     | Particle residence time.....  | 165 |
| 6.6.2.     | Moisture content of the particles .....   | 165 |
| 6.6.3.     | Markers for Maillard reactions .....  | 166 |
| 6.7.       | Conclusions.....  | 166 |
| Chapter 7. | Conclusion and further consideration.....   | 168 |
| 7.1.       | Overview of the thesis .....  | 169 |
| 7.2.       | Maillard reactions under different spray drying conditions.....   | 170 |
| 7.3.       | Effect of different designs of the spray dryer on the particle residence time<br>distribution and the quality of the final product..... | 171 |
| 7.4.       | Modelling Maillard reactions under different spray drying conditions .....  | 173 |
| 7.5.       | Recommendations and future works.....   | 173 |
| 7.5.1.     | Additional markers for thermal degradations.....  | 174 |
| 7.5.2.     | Maillard reactions kinetics at lower moisture contents .....  | 175 |
| 7.5.3.     | Effect of component segregations .....  | 175 |
| 7.5.4.     | Computational fluid dynamics (CFD) simulations for different designs of the<br>spray dryer  | 175 |
| 7.5.5.     | Effects of other spray drying conditions.....   | 176 |
| Chapter 8. | Impact of COVID-19 on the scope of this thesis.....   | 178 |
| 8.1.       | Overview of the COVID-19 impacts .....  | 179 |
| 8.2.       | Potential research projects and outcomes without COVID-19 restrictions .....  | 179 |

|            |  |     |
|------------|--|-----|
| 8.2.1.     | Measuring kinetic of Maillard reactions at lower moisture contents ..... | 179 |
| 8.2.2.     | Measuring furosine content in samples .....                              | 180 |
| 8.3.       | Conclusion .....   | 181 |
| References |  | 182 |
| Appendix:  |  | 196 |
| A.1.       | Codes for controlling automated dye injection system.....                | 196 |
| A.2.       | Codes for colour analysis.....   | 197 |
| A.3.       | Codes for CSTR-TIS model fitting.....                                    | 200 |
| A.4.       | Code for Fourier transform of measured signals .....                     | 203 |

**List of figures:**

Figure 1.1 Schematic diagram of a typical spray dryer. ....2

Figure 2.1 Overview of Maillard reactions scheme (reproduced based on Nursten, 2005).  
..... 19

Figure 2.2 Condensation and formation of Schiff base of lactose and lysine.....20

Figure 2.3 Formation of Amadori products. ....20

Figure 2.4 Open-chain form and closed-form of glucose. ....21

Figure 2.5 Amino acids in different pH environments. ....22

Figure 2.6 Schematic diagram of 3-deoxyosone-pathway via the 1,2 enolisation route. ..23

Figure 2.7 Schematic diagram of 1-deoxyosone-pathway via the 2,3 enolisation route. ..23

Figure 2.8 Schematic diagram of the 4-deoxyosone-pathway.....24

Figure 2.9 Kinetic model for the early stage of Maillard reactions ((Ge and Lee, 1997)..25

Figure 2.10 Kinetic model for Maillard reactions (Boekel and Martins, 2002). ....26

Figure 2.11 Summary of factors and their main effects on Maillard reactions in spray dryers.  
.....32

Figure 2.12 Schematic diagram of dominant components in different layers of spray-dried  
milk particles.....38

Figure 3.1 Schematic diagram of Buchi mini spray dryer B-290. ....52

Figure 3.2 Spray dryer with 4-inch cylindrical connection (Design 1). ....53

Figure 3.3 Spray dryer with 6-inch cylindrical connection (Design 2). ....54

Figure 3.4 Spray dryer with cylindrical drying chambers and box connection (Design 3).  
.....55

Figure 3.5 Spray dryer with conical drying chamber and box connection (Design 4). ....55

Figure 3.6 Particle residence time measurement device for Buchi mini spray dryer B-290  
version 1 (not to scale). ....61

Figure 3.7 Detailed dimensions of the Buchi mini spray dryer B-290. ....61

Figure 3.8 Light scattered by particles (a) particles without dye (b) particles with dye....62

Figure 3.9 Enlarged view of the signal measurement device. ....62

|   |    |
|---|----|
| Figure 3.10 3D printed holder for photomultipliers use with the lab-scale spray dryer. (a) photomultiplier end (sampling window) (b) laser pointer end (c) pass-through for drying chamber.....   | 63 |
| Figure 3.11 Detailed dimensions of the 3D printed holder for photomultipliers use with the lab-scale spray dryer. Left: bottom view Right: right-side view. ....  | 63 |
| Figure 3.12 Particle residence time measurement device for Buchi mini spray dryer B-290 version 2.....  | 64 |
| Figure 3.13 Schematic diagram of RTD measurement device on pilot-scale spray dryer (Design 1).....  | 64 |
| Figure 3.14 Schematic diagram of manual dye injection system for pilot-scale spray dryer. ....  | 65 |
| Figure 3.15 Schematic diagram of the automated dye injection system.....  | 66 |
| Figure 3.16 Schematic diagram of particle residence measurement device for pilot-scale spray dryer. ....  | 67 |
| Figure 3.17 Detailed dimensions of the 90° long radius elbow (R = 1.5D). Left: front view Right: top view. Flanges on the elbow are not shown. ....   | 67 |
| Figure 3.18 3D printed holder for photomultipliers used with the pilot-scale spray dryer. (a) Top view of the holder; (b) side view of the holder; (c) bottom view of the holder. ....  | 68 |
| Figure 3.19 Detailed dimensions of the 3D printed holder for photomultiplier use with the pilot-scale spray dryer. Left: side view of the fitting for measuring the particle residence time Right: top view of the fitting for measuring the particle residence time. ....  | 68 |
| Figure 3.20 Schematic diagram of standard lighting box. ....  | 70 |
| Figure 3.21 Standard colour correction card used in this thesis. ....   | 70 |
| Figure 4.1 The changes in AMP/Trp ratios as functions of inlet gas temperature for real food systems. ■ : reconstituted skim milk ● : fresh skim milk — : fitted curve for reconstituted skim milk ( $Y=4.35 \cdot 10^{-19} X^{8.8}$ , $R^2=0.92$ ) -- : fitted curve for fresh skim milk ( $Y=2.89 \cdot 10^{-34} X^{15}$ , $R^2=0.96$ ). .... | 77 |

|  |     |
|--|-----|
| Figure 4.2 Predicted temperature profile for the particles and the drying air with an inlet gas temperature of 130°C — : gas temperature -- : particle temperature.....  | 79  |
| Figure 4.3 The changes in AMP/Trp ratios as functions of inlet gas temperature for model systems. ■ : Lactose:WPI 1:2 ● : Lactose:WPI 2:1 — : fitted curve for reconstituted skim milk ( $Y=1.98*10^{-47}X^{4.5}$ , $R^2=0.81$ ) -- : fitted curve for fresh skim milk ( $Y=4.33*10^{-54}X^{8.4}$ , $R^2=0.84$ ).<br>..... | 81  |
| Figure 4.4 Colours of the spray-dried fresh skim milk from different inlet gas temperatures.<br>.....  | 84  |
| Figure 4.5 Chroma values as functions of the changes in AMP/Trp ratios for real food systems. ■ : experimental data points — : fitted curve ( $y=4.68X^{0.15}$ , $R^2=0.90$ ).<br>.....  | 85  |
| Figure 5.1 Particle residence time distribution in Buchi mini spray dryer B-290 (Schmitz-Schug et al., 2013).<br>.....   | 91  |
| Figure 5.2 Particle residence time distribution in Buchi mini spray dryer B-290.<br>.....  | 92  |
| Figure 5.3 Mean particle residence time ( $\tau$ ) ■: Design 1: 4-inch connection ●: Design 2: 6-inch connection ▲: Design 3: Box connection ▼ Design 4: Conical drying chamber.<br>.....  | 95  |
| Figure 5.4 Ratios between particle and gas residence time for different configurations and gas flow rates ■: Design 1: 4-inch connection ●: Design 2: 6-inch connection ▲: Design 3: Box connection ▼ Design 4: Conical drying chamber.<br>.....   | 98  |
| Figure 5.5 CFD simulation results for the first two designs. Left: Design 1 Right: Design 2 (Langrish et al., 2020).<br>.....  | 99  |
| Figure 5.6 CFD simulation results for Design 3 (Langrish et al., 2020).<br>.....   | 100 |
| Figure 5.7 Difference between cylindrical and conical drying chambers.<br>.....  | 101 |
| Figure 5.8 Number of equivalent CSTR in series (n) for different configurations and gas flow rates. ■: Design 1: 4-inch connection ●: Design 2: 6-inch connection ▲: Design 3: Box connection ▼ Design 4: Conical drying chamber.<br>.....   | 102 |
| Figure 5.9 Averaged normalised signals for all designs at the maximum gas flow rate (257-315) m <sup>3</sup> /hr (a): Design 1: 4-inch connection (b): Design 2: 6-inch connection (c): Design 3: Box connection (d): Design 4: Conical drying chamber.<br>.....   | 103 |

|  |     |
|--|-----|
| Figure 5.10 Dominant frequencies for different configurations and gas flow rates ■: Design 1: 4-inch connection ●: Design 2: 6-inch connection ▲: Design 3: Box connection ▼ Design 4: Conical drying chamber.....                         | 105 |
| Figure 5.11 Factors affecting the wall deposition and wall deposit re-entrainment.....   | 108 |
| Figure 5.12 SEM image of particle collected from different gas flow from maximum gas flow rate (a): Design 1: 4-inch connection (b): Design 2: 6-inch connection (c): Design 3: Box connection (d): Design 4: Conical drying chamber. .... | 120 |
| Figure 6.1 Schematic diagram for finite volume method (FVM) applied in this thesis. R: Radius of the droplet $\Delta R$ : thickness of the sub-layer.....  | 131 |
| Figure 6.2 Schematic diagram of different cells used in this thesis. CV-1: Core control volume CV-X: intermediate control volume CV – n: outermost control volume. ....  | 131 |
| Figure 6.3 Experimentally measured changes in AMP/Trp ratios under different temperatures as functions of heating time for model systems with different reactant ratios and moisture contents. ....  | 139 |
| Figure 6.4 Experimentally measured changes in AMP/Trp ratios for model systems with different reactant ratios with X=10 kg/kg heated at 100°C.....   | 143 |
| Figure 6.5 Example of the kinetic constant fitting process (X=10 kg/kg heated at 100°C with different reactant ratios).....  | 144 |
| Figure 6.6 Fitting result of the Arrhenius equation for the rate constant.....   | 148 |
| Figure 6.7 Moisture content dependency of the constant $k_{ref}$ in the Arrhenius equation.  | 150 |
| Figure 6.8 Moisture content dependency of the constant c in the Arrhenius equation....   | 150 |
| Figure 6.9 Temperature history of drying gas and particles (average) predicted by different modelling approaches (initial stage). (a) Lumped-parameter model (b) distributed-parameter model.....  | 154 |
| Figure 6.10 Particle (average) temperature history predicted by different modelling approaches (whole dryer).....  | 155 |
| Figure 6.11 Particle moisture content history predicted by different modelling approaches (initial stage). ....  | 155 |

|  |     |
|--|-----|
| Figure 6.12 Particle moisture content history predicted by different modelling approaches (whole dryer).....   | 156 |
| Figure 6.13 Moisture content history of the outermost layer of the particle (from the distributed-parameter model) and the value predicted by the lumped-parameter model. .... | 157 |
| Figure 6.14 Prediction result from the lumped- and distributed-parameter approaches. a – c: lumped-parameter model d – f: distributed-parameter model .....                    | 158 |
| Figure 6.15 Prediction result from the distributed-parameter model with a different number of sub-layers. a – c: 3 layers d – f: 5 layers g – i: 10 layers.....                | 160 |
| Figure 6.16 Predicted result from lumped parameter model and experimental data. ....   | 161 |
| Figure 6.17 Predicted reaction rate for each sublayer from the distributed-parameter model. ....   | 163 |
| Figure 6.18 Predicted result from distributed-parameter model and experimental data..  | 164 |

**List of tables:**

Table 2.1 Summary of relevant studies on Maillard reactions in spray dryers..... 15

Table 2.2 Fraction of open-chain form of glucose at different temperatures and pHs (reproduced based on Yaylayan et al., 1993).....21

Table 3.1 Materials used in this thesis. ....51

Table 3.2 Operating conditions for investigating the effect of operating conditions and feed compositions. ....57

Table 3.3 Operating conditions for measuring RTD in Buchi mini spray dryer B-290. ...59

Table 3.4 Operating conditions for measuring RTD in different designs of the spray dryer. ....60

Table 4.1 Summary of actual and estimated outlet gas temperatures for different inlet gas temperatures.....80

Table 4.2 Summary of colour analysis result for samples collected from different spray drying conditions. ....83

Table 5.1 CSTR fitting results for RTD measurement using different injection volumes and methods.....94

Table 5.2 Key difference between designs and internal volume of different designs. ....97

Table 5.3 Summary of gas velocity,  $Re$ ,  $Sr$  for different parts of the spray dryer at different drying gas flow rates..... 107

Table 5.4  $C_{max}$  and  $C_{min}$  were used for estimating outer normalised turbulent burst frequencies at different  $Re$  (Values of  $C$  are from Metzger et al. (2010)). .... 111

Table 5.5 Estimated turbulent burst frequency based on outer variables for Design 1&2 (diameter = 0.3 m). .... 112

Table 5.6 Estimated turbulent burst frequency based on outer variables for Design 3 (diameter = 0.3 m). .... 112

Table 5.7 Estimated turbulent burst frequency based on inner variables for Designs 1 - 3 (diameter = 0.3 m) .... 116

Table 5.8 RTD measurement result summary for experiments with salt solution..... 117



|   |     |
|---|-----|
| Table 5.9 Physical properties of spray-dried powder collected from different designs and gas flow rates. ....   | 119 |
| Table 6.1 Estimated binary diffusion coefficients of main components of milk at infinity dilution (Foerster et al., 2016).....                        | 135 |
| Table 6.2 Lactose solubility in water (Hudson, 1904).....   | 142 |
| Table 6.3 Whey protein isolate solubility in water (Pelerine and Gomes, 2008).....  | 142 |
| Table 6.4 Fitted kinetics parameters (k in cps/cps/S *10 <sup>-5</sup> ) of experimental data (Zero-order).<br>.....                                  | 145 |
| Table 6.5 P values for the impact heating temperature on the fitted reaction kinetic constants at the same moisture content and reactant ratio. ....  | 146 |
| Table 6.6 P values for the impact moisture content on the fitted reaction kinetic constants at the same heating temperature and reactant ratio. ....  | 146 |
| Table 6.7 P values for the impact reactant ratios on the fitted reaction kinetic constants at the same heating temperature and moisture content. .... | 146 |
| Table 6.8 P values for the impact reactant ratios on the fitted reaction kinetic constants under the same heating temperature and reactant ratio..... | 148 |
| Table 6.9 Fitted parameters for a model describing the temperature and moisture content dependency of Maillard reaction rate constants.....           | 152 |
| Table 6.10 Initial conditions of the base case simulation. ....   | 153 |

## Chapter 1. Introduction

In this chapter, the general background and motivation of this thesis are given. The overall aim and the structure of this thesis are also provided.

This chapter contains published materials from the following publications:

**Zhou, Z.**, Langrish, T.A.G., 2021. A review of Maillard reactions in spray dryers. *J. Food Eng.* 305, 110615. <https://doi.org/10.1016/j.jfoodeng.2021.110615>

**Zhou, Z.**, Langrish, T.A.G., 2021. Color formation and Maillard reactions during the spray drying process of skim milk and model systems. *J. Food Process Eng.* <https://doi.org/10.1111/jfpe.13936>

**Zhou, Z.**, Langrish, T.A.G., Cai, S., 2022. Using particle residence time distributions as an experimental approach for evaluating the performance of different designs for a pilot-scale spray dryer. *Processes* 11, 40. <https://doi.org/10.3390/pr11010040>

I am the first and the corresponding author for the journal articles. I designed the study, analysed the data and wrote the majority of the drafts with the guidance of the supervisor of this thesis, Professor Timothy Langrish. Professor Langrish has assisted with the editing and structure of the manuscripts. Other co-contributors of the works have assisted with the design of the experiment, data acquisition, or editing of the manuscript.

Permission for including published materials in this chapter has been granted by the supervisor of this thesis, Prof. Timothy Langrish.

## 1.1. Spray drying

Drying is the process of removing moisture from materials. Drying has been widely used to extend the shelf life of perishable goods and reduce the cost of transportation. There are many drying methods, including but not limited to freeze-drying, spray drying, oven drying and fluidised bed drying (Fathi et al., 2022). Spray drying is one of the most common methods for drying liquid stock into powders and has been widely used in many industries since the 18<sup>th</sup> century (Caric and Kalab, 1987). A schematic diagram of a typical spray dryer is shown in Figure 1.1.

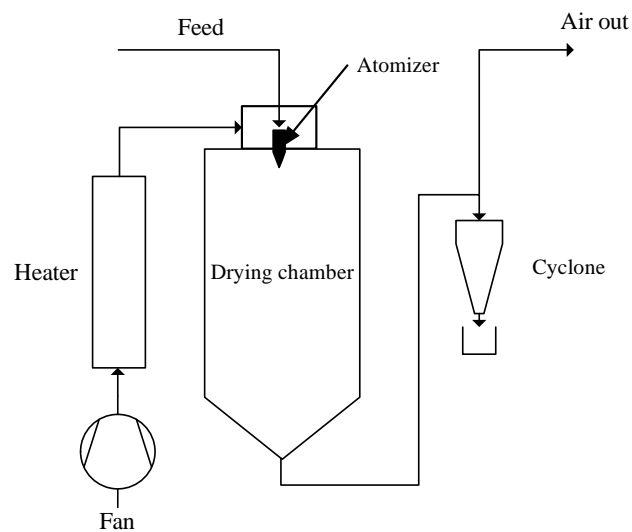


Figure 1.1 Schematic diagram of a typical spray dryer.

A typical spray dryer setup consists of a heating unit, an atomising unit, drying chambers, and a powder collection unit. The heating unit heats up the drying medium to a desirable temperature. Depending on the application, the drying medium usually consists of air or other inert gases (Nunes et al., 2019). The atomising unit atomises the feed into small droplets to provide a higher surface-to-volume ratio to accelerate the drying process. The drying chamber of the spray dryer is where most of the heat and mass transfer between the drying medium and feed droplets occurs. The solvent in the feed droplets transfers to the drying medium within the drying chamber. The hot drying medium also increases the droplet temperature via heat transfer, thus increasing the evaporation rate. At the end of the drying process, dry particles are collected by a cyclone collector or collectors. Sometimes, bag filters are also used after the cyclone

collector to collect fine particles. Fluidised beds are sometimes combined with spray dryers to achieve the desired product properties (Masters, 1972).

Besides freeze-drying and other low-temperature drying methods, spray drying is one of the most commonly used operations in the drying process for many thermally-sensitive products, including foods and pharmaceutical products (Fathi et al., 2022). Compared with freeze drying, spray drying is a well-developed continuous drying method requiring minimal manual handling (Haseley and Oetjen, 2018). Furthermore, the operating and capital costs of spray dryers are also significantly lower than freeze dryers due to their simpler design and higher energy efficiency (Roser, 1991; Santivarangkna et al., 2007).

## 1.2. Milk powder production

Milk is a typical perishable good, which can be easily spoiled if not stored properly. Under optimum storage conditions, pasteurised whole milk can only last for up to two weeks (Australia New Zealand Food Standards, 2006). In order to extend the shelf life of whole milk, whole milk is made into various dairy products, including cheeses, yoghurt and milk powder. Milk powder is one of the most common dairy products that is produced from milk. Removing most of the water from milk extends the shelf life and reduces storage and transportation-related costs (Fathi et al., 2022). Milk powders are usually produced via spray drying. During the production of milk powders, pasteurised milk is pre-concentrated to 48 - 52% solids content via falling-film evaporators to reduce energy consumption in drying. Then the concentrated feed is fed into a spray dryer, where the feed will be spray dried and become powder. Due to the heat exposure during the spray drying process, the quality of the final product may be affected. After the spray-drying process, the spray-dried powder will go through a series of conditioning treatments (Pisecky, 1997). Milk and milk-like model systems have been chosen as the main materials used in this thesis mainly due to their wide applications and the importance of food safety in the dairy industry.

### 1.2.1. Physical properties

The quality of the spray-dried products mainly includes considering the physical and chemical properties of the product. Physical properties of spray-dried products include but are not limited to, the moisture content, the particle size distribution, and the microstructure of the spray-dried products. Some of these properties are critical to the functionality of the powder (Kim et al., 2002; Pisecky, 1997). For example, the moisture content may affect the shelf life of the spray-dried product. If the moisture content is above a specific value, it will encourage the growth of microorganisms or chemical reactions that may lead to a shorter shelf life or the spoilage of the product (Nursten, 2005). The particle size of the powder is another important property that needs to be considered. Particle size mainly affects the re-wettability of the powder and the ease of storing and transporting the powder. In general, if the particle size is too small, it may lead to difficulties in re-dissolving the powders. For milk powders, a particle diameter of 200 - 300  $\mu\text{m}$  is considered the optimal range (Pisecky, 1997).

### 1.2.2. Thermal degradation

Besides the physical properties of the spray-dried product, changes in chemical composition during the spray-drying process are also important. Studies have shown that people are more and more interested in the quality of foods in terms of food safety and the nutritional value of food (Lakni and Jayasinghe-Mudalige, 2010). Due to the thermal exposure of the product during the spray drying process, chemical reactions that are flavoured at elevated temperatures may occur and change the composition of the final product. The changes in chemical composition are commonly known as thermal degradations. There are mainly four types of thermal degradation that may occur during the spray drying process for milk.

The first type of thermal degradation is protein denaturation and aggregation (Jaskulski et al., 2017). Milk is a material that is rich in proteins. Proteins may lose their special structure due to thermal exposure during spray-drying processes. This process is commonly known as protein denaturation (Bylund and Svensson, 1995). Protein denaturation has many consequences, including reduced bioavailability and solubility, which may adversely affect the quality of the final products (Meshram et al., 2018; Singh et al., 2015). In industry, milk

powders are classified into three broad classes based on the whey protein nitrogen index (WPNI), which measures the degree of protein denaturation (Pisecky, 1997).

Enzymes are proteins that can act as catalysts to affect the reaction rate of a specific biochemical reaction. As with other proteins, enzymes are subject to "denaturation" due to thermal exposure during spray-drying processes (Meshram et al., 2018; Fox and Kelly, 2006). Based on this characteristic of enzymes, some enzymes in milk have been used as markers for evaluating the extent of thermal exposure for hygiene purposes or simulating the extent of reactions (Fox, 2002; Lorenzen et al., 2010; Ritota et al., 2017; Wijlhuizen et al., 1979).

Other than proteins, milk is rich in sugars, mainly lactose. Under elevated temperatures, lactose may undergo isomerisation and form lactulose with appropriate catalysts (Adachi, 1958; Ritota et al., 2017). Lactose is also involved in other reactions, and lactose isomerisation is more favoured at higher temperatures. As a result, lactulose is commonly used as a marker for high-temperature exposure combined with other markers for thermal exposure (Nursten, 2005).

Lactose and proteins contribute to more than 60% of the solids in bovine milk on a mass basis (Pisecky, 1997). Thus, the interactions between lactose and protein under elevated temperatures are important factors that must be considered. The reactions between reducing sugars like lactose and proteins are commonly known as the non-enzymatic browning reactions or the Maillard reactions (Maillard, 1912), which is the main focus of this thesis.

### 1.2.3. Maillard reactions

Maillard reactions, named after Louis Camille Maillard, are reactions between reducing sugars and amino acids. Maillard reactions involve more than 200 reactions that have various consequences (Maillard, 1912; Nursten, 2005). Due to the complex nature of Maillard reactions, the exact reaction pathways, reaction products, and their effect on humans are complicated.

Some of the Maillard reaction products are less desirable. During the early stage of Maillard reactions, lysine residues on proteins react with reducing sugars via Schiff base formation, followed by Amadori transformation. As a result, the bioavailability of proteins decreases (Birlouez-Aragon et al., 2004; Schmitz et al., 2011; Boekel, 1998). Ascorbic acid (Vitamin C)

may also be involved in the early stage of Maillard reactions, and further reduces the nutritional values of the product (Nursten, 2005; Zhong et al., 2019). Advanced Glycosylation End (AGE) products, which are considered a class of harmful products linked to diabetes and other diseases, are formed during the intermediate stage of the Maillard reactions (Nursten, 2005; Uribarri et al., 2010). Other than AGE products, studies have also reported that some of the intermediate products are mutagenic or carcinogenic (Friedman, 1996; Lee and Shibamoto, 2002). Some of the intermediate products produce visible browning, which is often regarded as the sign of the start of the intermediate stage of Maillard reactions (Nursten, 2005). Protein crosslinking during the final stage of the Maillard reactions may decrease the solubility of the spray-dried products (Nursten, 2005). Other than reducing the solubility of the product, nitrogen-containing browning pigments (melanoidins) are formed as a result of the polymerisation of products formed during the previous stages of Maillard reactions (Hodge, 1953). Melanoidins are mainly responsible for browning in the final product. During the intermediate and the final stages of Maillard reactions, small flavour species are formed and contribute to the characteristic flavour and smell in the final product (Park et al., 2016; Reineccius, 1999). These flavoured products may be desirable in some cases. However, they may be less desirable in spray-dried powders.

On the other hand, studies have reported that some Maillard reaction products have antioxidant properties (Nursten, 2005; Samborska et al., 2019). Maillard reaction conjugates are sometimes used as encapsulation agents or emulsifiers during some spray-drying processes (Lee et al., 2017, 2015). Maillard reaction products prepared from specific systems are also believed to have antimutagenic, antibiotic and antiallergenic effects (Einarsson, 1987; Einarsson et al., 1988, 1983; Kato et al., 1987; Yen and Hsieh, 1994).

In conclusion, the effect of Maillard reactions on the quality of the spray-dried product is complicated, which is related to the complex reaction scheme. Given the importance of food safety, it is important to study the kinetics of Maillard reactions that occur during the spray drying process for milk.

### 1.3. Importance of spray dryer designs

Historically, studies of reactions during the spray drying processes have mainly focussed on the operating conditions and the feed itself (Koca et al., 2015; Park et al., 2016). Only limited attention has been paid to the impact of the design of the spray dryer on the reactions that occur during spray drying (Jeantet et al., 2008; Schmitz-Schug et al., 2013). Redesigning and improving spray dryers have always been important parts of drying technology research. One of the important aspects of the spray-dryer redesign process is reducing the extent of wall deposition. Wall deposition involves particles and droplets depositing on the inner walls of the equipment. Other than the loss of products and related fire hazards, the re-entrainment process of wall depositions is another important factor that may affect the quality of the spray-dried products. Wall depositions may affect the quality of the spray-dried products through changing the residence time of the material in the equipment (Keshani et al., 2015). Re-entrainment of wall depositions is the process of particles on the inner wall of the spray dryer re-entraining into the gas flow after staying on the wall for a period of time. Compared with those particles that do not interact with the wall, wall deposits that are re-entrained have a greater extent of thermal exposure, which may and affect the product quality adversely (Francia et al., 2015; Hanus and Langrish, 2007a; Mazza et al., 2003). The re-entrained wall deposits may contaminate the final product. Re-entrainment is an important factor that needs to be considered when studying Maillard reactions that occur during spray drying.

Traditionally, optimisation and redesign processes are based on trial-and-error methods and simplified mathematical modelling. These traditional approaches are time-consuming, expensive or can only provide a rough approximation of the actual process. With the advancements in computational power, the use of more complex modelling methods has become practical with the assistance of computers. One of the examples is computational fluid dynamics (CFD). CFD has been commonly used to study the flow of fluids in many areas. CFD simulations can provide theoretical insights into the flow regime and gas and particle flow patterns within the equipment. CFD technology has made the redesign process less time-consuming and more cost-effective. However, assumptions in calculations are still



required for CFD simulations due to the need to model turbulence, connected with the time required to obtain well-converged simulations that capture all the required physical phenomena of turbulence, time-dependent flow, and multiphase flow (including drying, particle size changes, and stickiness). Thus, validations of the simulation results are still essential (Jeantet et al., 2008).

One of the key performance indicators for the performance of a spray dryer is the particle residence time distribution at a given operating condition. The particle residence time measures the time that the particles stay in the equipment. The particle residence time distribution (RTD) can provide significant insight into the combined effect of the material properties, designs and operating conditions (Jeantet et al., 2008). It is also a useful tool for validating CFD simulation results. In the case of spray drying, the particle residence time is the contact time between the drying medium and the particles, which also determines the total time for any chemical reactions. Similar to most reactions, Maillard reactions are time-dependent (Hodge, 1953; Morales and Boekel, 1998). Therefore, investigating how the particle residence time is affected by the design of a spray dryer is relevant to the study of Maillard reactions in spray dryers.

#### 1.4. Segregation during spray drying

Component segregation is a physical process where components of a mixture separate into different layers (Baklouti et al., 1998; Kim et al., 2003). Segregation is expected to occur during the spray-drying process of multi-component feeds, such as milk. Many studies have reported the segregation processes that occur during the spray drying process of milk, due to the differences in physical properties of proteins and sugars (solubilities and diffusivities). The surface of the milk powders is mainly covered in fats or proteins, while the core of the spray-dried powder mainly consists of sugars (lactose, in milk) (Fäldt and Bergenståhl, 1994; Kim et al., 2003; Nijdam and Langrish, 2006). This process of segregation results in a significant difference in the protein to lactose ratios from the outside to the inside of the particles. Proteins and reducing sugars are the two main reactants for Maillard reactions, and thus the kinetics of Maillard reactions are likely to be affected by the segregation process (Hodge, 1953). Therefore, it is also important to consider the segregation process that occurs

during the spray drying process as a part of the study for the kinetics of Maillard reactions in spray dryers.

### 1.5. Thesis Aim

The aim of this thesis is to investigate the Maillard reactions that occur during the spray drying process from an engineering point of view with a more systematic approach. Milk and milk-related materials have been chosen as the raw materials for the spray drying process due to their common usage, significant experience in research, and relative safety and non-toxicity. Studies on the kinetics of reactions that occur during the spray drying process have typically been focused on the operating conditions (Koca et al., 2015; Park et al., 2016). In contrast, limited attention has been paid to the design characteristics (dimensions and geometry) of the spray dryer itself. In addition to traditional factors, such as temperature and feed composition, the design characteristics of the spray dryer should also be considered while investigating the kinetics of any reactions that occur during spray-drying processes. Physical processes, such as component segregation, which occur during the spray-drying processes, are also important factors and need to be considered. In summary, this thesis aims to address the following objectives:

- Investigate how operating conditions and feed compositions may affect the kinetics of Maillard reactions in spray dryers.
- Investigate how designs of drying chambers may affect particle residence time, the re-entrainment behaviour of wall deposits, and the impact of these different designs on the quality of the spray-dried product.
- Propose a model for modelling of Maillard reactions that occur during the spray drying process with the inclusion of the segregation process in this modelling approach.

## 1.6. Thesis structure

To address the aims of the thesis, this thesis has been divided into eight chapters.

### **Chapter 1: Introduction**

The first chapter is the introduction chapter. In this chapter, the general background, motivations and aims of this research project have been briefly introduced.

### **Chapter 2: Literature review**

The second chapter is the literature review chapter. In this chapter, current developments in fields that are relevant to this thesis have been summarised, and the background of the research has been further explained. The research gaps that are aimed to be addressed in this thesis have been discussed in greater detail.

### **Chapter 3: Materials and methods**

In this chapter, the materials and methods used in this thesis have been discussed in more depth.

### **Chapter 4: Maillard reactions under different spray drying conditions**

The fourth chapter mainly focused on how different operating conditions and feed compositions affect the kinetics of the Maillard reactions in spray dryers.

### **Chapter 5: Effect of different designs of the spray dryer on the particle residence time distribution and the quality of the final product**

The fifth chapter mainly focused on how chamber designs may affect the particle residence time and the potential impact of different designs on the quality of the final product.

### **Chapter 6: Modelling Maillard reactions under different spray drying conditions**

The sixth chapter mainly focused on developing a model for simulating component segregation and its potential connection to the kinetics of Maillard reactions using both the lumped and distributed-parameter modelling approach.

## **Chapter 7: Conclusions and further considerations**

The seventh chapter contains conclusions and further recommendations. In this chapter, findings in the previous chapters have been discussed and summarised, and future studies that can be developed based on these findings were also suggested.

## **Chapter 8: Impact of COVID-19 on the scope of this thesis**

The eighth chapter highlighted the impact of COVID-19 related government-imposed restrictions on the scope of this thesis, as per the requirement of thesis examination under emergency conditions.

## **Appendix:**

Supporting materials, including codes developed for control of the automated systems and data processing are included in this section.

## Chapter 2. Literature review

In this chapter, current developments in relevant fields to this thesis have been summarised, and the background of the research has been further explained. The research gaps that are aimed to be addressed in this thesis have been discussed in greater detail.

This chapter is developed based on a published journal article: "*A review of Maillard reactions in spray dryers.*" that was published in the Journal of Food Engineering. I am the first and the corresponding author for this journal article. I designed the study, analysed the data, and wrote the majority of the draft with the guidance of the supervisor of this thesis, Professor Timothy Langrish. Professor Langrish has assisted with the editing and structure of the manuscript.

Permission for including published materials in this chapter has been granted by the supervisor of this thesis, Prof. Timothy Langrish.

---

| <b>Symbols</b>        |                                |
|-----------------------|--------------------------------|
| <i>A</i>              | Amino acid                     |
| <i>AP</i>             | Amadori product                |
| <i>AS</i>             | Schiff base product            |
| <i>a<sub>w</sub></i>  | Water activity                 |
| <i>DG</i>             | Deoxyglucosone                 |
| <i>f</i>              | Normalised drying rate         |
| <i>k</i>              | Reaction kinetic constant      |
| <i>M</i>              | Melanoidins                    |
| <i>N</i>              | Specific drying rate           |
| <i>P<sub>v</sub></i>  | Vapour concentration           |
| <i>R</i>              | Ideal gas constant             |
| <i>S</i>              | Reducing sugar                 |
| <i>T<sub>g</sub></i>  | Glass transition temperature   |
| <i>X</i>              | Moisture content               |
| <i>ΔE<sub>v</sub></i> | Activation energy              |
| <i>Φ</i>              | Dimensionless moisture content |

---

## 2.1. Introduction

Spray drying has been used since the 18<sup>th</sup> century as a method for extending the shelf life of dairy and other food products (Caric and Kalab, 1987). The quality of spray-dried products is commonly assessed on the basis of physical properties, such as moisture content, wettability, and particle size (Pisecky, 1997). With the growing interest in the nutritional value and the integrity of components in foods, it is important to understand the mechanism of thermal degradation in spray dryers (Lakni and Jayasinghe-Mudalige, 2010).

One of the common types of thermal degradation that occurs during the spray drying processes of many food products is Maillard reactions (Schuck, 2006). Maillard reactions are chemical reactions that occur between amino acids and reducing sugars (Maillard, 1912). During the spray drying process of milk or other dairy products, depending on the processing conditions, Maillard reactions may occur. Maillard reactions have many consequences, including the loss of nutritional value, the formation of nitrogen-containing brown pigments (melanoidins), the formation of potential mutagenic products, and the formation of flavour products (Morales and Boekel, 1998; Nursten, 1986).

Current studies on Maillard reactions in spray dryers are mainly focused on the following areas: the effect of the operating conditions (e.g., inlet gas temperature, feed flow rate) on the quality of spray-dried products (Koca et al., 2015; Park et al., 2016), using Maillard reactions products as emulsifiers or encapsulation agents in spray-drying processes (Lee et al., 2017, 2015), Maillard reactions that occur during the storage of spray-dried products, and changes in physical or sensory properties in the spray-dried products that may be related to Maillard reactions (Carter et al., 2018; Ceylan Sahin et al., 2018; Park et al., 2016). A summary of some relevant studies is shown in Table 2.1. Although the kinetics of Maillard reactions in liquid systems have been studied extensively, little attention has been paid to the kinetics of Maillard reactions inside spray dryers. Nevertheless, spray dryers of various sizes and configurations have been used in current studies, which all have different characteristics, making it difficult to assess the wider applicability of their findings. Thus, a more systematic approach to the question is still lacking.

Table 2.1 Summary of relevant studies on Maillard reactions in spray dryers.

| Authors                       | Food systems   | Spray drying conditions  | Degree of Maillard reactions   |
|-------------------------------|--|--|--|
| Tomlinson et al. (1993)       | Model system:<br>Glucose: 1M<br>Glycine: 1M  | Bench-scale spray dryer<br>Inlet/Outlet gas temperature:<br>235°C /170°C<br>Flowrate: 20 mL/min  | Structure elucidation of Maillard reaction product   |
| Vasbinder and de Kruif (2003) | Gelatin hydrolysate and maltodextrin at a ratio of 2:1 (w/w)<br>Solid conc. 2% w/v | Bench-scale spray dryer<br>Inlet/outlet gas temperature:<br>160°C - 200°C/92°C -112°C;<br>Flowrate: 4.0 mL/min   | Colour analysis based on CIELab colour space: L*: 15-20, a*:-0.38 - 0.14, b*:-5 -16, ΔE: 5 - 11  |
| Miao and Roos (2004)          | Model system:<br>Lactose 45 wt%, trehalose 45 wt%, xylose 5wt%, and lysine wt5%    | Samples were conditioned to different moisture contents<br>Heated 40 - 90°C for 5 - 15 min<br>Pilot-scale spray dryer<br>Inlet/outlet gas temperature:<br>160°C - 230°C/60°C - 100°C                         | Optical density at 280nm (0 - 450 OD/g of dry mass) and 420nm (0 - 80 OD/g of dry mass)  |
| Koca et al. (2015)            | Cheese slurry<br>Solid conc. 25 wt%  | Atomisation pressures :<br>294 kPa - 588 kPa<br>Feed flow rate was controlled to maintain a specific outlet gas temperature  | Measured as Non-enzymatic browning (NEB):<br>Chroma values:10 - 20:<br>Browning index: 11 - 30.<br>Degree of NEB: 0.12 - 0.343 optical density/g of dry mass |
| Huang et al. (2016)           | Glycine and sucrose at ratio of 2:1 (w/w)<br>Solid conc. 1.5% w/v                  | Bench-scale spray dryer<br>Inlet/outlet gas temperature:<br>160°C - 230°C/75°C - 107°C<br>Feed flow rate: 5g/min - 25g/min<br>Pilot-scale spray dryer<br>Inlet/outlet gas temperature:<br>160°C - 260°C/90°C | Browning pigment formation and intermediate product as absorbance at 294 nm and 420 nm, respectively.<br>HMF concentration: 0 - 0.8 w/w%                     |
| Park et al. (2016)            | Skim milk<br>Solid conc. 30 - 50 wt%   | Feed flow rate was controlled to maintain the same outlet gas temperature  | Furosine: 10 - 20 mg/100g of protein<br>Changes in sensory properties and volatile compounds   |



Table 2.1 Continued.

| <b>Authors</b>                      | <b>Food systems</b>  | <b>Spray drying conditions</b>  | <b>Degree of Maillard reactions</b>  |
|-------------------------------------|--|---|--|
| Rongsirikul and Hongsprabhas (2016) | Whey protein concentrates with/without modification and trehalose at a ratio of 3:7<br>Solid conc. 20% w/v | Bench-scale spray dryer<br>Inlet /Outlet gas temperature:<br>130°C /100°C<br>Flowrate: 4.0 mL/min   | Browning pigment formation as absorbance at 420 nm.  |
| Fialho et al. (2018)                | Lactose-hydrolyzed concentrated milk and concentrated milk.<br>Solid conc. 40% w/w dry mass                | Bench-scale spray dryer<br>Inlet/outlet gas temperature:<br>160°C/53 - 93°C<br>Feed flow rate: 5g/min - 25g/min   | Colour analysis based on CIELab colour space: L*: 86 - 96<br>HMF concentration: 0 - 130 mg/kg  |
| Katekhong and Charoenrein (2018)    | Egg white  | Pilot-scale spray dryer<br>Inlet /Outlet gas temperature:<br>140°C - 180°C/80°C<br>Feed flow rate was controlled to maintain the same outlet gas temperature (13 - 20 mL/min) | Visual appearance and Colour analysis based on CIELab colour space: $\Delta E$ : 0 - 15<br><br>Available lysine: 1.63 - 11.3 g/100g of protein<br>Furosine : 0.44 - 11.1 mg/100g of protein                |
| Gómez-Narváez et al. (2019)         | Model system:<br>2.91% moisture, 5.62% ash, 11.07% protein, 77.78% lactose                                 | Samples were conditioned to different moisture contents<br>Heated at 60 - 90°C for 2 - 40 min   | HMF: ND - 57.7 mg/100g of protein<br>Browning index: 0.01 - 0.11<br>Colour analysis based on CIELab colour space: $\Delta L^*$ : -10 - 0, $\Delta a^*$ : 0 - 8, $\Delta b^*$ : 0 - 15, $\Delta E$ : 0 - 18 |

Table 2.1 Continued.

| <b>Authors</b>              | <b>Food systems</b>  | <b>Spray drying conditions</b>  | <b>Degree of Maillard reactions</b>   |
|-----------------------------|--|---|---|
| Zhong et al. (2019)         | Ascorbic acid (vitamin C) and whey protein isolate (WPI) at different ratios (0 - 1:2) (10 wt% WPI, and concentration of Vitamin C varies based on ratios) | Bench-scale spray dryer<br>Inlet/outlet gas temperature: 150°C - 72°C<br>Feed flowrate: 8 mL/min<br>Samples were aged at 20°C for 21 days | Colour analysis based on CIELab colour space: Red/green values (a*) (-5 - 30)<br>Fluorescence measurements with excitation wavelengths of 380/500nm, and emission wavelengths 440/600nm<br>Available lysine: 52.5 - 60.5 mmol/100g of protein |
| Gómez-Narváez et al. (2022) | Nano-filtered whey: 2.91% moisture, 5.62% ash, 11.07% protein, 77.78% lactose  | Samples were conditioned to different moisture contents<br>Heated at 60 - 90°C for 2 - 40 min   | Furosine : 4.4 - 10.0 mmol/100g of protein<br>Browning index: 20.7 - 21.8 Abs/100g of protein   |

Due to the rapid changes in the moisture content and the temperature of particles in most spray dryers, the mechanisms of the Maillard reactions in spray dryers may be different to these reactions in liquid systems, and there is a need to investigate this area. The structure of this review can be summarised as follows. The chemical reactions and kinetics of the Maillard reaction scheme have been reviewed first, and then the difference between Maillard reactions in liquid systems and in spray dryers has been outlined. General factors, such as the composition of the feed, the pH values, and the water activity, have then been discussed. Significant attention has been paid to the factors that are mainly related to the spray-drying process. Spray-drying specific factors, including component segregation due to the spray-drying process, wall deposition and re-entrainment and the particle residence times in spray dryers, have been discussed in the context of Maillard reactions.

## 2.2. Maillard reactions

The exact mechanisms of Maillard reactions remain unclear due to their complicated natures (Nursten, 2005). Essentially, Maillard reactions are a group of reactions that occurs between amino acids and reducing sugars, and these reactions are more favoured at elevated temperatures (Maillard, 1912). Hodge (1953) developed a simplified version of the Maillard reactions scheme where most of the reaction routes are included within that scheme. Nursten later included a reaction route where fission products are formed from Schiff based products to account for the more recent discoveries in the kinetics of Maillard reactions (Nursten, 2005).

In general, Maillard reactions can be divided into three different stages. In the study of Hodge (1953), the Maillard reaction scheme has been divided into three different stages, namely the initial stage, the intermediate stage, and the final stage, as shown in Figure 2.1.

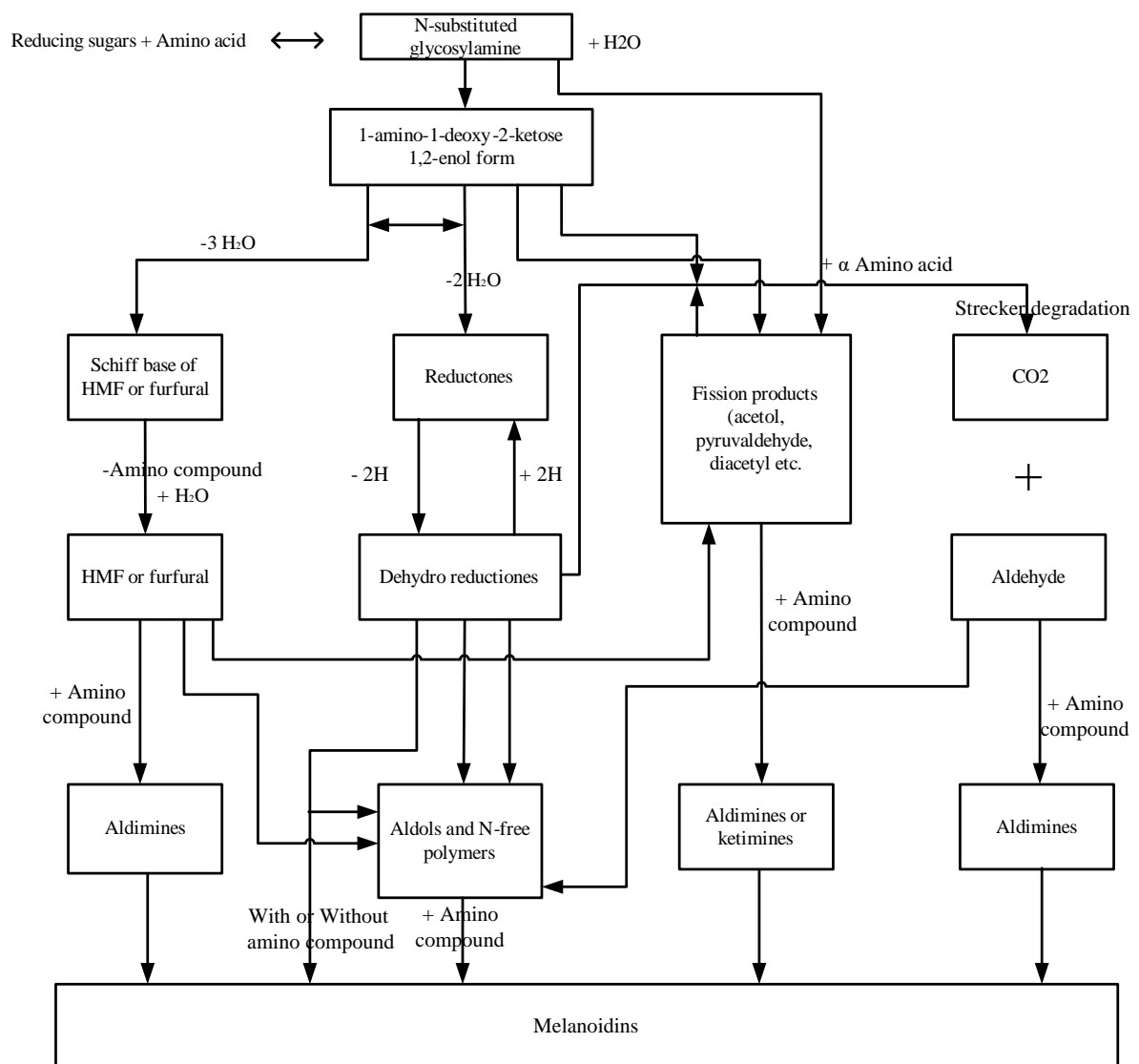


Figure 2.1 Overview of Maillard reactions scheme (reproduced based on Nursten, 2005).

### 2.2.1. The early stage of Maillard reactions

During the early stage of Maillard reactions, reducing sugars (carbohydrates) react with amino acids via Schiff base formation. Then Schiff base products are rapidly transformed into Amadori products via the Amadori transformation. The Amadori rearrangement is generally considered to be an irreversible process. However, some studies have suggested a different opinion (Boekel, 2001). A significant amount of lysine was recovered by incubating 15nM N-formyl-N-fructosyl-lysine (fFL) in pH 7.4 buffer for 15 days at 37 °C. Ahmed et al. (1986, 2002) considered the reproduction of lysine to be a result of the reversal of the Amadori rearrangement. Later study by Davidek et al. (2002) showed that the reaction rate for the

reversal of an Amadori product is low, and the Amadori rearrangement can still be considered to be effectively irreversible (Davidek et al., 2002; Nursten, 2005; Boekel, 1998).

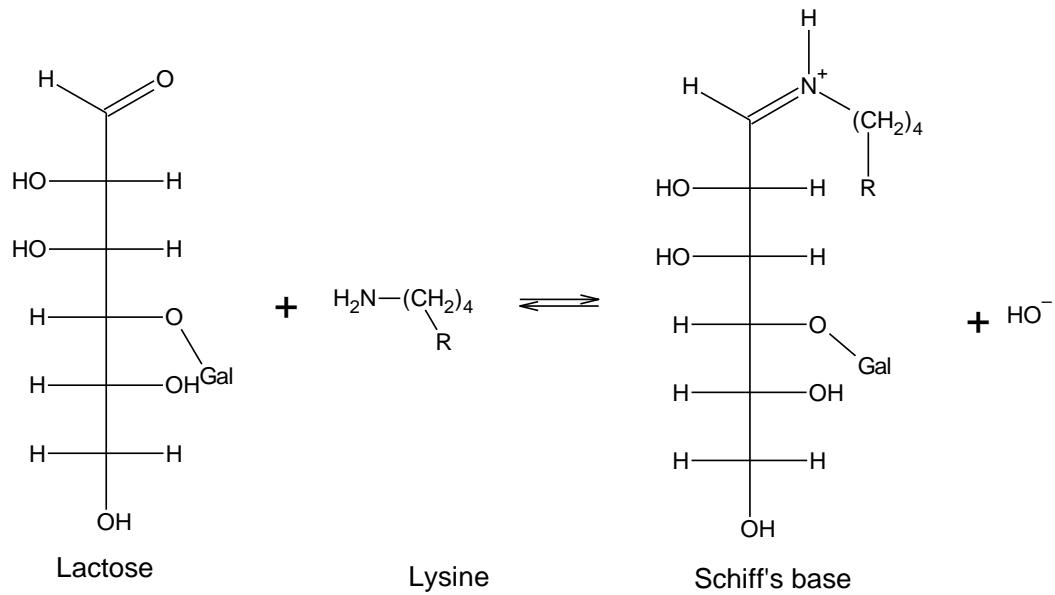


Figure 2.2 Condensation and formation of Schiff base of lactose and lysine.

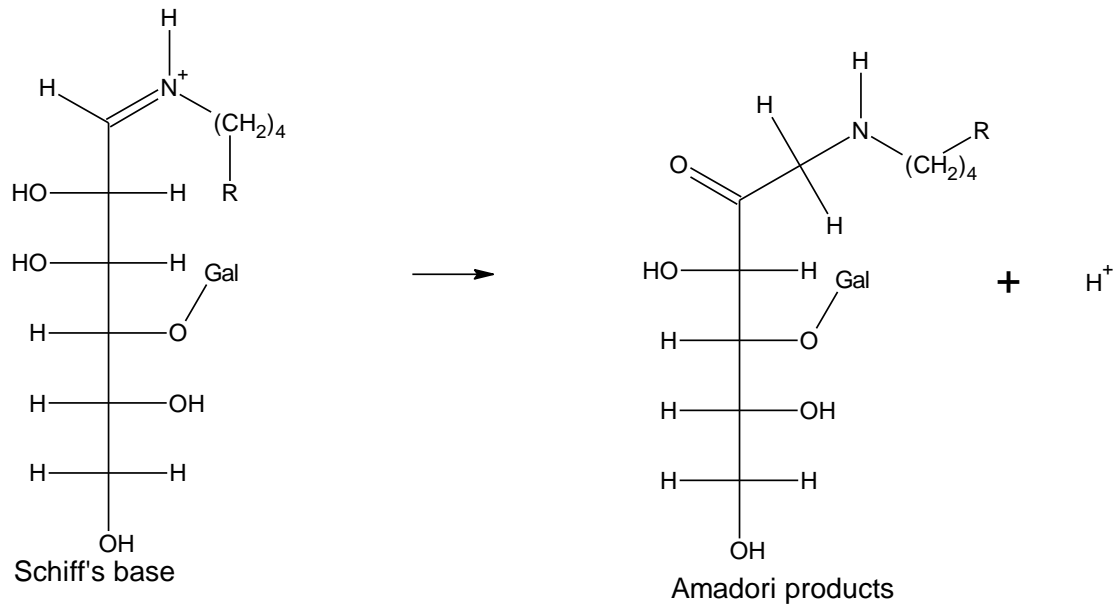


Figure 2.3 Formation of Amadori products.

As with other reactions, the reaction rate for Amadori product formation is dependent on the reactant concentration. Both amino acids and reducing sugars are present in two forms in aqueous systems, reactive and unreactive forms (Boekel, 2001).

Sugars consist of two forms in aqueous solutions, open-chain and closed forms, where the open-chain form is considered to be the reactive form (Figure 2.4). The ratio between the open-chain and closed form depends on the pH and the temperature of the environment. Studies show that the open-chain form is more favoured at greater pHs and temperatures (Yaylayan et al., 1993). The fractions for the open-chain form of D-glucose in aqueous solutions at different temperatures and pHs have been investigated by Yaylayan et al. (1993), and their results are shown in Table 2.2.

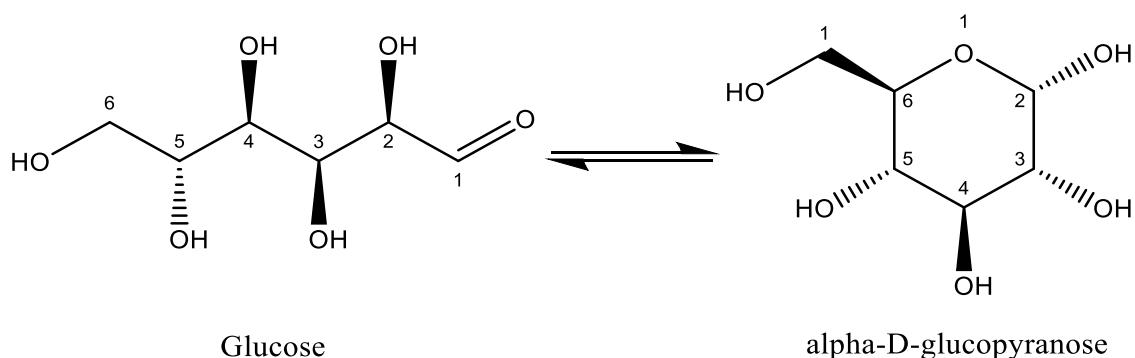


Figure 2.4 Open-chain form and closed-form of glucose.

Table 2.2 Fraction of open-chain form of glucose at different temperatures and pHs (reproduced based on Yaylayan et al., 1993).

| Temperature (°C) | pH 2 | pH 3 | pH 7 | pH 8 | pH 9 |
|------------------|------|------|------|------|------|
| 25               | 0.9  | 0.9  | 0.7  | 0.7  | 0.8  |
| 30               | 1.5  | 1.5  | 1.3  | 1.5  | 1.5  |
| 35               | 2.3  | 2.3  | 2.1  | 2.3  | 2.2  |
| 40               | 3.1  | 3.1  | 2.9  | 3.2  | 3.1  |
| 45               | 4    | 4    | 3.8  | 4.2  | 4.1  |
| 50               | 5    | 5.1  | 4.9  | 5.2  | 5.2  |
| 55               | 6.1  | 6.2  | 6    | 6.4  | 6.4  |
| 60               | 7.3  | 7.4  | 7.2  | 7.6  | 7.8  |
| 65               | 8.6  | 8.7  | 8.5  | 8.9  | 9.2  |
| 70               | 10   | 10.1 | 10   | 10.3 | 10.8 |
| 75               | 11.5 | 11.5 | 11.5 | 11.7 | 12.5 |
| 80               | 13.1 | 13.1 | 13.1 | 13.3 | 14.3 |

Similar to sugars, proteins (amino acids) also consist of two different forms in aqueous solutions, protonated and unprotonated forms. The unprotonated protein form is considered to be the reactive form of proteins (Figure 2.5) (Boekel, 2001). The equilibrium between protonated and unprotonated proteins depends on the pH of the environment and the pKa of

the amino acid. Usually, less than 1% of the protein remains unprotonated when the pH is below 7 (Boekel, 2001).

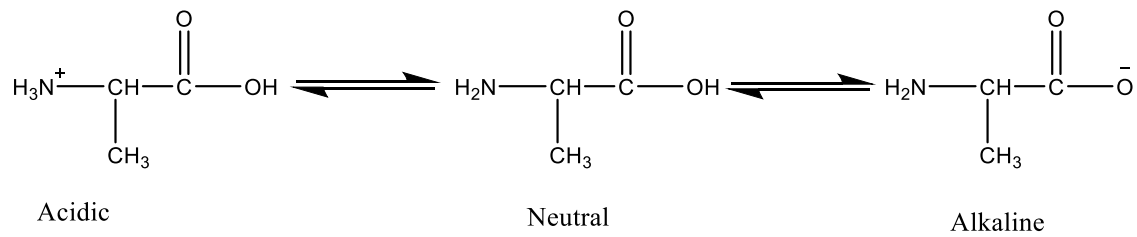


Figure 2.5 Amino acids in different pH environments.

The ratios between different reactants also play an important role in the early stage of Maillard reaction kinetics. Copado et al. (2017) created microcapsules formulated with different concentrations of chia oil and with different carbohydrate-to-protein ratios in a freeze dryer. They found that a higher carbohydrate-to-protein ratio increased both the rate and the extent of Maillard reactions for their system.

### 2.2.2. The intermediate stage of Maillard reactions

After the initial stage of the Maillard reactions, the Amadori products start to break down into different small pigments, depending on the pH of the environment. There are three main different breakdown routes: 1. The 3-deoxyosone pathway via the 1,2 enolisation route under acidic environments (Figure 2.6). 2. The 1-deoxyosone pathway via the 2,3 enolisation route under neutral and alkaline environments (Figure 2.7). 3. The 4-deoxyosone pathway under slightly alkaline conditions (Figure 2.8) is less common than the other two pathways (Boekel, 1998).

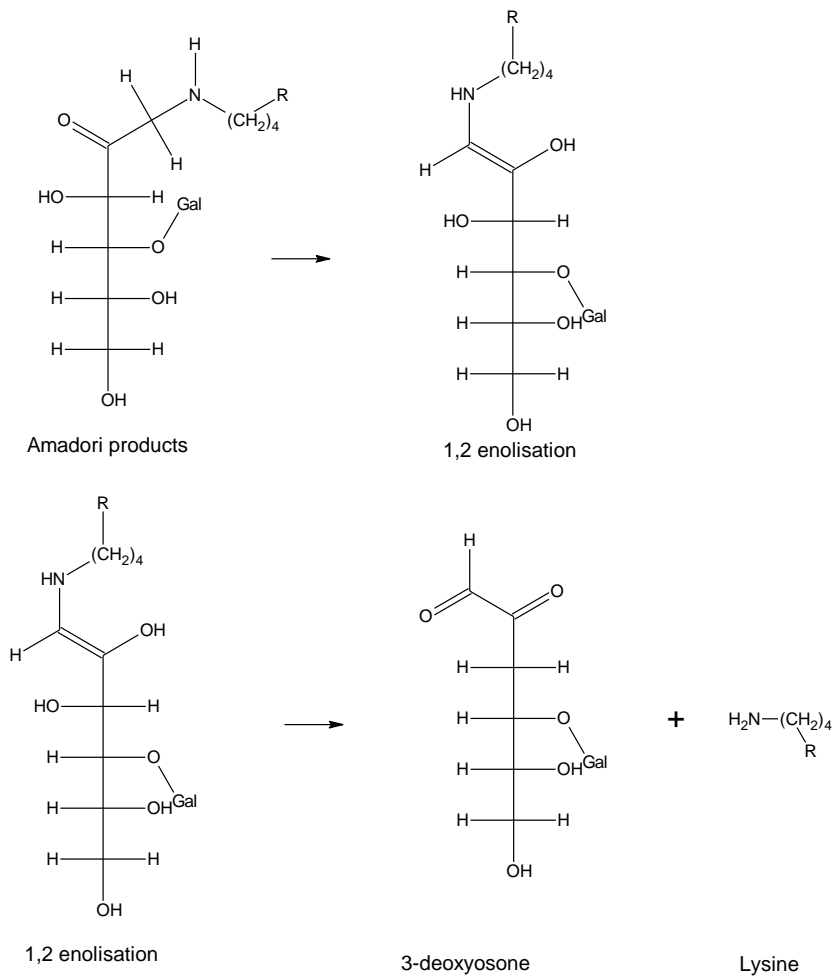


Figure 2.6 Schematic diagram of 3-deoxyosone-pathway via the 1,2 enolisation route.

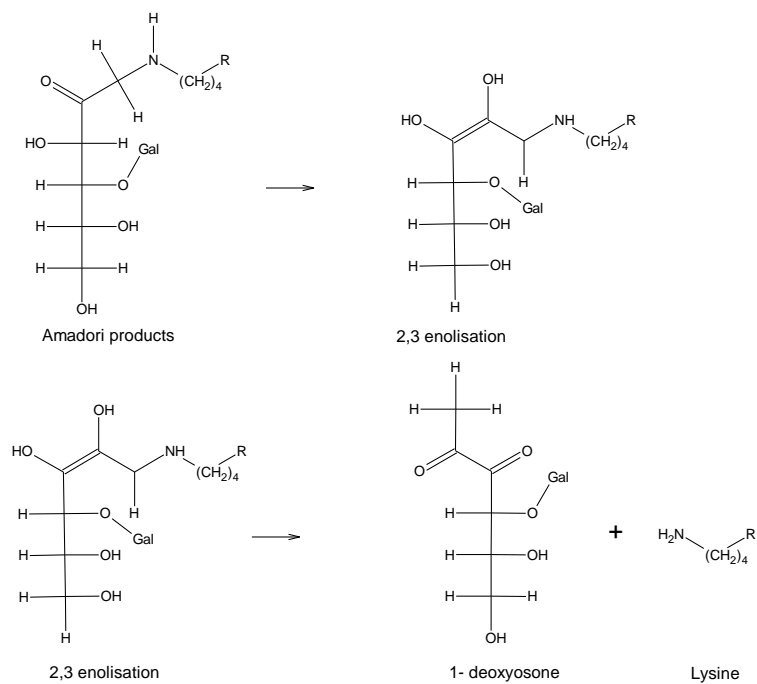


Figure 2.7 Schematic diagram of 1-deoxyosone-pathway via the 2,3 enolisation route.



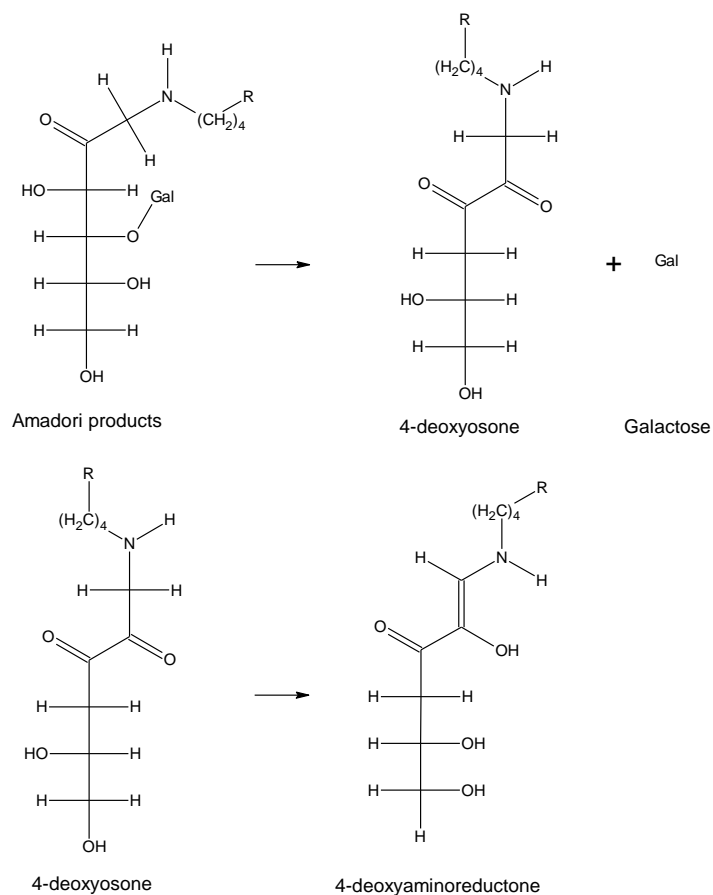


Figure 2.8 Schematic diagram of the 4-deoxyosone-pathway.

All three different breakdown pathways involve the formation of deoxyosones, which are reactive intermediate products. Some of the breakdown products of these reactive intermediates are known as advanced glycosylation end products (AGEs). These products have strong ultraviolet absorbance prior to the start of visible browning, and they can be used as indicators for the start of the intermediate stage of Maillard reactions (Nursten, 2005). Some of the methods used for estimating the extent of thermal degradation of food products have also been developed based on these products (Birlouez-Aragon et al., 1998; Keeney and Bassette, 1959). Furfural and reductones are formed during this stage and have been found to be related to the browning outcomes in the later stages (Hodge, 1953).

### 2.2.3. The final stage of Maillard reactions

During the final stage of Maillard reactions, the intermediate products that are produced during previous stages react with each other via polymerisation, and nitrogen-containing brown pigments (melanoidins) are formed. Melanoidins have high molecular weights (up to about

100000 g/mol). The exact mechanism for the formation of melanoidins and their structures remains unclear. The main reactions involved in the formation of melanoidins are expected to include aldol condensation, aldehyde-amine polymerisation, and the formation of heterocyclic nitrogen compounds (Hodge, 1953).

#### 2.2.4. Application of Maillard reactions in spray drying

Maillard reaction products are sometimes used as emulsifiers or encapsulation agents coupled with spray drying or other drying processes (Lee et al., 2017). The uses of Maillard reaction products as encapsulants for palm-based medium- and long-chain triacylglycerol were studied by Lee et al. (2015). They found that the Maillard reactions can be controlled satisfactorily by choosing a suitable mixture of sodium caseinate, soy proteins, and maltodextrin when heated as a solution for a particular temperature and time and that Maillard reaction products can act as natural emulsifiers and encapsulation agents. The anti-oxidant properties of Maillard reaction products have been reported in many studies (Lee et al., 2017). In a study by Samborska et al. (2019), the effects of low-temperature spray drying with dehumidified inlet air on the phenolic content, antioxidant activity and level of aroma compounds in rapeseed honey have been investigated. Maltodextrin and NUTRIOSE® were used as carriers, and skim milk was assessed as a substitute for water. The authors suggested that Maillard reaction products may contribute to the increased anti-oxidant activity in the spray-dried powders (Samborska et al., 2019).

### 2.3. Kinetic studies of Maillard reactions

#### 2.3.1. Kinetic studies of Maillard reactions in liquid systems

To understand the kinetics of the Maillard reactions in spray dryers, kinetic modelling is necessary. Ge and Lee (1997) proposed a model for the early stage of Maillard reactions, as shown in Figure 2.9.

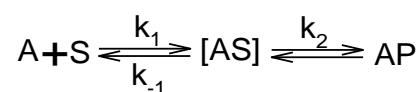


Figure 2.9 Kinetic model for the early stage of Maillard reactions ((Ge and Lee, 1997).

Here  $A$  is an amino acid;  $S$  is a reducing sugar;  $AS$  is the Schiff base product, and  $AP$  is the Amadori product.

In their results,  $k_{-1}$  and  $k_2$  are significantly greater than  $k_1$ , which suggests that the formation of Schiff base is the rate-limiting step for the early stages of Maillard reactions. The formation of Amadori product is strongly temperature-dependent and favoured at higher temperatures, as suggested by the higher activation energy for step 2 compared with step 1 and the reverse of step 1 (Ge and Lee, 1997).

Since there are various products that may be formed during Maillard reactions, and they may interact with each other, using a multi-response modelling approach is necessary. A multi-response modelling approach is an approach that includes multiple and potentially simultaneous chemical reactions in a complex reaction scheme; this approach predicts the changes (responses) in both reactants and products at the same time. This terminology has been used by Martins et al. (2000). They have explained the distinction between this concept and the concept of "*analysing and modelling more than one component simultaneously*". Mundt et al. (2002) have proposed a multi-response model for the maltose-glycine system. The multi-response scheme gave a good fit to the experimental results. The multi-response scheme has been further developed and extended by including key intermediates that are produced during different stages of the Maillard reactions, as shown in Figure 2.10 (Martins and Boekel, 2002).

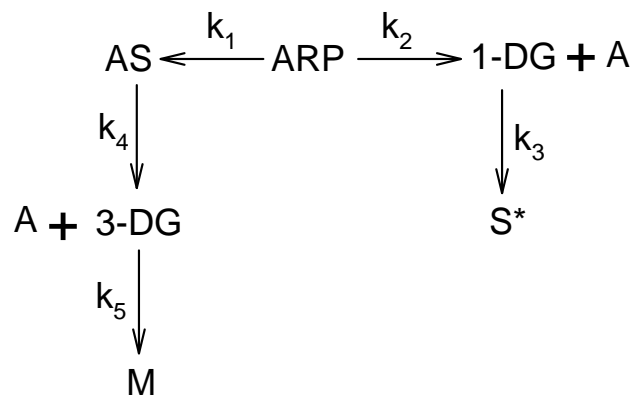


Figure 2.10 Kinetic model for Maillard reactions (Boekel and Martins, 2002).

The extended reaction scheme showed a good fit with experimental data obtained from the glucose-glycine system. Their results also suggested that the 3-DG pathway is the main pathway for the formation of melanoidins. In their later study for the glucose-glycine model system, glucose was found to be involved in reactions to a greater extent. Based on their results, they concluded that this phenomenon is due to (1) glucose isomerisation; and (2) glycine is being regenerated during the second stage of the Maillard reactions (Boekel and Martins, 2002).

The multi-response modelling approach has also been used in many other studies (Bertrand et al., 2015; Chansataporn et al., 2019; Kocadağlı and Gökmen, 2016). There are also some other kinetic models that focus on other products that are produced due to Maillard reactions. For example, the kinetics of flavour compound formation due to Maillard reactions have also been studied by Jousse et al. (2002). The kinetics of the formation of some other components, such as fluorescent products, are still unclear (Matiacevich et al., 2005)

### 2.3.2. Kinetic studies of Maillard reactions applicable to spray drying

Most of the studies mentioned above are based on liquid systems, where the kinetic parameters may be different from those in solid systems or systems with much lower moisture content. The differences in the moisture contents may result in different component mobilities in the systems and, thus different kinetic parameters. The effect of the water activity and component mobilities will be discussed in more detail in subsequent sections.

Some studies have investigated the effect of moisture content and temperature on Maillard reactions under conditions that are applicable to spray drying. A freeze-dried mixture of lactose, trehalose, xylose and lysine in a 45:45:5:5 weight ratio was used in the work of Miao and Roos (2004). Freeze-dried powders were conditioned to different moisture contents by placing them above different saturated salt solutions. Samples were then heated at different temperatures (40°C - 90°C) in sealed containers for different lengths of time. The extent of Maillard reactions in their study was based on measuring the optical density (OD) at 280 nm and 420 nm. In their study, the kinetics of Maillard reactions have been modelled as a zero-order reaction. A zero-order reaction model fitted the browning process in the samples well, but it

does not provide insights into the reaction mechanism for complex reaction schemes, such as the overall Maillard reactions. Additionally, the browning behaviours observed in Maillard reactions do not occur until the advanced stages of the Maillard reactions, which means that the products of the early Maillard reactions were not measured in their study. In a later study, Aalaei et al. (2019) found that, despite different infant formula powders having similar lysine levels (markers for early-stage reactions), the levels of CML (N( $\epsilon$ )-Carboxymethyllysine, a marker for advanced-stage reactions) varied sevenfold, indicating that the advanced stages of Maillard reactions vary considerably between different spray-dried samples. Their results suggested that the kinetics for different stages of Maillard reactions may be different from each other. Therefore, it is necessary to monitor more than one stage of the Maillard reaction scheme in a kinetic study of Maillard reactions. In addition, Ren et al. (2015) confirmed that the early stages of Maillard reactions are the rate-limiting steps in the overall reaction, which further emphasises the importance of monitoring the early Maillard reaction products that occur in spray dryers.

Gómez-Narváez et al. (2019) performed a similar study when they were assessing the usefulness of different markers for Maillard reactions under conditions that are applicable to the spray drying process. In their study, freeze-dried whey powders were conditioned to different water activities ( $a_w$ , 0.11 - 0.71) using four different saturated salt solutions in a similar approach to that of Miao and Roos (2004). Conditioned samples were subsequently heated at 60°C, 75°C, and 90 °C for up to 40 minutes. Then the samples were analysed using different analytical methods. Their results suggested that furosine and bioavailable lysine are sensitive markers for Maillard reactions under spray drying conditions, while HMF is less useful as a marker. Studies have shown that the formation of HMF could also be caused by other reactions other than Maillard reactions. The conversion rate of HMF from the Amadori product is low, and most of the HMF comes from lactose rather than the Maillard reactions (Morales et al., 1997). As a result, HMF could still be used as an indicator of heat-induced damage under more severe conditions. The colour formation was also found to agree with the markers of furosine and bioavailable lysine, although the sensitivity was reduced at lower

temperatures. Both the studies of Miao and Roos (2004) and Gómez-Narváez et al. (2019) showed how Maillard reactions could be affected by the moisture content and temperature at conditions applicable to spray drying.

A recent study by Gómez-Narváez et al. (2022) attempted to model the effect of different spray-drying conditions on the extent of Maillard reactions in spray-dried whey powders. Similar to their previous study (Gómez-Narváez et al., 2019), freeze-dried whey powders (lac:Protein 7:1 w/w) were conditioned to four different water activities ( $a_w$ , ranging from 0.14 - 0.71) using saturated salt solutions. Conditioned samples were subsequently heated at 60°C, 75°C, and 90°C for up to 40 minutes. Thermal degradation markers, including available lysine, furosine, and browning index of the heated samples were measured. The changes in these markers were modelled using first-order kinetic reaction models. The developed reaction kinetics models were then combined with a drying kinetic model to predict the Maillard reactions and protein denaturation occurring during a spray-drying process. The predicted results were compared with experimentally-measured values obtained from spray drying a whey solution using a laboratory-scale spray dryer (Buchi mini spray dryer B-290). Their model successfully predicted the extent of protein denaturation (in terms of loss in lysine bioavailability). However, the prediction for the extent of Maillard reactions in the spray-dried product was less successful. This outcome is likely due to three factors:

1. The drying kinetic modelling approach, namely the characteristic drying curve (CDC) approach. The CDC modelling approach is a lumped-parameter approach, and it treated the particles as a whole (Keey, 1978). As a result, the temperature, moisture, and component ratios gradients across the particles during the spray-drying process have not been included. The effects of these factors and the drying kinetic modelling will be discussed in a subsequent section of this chapter.
2. Another cause of the disagreement between the predicted and experimentally measured values in Gómez-Narváez et al. (2022) is likely to be due to the choice of modelling approaches for the reaction kinetics. As mentioned previously, the Maillard reactions have a complex reaction scheme and involve a series of reactions (Nursten, 2005). Thus,

a more comprehensive approach, such as the multi-response modelling approach used in studies for Maillard reactions in liquid systems (Martins and Boekel, 2005), may be more suitable for establishing a better understanding of the kinetics of Maillard reactions in spray dryers. Kocadağlı and Gökmen (2016) have investigated the kinetics of Maillard reactions in systems with low moisture content systems using heated glucose/wheat flour model systems (1:10 w/w, 7% humidity) at 160, 180 and 200°C for up to 20 min. A multi-response modelling approach was used in their study. Their study has shown that the multi-response modelling approach is applicable to systems with low moisture contents. Although the temperatures used in their studies were much higher than the particle temperatures that might be expected in a spray dryer (Chiou et al., 2008), some of their findings may still be applicable for particles that stick to the walls of spray dryers.

3. The dryer model itself was the simplest possible model for a spray dryer, which assumes that the gas has the same temperature and humidity (for both air and solids) everywhere inside the dryer, and this temperature is the same as the outlet gas temperature. This type of model was described by Langrish (2009) as the coarsest scale modelling, with a well-mixed dryer where the gas and solid temperatures, humidities and moisture contents may be estimated only using mass and energy balances and sorption isotherms. A dryer model is possible for a straightforward personal computer solution that gives more detailed information, called finer-scale modelling. This approach *"treats dryers as having the gas and solids flowing in parallel to each other"* (Langrish, 2009). This more detailed approach has been used in later chapters of this thesis.

Last but not least, in the studies mentioned above, single model systems were used instead of a set of model systems with different ratios between the reactants, and thus the effects of different ratios between reactants at various moisture contents and temperatures were not studied.

### 2.3.3. Studies on Maillard reactions in spray-dried powders during storage

Many other studies have addressed the problem of Maillard reactions in stored spray-dried powders (Hurrell et al., 1983; Nishanthi et al., 2018). Although most of the studies use lower temperatures and longer durations than those that could be expected in a spray dryer (Chiou et al., 2008), their findings about Maillard reactions may still be applicable for Maillard reactions in spray dryers. A study by Hurrell et al. (1983) found that Maillard reactions in milk powder were more rapid when the samples were stored at temperatures above 70°C than those stored at 40°C - 50°C. Their results suggested that the rates of Maillard reactions may increase significantly when the samples are kept above a certain temperature. Similar temperature-dependent behaviour was also reported in other studies (Miao and Roos, 2004). Nishanthi et al. (2018) monitored the physical properties of different types of whey protein powders during storage at temperatures of 4°C, 25°C, and 45°C and relative humidities of 22% and 33% for 90 days. The Maillard reaction was found to be involved in changes to the surface composition and the physical properties of the powders (Huang et al., 2020; Nishanthi et al., 2018).

### 2.4. Factors affecting the kinetics of Maillard reactions in spray dryers

Studies on the kinetics of Maillard reactions in liquid systems have shown that the kinetics of Maillard reactions may be affected by various factors, including but not limited to temperature, pH, and reaction time (Nursten, 2005). Some of the factors may be applicable to the kinetics of Maillard reactions in spray dryers, while others are not so clearly linked. In general, Nunes et al. (2019) have covered general factors that affect Maillard reactions in infant formulae. However, the connection between those factors and connected to the spray-drying process was not discussed, and spray-drying specific factors were not mentioned. Thus, a more detailed review of Maillard reactions in spray dryers is required. A summary of different factors that may change the kinetics of Maillard reactions in spray dryers is shown in Figure 2.11.



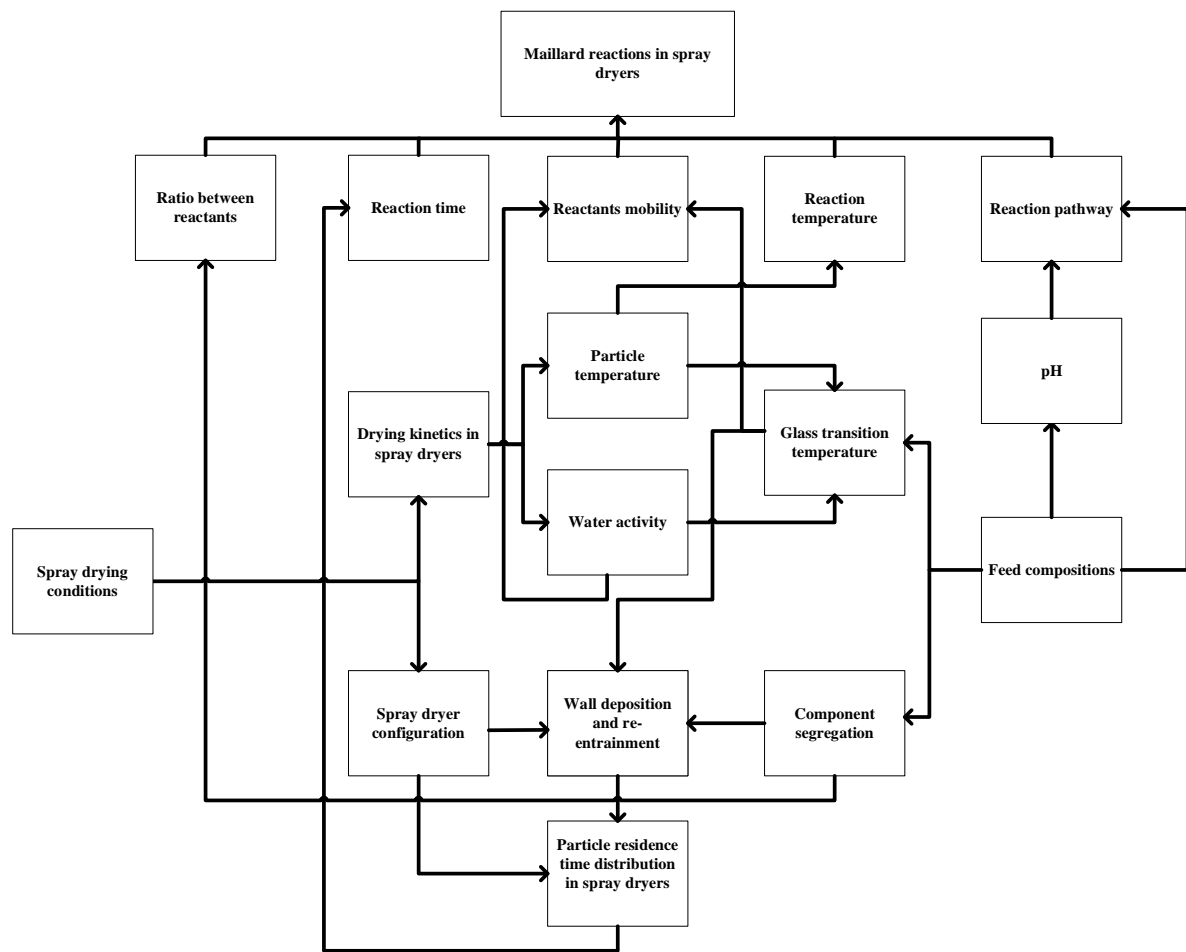


Figure 2.11 Summary of factors and their main effects on Maillard reactions in spray dryers.

#### 2.4.1. Effect of feed composition

Other than the concentration of sugars and amino acids in their reactive forms, other components in the feed may also play an important role in the kinetics of Maillard reactions in spray dryers. The study of Claeys et al. (2003) showed that the fat present in milk promotes the formation of furosine during the thermal processing of milk when the temperature is below 130 °C. Furosine is an acidic degradation product of the Amadori product and is often used as a marker for the early stage of Maillard reactions (Finot et al., 1981). Their results suggested that reducing the fat content in the feed may be an effective way to reduce the extent of Maillard reactions occurring during the spray-drying process. Furthermore, Nijdam and Langrish (2005) showed that the spray drying of skim milk (low fat contents) results in a higher recovery rate of the spray-dried product by comparing the product recovery rate of spray-drying skim and whole milk.

Ascorbic acid (Vitamin C) in the feed may also contribute to Maillard reactions that occur during spray drying. In the study of Zhong et al. (2019), redness generation was observed in the spray-dried ascorbic acid-WPI mixture, possibly due to Maillard reactions. Other literature also reported the involvement of ascorbic acid in Maillard reactions (Nursten, 2005). It is important to investigate the role of ascorbic acid in the kinetic of Maillard reactions in spray dryers, as it is commonly used as an additive in spray-dried products, such as infant formula. Additionally, the redness generation observed in the particles from the study of Zhong et al. (2019) was found to give suitable materials for use as a potential thermal exposure indicator.

The effect of the minerals (i.e., metal ions) on the kinetics of the Maillard reactions is rather complex, as they may inhibit the formation of some products, while the formation of other products is promoted. Akagawa et al. (2002) investigated the influence of metal ions, anions (e.g., phosphate, carbonate), oxygen and some other chelating agents on the early stages of Maillard reactions. Their results suggested that metal ions accelerate the degradation of Amadori products, while chelating agents reversed the effects (Gökmen and Şenyuva, 2007). They also found that the formation of Amadori products is accelerated by phosphate and carbonate ions.

Carrier agents (sometimes described as drying aids), such as maltodextrin, gum arabic, and starches are commonly used in the spray drying processes for sugar-rich materials (Shishir and Chen, 2017). Michalska et al. (2019) studied the effect of freeze-, vacuum- and spray-drying on the polyphenolic contents of blackcurrant juice powders. Greater degradation of anthocyanins and a significantly higher hydroxymethyl-1-furfural (HMF) content was found in powders containing inulin than those containing maltodextrin after vacuum drying at 90°C. This difference in the powders might be due to the fructose in the inulin being involved in the formation of HMF via Maillard reactions or caramelisation at high temperatures (Michalska et al., 2019). This finding regarding inulin is significant and interesting, since common carriers used in spray dryers are basically poly-carbohydrates, which may also contribute to Maillard reactions in spray dryers (Shishir and Chen, 2017). Thus, more investigation about the effect of different carriers on the kinetics of Maillard reactions is required.

#### 2.4.2. Effect of oxygen

Oxygen plays an important role in the Maillard reaction scheme, but it is not essential to the Maillard reactions. The presence of oxygen may promote the formation of the reductones, but it may also oxidise some reactants and reduce the reaction rate (Nursten, 2005). Pokorný et al. (1988) found that the absence of oxygen can limit the reaction rate in their model systems. Their model systems were glucose and L-alanine, and the products were Amadori ones. They reported that, when air was replaced by bubbling nitrogen into the reaction system, the reaction rate was nearly halved. This result is likely to be due to the formation of reactive hexosulose (I) in the presence of oxygen. Oxygen may also play an important role in some systems by promoting lactose degradation (McSweeney and Fox, 2009). The solubility of reactive oxygen in liquids decreases with higher temperatures (unlike the solubility of most solids in liquids), so the impact of oxygen in liquid droplets inside spray dryers may be somewhat limited, because the droplet and particle temperatures increase towards the outlet temperature in spray dryers as shown in Chiou et al. (2008). However, the role of oxygen in dry particles or powders inside spray dryers may be more important, because the access to oxygen does not limit by the solubility of oxygen in the reaction medium. Nunes et al. (2019) reported that, using nitrogen gas as the drying gas has been found to reduce the extent of Maillard reactions in the production of infant formulae. The situation may be further complicated by the possibility that Maillard reaction products may have some antioxidant activity, as pointed out in the review by Lee et al. (2017).

#### 2.4.3. Effect of pH

As mentioned in section 2.2.2, the pH of the system affects the concentration of available (reactive) reactants and the degradation pathway of Amadori products (Boekel, 1998; Yaylayan et al., 1993). The rate of reaction generally increases with the pH. Verardo et al. (2017) reported that the furosine level (a marker for the early stage of Maillard reactions) in a spray-dried pasteurised egg mixture was 55 times higher than that in the ordinary pasteurised egg. The large differences in the furosine levels in their samples may have been due to Maillard reactions that were encouraged by the alkaline and high protein content environment. The effect of the

pH is also dependent on the composition of the systems. For systems with disaccharides, the reaction rate will be more favoured at lower pH as these conditions promote the degradation of the disaccharides to form reducing sugars (Huang et al., 2016; Lea and Hannan, 1949). During the second stage of Maillard reactions, formic acid and other organic acids are formed. The formation of these organic acids may reduce the pH of spray-dried droplets and change the reaction rate or shift the degradation pathway of Amadori products. However, these organic acids are volatile and can be evaporated easily during the spray-drying process, and the impact of the formation of these acids on the kinetics of Maillard reactions in spray drying may not be so significant. Nevertheless, the formation and evaporation of the organic acids may cause changes in the morphology of the spray-dried particles (Huang et al., 2016).

#### 2.4.4. The role of water

Water activity ( $a_w$ ) is another factor that affects the kinetics of Maillard reactions in spray dryers. At high water activity, the dilution effect leads to low reactant concentrations, reducing the rate of the reactions. At a low water activity, low mobility of the molecules also reduces the rate of reactions. The water activity giving the maximum reaction rate for Maillard reactions was found to correspond to a moisture content of approximately 50 wt% (Nursten, 2005). Spray-dried products typically have a moisture content of no more than 3 - 4 wt% to prevent the growth of micro-organisms, to prolong the shelf-lives of the products (Nursten, 2005). In practice, the feeds are usually dewatered before spray drying to 48 - 52 wt% solid content to reduce energy consumption during drying (Pisecký, 1997). The initial moisture content of the feed may have a limited impact on the kinetics of the Maillard reactions in spray dryers, since most of the water evaporates rapidly in a short time, and the particle temperature rises slowly due to the cooling effect of the rapid evaporation.

In addition to affecting the concentration and mobility of the reactants, water may also play an important role in the kinetics of Maillard reactions in spray dryers. During the formation of Amadori products, a water molecule is eliminated. Thus, there are two possible degradation pathways for Amadori products, hydrolysis or direct cleavage (Kocadağlı and Gökmen, 2016). When the water becomes a limiting reactant, the hydrolysis pathway is expected to be limited,

while the dehydration pathway is preferred. As a result, certain reaction pathways, such as direct dehydration of glucose, are expected to be favoured at high temperatures and low moisture contents. This type of situation is applicable to particles near the outlet of spray dryers and particles stuck to the dryer walls (Kocadağlı and Gökmen, 2016).

Water is produced during different stages of the Maillard reactions, and a substantial proportion of water is produced during the second stage of the Maillard reactions (Nursten, 1986). The production of water due to Maillard reactions that may occur inside a spray dryer is likely to have a limited impact on the kinetics of Maillard reactions in spray dryers since the amount of water produced is typically insignificant compared with the amount of water in the droplets and the drying rate of the powders. On the other hand, the production of water during the storage of the spray-dried product may be an important factor, since the products typically have a low moisture content (Pereyra Gonzales et al., 2010). In a study by Ceylan Sahin et al. (2018), different water activities were found in spray-dried samples stored using different packaging materials. Samples with higher water activity were also found to have a greater extent of Maillard reactions. Water production in low water activity products (e.g., spray-dried powders) products may also promote the growth of micro-organisms.

#### 2.4.5. Glass transition temperature ( $T_g$ )

The glass transition temperature is the temperature at which amorphous materials transform from hard glassy to sticky rubbery states (Reid and Levine, 1991; Roos, 2016; Sherrington, 1993). As mentioned in the previous section, the physical state of the reactants has a critical role in the kinetics of Maillard reactions for "dry" systems. Glass transition will affect the physical properties of the material and may increase the amount of wall deposition in spray dryers (Roos, 2009; Straatsma et al., 1999). Other than affecting the stickiness of the particles, glass transition also affects the mobility of the molecules in the spray-dried powders. When the materials are in a glassy state, the molecule mobility is somewhat limited, while in the rubbery state, greater molecular mobility is observed (Roos, 2002; Sherrington, 1993). Different molecular mobilities may affect the reaction kinetics of the Maillard reactions. An increase in the reaction rate of Maillard reactions has been observed when the temperature is above the

glass transition temperature, and the glass transition temperature of the samples ( $T_g$ ) is depressed significantly due to water production via Maillard reactions (Roos, 2002; Sherrington, 1993). Other than water, melanoidin produced in the final Maillard reactions may also contribute to the change in glass transition temperature. Ames et al. (2000) proposed a recipe for producing a standard melanoidin from glucose and glycine to better understand the properties of melanoidins. The glass transition temperature of the standard freeze-dried melanoidin was investigated by Anese et al. (2001) and found to be 56°C. The physical properties of the melanoidins differing dependent on their formation pathways, and the overall glass transition temperature of the particle is expected to be affected by the formation of melanoidins. In the study of Miao and Roos (2004), a critical value of difference between the particle and its glass transition temperature ( $T-T_g$ ) was observed. When the temperature difference was above this critical value, a significant increase in the rate of Maillard reactions was observed for the occurrence of Maillard reactions. A later study by Gómez-Narváez et al. (2019) on whey powders also suggested that lactose in the rubbery-like state promotes Maillard reactions. During the spray drying process, the moisture contents of the particles change rapidly, and thus the glass transition temperatures of the particles also change. The results of Miao and Roos (2004) suggested that the change in the glass transition temperature during the spray drying process is also an important factor that needs to be considered when studying Maillard reactions in spray dryers.

#### 2.4.6. Segregation

Segregation is a process where different components in a mixture separate from each other during processing. Many studies have reported heterogeneous distributions of components in spray-dried products, which has suggested that segregation does occur during the spray-drying process of a multi-component system (Baklouti et al., 1998; Kim et al., 2003). These studies found that, for spray-dried protein-sugar systems, the surface of the particles is generally rich in protein. When fat is present in the systems, the surfaces of the particles are dominated by fats instead of proteins, likely due to the fact that fats are more surface-active than proteins (Kim et al., 2003).

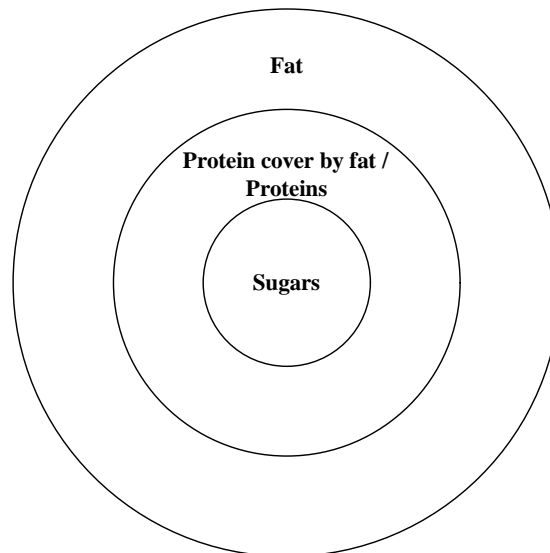


Figure 2.12 Schematic diagram of dominant components in different layers of spray-dried milk particles.

For Maillard reactions in spray dryers, amino acids are most likely to come from proteins, and reducing sugars are found in carbonyl compounds. These two types of compounds have significantly different physical properties, which may cause segregation behaviour inside particles during the spray-drying process, according to the hypotheses identified above (Charlesworth and Marshall, 1960; Fäldt and Bergenståhl, 1994; Meerdink, 1994). For example,  $\alpha$ -Lactalbumin, one of the main components of whey protein isolate (WPI), has a diffusion coefficient of  $0.12 \times 10^{-9} \text{ m}^2/\text{s}$  in water at  $25^\circ\text{C}$  (Saltzman et al., 1994), while lactose has a much higher diffusion coefficient under the same conditions ( $0.566 \times 10^{-9} \text{ m}^2/\text{s}$ ) (Killie et al., 1991). Proteins also have higher surface activities than sugars (Fang et al., 2013). These two components are found in skim milk, in significant quantities, and various studies have reported that segregation occurs during the spray-drying process of milk or similar systems (Fäldt and Bergenståhl, 1994; Kim et al., 2003; Nijdam and Langrish, 2006; Wang et al., 2013).

As a result of component segregation during the spray-drying process, the ratios of each component in various layers of the particles will be different. The different compositions of each layer may change the reaction kinetics. For example, for the outer layers of skim milk particles during the spray-drying process, the concentrations of lactose are likely to be the rate-limiting factor for the initial stages of Maillard reactions, since proteins are the dominant component. However, in the inner layer of the particles, the concentration of protein is likely

to be the rate-limiting factor, since lactose is the dominant component (Fäldt and Bergenståhl, 1994).

The impact of segregation on the overall extent of the Maillard reactions in spray-dried products was not considered in most of the studies investigating Maillard reactions in spray dryers. More investigation is required to understand the segregation process and how this phenomenon may be used to improve the quality of the final product.

#### 2.4.7. Wall deposition and re-entrainment

During the spray drying process, some of the particles may deposit onto the inner walls of spray dryers, and this process is known as wall deposition. The main consequences of wall deposition include the loss of products, the build-up of material within the spray dryer, the effects on the gas flow patterns, the contamination caused by re-entrainment, and extended particle residence times (Keshani et al., 2015). Extended particle residence times mean extended reaction times for the Maillard reaction. Wall deposition can be affected by the configurations of the spray dryers. The geometry of the spray dryer is important, and inappropriate geometries, sizes and shapes of spray dryers may result in an increased amount of deposition (Masters, 1979; Oakley, 1994). The wall material may also play an important role in wall deposition (Huang et al., 2003; Huang and Mujumdar, 2006). Experimental work by Ozmen and Langrish (2003) showed that reducing the amount of swirl in the air flow at the entrance of the spray dryer may also reduce the amount of wall deposition.

Other than the configuration of the spray dryer, material stickiness also affects the wall deposition rate in a spray dryer. The study of Ozmen and Langrish (2003) showed that less deposition is observed when the temperature of the particles is below the sticky-point value. Component segregation will also affect the amount of wall deposition. Migration of components that have higher glass transition temperatures to the surfaces of the droplet will result in a protective layer and will result in less wall deposition (Keshani et al., 2013; Kim et al., 2003; Wang and Langrish, 2009a).



Re-entrainment of wall deposition has been reported in some studies (Francia et al., 2015; Keshani et al., 2013; Kim et al., 2003; Wang and Langrish, 2009a). Re-entrainment of wall deposition is very likely to cause an increase in the particle residence time above the time expected if particles flowed with the gas without interacting with the walls (Hanus and Langrish, 2007a; Kieviet and Kerkhof, 1995; Mazza et al., 2003). The physical processes and phenomena of wall deposition, re-entrainment, agglomeration and residence time distribution are all interlinked, in the sense that the deposition of particles on the walls, and then subsequent re-entrainment, increases the effective residence time of particles, and also causes agglomeration of particles (Francia et al., 2015). In their study, the formation of wall deposition in a swirl spray dryer was found to be a dynamic process. During the spray drying process, deposits on the walls of spray dryers are constantly renewed. They also found that the age of particles in a swirl spray dryer may be extended by the formation of deposits and the re-entrainment process by 10 - 100 times compared with the airborne residence time. Furthermore, they also found that more than 20% of detergent particles collected from a swirl counter-current spray dryer have been re-entrained from the wall deposits. A similar process can be expected in other types of spray dryers.

Longer particle residence times will result in greater extents of Maillard reactions, since Maillard reactions are clearly time-dependent (Hodge, 1953; Boekel, 1998). Therefore, the residence time of particles and how they are affected by wall deposition is another important factor that needs to be considered when studying Maillard reactions in spray dryers.

#### 2.4.8. Particle residence time distribution in spray dryers

The particle residence time in spray dryer is another important factor that needs to be considered when studying Maillard reactions in spray dryers (Schmitz-Schug et al., 2013; Boekel, 1998), and it is linked to the phenomenon of re-entrainment that has just been discussed. The particle residence time consists of particles that travel through two routes, creating a primary particle residence time and a secondary particle residence time. The primary particle residence time is the amount of time for particles to move from the outlet of the nozzle to the outlet of the dryer or wall directly in the air flow. Secondary residence time is the amount of

time that a particle stays on the wall, gets re-entrained and then moves to the outlet of the dryer (Anandharamakrishnan et al., 2010).

Kieviet investigated the particle residence time in a co-current spray dryer using the modelling and experimental methods. In his study, the average primary particle residence time (estimated based on the model developed) was found to be significantly shorter than the gas residence time, possibly due to the initial speed of particles coming out of the nozzle (Kieviet, 1997). A similar result was also obtained in a later study by Anandharamakrishnan et al. (2010). Different particle residence times have been reported in different studies. The reported mean particle residence times range from as short as 58.5 seconds to as long as 12 minutes, depending on the configuration of the spray drying system (Gianfrancesco, 2009; Jeantet et al., 2008; Schmitz-Schug et al., 2013). In the study of Kieviet (1997), some particle residence times can be up to 10 min, despite the relatively short mean particle residence time (less than a minute). Extended mean particle residence times within the spray dryer may give a greater extent of thermal degradation of the product (Kieviet, 1997). In order to understand the kinetics of Maillard reactions in spray dryers, it is necessary to establish a good understanding of the particle residence times within the spray dryer. In previous studies, particle residence times have been measured by introducing tracers (e.g., maltodextrin, sodium chloride, colour dye) and collecting samples during the spray drying process (Gianfrancesco, 2009; Jeantet et al., 2008; Kieviet, 1997; Schmitz-Schug et al., 2013). However, there are significant limitations in the methods used in their studies; The sampling rates were limited by their sampling device. For example, in the study of Francia et al. (2015), samples were collected from the belt located at the outlet of the spray dryer, and the sampling intervals were 15 seconds. This sampling frequency was sufficient for determining the residence time of re-entrained wall deposits, but insufficient for measuring the airborne phase residence time, as this airborne residence time is expected to be less than 35 - 45 seconds (Harvie et al., 2002). Furthermore, some very fine particles exiting from the top of the spray dryer were not measured. Thus, a better sampling technique may be required for future studies and need to be extended to other types of spray dryers and feeds.

In order to have a better experimental determination of the particle residence times, an advanced non-intrusive method is required. Introducing and activating fluorescence material during the spray drying process may be an effective method. Fluorescent tracers can be detected within the spray dryer (inlet, outlet, and in-between) using photomultipliers. This type of non-intrusive method may avoid affecting the gas flow pattern within the spray dryer and, thus the particle residence times. Furthermore, photomultipliers may have a much faster sampling rate, compared with traditional methods. However, there are still some potential issues, such as powder deposits on the sensors, which may affect the accuracy of the results and need to be addressed. Lastly, the hazards related to the fluorescent powder produced during the experiment should also be taken into consideration. Other than introducing fluorescent dye into the feed, using phase doppler anemometry (PDA) or other types of laser detection devices in spray dryers is also an option for estimating the particle residence times. Such approaches were used in the study of Ruprecht and Kohlus (2018) for determining the particle size distributions from different spray dryers.

#### 2.4.9. Drying kinetics in spray dryers

The drying kinetics of the particles in a spray dryer may also affect the kinetics of Maillard reactions in spray dryers. In a spray dryer, the thermal exposure of the powder is the same as the thermal exposure of the particles, so the particle temperature is very relevant to this discussion. The particle temperature has been shown to be very close to that of the outlet gas temperature in most of a co-current spray dryer by Chiou et al. (2008). The only reason why a spray-drying situation might be different (particle temperature close to outlet gas temperature) is that there might be a significant unhindered (constant rate) drying period, when the particle temperature might be closer to the wet-bulb temperature of the air for some part of the overall drying period. However, most foods do not show a significant constant-rate period during drying (Langrish and Kockel, 2001). Hence the gas outlet temperature, if measured, can normally be used as an estimate of the particle, powder and material temperatures during spray drying, which are the reaction temperatures for the Maillard reactions.

Furthermore, the outlet gas temperature alone is not sufficient for describing the impact of different spray drying conditions on the kinetics of the Maillard reactions in the spray dryer. In a later study by Park et al. (2016), the feed flow rate was changed during the experiments to maintain the same outlet gas temperature, where different feed solid contents and inlet gas temperatures were used for the experiments. In this paper, higher furosine levels were found as the inlet temperature and the solids concentration increased. The increase in the inlet temperature should result in more thermal exposure for the particles, giving a greater extent of Maillard reactions, hence increasing the furosine levels. The increase in the solids concentration is also likely to lead to a greater extent of Maillard reactions (greater furosine levels) due to changes in the atomisation behaviour, as follows. Higher solids concentrations tend to give larger droplets, and larger droplets take longer to dry out and are wetter for longer, so the liquid-phase reaction times are longer for larger droplets. Therefore, larger droplets (from higher solids concentrations) are also likely to show more Maillard reaction products, such as furosine, as observed in this paper. In the study of Zbicinski et al. (2002), the drying kinetics of maltodextrin and Bakers' yeast were investigated in situ during spray drying. In their results, different atomisation ratios were found to give different drying kinetics. Therefore, it is also necessary to consider the drying kinetics of particles in spray dryers when investigating the Maillard reactions in this equipment.

For modelling the drying kinetics of particles in spray dryers, there are two main types of modelling approaches: lumped-parameter models and distributed-parameter models. In lumped-parameter models, the droplet and particle are assumed to be homogeneous, and the temperatures and concentrations in different layers of the particles are assumed to be the same. Examples of this approach are the concept of a characteristic drying curve (CDC) and the reaction engineering approach (REA) (Chen and Lin, 2005; Keey, 1978; Tran et al., 2017).

#### *2.4.9.1. Characteristic drying curve (CDC) models*

The concept of a characteristic drying curve (CDC) model assumes that the shape of the drying curve is the same for a specific material, regardless of the drying conditions (Keey, 1978). The drying rate is estimated based on the maximum drying rate (drying rate during the

first stage of drying where the drying rate is not affected by the presence of solids) and moisture content (Keey, 1978):

$$f = \frac{N}{N_{max}} = fn(\Phi) \quad 2.1$$

$$\Phi = \frac{X - X_e}{X_{cr} - X_e} \quad 2.2$$

Where  $f$  is the normalised drying rate,  $N$  is the drying rate,  $X$  is the moisture content, and  $\Phi$  is the dimensionless moisture content. The subscripts  $cr$  and  $e$  refer to the critical point and the equilibrium moisture content, respectively. The shape of the drying curve is the shape of the curve where  $f$  is plotted as a function of  $\Phi$ .

Langrish and Kockel (2001) assessed different experimental data for the spray drying of both whole milk and skim milk and concluded that a linear function was a good approximation to the shape of the characteristic drying curve.

$$f = \Phi \quad 2.3$$

Other than linear characteristics curve, non-linear characteristics curve has also used for modelling the drying kinetics (Tran et al., 2017):

$$f = 1 \quad X > X_{cr} \quad 2.4$$

$$f = \phi^{a*\phi+b} \quad X < X_{cr} \quad 2.5$$

Where  $a$  and  $b$  are constants based on the gas velocity and gas temperature.

Good agreement was obtained by Tran et al. (2017) between the predictions of the CFD model and the experimental data obtained via spray drying skim milk (30 wt%) with an inlet gas temperature of 150°C and different feed flow rates.

The CDC modelling approach was also used with CFD to predict the thermal degradation that occurs during spray-drying processes. Jaskulski et al. (2017) have developed a CFD model for predicting whey protein denaturation during the spray-drying process. In their study, the drying kinetics model was modelled using the CDC approach. Their results showed good agreement with the experimental data obtained using an inlet gas temperature of 150°C and different feed flowrates ranging from 130 - 216 mL/min.

#### 2.4.9.2. Reaction engineering approach (REA)

Other than the well-known CDC approach, a reaction engineering approach (REA) has been developed based on experimental data. In REA models, the drying rate is based on the difference in vapour concentrations between the surface of the particles and the bulk gas (Chen and Lin, 2005).

$$N = -h_m * (\rho_{v_{sat}} * \exp\left(-\frac{\Delta E_v}{RT}\right) - \rho_{v_b}) \quad 2.6$$

Where  $N$  is the specific drying rate (kg/m<sup>2</sup>/s),  $\rho_{v_{sat}}$  and  $\rho_{v_b}$  are the vapour concentration at the interface and bulk vapour concentration, respectively,  $R$  is the ideal gas constant, and  $T$  is the temperature. The parameter  $\Delta E_v$  is the activation energy required for drying, which measures the difficulty of the drying process.

#### 2.4.9.3. Common features of lumped-parameter models

Both CDC and REA models can provide a good approximation to the drying process. REA models trends to be a better approximation under some conditions, but the difference between them is not very significant (<5%) (Chen and Lin, 2005). There are also other different lumped-parameter approaches, such as the short-cut approach proposed by Thijssen and Coumans (1985). They will not be discussed in detail here, as they share similar advantages and disadvantages.

Although the lumped-parameter approach (CDC) has been found by Jaskulski et al. (2017) to be suitable for predicting the temperatures and moisture contents that affect certain types of reactions (protein denaturation) during the spray-drying process, it may be less suitable for the predicting Maillard reactions in the spray-drying process. In the later study by Gómez-Narváez et al. (2022), the CDC approach was also used for predicting thermal degradation during the spray-drying process of a whey solution. They successfully predicted the extent of protein denaturation while being less successful with predicting the extent of Maillard reactions in the spray-dried product. The main difference between protein denaturation and Maillard reactions is that more than one component is involved in Maillard reactions, while protein denaturation involves a more limited range of components (Nursten, 2005). When there is more than one

component involved in the reaction, the impact of segregation during the spray drying process may become more significant. Due to the lumped-parameter nature of their approach, the impact of segregation was not considered.

#### 2.4.9.4. *Distributed-parameter models*

In contrast to lumped-parameter models, distributed-parameter models do not assume that the temperatures and moisture contents inside the particles are homogenous. Individual droplets are divided into different sublayers in a typical distributed-parameter model. The heat and mass balance for each sublayer is calculated individually, thus allowing the different temperatures and concentration profiles in each individual layer to be predicted. Such an approach has been used to predict the component segregation process that occurs during the spray-drying process of multi-component droplets (Gac and Gradoń, 2013; Wang et al., 2013). However, such an approach has not been applied to predict reactions that occur during spray drying. In theory, distributed parameters modelling approach may be more suitable for modelling multi-component reactions, including Maillard reactions, that occur in spray dryers compared with lumped-parameter models. Despite the clear theoretical advantage of distributed-parameter models over the lumped-parameter models, the difference in estimating the overall extent of the reactions in the spray-dried product may be small. Last but not least, distributed-parameter models are also more computationally expensive to solve.

#### 2.4.10. Artificial neural networks (ANN) models

In light of recent computer science developments, artificial neural networks (ANN) have also been used as an alternative method for modelling the spray-drying process (Keshani et al., 2012). Compared with conventional models (i.e., models developed based on physical principles), ANN models do not rely on the understanding of the process, which makes ANN models good for predicting the outputs of a complex system based on the inputs. Some of the studies in the past have shown the value of utilising ANN models for predicting the behaviour of the drying process and the properties of the product. In the study of Keshani et al. (2012), an ANN model was used to predict the amount of wall deposition for lactose-rich systems. Their ANN model was found to be able to provide a good prediction for wall deposition within

the range of conditions used for training their ANN model. In the study of Cheggini et al. (2008), an ANN model was used to predict the drying process and the physical properties of the spray-dried orange juice. The ANN model they trained also gave good agreement with the experimental results ( $R^2 = 0.93$ ).

However, the advantage of ANN models is also their biggest drawback. ANN models have been developed based on a black-box relationship between the input variables and the output variables, which means the mechanisms behind the processes remain unclear. ANN models that are trained based on data collected from specific instruments are also limited to those specific instruments. As a result, ANN models are ideal for optimising the spray drying process for a specific material in a particular spray dryer within a certain range of operating conditions. However, ANN models are less suitable for extending the results obtained from one system to another. In addition, ANN models also require a large number of samples to avoid overfitting, which can be time-consuming and costly.

## 2.5. Conclusions

In this review, many factors that may affect the mechanism of Maillard reactions in spray dryers have been reviewed. The mechanisms of Maillard reactions in spray dryers may be different from those in liquid systems due to the rapid changes in temperature and moisture content in the equipment. Although the mechanisms of Maillard reactions in liquid systems have been studied extensively, only limited studies have addressed this reaction in the context of the liquid to solid transformation (Gómez-Narváez et al., 2019; Grigioni et al., 2007; Miao and Roos, 2004; Park et al., 2016). Most of the research about Maillard reactions for powders is focused on how the operating conditions or the storage conditions affect the extent of Maillard reactions in spray-dried products, but the mechanism of Maillard reactions occurring in spray dryers has not been investigated. Nevertheless, different spray dryers were used in those studies, and they all have different characteristics which may affect their results. However, the impact of the characteristics of the spray dryers was not considered in those studies. Therefore, establishing a better understanding of the mechanisms of Maillard reactions in spray



dryers by including the characteristics of the spray dryers is a worthwhile direction for this research.

## Chapter 3. Methods and materials

In this chapter, the materials and methods used in this thesis were discussed in detail.

This chapter contains published materials from the following publications:

### **Journal article:**

**Zhou, Z.**, Langrish, T.A.G., 2021. A review of Maillard reactions in spray dryers. *J. Food Eng.* 305, 110615. <https://doi.org/10.1016/j.jfoodeng.2021.110615>

**Zhou, Z.**, Langrish, T.A.G., 2021. Color *formation* and Maillard reactions during the spray drying process of skim milk and model systems. *J. Food Process Eng.* <https://doi.org/10.1111/jfpe.13936>

**Zhou, Z.**, Langrish, T.A.G., Cai, S., 2022. Using particle residence time distributions as an experimental approach for evaluating the performance of different designs for a pilot-scale spray dryer. *Processes* 11, 40. <https://doi.org/10.3390/pr11010040>

### **Conference proceeding:**

I am the first and the corresponding author for the published materials above. I designed the study, analysed the data, and wrote the majority of the draft with the guidance of the supervisor of this thesis, Professor Timothy Langrish. Professor Langrish has assisted with the design of the experiment, data acquisition, and manuscript editing.

Permission for including published materials in this section has been granted by the supervisor of this thesis, Prof. Timothy Langrish.

---

| <b>Symbols</b> |                                      |
|----------------|--------------------------------------|
| $*$            | Convolution                          |
| $\cdot$        | Point-wise operation                 |
| $C$            | Chroma                               |
| $C(t)/dt$      | Dye injection rate                   |
| $D$            | Diameter                             |
| $E$            | E index                              |
| $E(t)$         | Signal                               |
| $F$            | Fourier transform                    |
| $n$            | Number of equivalent reactors        |
| $X$            | Moisture content                     |
| $\tau$         | Overall mean particle residence time |

---

### 3.1. Materials

A list of all materials used in this thesis is shown in Table 3.1. Unless stated otherwise, all materials used in this thesis were Laboratory grade or better. The materials are listed in alphabetical order.

Table 3.1 Materials used in this thesis.

| <b>Materials</b>     | <b>Formula</b>                                  | <b>Purity</b>               | <b>Supplier</b>             |
|----------------------|---|-----------------------------|-----------------------------|
| Fresh skim milk      | N/A   | Food grade,<br>99% fat-free | Coles, Australia            |
| Galicia acetate acid | CH <sub>3</sub> COOH                            | Laboratory reagent          | Sigma-Aldrich,<br>Australia |
| Lactose              | C <sub>12</sub> H <sub>22</sub> O <sub>11</sub> | Analytical reagent          | Sigma-Aldrich,<br>Australia |
| Potassium acetate    | CH <sub>3</sub> CO <sub>2</sub> K               | Analytical reagent          | Sigma-Aldrich,<br>Australia |
| Red food dye         | N/A   | Food grade                  | Queens, Australia           |
| Skim milk powders    | N/A   | Food grade,<br>99% fat-free | Coles, Australia            |
| Whey protein isolate | N/A   | Food grade, fat-free        | Iso-natural, Australia      |

### 3.2. Spray dryers

The work in this thesis is mainly based on the spray drying of milk and milk-like model systems. Two different scales of spray dryers were used in this thesis, laboratory-scale and pilot-scale.

#### 3.2.1. Laboratory-scale spray dryer

The Buchi mini spray dryer B-290 (Switzerland) is a well-developed, widely-used laboratory-scale spray dryer (Gómez-Narváez et al., 2022; Nijdam and Langrish, 2005; Schmitz-Schug et al., 2013; Zhong et al., 2019). In this thesis, it was used for preliminary investigations and the development and validation of analytical methods. A Buchi two-fluid atomiser was used for atomising the feed ( $D_{nozzle} = 0.7$  mm,  $D_{nozzlecap} = 1.5$  mm, Buchi, Switzerland). Feed solutions are delivered to the atomiser via the peristaltic pump on the spray dryer. A schematic diagram of the Buchi mini spray dryer B-290 is shown in Figure 3.1.

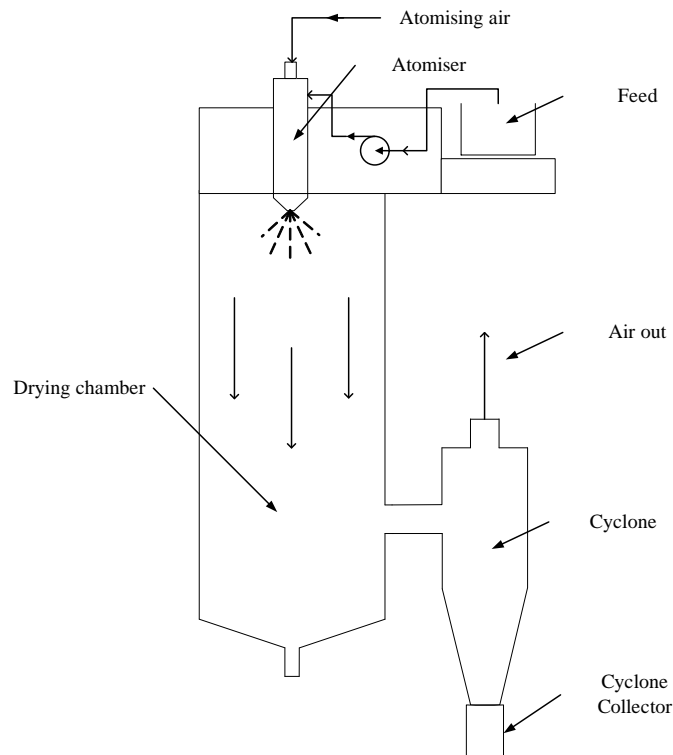


Figure 3.1 Schematic diagram of Buchi mini spray dryer B-290.

### 3.2.2. Pilot-scale spray dryer

To address the aim of investigating the impact of different designs and scales of the spray dryers, a pilot-scale spray dryer with different drying chamber designs was used in this thesis. The first two designs of this pilot-scale spray dryer were built based on the findings of Huang et al. (Huang et al., 2018). Briefly, the first two designs of the pilot-scale spray dryer consist of two main drying columns connected via a 4-inch or 6-inch cylindrical connection. Most parts of the spray dryer are constructed with 1.6 mm thick 304 stainless steel (SS-304). The surface of the spray dryer is covered with 25 mm mineral wool to reduce heat loss to the surroundings and avoid burns. Drying gas is provided by three F24 centrifugal fans (Aerotech Fans Pty Ltd., Australia) in a push-and-pull configuration, providing a gas flow rate of up to 315 m<sup>3</sup>/hr, depending on the configuration. The same two-fluid atomiser used in Buchi mini spray dryer B-290 is used for atomising the feed. Detailed dimensions of the pilot-scale spray dryer are shown in Figures 3.2 – 3.3. For the sake of brevity, the design with a 4-inch cylindrical connection will be referred to as "Design 1" or "4-inch connection design" for short in later sections of this thesis. The same applies to the design with a 6-inch cylindrical connection, and it will be referred to as "Design 2" or the "6-inch connection design".

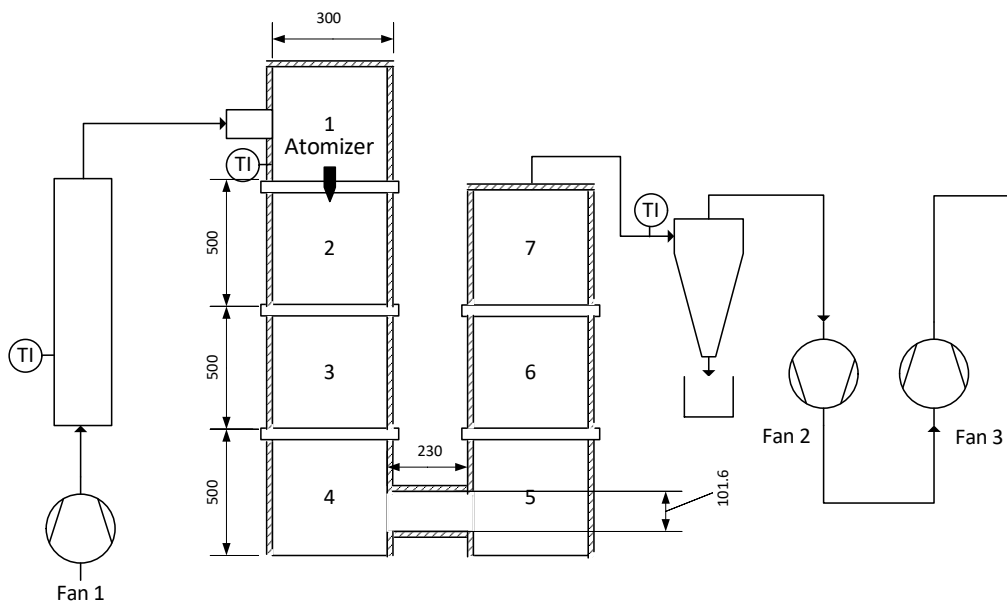


Figure 3.2 Spray dryer with 4-inch cylindrical connection (Design 1).



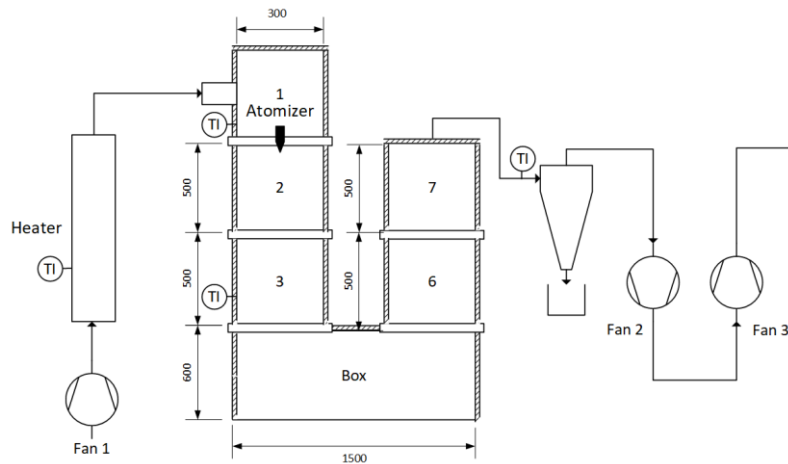


Figure 3.4 Spray dryer with cylindrical drying chambers and box connection (Design 3).

Preliminary investigations have shown that a significant amount of the wall deposition occurs in the first two drying chambers of the spray dryer except for the bottom of the dry columns (Langrish et al., 2020). This phenomenon is likely caused by the direct contact between the spray and the inner wall of the spray dryer. Thus, in the fourth design, the first two drying chambers have been redesigned in a conical shape to better fit the conical spray pattern produced by the two-fluid atomiser. The expansion angle of the conical section has been chosen to be  $8.5^\circ$ , which is intended to avoid flow separation due to the expansion while keeping the footprint of the spray dryer within reasonable limits. The box connection between the two drying columns has also been redesigned accordingly. A schematic diagram and detailed dimensions of the fourth design are shown in Figure 3.5. The fourth design of the pilot-scale spray dryer will be referred to as "Design 4", "Conical drying chambers with box connection", or "Conical drying chambers" for brevity.

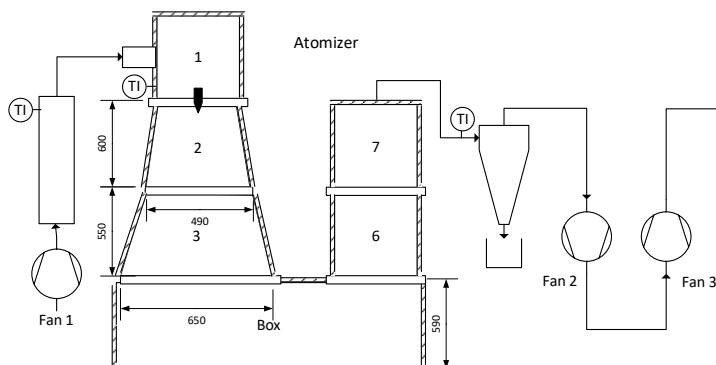


Figure 3.5 Spray dryer with conical drying chamber and box connection (Design 4).



### 3.3. Spray drying

#### 3.3.1. Effect of different operating conditions and feed compositions on the kinetics of Maillard reactions in spray dryers

The following approach was used to investigate the effect of different operating conditions and feed composition on the kinetics of Maillard reactions. Three types of feed solutions were used, reconstituted skim milk or milk-like model systems and fresh skim milk. Feed solutions using skim milk powders or the lactose-WPI model system were prepared by dissolving solids in distilled water at room temperature (20°C) to make up a feed solution. Skim milk powders, whey protein isolate (WPI), and lactose are stored in sealed containers before use under recommended storage conditions. The solid content of the reconstituted solution is 8.8 wt% which is the same as the solids content in skim milk. For experiments that used fresh skim milk as the feed, fresh skim milk was stored in a fridge at 4°C for no longer than three days and brought back to room temperature (20°C) prior to spray drying. All related experiments were carried out using the pilot-scale spray dryer (Design 3) (Figure 3.4). The spray drying conditions consisted of an inlet gas flow rate up to 257 m<sup>3</sup>/hr and an atomising air flow rate of 10 mL/min at a compressed air pressure of 220 kPa. Different inlet gas temperatures ranging from 130°C to 190°C were used to investigate the effect of the temperatures on the kinetic of Maillard reactions in spray dryers. Detailed spray-drying conditions are summarised in Table 3.2. The spray-dried milk powder was collected from the circular collector located at the bottom of the cyclone (approximately 80% of the total solids in the feed). Spray-dried samples have a mean particle size ranging from 9 to 12 µm and have a moisture content of 1.5 ± 0.6% by weight. Collected samples were placed in a sealed bag and stored at -20°C to avoid moisture absorption and to minimise the extent of Maillard reactions during storage. Each experimental condition was repeated three times.

Table 3.2 Operating conditions for investigating the effect of operating conditions and feed compositions.

| Feed                                  | Inlet gas temperature (°C) | Feed flow rate (mL/min) | Outlet gas temperature (°C) |
|---------------------------------------|----------------------------|-------------------------|-----------------------------|
| Skim milk powder<br>/ Fresh skim milk | 130                        | 27                      | 101                         |
|                                       | 150                        | 27                      | 114                         |
|                                       | 170                        | 27                      | 130                         |
|                                       | 180                        | 27                      | 136                         |
|                                       | 190                        | 27                      | 145                         |
| WPI: Lactose<br>1:2 / 2:1             | 150                        | 27                      | 116                         |
|                                       | 170                        | 27                      | 130                         |
|                                       | 180                        | 27                      | 138                         |
|                                       | 190                        | 27                      | 146                         |

In addition to the pilot-scale spray dryer, a laboratory-scale spray dryer (Buchi mini spray dryer B-290) was also used in the spray drying experiment of real food systems. The spray drying conditions are the same as those for the pilot scale spray dryer, but with a lower inlet gas flow rate of 35 m<sup>3</sup>/hr and an atomising air flow rate of 10 mL/min at 200 kPa. Spray-dried samples were collected and stored in the same manner as those samples collected from the pilot-scale spray dryers.

### 3.3.2. Effect of different designs and sizes of the spray dryer on particle residence time distribution

To compare the impact of different designs on the extent of Maillard reactions in the final products, fresh skim milk and salt solution with the same concentration (8.8 wt%) was spray-dried using four different designs of the pilot-scale dryer in a similar manner. Due to the limitation of the operating temperature of the photomultiplier used for sampling the response signals produced, an inlet gas temperature of 100°C was used instead of the temperature listed above. The feed flow rates have also been halved to prevent blockages in the sampling window. In addition to the difference in inlet gas temperatures and feed flow rates, and different drying gas flow rates (ranging from 257 – 315 m<sup>3</sup>/hr) were used to investigate the impact of different drying gas flow rates on the particle residence time distribution within the dryer. Other spray-drying conditions remained unchanged.

### 3.4. Particle residence time distribution measurement

As discussed in Chapter 2, the particle residence time distribution (RTD) is an important factor that mainly affects the reaction time and drying kinetics. Particle residence time is affected by the design and size of spray dryers (Francia et al., 2015; Keshani et al., 2015; Schmitz-Schug et al., 2013; Boekel, 1998). Particle residence time measurements are powerful tools that can provide an experimental overview of the performance of the spray dryer design under different operating conditions (Jeantet et al., 2008). An experimentally measured particle residence time reflects the combined effect of the chamber design and physical properties of the materials being spray-dried under different operating conditions. Due to the importance of the particle residence time, measuring the particle residence time and investigating the effect of designs and size of the spray dryer is desirable.

#### 3.4.1. Particle residence time distribution

The RTD measurement systems can be divided into input, processes, and response. Inputs to the systems are normally introduced as either pulse or step changes, and then the responses of the processes are measured. In general, the RTD measurement process can be represented by equation 3.1.

$$E_{response}(t) = E_{input}(t) * RTD \quad 3.1$$

Where  $E_{response}(t)$  is the response signal,  $E_{input}(t)$  is the input signal, and  $RTD$  is the function of the particle residences time distribution. \* in this equation represents the convolution product.

The particle residence time distribution function can be extracted from the deconvolution result of the response signal and input signal. The convolution and deconvolution processes were carried out using the convolution theorem (equation 3.2):

$$\mathcal{F}(g * h) = \mathcal{F}(g) \cdot \mathcal{F}(h) \quad 3.2$$

Where  $\mathcal{F}$  represents a Fourier transform, \* represents the convolution product, and  $\cdot$  is point-wise multiplication. From equations 3.1 - 3.2, can have the following equations:

$$\mathcal{F}(E_{response}(t)) = \mathcal{F}(E_{input}(t)) \cdot \mathcal{F}(RTD) \quad 3.3$$

$$\mathcal{F}(RTD) = \mathcal{F}(E_{response}(t)) ./ \mathcal{F}(E_{input}(t)) \quad 3.4$$

$$RTD = \mathcal{F}^{-1}(\mathcal{F}(E_{response}(t)) ./ \mathcal{F}(E_{input}(t))) \quad 3.5$$

In this thesis, all Fourier transform and inverse Fourier transform operations were performed using the Fast Fourier Transform (FFT) algorithm in MATLAB.

When the input is introduced as pluses, the *RTD* function can be calculated as follows:

$$RTD = \frac{E_{response}(t)}{\int_0^{\infty} C(t) dt} \quad 3.6$$

Here,  $C(t) dt$  is the rate of tracer injection.

### 3.4.1. Spray drying conditions used for particle residence time distribution measurement

For particle residence time distribution measurement, both the lab-scale spray dryer and pilot-scale spray dryer were used. An inlet gas temperature of 100°C was used for all particle residence time measurement experiments due to the limitations on the operating condition of the photomultiplier. All experiments were repeated at least three times. Operating conditions for measuring particle residence time distribution in the lab-scale spray dryer are summarised in Table 3.3.

Table 3.3 Operating conditions for measuring RTD in Buchi mini spray dryer B-290.

| Parameters                         | Values |
|------------------------------------|--------|
| Inlet gas temperatures (°C)        | 100    |
| Feed flow rate (mL/min)            | 3      |
| Gas flow rate (m <sup>3</sup> /hr) | 38     |
| Atomising air flow rate (mL/min)   | 10     |
| Atomising air pressure (bar)       | 2.2    |

For measuring the particle residence time distributions in different designs of the pilot-scale spray dryer, different drying gas flow rates and all four designs of the spray dryer were used. The feed flow rate also halved compared with the flow rate used to investigate the effect of the operating conditions on Maillard reactions. By halving the feed flow rate, the chance of particles depositing onto the sampling window is reduced, thus causing less interference with the measured signals. Detailed operating conditions are summarised in Table 3.4.

Table 3.4 Operating conditions for measuring RTD in different designs of the spray dryer.

| <b>Parameters</b>                  | <b>Values</b> |
|------------------------------------|---------------|
| Inlet gas temperatures (°C)        | 100           |
| Feed flow rate (mL/min)            | 13.5          |
| Gas flow rate (m <sup>3</sup> /hr) | 99 - 315      |
| Atomising air flow rate (mL/min)   | 10            |
| Atomising air pressure (bar)       | 2.2           |

### 3.4.2. Particle residence time measurement devices for laboratory-scale spray dryer

In Ruprecht and Kohlus (2018), the particle concentrations and diameters are measured using scattered laser from the particles. This type of measurement can be considered a non-intrusive method that will not disturb the gas flow within the spray dryer. A similar laser scattered measurement device has been developed and built in this thesis.

The particle residence time measurement device was tested on the Buchi mini spray dryer B-290 before the measuring system was implemented onto the pilot scale spray dryer. In the first version of the RTD measurement device, the input into the system was introduced as step changes in feed compositions. In this thesis, two types of feed were used, fresh skim milk and red dye solutions. The step changes in the feed composition were introduced by changing the position of the three-way valve periodically during the spray drying process. By changing the position of the three-way valve, feed into the system was switched between the red dye solution and fresh skim milk. A schematic diagram of the particle residence time distribution (RTD) measurement device is shown in Figure 3.6.

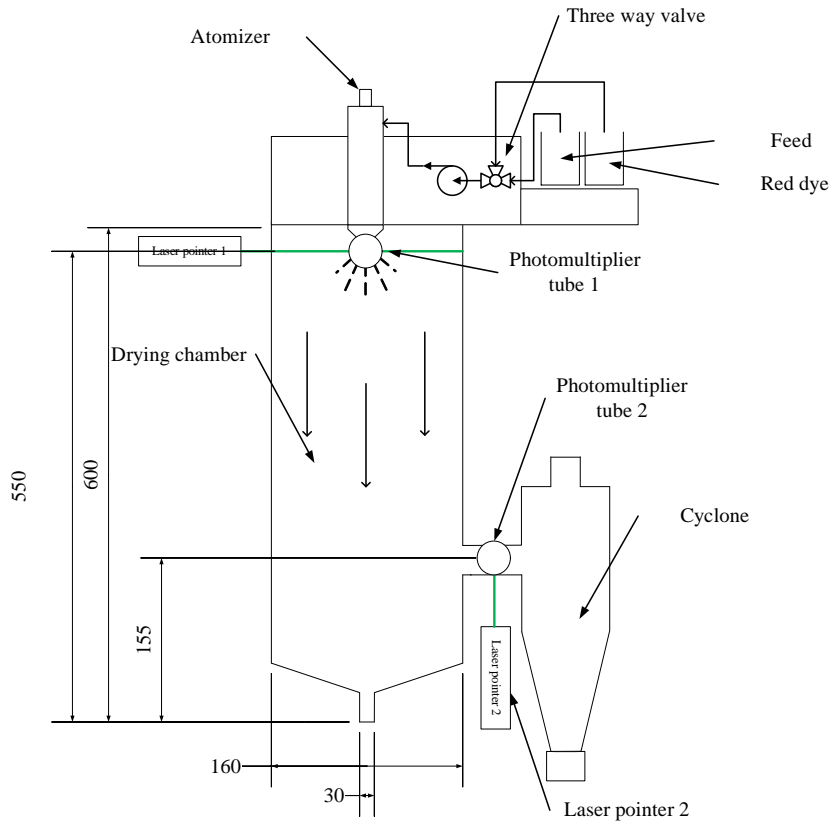


Figure 3.6 Particle residence time measurement device for Buchi mini spray dryer B-290 version 1 (not to scale).

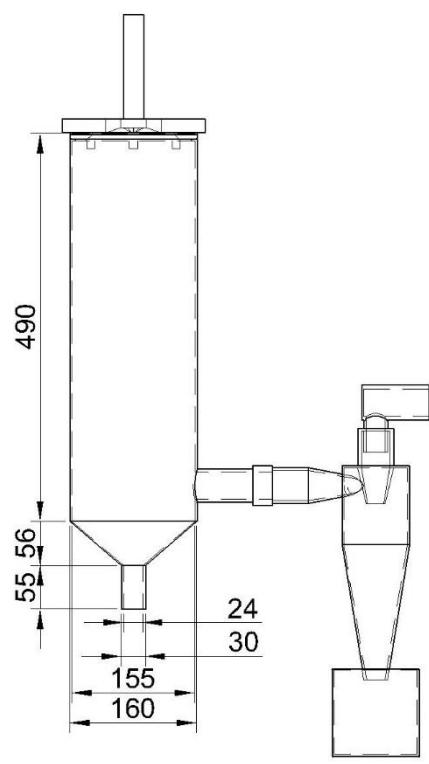


Figure 3.7 Detailed dimensions of the Buchi mini spray dryer B-290.

For measuring the input signal ( $E_{input}(t)$ ) and the response signal ( $E_{response}(t)$ ) of the system, two sets of laser pointers and photomultipliers were used. When particles pass through the sampling window, the laser from the laser pointer is scattered by the particles. Particles with different dye concentrations scattered the light differently (Figure 3.8). The difference in the intensity of the scattered light was measured using the photomultiplier perpendicular to the laser pointer (Figure 3.9). The changes in light intensity are regarded as the actual input/response signal of the system.

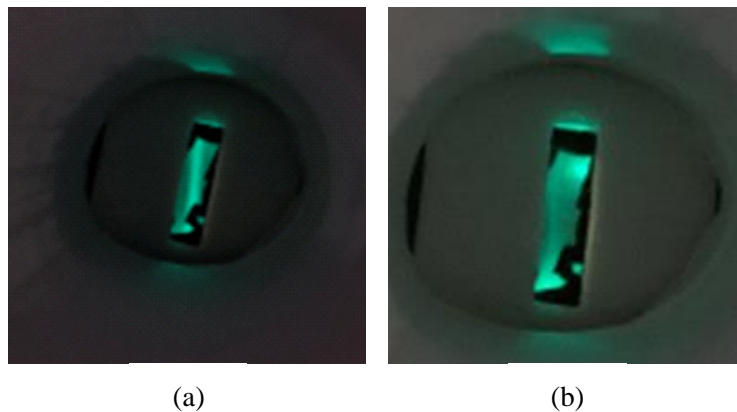


Figure 3.8 Light scattered by particles (a) particles without dye (b) particles with dye.

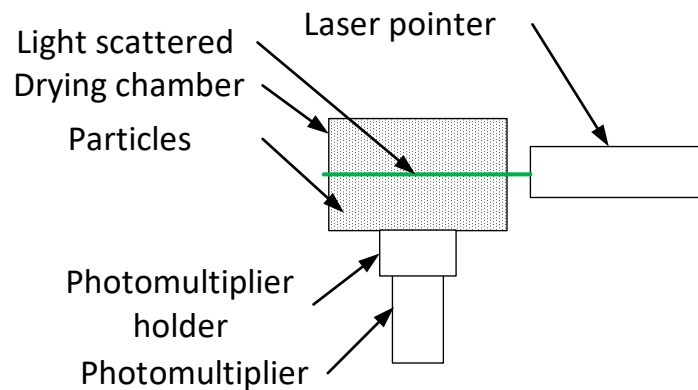


Figure 3.9 Enlarged view of the signal measurement device.

For better stability of the measurement devices, 3D printed holders for the photomultipliers were also developed and built as part of the method development process (Figure 3.10).

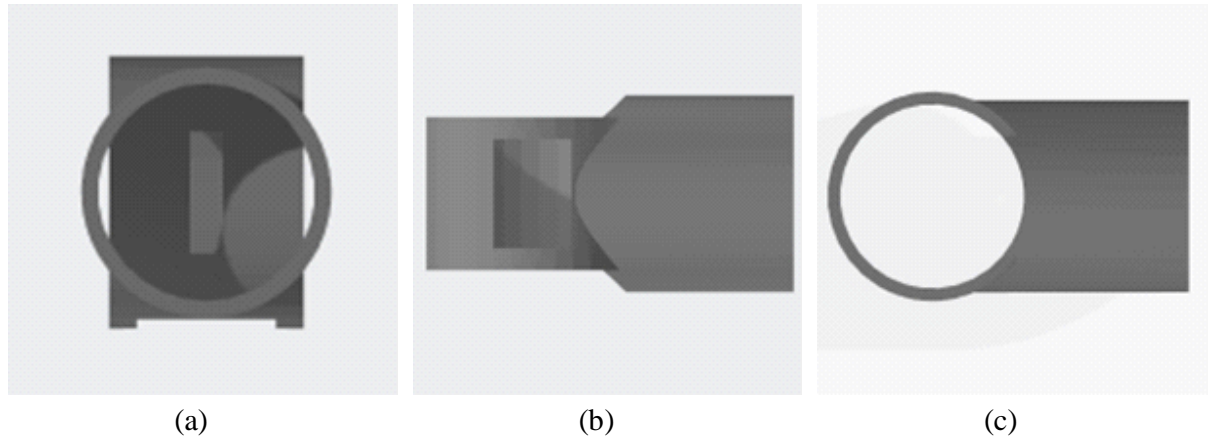


Figure 3.10 3D printed holder for photomultipliers use with the lab-scale spray dryer. (a) photomultiplier end (sampling window) (b) laser pointer end (c) pass-through for drying chamber.

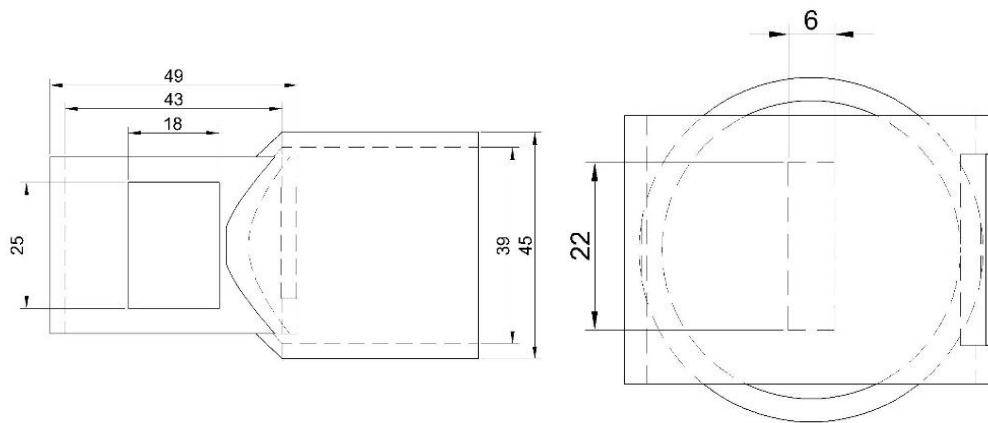


Figure 3.11 Detailed dimensions of the 3D printed holder for photomultipliers use with the lab-scale spray dryer. Left: bottom view Right: right-side view.

In the first version of the RTD measurement devices, the tubing connections between the three-way valve and the atomiser led to the mixing of two different feeds, which affected the accuracy of the measurements. In order to reduce interference from dead time lags and mixing due to the tubing lengths, modifications were made in the second version of the RTD measurement system. The three-way valve was moved next to the inlet of the atomiser, and the dye was injected as pulses. During the experiments, the three valves were only opened before injection, and 2 mL of dye solution was manually injected into the system via a syringe. A schematic diagram of the RTD measurement device version 2 is shown in Figure 3.12.



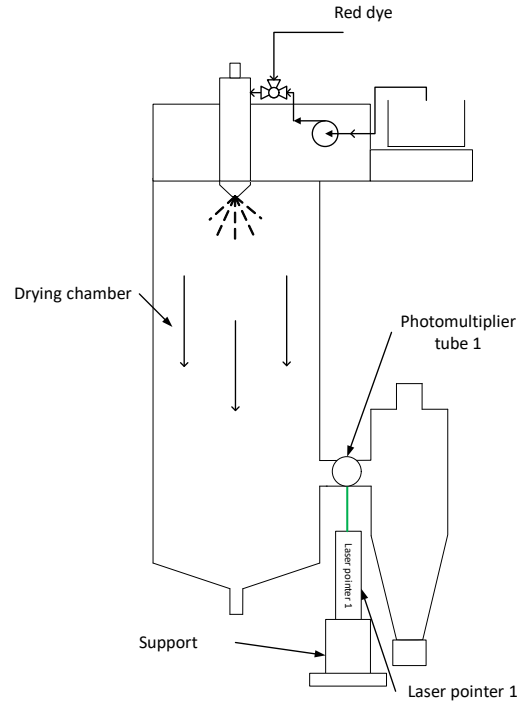


Figure 3.12 Particle residence time measurement device for Buchi mini spray dryer B-290 version 2.

### 3.4.3. Particle residence time measurement device for pilot-scale spray dryer

After successfully measuring RTD in the laboratory-scale spray dryer, the particle residence time measurement device was modified for the pilot-scale spray dryer. A schematic diagram of the RTD measurement device on a pilot-scale spray dryer is shown in Figure 3.13.

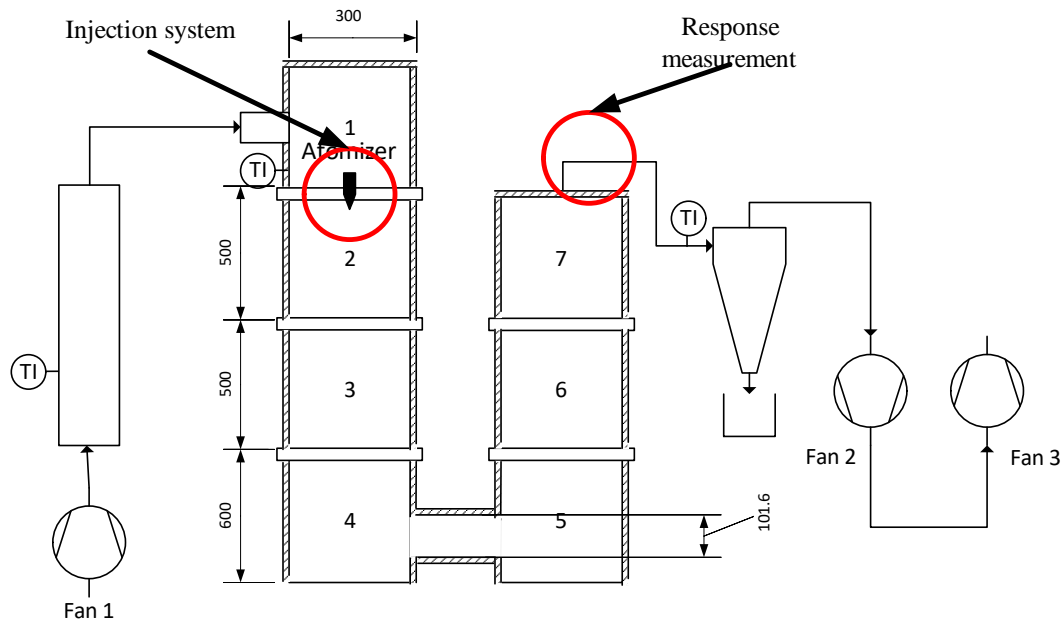


Figure 3.13 Schematic diagram of RTD measurement device on pilot-scale spray dryer (Design 1).

Similar to the RTD measurement devices for the laboratory-scale spray dryer, the RTD measurement device for the pilot-scale spray dryer also consisted of two parts, a dye injection system and a response measurement device. Dye solutions were injected into the system as pluses, and the responses of the system to dye injections were measured at the outlet of the drying chamber prior to the cyclone collector.

#### 3.4.3.1. Manual dye injection

At the early stage of the experimental design, manual injections were used to investigate the effect of different amounts of dye injection, signal-to-noise ratio (SNR) and feasibility of the method. For manual injection, dye solutions were injected using  $D = 2$  mm tubing, which is connected to a syringe containing the dye solution. A valve is located between the syringe and the inlet of the atomiser to prevent the back-flow of the dye or the feed. During the experiments, the valve was opened before injections and closed after injections. Dye solutions were injected into the system via a syringe every 180 s. All manual injection experiments were carried out using Design 3 at a gas flow rate of  $257 \text{ m}^3/\text{hr}$ . A schematic diagram of the manual injection system can be found in Figure 3.14.

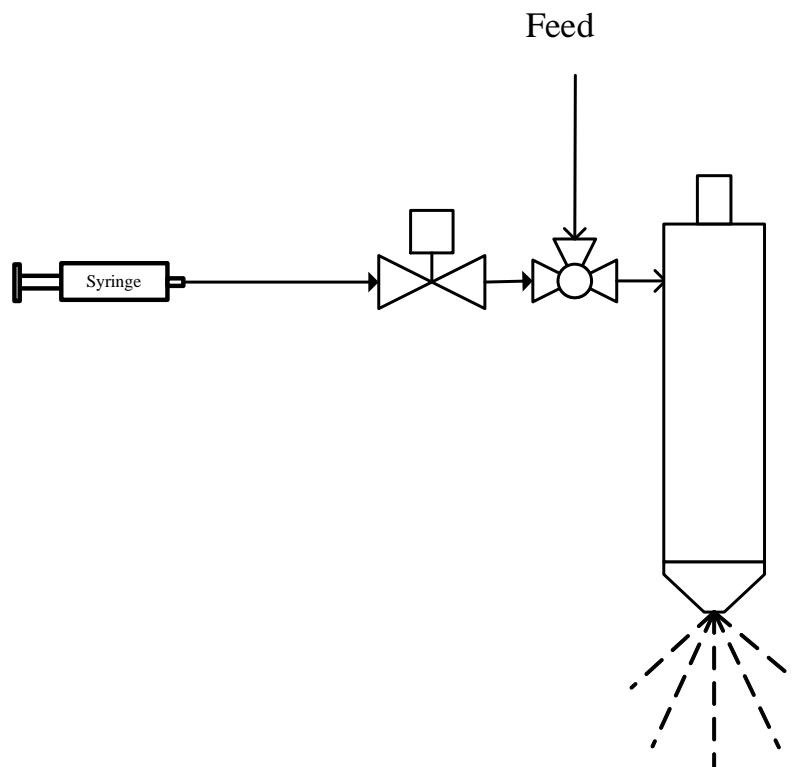


Figure 3.14 Schematic diagram of manual dye injection system for pilot-scale spray dryer.

### 3.4.3.2. Automated dye injection

After validating the method with manual dye injections, an automated dye injection system has been developed and built. The automated dye injection is designed to eliminate interference due to human factors (i.e., human reaction time and inconsistency between injections). In addition to eliminating the human factor, a shorter tubing could be used to further reduce the lag time due to the tubing. The automated dye injection consisted of a pump for delivering dye, a diaphragm valve to prevent backflow, and a single-board computer (Raspberry Pi 4) to control the pump and valve (Figure 3.15). The pump and valve were controlled in an On-Off control configuration via a relay module. The single-board computer controlled the relay module by sending high or low voltage signals through general-purpose input/output (GPIO) ports. The automated dye injection system automatically injected 2 mL of dye into the system within 0.5 seconds every 180 seconds during experiments. The Python code for dye injection control is shown in the appendix (Section A.1).

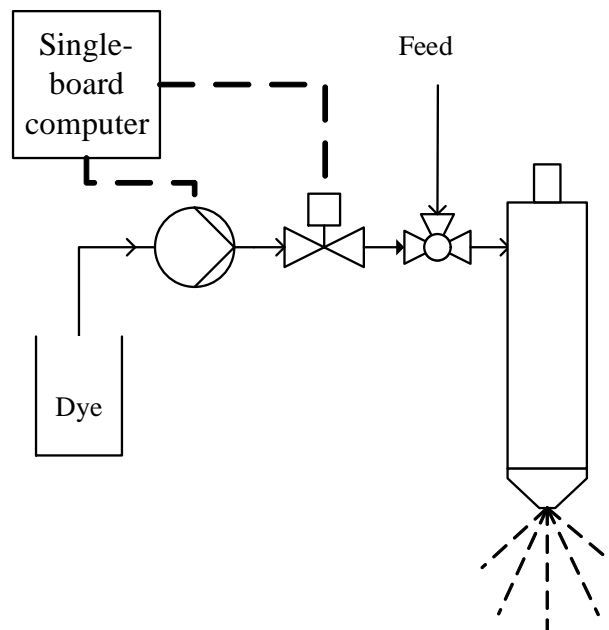


Figure 3.15 Schematic diagram of the automated dye injection system.

To measure the response of the system, a set of photomultipliers and laser pointers were used between the outlet of the drying chamber and the cyclone collector (Figure 3.16).

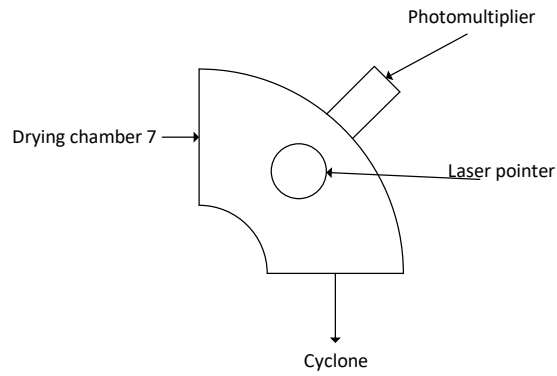


Figure 3.16 Schematic diagram of particle residence measurement device for pilot-scale spray dryer.

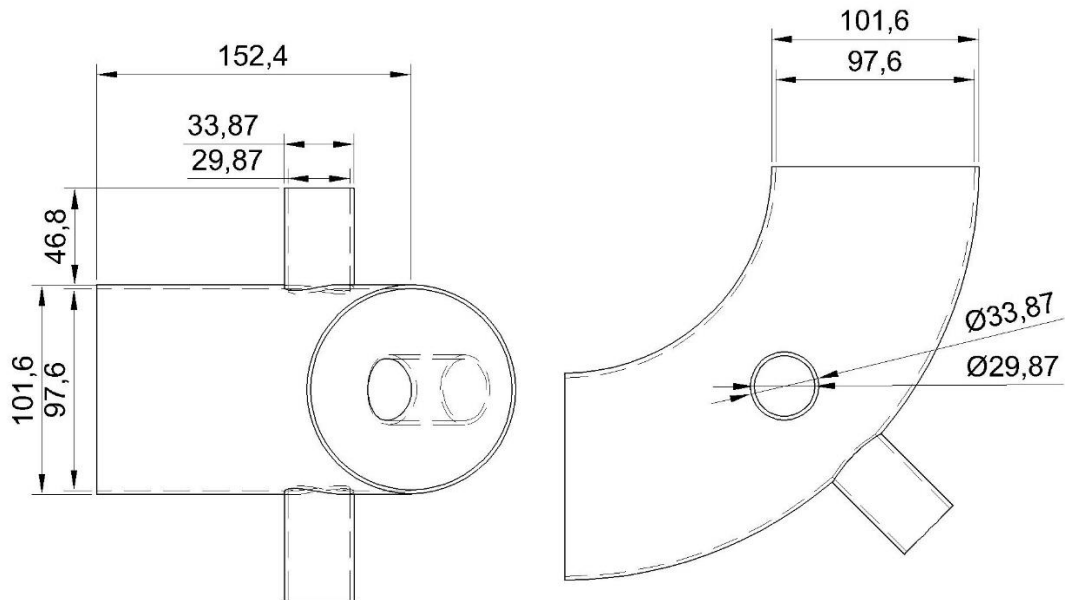


Figure 3.17 Detailed dimensions of the 90° long radius elbow ( $R = 1.5D$ ). Left: front view Right: top view. Flanges on the elbow are not shown.

A 3D printed holder for the photomultiplier was designed and built for better stability of the measurement devices (Figure 3.18).

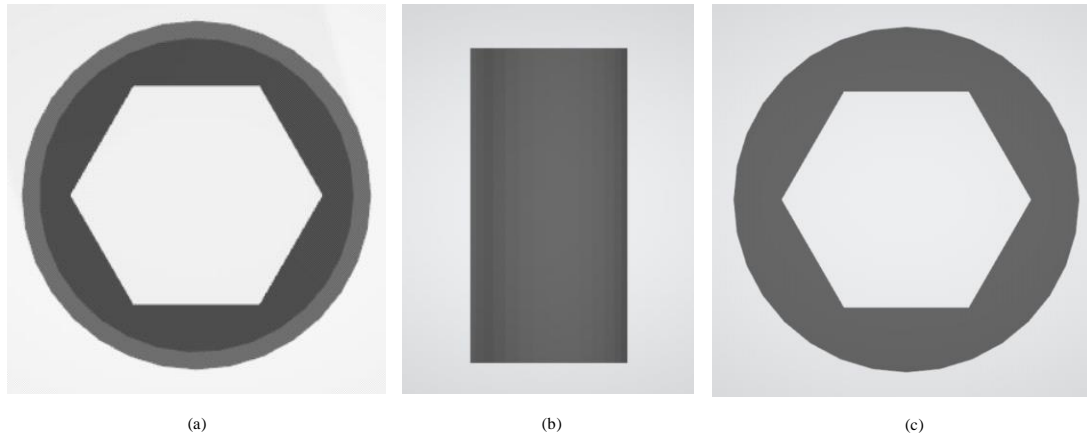


Figure 3.18 3D printed holder for photomultipliers used with the pilot-scale spray dryer. (a) Top view of the holder; (b) side view of the holder; (c) bottom view of the holder.

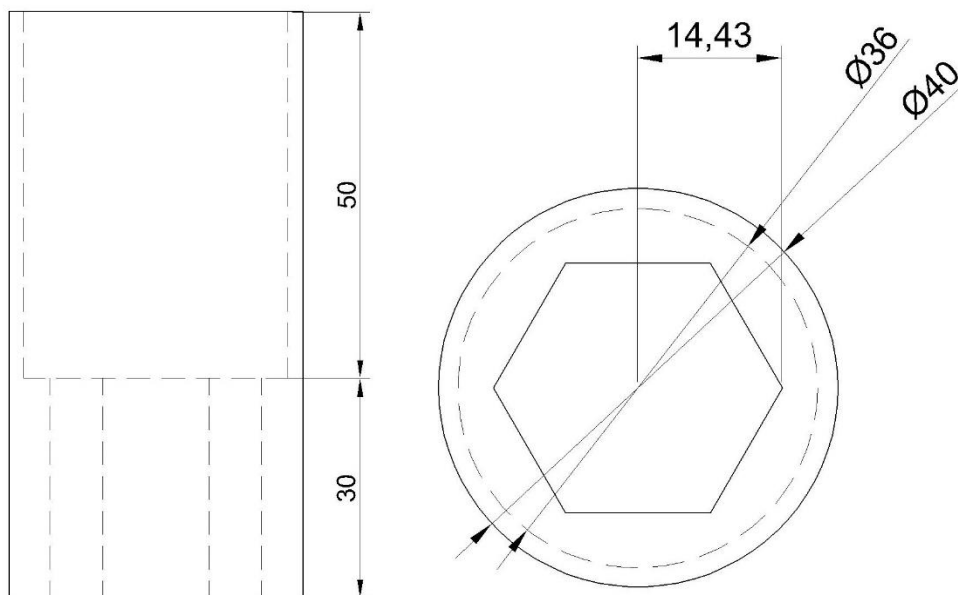


Figure 3.19 Detailed dimensions of the 3D printed holder for photomultiplier use with the pilot-scale spray dryer. Left: side view of the fitting for measuring the particle residence time Right: top view of the fitting for measuring the particle residence time.

It is difficult to compare two different RTD curves directly. To quantitatively analyse the measured RTD curves, all measured signals were normalised and fitted with a continuous-stirred-tank-reactor tank-in-series (CSTR-TIS) model (equation 3.7). The model parameters were fitted using MATLAB based on the least-squares method. MATLAB code for model fitting is shown in the appendix (Section A.3).

$$RTD(t) = \frac{n}{(n-1)!} * \exp\left(-n * \frac{t}{\tau}\right) * \left(\frac{n * t}{\tau}\right)^{n-1} \quad 3.7$$

Where  $\tau$  is the overall mean particle residence time, and  $n$  is the number of equivalent reactors in series (Ruprecht and Kohlus, 2018).

There are two parameters in the CSTR-TIS model, the overall mean particle residence time ( $\tau$ ) and the number of equivalent reactors in series ( $n$ ). The overall mean particle residence time represents the average time that particles stay in the spray dryer. The number of equivalent reactors ( $n$ ) describes the spread of the residence time distribution, and the larger the value of  $n$ , the tighter the spread of the RTD (i.e., it becomes closer to a plug-flow reactor).

#### 3.4.4. Analysis of the fluctuations in the signal

Normalised signals were transformed from the time domain to the frequency domain via Fourier transform to analyse the frequency of fluctuations observed in the measured signals. The last 60 seconds of each measured signal were analysed to reduce the interference from the main peak. Fourier transformations of the signals were performed using the Fast Fourier Transform (FFT) algorithm available in MATLAB. The MATLAB code for signal processing is shown in the appendix (Section A.4).

### 3.5. Product quality assessments

#### 3.5.1. Colour measurement

As discussed in Chapter 2, colour formation in the spray-dried powder is one of the key characteristics of Maillard reactions during the spray-drying process. Colour analysis of the final products was carried out using a standard lighting box with four lamps (cold white) using the method described in Zhong et al. (2019).

The colour analysis procedure consisted of the following steps: turning on the lamps in the standard lighting box, filling a square polystyrene container (10 mm\*10 mm\*5 mm) with the sample, and placing the container at the centre of the standard lighting box (Figure 3.20); fixing a camera on a clamp 50 mm above of the sample; setting a 10s timer for the camera and closing

the front cover of the lighting box; removing the front cover of the standard lighting box and transferring the photo from the camera to the computer for further analysis by MATLAB.

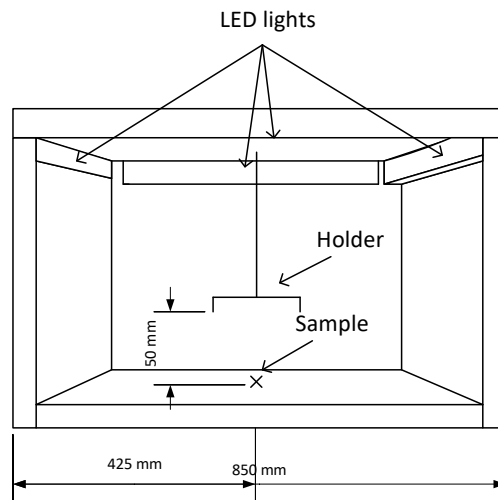


Figure 3.20 Schematic diagram of standard lighting box.

In addition, a standard colour correction card (X-rite, USA) was used to ensure the accuracy of the colour measurements (Figure 3.21).



Figure 3.21 Standard colour correction card used in this thesis.

The colour of the sample was described using the averaged L, a\*, b\* values of the central region (50\*50 pixel) of the collected photos based on the CIELAB colour space. L, a\*, b\* values represent the lightness (0 - 100 from black to white), red and green components (-100 - 100 from red to green) and yellow and blue components (-100 – 100 from yellow to blue), respectively. From the L, a\*, b\* values, the E indices ( $E = \sqrt{L^2 + a^{*2} + b^{*2}}$ ) and the Chroma values  $C = \sqrt{a^{*2} + b^{*2}}$  were also assessed. The overall E index (E) has been used to describe the colour of the sample in other studies for liquid milk and infant formulas. The differences in the E indices may be used to represent differences between the colours of the powders (Bosch et al., 2007; Morales and Boekel, 1998). The Chroma value (C) is another parameter used for describing the colour of the samples. The Chroma value is only dependent on the colour component (a\* and b\*) of the samples and is not affected by the lightness (L). The Chroma value is used to describe the intensity of the colour, and changes in either the positive or the negative directions of the a\* and b\* values will change the Chroma value (Rhim et al., 1988). All colour analysis mentioned above were performed in MATLAB, and the MATLAB codes used for analysis has been provided in the appendix (Section A.2.)

### 3.5.2. Fluorescence of Advanced Maillard products and Soluble Tryptophan (FAST)

The FAST method proposed by Birlouez-Aragon (1998) was used to determine the extent of Maillard reactions based on the fluorescence of tryptophan and advanced Maillard reaction products in the soluble fraction of milk at a pH of 4.6. Spray-dried samples were reconstituted with distilled water to 8.8 wt%, which was the original solids content in the fresh milk; reconstituted samples were mixed with a pH 4.6 buffer solution (acetate buffer, 0.1 M) at a 1:5 ratio and centrifuged at 3620 g for 30 min to separate the insoluble fraction. The supernatant was further diluted ten times with distilled water. The fluorometric measurement of the diluted samples was carried out by using a Horiba FluoroMax-4 spectrometer (Kyoto, Japan). The excitation and emission wavelengths were set to 290/340 nm and 350/440 nm to detect tryptophan and advanced Maillard reaction products, respectively. The extent of the Maillard reactions was expressed as the ratio between the fluorescence of advanced Maillard reaction products and tryptophan (AMP/Trp ratio).



### 3.5.3. Particle size distribution

The particle size distribution may be affected by the operating conditions of the dryer and the atomiser and the design of the spray dryer. Thus, the particle size distribution was determined for samples collected from different operating conditions. The particle size distribution was measured using a Malvern Mastersizer 3000 (Malvern Instruments, UK) a universal feeding funnel and a 100% feed flow rate at 2.2 bar.

### 3.5.4. Scanning electron microscopy (SEM)

The particle morphology was observed using Scanning Electron Microscopy (SEM). Samples were fixed on the sample stem via carbon tape. Then the sample was coated with gold using a Quorum-SC7620 Mini Sputter Coater (Quorum Technologies, UK). Images of the coated samples were observed at 1000X, 3000X and 5000X magnification with a Phenom-Prox SEM (Phenom-World, Netherlands).

### 3.5.5. Moisture content measurement

The moisture content of the samples was measured using the loss-on-drying method described in Ozmen and Langrish (2002). In summary, approximately 1g of the collected samples were placed on a Petri dish and placed in a drying oven at 85°C for a period of 23 hours. The moisture content of the samples was calculated based on the change in mass.

## 3.6. Heating model systems under isothermal conditions

In order to predict the Maillard reactions in spray dryers along with the segregation process, the combined effect of moisture content, component ratio, and temperature on the reaction kinetics of Maillard reactions needs to be investigated. Model systems with different moisture contents and lactose-to-WPI ratios were prepared. Three different ratios between lactose and WPI were used: 1:1, 1:2 and 2:1 to represent the heterogeneous distribution of different components across the particle in different layers of the particles due to the segregation process. Three different moisture contents were used:  $X = 1$  kg/kg,  $X = 5$  kg/kg, and  $X = 10$  kg/kg, since most of the segregation process occurs within this range of moisture content (Putranto et al., 2017). Despite droplet drying being a liquid-solid system and the kinetics of Maillard reactions

in liquid systems having been studied extensively, there are no data available in the literature that are suitable for the needs of this thesis. Samples prepared were subsequently heated isothermally at between 60°C, 80°C, and 100°C for up to 35 minutes in a sealed glass bottle in a fan-forced oven. After heating, the samples were cooled using an ice-water mixture to reduce the extent of subsequent reactions.

### 3.7. Conclusions

This thesis has involved five different spray dryers, four different configurations of a pilot-scale spray dryer and one laboratory-scale spray dryer, for spray-drying experiments. The effects of feed compositions and operating conditions on Maillard reactions in spray dryers were investigated. The effects of feed compositions were investigated by spray drying different feeds, including real food systems (fresh skim milk and reconstituted skim milk) and model systems with different compositions. The effects of different inlet gas temperatures and dimensions of the spray dryers were also investigated using one of the configurations of the pilot-scale spray dryer and the laboratory-scale spray dryer. The extent of Maillard reactions in samples collected from the spray-drying experiments was evaluated using fluorometric and colourimetric methods. The physical properties of the collected samples were examined using a particle size analyser for the particle size distribution, scanning electron microscopy (SEM) for particle morphology, and a loss-on-drying method for the moisture contents.

For particle residence time distribution (RTD) measurements, a laser-based non-intrusive measuring system was developed in this thesis. RTD of spray dryers with different designs and dimensions were measured using the developed system for comparing the performance of different spray dryers. Additionally, the measurement results for the laboratory-scale spray dryer were also compared with reported values in similar studies for validation.

Finally, isothermal heating experiments of samples with different moisture contents and compositions were also carried out as part of developing simulation models for Maillard reactions kinetics in spray dryers.

## Chapter 4. Maillard reactions with different inlet gas temperatures and feed compositions

This chapter mainly focuses on how operating conditions and feed composition affect the kinetics of the Maillard reactions in spray dryers.

This chapter is developed based on a published journal article: "*Colour formation and Maillard reactions during the spray drying process of skim milk and model systems*" that was published in the Journal of Food Engineering. I am the first and the corresponding author for this journal article. I designed the study, analysed the data, and wrote the majority of the draft with the guidance of the supervisor of this thesis, Professor Timothy Langrish. Professor Langrish has assisted with the design of the experiment, data acquisition and editing of the manuscript.

Permission for including published materials in this section has been granted by the supervisor of this thesis, Prof. Timothy Langrish.

---

| <b>Symbols</b> |         |
|----------------|---------|
| <i>C</i>       | Chroma  |
| <i>E</i>       | E index |

---

#### 4.1. Introduction

Spray drying is a common method used for drying liquid feedstocks. Other than the requirements for low final moisture content and other physical properties of dried products, the flavour, the nutritional values, and the appearance of the dried milk are also important, so the loss of volatile components and heat-induced degradation (e.g., Maillard reactions) should be minimised during the spray-drying process. It is, therefore, important to understand how the spray-drying process affects the properties of the final products. Maillard reactions may cause changes in the physical properties of the product (e.g., colour, rheological properties), loss of nutritional values and produce mutagenic or even potentially carcinogenic products (Brands et al., 2000; Friedman, 1996; Lucey, 2002). Thus, it is important to investigate the Maillard reactions that occur during spray-drying processes.

Due to the complex nature of the spray-drying process, Maillard reactions that occur during the spray-drying process have been less well-studied compared with those in liquid systems (Jaskulski et al., 2017; Schmitz-Schug et al., 2016; Wijlhuizen et al., 1979). As mentioned in Chapter 2, Maillard reactions in spray dryers may be affected by many factors, including temperatures, moisture contents, water activities, compositions of the foods and the characteristics of the spray dryer. Maillard reactions consist of three different stages. During the early stage of the Maillard reactions, reducing sugars bond to amino acids via Schiff bonds and produce protein-bonded Amadori products. During the advanced stage, Amadori products transform into advanced Maillard reaction products via different pathways depending on the conditions (Morales and Boekel, 1998). In the final stage of the Maillard reaction, high molecular weight nitrogenous brown pigments (melanoidins) are formed. The formation of melanoidins is the main cause for the browning of the final product. Therefore, it is also important to understand how the colour formation of the milk powder is related to the extent of Maillard reactions.

This chapter mainly focused on how different operating conditions, including inlet gas temperatures and feed compositions, may affect Maillard reactions in the spray-dried product, including the use of model systems.

#### 4.2. Fluorometric measurement results – Fresh skim milk & reconstituted skim milk

The amounts of advanced Maillard reaction products have been measured using the FAST method proposed by Birlouez-Aragon et al. (1998), and the changes have been expressed as percentage changes compared with the feed. A detailed description of the FAST method and spray drying conditions has been provided in Chapter 3. Two different feeds, fresh skim milk and reconstituted skim milk (8.8 wt%), were spray dried using inlet gas temperatures ranging from 130°C to 190°C.

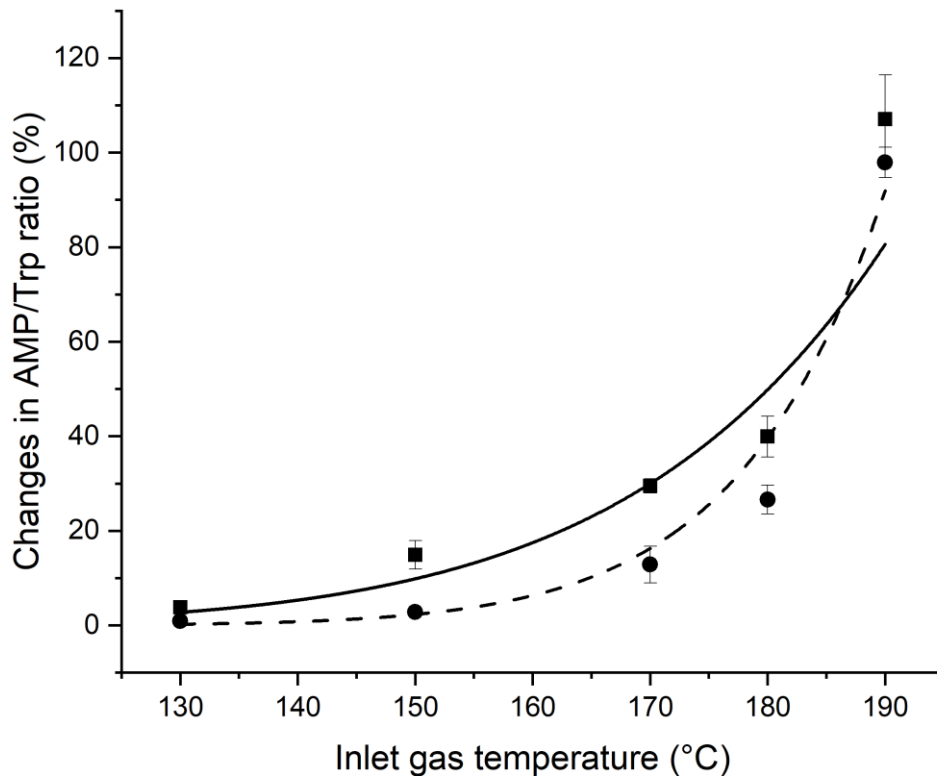


Figure 4.1 The changes in AMP/Trp ratios as functions of inlet gas temperature for real food systems. ■: reconstituted skim milk ●: fresh skim milk —: fitted curve for reconstituted skim milk ( $Y=4.35*10^{-19}X^{8.8}$ ,  $R^2=0.92$ ) --: fitted curve for fresh skim milk ( $Y=2.89*10^{-34}X^{15}$ ,  $R^2=0.96$ ).

As shown in Figure 4.1, the extent of Maillard reactions in spray-dried samples collected from the pilot-scale spray dryer increased, even at the lowest inlet gas temperature (130°C). This result confirmed that Maillard reactions do occur during the spray-drying process of skim milk at all inlet gas temperatures used in this thesis. Under the same spray drying condition,

the powder obtained from reconstituted skim milk always gave a greater extent of Maillard reactions. The difference in the results was probably caused by the reconstituted samples having more early/advanced Maillard reactions products in the feed, due to having already been spray dried. The work of Nijdam and Langrish (2005) has also shown that reconstituted skim milk behaves similarly to fresh skim milk in many respects, apart from the fact that it has already been spray dried.

There was a significant increment in the extent of Maillard reactions when the inlet gas temperature increased from 180°C to 190°C for both reconstituted and fresh skim milk ( $P < 0.01$ ). Compared with inlet gas temperature, the particle temperature history is more critical for investigating the kinetic of Maillard reactions that occur during spray drying. Spray drying processes can be classified into two stages: the un-hindered drying stage and hindered drying stage. During the un-hindered drying stage, "free" water on the surface of the particles evaporates rapidly; thus, the particle temperature increases slowly due to the cooling effect of evaporation. As the drying process for a particle enters the hindered stage, the drying rate decreases, and the temperature of the particle rises rapidly (Wijlhuizen et al., 1979). Heat-included degradation and loss of the volatile product are more likely to occur during this stage (Birchal and Passos, 2005). Many studies, for example, Langrish and Kockel (2001) have shown that some materials, such as milk, may not have a long unhindered drying stage, and the particle temperature will approach the outlet gas temperature during the long hindered drying period. The particle and gas temperature history are estimated using parallel-flow design equations described in Langrish (2009). The equations used are provided in Chapter 6. The predicted particle and gas temperature is plotted against the distance from the atomiser for an inlet gas temperature of 130 °C shown in Figure 4.2.

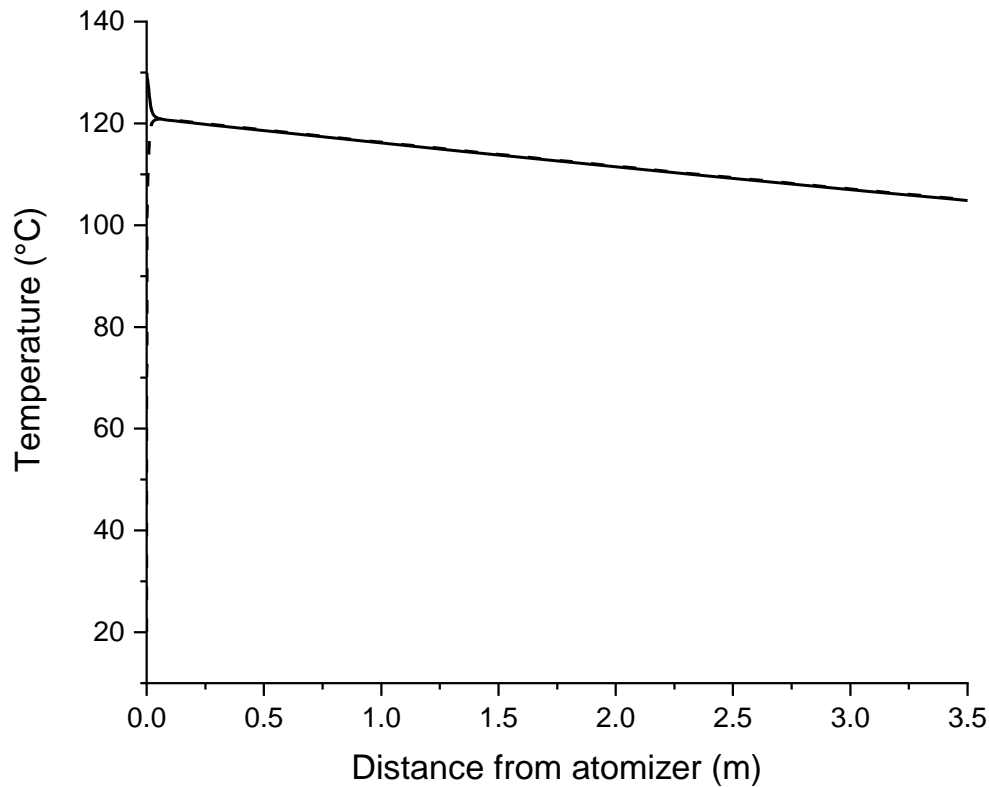


Figure 4.2 Predicted temperature profile for the particles and the drying air with an inlet gas temperature of 130 °C —: gas temperature --: particle temperature.

As shown in Figure 4.2, the particle temperature approaches the gas temperature very quickly after the start of the dryer. The difference between the estimated outlet gas temperature and the actual outlet gas temperature can be accounted for by including an overall heat loss coefficient to the environment. Considering the fact that the spray dryer is well insulated, an overall heat loss coefficient (multiplied by the surface area) to the environment of  $5 \text{ Wm}^{-2}\text{K}^{-1}$  fits the experimentally-observed outlet temperatures within 4°C. Summaries of the simulation results and the differences between the estimated temperatures and actual temperatures are shown in Table 4.1.



Table 4.1 Summary of actual and estimated outlet gas temperatures for different inlet gas temperatures.

| Inlet gas temperature (°C) | Actual Outlet gas temperature (°C) | Estimated outlet gas temperature (°C) |
|----------------------------|------------------------------------|---------------------------------------|
| 130                        | 101                                | 105                                   |
| 150                        | 114 - 116                          | 118                                   |
| 170                        | 130                                | 130                                   |
| 180                        | 136 - 138                          | 135                                   |
| 190                        | 145 - 146                          | 141                                   |

The corresponding outlet gas temperatures for 180°C and 190°C experiments were 136°C and 145°C, respectively. The significant increase in MRPs between these two inlet temperatures suggested that there may be a critical reaction where the rate of one reaction in the Maillard reaction scheme increases significantly between  $136 \pm 1^\circ\text{C}$  and  $145 \pm 1^\circ\text{C}$ . Other studies also showed a similar trend, where the rate of Maillard reaction increases significantly when the temperature is above a certain value (Miao and Roos, 2004). The study of Miao and Roos showed a significant increase in the rate of Maillard reaction when the particle temperature is 10 - 40°C above the glass transition temperature of the particle (Miao and Roos, 2004). Similar behaviour has also been reported in an earlier study by Karmas et al. (1992). A later study by Roos showed that the physical state of lactose also plays an important role in Maillard reactions in milk or milk-like model systems (Roos et al., 1996). The latest study by Gómez-Narváez et al. (2019) also showed that the Maillard reaction could be promoted by lactose in the rubbery-like state, since the mobility of the molecules increases in the glass transition state. This increase in the rate of Maillard reactions may also be related to the change in the structure of proteins. Studies have shown that  $\beta$ -Lactoglobulin ( $\beta$ -Lg), which is the major whey protein found in milk, may lose its spiral structure due to heating and exposing more reactive functional groups (Qian et al., 2017; Vasbinder et al., 2003). More exposed functional groups may promote the sugar-amide reaction (early stage of Maillard reactions) and thus increase the rate of Maillard reactions.

#### 4.3. Fluorometric measurement results – lactose-WPI model systems

Two milk-like model systems were also spray dried using the pilot-scale spray dryer under similar conditions. The extent of Maillard reactions in the spray-dried samples was also

measured using the FAST method described in Chapter 3. The advantage of the model system over the real food system is that the ratio of different components (mainly lactose and WPI) can be controlled. Thus, the effect of different reactant ratios on the kinetics of Maillard reactions can be investigated, and the reaction-rate-limiting component can be identified. In addition to component ratios, the result obtained from the model system is more reproducible, since the model systems are free of other components that may also affect the kinetics of Maillard reactions (Akagawa et al., 2002; Nursten, 2005). Furthermore, model systems also eliminated possible changes in composition due to seasonal variation in real food systems (Grigioni et al., 2007).

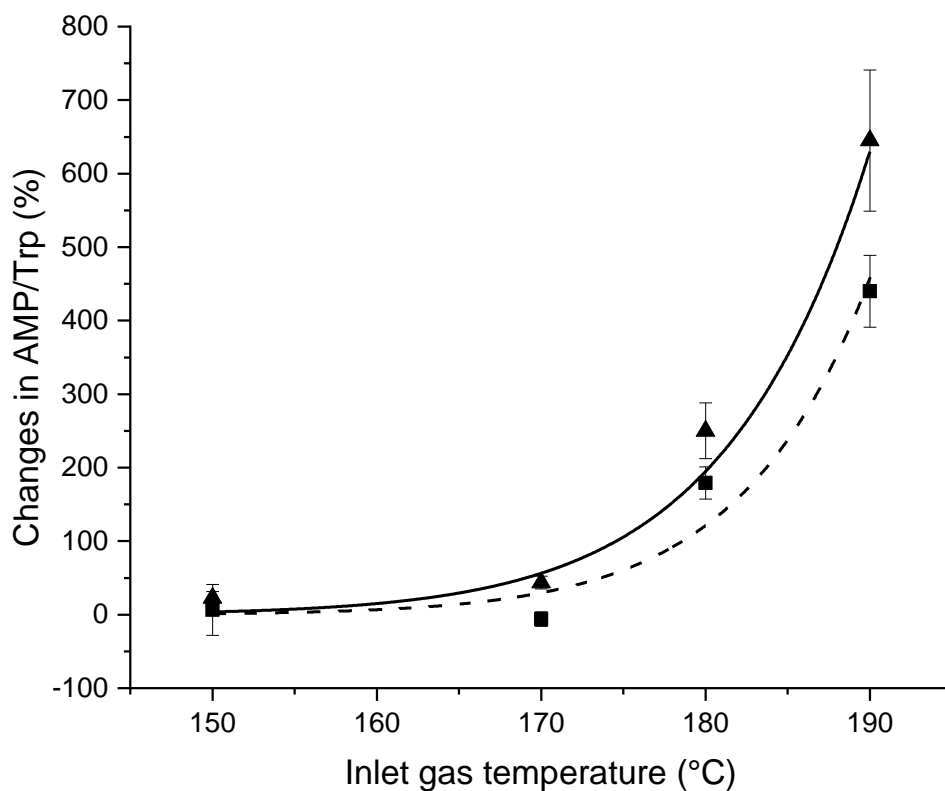


Figure 4.3 The changes in AMP/Trp ratios as functions of inlet gas temperature for model systems. ■: Lactose:WPI 1:2 ●: Lactose:WPI 2:1 —: fitted curve for reconstituted skim milk ( $Y=1.98*10^{-47}X^{4.5}$ ,  $R^2=0.81$ ) --: fitted curve for fresh skim milk ( $Y=4.33*10^{-54}X^{8.4}$ ,  $R^2=0.84$ ).

Similar to the fresh and reconstituted skim milk, the extent of the Maillard reactions in the samples increased with greater values of the inlet gas temperature (Figure 4.3). Under the same

spray drying conditions, model systems with higher WPI contents showed a greater extent of Maillard reactions compared with ones having lower WPI contents. This result suggested that WPI was the rate-limiting reactant for these model systems. The rate of changes in the AMP/Trp ratio increased significantly when the inlet gas temperature was above 170°C (which gave an outlet gas temperature of 130°C) for both model systems, and the corresponding critical temperature appears to be between 130-138°C.

The lower critical temperature suggests that these model systems may be more sensitive to higher temperatures compared with real food systems. Furthermore, these model systems appear to be more greatly affected by Maillard reactions, as indicated by a much higher AMP/Trp ratio in the spray-dried powders, compared with fresh and reconstituted skim milk. This observation might arise because both model systems have higher WPI to lactose ratios than the real food system. Additionally, the WPI and lactose powders have gone through more processing steps that may change the state of the reactants and make them more sensitive to thermal degradation processes, such as Maillard reactions. Last but not least, other components, such as minerals present in the real food system, may also affect the kinetics of the Maillard reactions and lead to a slightly different behaviour between the model system and the real food system (Akagawa et al., 2002).

#### 4.4. Colour analysis of the samples

During the final stage of the Maillard reactions, melanoidins are formed. Melanoidins are brown nitrogen-containing pigments and are the main cause of browning in spray-dried powders. The browning in the spray-dried powders can also be used as an indicator for the final stage of Maillard reactions.

Table 4.2 Summary of colour analysis result for samples collected from different spray drying conditions.

| Inlet gas temperature & conditions |                    | L           | a*         | b*         | E          | C          |
|------------------------------------|--------------------|-------------|------------|------------|------------|------------|
| Fresh skim milk                    | 130°C              | 86.6 ± 1.1  | -1.0 ± 0.2 | 4.6 ± 0.4  | 86.7 ± 1.1 | 4.7 ± 0.4  |
|                                    | 150°C              | 88.2 ± 0.4  | -0.9 ± 0.2 | 5.4 ± 0.4  | 88.7 ± 0.4 | 5.4 ± 0.3  |
|                                    | 170°C              | 88.4 ± 0.1  | -1.2 ± 0.1 | 6.6 ± 0.2  | 89.6 ± 0.1 | 6.7 ± 0.2  |
|                                    | 180°C              | 84.8 ± 0.1  | -1.2 ± 0.1 | 7.5 ± 0.3  | 85.2 ± 0.1 | 7.6 ± 0.3  |
|                                    | 190°C              | 88.7 ± 0.4  | -0.9 ± 0.3 | 9.8 ± 0.6  | 89.3 ± 0.4 | 9.8 ± 0.6  |
| Reconstituted skim milk            | 130°C              | 92.3 ± 0.7  | 0.3 ± 0.5  | 6.8 ± 0.5  | 92.6 ± 0.7 | 6.9 ± 0.5  |
|                                    | 150°C              | 92.4 ± 0.7  | -1.3 ± 0.4 | 7.7 ± 0.6  | 92.7 ± 0.7 | 7.8 ± 0.7  |
|                                    | 170°C              | 92.5 ± 0.15 | -0.3 ± 0.7 | 8.1 ± 0.3  | 92.8 ± 0.1 | 8.1 ± 0.3  |
|                                    | 180°C              | 93.4 ± 0.4  | 0.2 ± 0.5  | 8.6 ± 0.5  | 93.8 ± 0.3 | 8.6 ± 0.5  |
|                                    | 190°C              | 91.9 ± 1    | 0.1 ± 0.3  | 12.0 ± 1.3 | 92.6 ± 1.0 | 12.1 ± 1.3 |
| Model system                       | Lac: WPI 1:2 170°C | 95.4 ± 0.5  | -2.0 ± 1.4 | 18.7 ± 1.0 | 97.3 ± 0.5 | 18.9 ± 1.0 |
|                                    | Lac: WPI 2:1 170°C | 95.7 ± 0.5  | -2.2 ± 0.2 | 14.0 ± 1.2 | 96.8 ± 0.4 | 14.2 ± 1.4 |
|                                    | Lac: WPI 1:2 180°C | 96.0 ± 0.5  | -3.3 ± 0.2 | 21.4 ± 1.2 | 98.4 ± 0.3 | 21.7 ± 1.2 |
|                                    | Lac: WPI 2:1 180°C | 96.2 ± 0.4  | -2.6 ± 0.4 | 18.2 ± 0.1 | 98.0 ± 0.5 | 18.4 ± 0.2 |
|                                    | Lac: WPI 1:2 190°C | 94.9 ± 0.4  | -3.4 ± 0.3 | 27.0 ± 1.9 | 98.8 ± 0.5 | 27.2 ± 1.9 |
|                                    | Lac: WPI 2:1 190°C | 95.6 ± 0.2  | -2.8 ± 0.5 | 21.3 ± 0.7 | 98.0 ± 0.1 | 21.5 ± 0.7 |

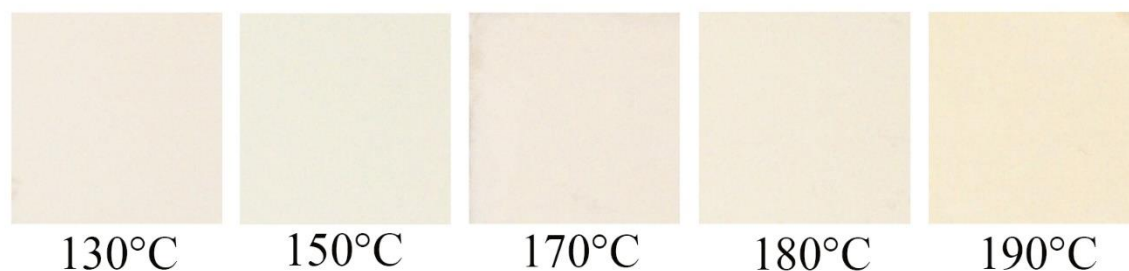


Figure 4.4 Colours of the spray-dried fresh skim milk from different inlet gas temperatures.

The mean L, a\*, and b\* values of the samples collected from different spray drying conditions are shown in Table 4.2. In general, the lightness (L) of the samples produced from the same feed decreased with increases in the inlet gas temperature. The increase in darkness may have been caused by the formation of the brown pigments (melanoidins) produced during the final stage of the Maillard reactions. The a\* value (red and green) of the samples did not change significantly with the different spray-drying conditions, which was also reported in other studies of the colour formation due to Maillard reactions in liquid milk and infant formulae (Bosch et al., 2007; Morales and Boekel, 1998). The b\* values increased with the severity of the spray-drying conditions, which suggested an increase in the yellow component of the colour that is consistent with the visual assessment (browning).

Standalone L, a\* or b\* values are not sufficient to describe the colour of the powders collected. The overall E index (E) has been used to describe the colour of the sample in other studies for liquid milk and infant formulas (Morales and Boekel, 1998). The E index can be calculated as the square root of the sum of the squares of L, a\*, b\* ( $E = \sqrt{(a^{*2} + b^{*2} + L^2)}$ ). In this thesis, the values of the E indexes are mainly dependent on the lightness (L) of the samples, as the L values of the spray-dried samples are much larger in magnitude when compared with the values of a\* and b\*. As a result, the E index might not be suitable for describing the browning due to Maillard reactions during the spray-drying process of milk or milk-like systems.

The Chroma value (C) is another parameter used for describing the colour of the samples. The Chroma value is based on the a\* and b\* values and does not involve the L values. Therefore,

the calculated Chroma values can better reflect the changes in the colour of the samples and be less affected by interference from lightness (L). As shown in Table 4.2, higher chroma values have been obtained for the samples collected from experiments with a higher inlet gas temperature and the same type of feed, and the model system with a lactose to WPI ratio of 1:2 and an inlet gas temperature of 190°C has given the largest chroma values.

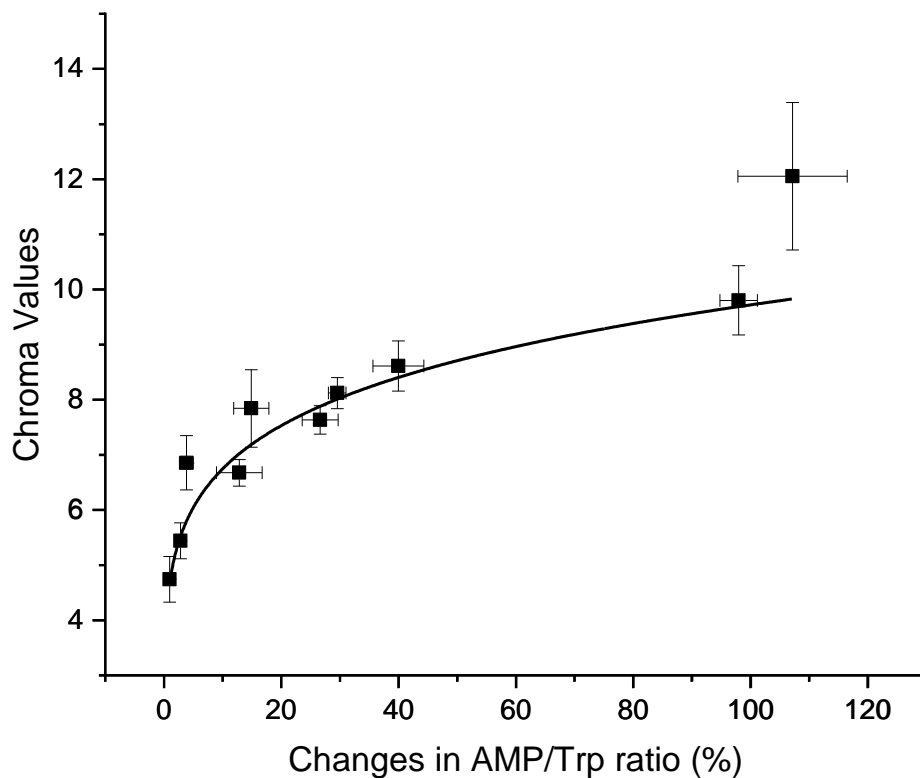


Figure 4.5 Chroma values as functions of the changes in AMP/Trp ratios for real food systems. ■: experimental data points —: fitted curve ( $y=4.68X^{0.15}$ ,  $R^2=0.90$ ).

The trend of the changes in chroma values of the samples is similar to the trend observed in the changes for the AMP/Trp ratio (an indicator of Maillard reactions), suggesting that the changes in the Chroma values are probably due to Maillard reactions. The experiment data for AMP/Trp ratio at 110% appear to be an outlier, which is likely due to the complex colour development under more severe conditions (Morales and Boekel, 1997). As shown in Figure 4.5, both the Chroma values and the changes in the AMP/Trp ratios of the spray-dried

reconstituted skim milk are higher than those for the spray-dried fresh skim milk. This observation is likely to be due to the skim milk powders having more thermal exposure than seen with liquid skim milk during production. Thermal exposure prior to the spray-drying process may lead to different initial concentrations of early Maillard reactions products and more structural changes of the proteins, which may make the reconstituted skim milk slightly more sensitive to Maillard reactions occurring during the spray-drying process. Nevertheless, the correlation between the Chroma values and the changes in AMP/Trp ratio is very similar for both the spray-dried reconstituted skim and fresh skim milk, which is consistent with the findings of other studies (Nijdam and Langrish, 2005). A correlation exists between the colour intensity of the spray-dried products and the formation of advanced Maillard reaction products, which can be potentially further developed as a rapid, cost-effective quality evaluation method for spray-dried products.

A power-law model was found to be most suitable for describing the correlation between the increase in the amounts of advanced Maillard reaction products and the colour intensity of the sample. Part of the reason for this result is due to the extent of browning being measured in terms of the CIElab colour space, which is based on a 0 - 100 scale, while the extent of the Maillard reaction is not limited in this way. In the study of Morales and Boekel (1997) on the heated casein/sugars solution system, a reduction in the Chroma values was observed under more severe conditions due to more complex colour development, which resulted in a reduction in the  $b^*$  values of the samples. The complex colour development might also have influenced this thesis by creating a non-linear correlation between the Chroma values and the change in the amounts of AGE products in the samples when more severe conditions were used.

#### 4.5. Maillard reactions occur during the spray drying process within the laboratory-scale spray dryer

With the laboratory-scale spray dryer, no significant change was observed in the AMP/Trp ratio in the spray-dried products collected from the most severe spray-drying conditions (inlet gas temperature of 190°C). This result may be caused by the laboratory-scale spray dryer having a much shorter particle residence time. Schmitz-Schug et al. (2013) have reported that

the mean particle residence for a laboratory-scale spray dryer is less than 10 seconds, while in a pilot-scale spray dryer, the mean particle residence time is expected to be longer than 20 seconds. In addition to the difference in the mean particle residence time, the particle residence times in spray dryers also have non-uniform distributions, and particles can stay up to 18 minutes in pilot-scale spray dryers (Schmitz-Shug et al., 2013). The short particle residence time in the laboratory-scale spray dryer may lead to a very low extent of Maillard reactions, and thus the products may not be detectable by the methods used in this thesis. The actual particle residence time distribution for the laboratory-scale spray dryer (Buchi mini spray dryer B-290) has been measured and discussed in Chapter 5.

#### 4.6. Conclusions

In this chapter, the extent of Maillard reactions of the spray-dried milk and milk-like model system under different spray-drying conditions have been investigated. Fluorescence analysis has shown that the extent of thermal degradation increased with the severity of the spray-drying conditions. The reaction rate for Maillard reactions increased significantly when the inlet gas temperature increased from 180°C to 190°C, suggesting that protein unfolding also plays an important role in the thermal degradation of milk in spray dryers. The non-uniform distribution of particle residence time in the pilot-scale dryer suggested that the design and operation of the spray dryer used for drying may also affect the extent of thermally-induced reactions during spray-drying processes. This work also reinforces the point made in Nijdam and Langrish (2005), that the behaviour of reconstituted milk from milk powder is similar to that of fresh milk, in the sense that the reconstituted milk falls on a continuous curve that has additional heat treatment to fresh milk, but which is not a separate and completely different material. Based on the result from spray drying model systems, WPI may be the rate-limiting reactant for Maillard reactions that occurs during the spray drying process. The colour analysis of the samples has indicated that the colour change of the milk powder may be caused by Maillard reactions and has shown a strong correlation with the content of the Advanced Maillard reaction products, which can be used as an indicator of the progress of Maillard reactions.



## Chapter 5. Effect of different designs of the spray dryer on the particle residence time distribution and the quality of the final product

This chapter mainly focuses on how different designs of the spray dryer affect the particle residence time distribution and, thus the quality of the final product.

Preliminary data from the chapter was published as a conference proceeding under the title of *"Particle residence time distributions in different configurations of a pilot-scale spray dryer"* for the 22nd International Drying Symposium (IDS 2022). This proceeding was later developed into a journal article with added experimental data and further discussion of the data.

This chapter is developed based on a published journal article: *"Using particle residence time distributions as an experimental approach for evaluating the performance of different designs for a pilot-scale spray dryer"*, which was published in the Processes as a part of the special issue *"Advances in Drying Technologies—Selected Papers from the 22nd International Drying Symposium (IDS 2022)"*.

I am the first and the corresponding author for this journal article. I designed the study, analysed the data, and wrote the majority of the draft with the guidance of the supervisor of this thesis, Professor Timothy Langrish. Professor Langrish and Sining Cai have assisted with the design of the experiment, data acquisition and editing of the manuscript.

Permission for including published materials in this section has been granted by the supervisor of this thesis, Prof. Timothy Langrish.

---

| <b>Symbols</b> |   |
|----------------|---|
| $\mu$          | Dynamic viscosity                             |
| $D$            | Diameter                                      |
| $f$            | Frequency                                     |
| $ff$           | Fanning friction factor                       |
| $L$            | Characteristic dimension                      |
| $n$            | Number of equivalent reactors                 |
| $Re$           | Reynolds number                               |
| $Sr$           | Strouhal number                               |
| $U_{\infty}$   | Freestream velocity of the fluid              |
| $u_{\tau}$     | Shear velocity                                |
| $x$            | Distance from the start of the boundary layer |
| $\delta$       | Thickness of the boundary layer               |
| $\Delta P$     | Pressure drop                                 |
| $\varepsilon$  | Chamber coefficient /Roughness of the surface |
| $\nu$          | Kinematic viscosity                           |
| $\rho$         | Density                                       |
| $\tau$         | Residence time                                |
| $\tau_w$       | Wall shear stress                             |

---

## 5.1. Introduction

For thermally-sensitive products, the quality of the final products (e.g., the extent of thermal degradation) is mainly dependent on their integrated thermal-time exposure during thermal processing (Jeantet et al., 2008). In the case of spray drying, the extent of thermal exposure (temperature) is mainly dependent on the operating conditions, including but not limited to inlet gas temperatures and feed to drying gas ratio. The impact of different operating conditions of the spray drying process on the quality of the final product has been investigated in Chapter 4, and also in many other studies (Koca et al., 2015; Park et al., 2016). The duration of the thermal exposure, also known as the particle residence time, is dependent on both the characteristics of the spray dryer and the properties of the product itself. A few studies have experimentally measured the particle residence times in spray dryers (Ali et al., 2017; Gianfrancesco, 2009; Jeantet et al., 2008; Kieviet and Kerkhof, 1995; Schmitz-Schug et al., 2013). However, in the studies mentioned above, only one drying chamber design has been used for each study. Thus, the effect of different chamber designs on the measured particle residence time distribution has not yet been investigated.

The main objective of this chapter is improving the drying chamber designs further to achieve a lower extent of wall-particle interaction and improve the final product quality. The performance of different spray dryer designs has been evaluated based on the measured particle residence time distribution and the properties of the final spray-dried products.

## 5.2. Method validation

### 5.2.1. Validation against published data

The method used for measuring the particle residence time distribution (RTD) in this thesis is modified based on Ruprecht and Kohlus (2018). In Ruprecht and Kohlus's study (2018), a phase doppler anemometry (PDA) device was used to measure the number of particles passing through the drying chamber. In this thesis, a method based on laser scattering was developed for the purpose of measuring the particle residence time distribution. Similar to many other locally-manufactured methods, it is crucial to validate the method with data from published data obtained using more established methods.

As mentioned previously, limited studies have investigated the particle residence time distribution (Ali et al., 2017; Gianfrancesco, 2009; Jeantet et al., 2008; Kieviet and Kerkhof, 1995; Schmitz-Schug et al., 2013), and the equipment or feed compositions are significantly different to those used in this thesis. It appears that the study on particle residence time distribution for model infant formula in Buchi B-290 mini spray dryer by Schmitz-Schug et al. (2013) is the closest published literature to this thesis. In their study, coloured salt (NaCl) solution was used as the tracer, and samples were sampled manually at the outlet of the cyclone. For the first 10 seconds, the sampling interval is 5 seconds and then every 10 seconds until 80 seconds, then 120 seconds, 160 seconds and 220 seconds. The particle residence time distributions were estimated based on the colour intensity of the sample collected. This type of method has also been used in many other studies (Ali et al., 2017; Chen et al., 2020; Jeantet et al., 2008; Kieviet, 1997). Therefore, it can be regarded as a "reference method" in this thesis for the purpose of validating the method developed here. In their study, the mean particle residence time ( $\tau_{50}$ ) was found to be 6 seconds.

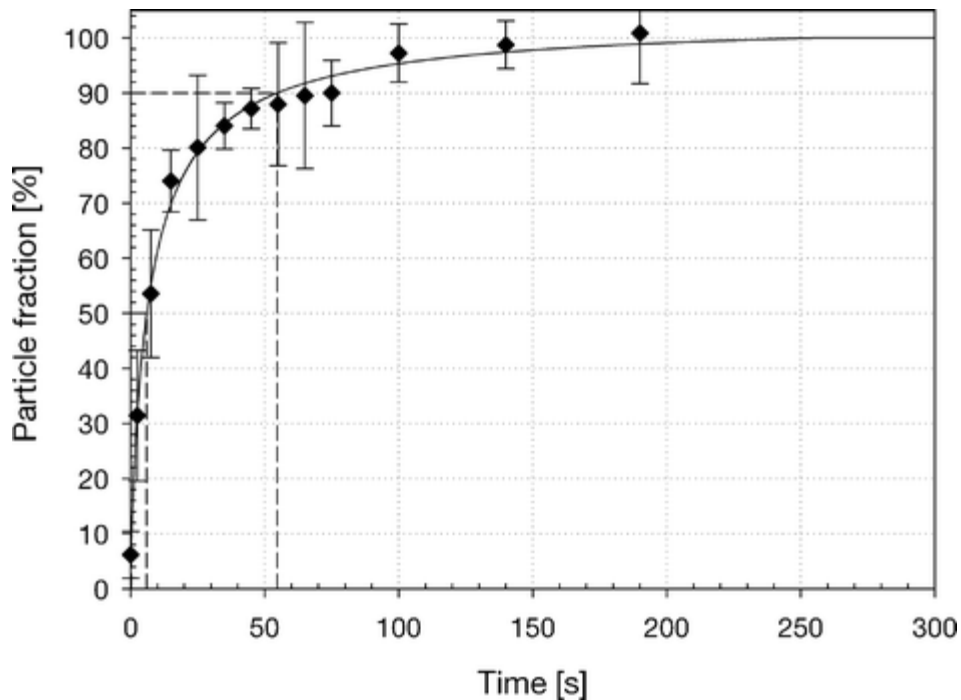


Figure 5.1 Particle residence time distribution in Buchi mini spray dryer B-290 (Schmitz-Schug et al., 2013).

In this chapter, the particle residence time distribution in the Buchi mini spray dryer B-290 has been measured using fresh skim milk under similar spray-drying conditions to the study of

Schmitz-Schug et al. (2013). The measured particle residence time distribution was fitted with the CSTR-TIS model. As shown in Figure 5.2, the CSTR-TIS model fitted well with the measured signal. The average measured mean particle residence time in the Buchi mini spray dryer B-290 was  $3.3 \pm 0.5$  seconds. The measured mean particle residence times are slightly shorter than the reported mean particle residence time is shorter than the reported values ( $\tau_{50} = 6$  s) but still within the same magnitude.

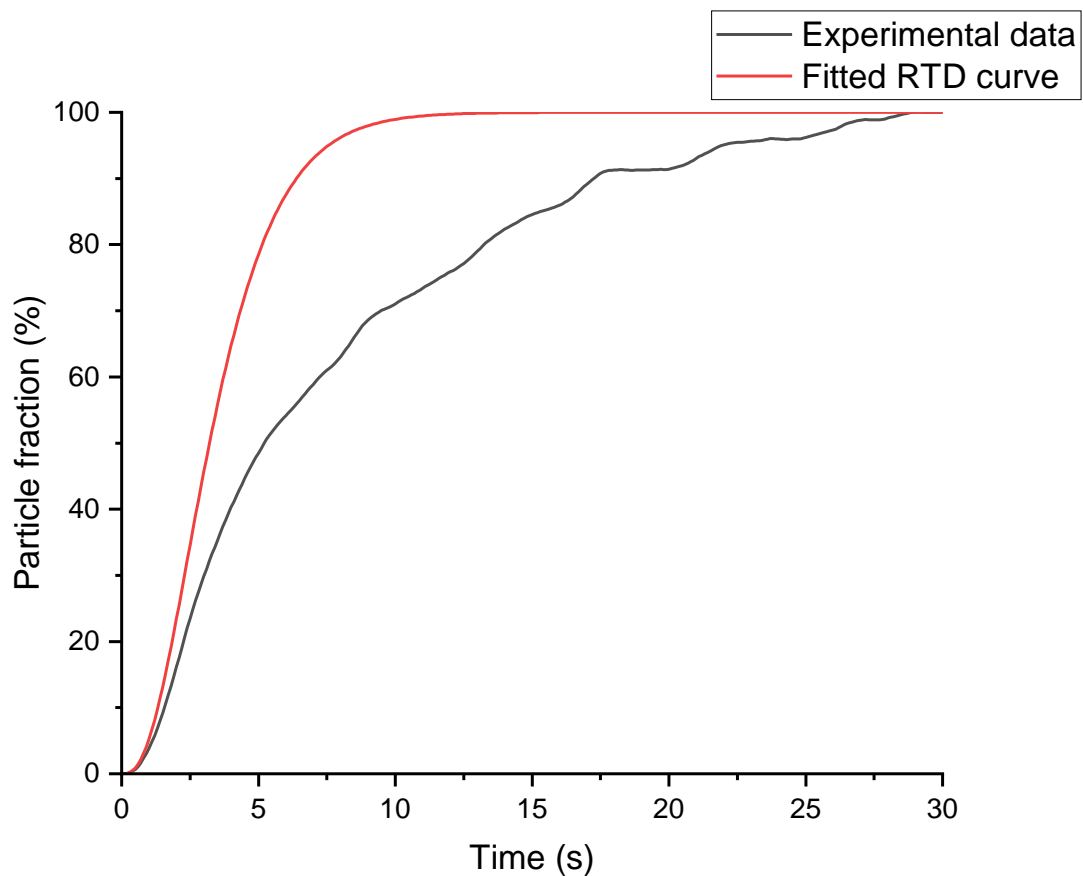


Figure 5.2 Particle residence time distribution in Buchi mini spray dryer B-290.

The difference between the measured value and the reported values is due to the difference between the two measurement methods. As discussed in Chapter 2, the method used in the study of Schmitz-Schug et al. (2013) can be classified as an "intrusive" method, and the sampling frequency is solely dependent on the efficiency of the sampling devices. The particle residence time reported is close to the sampling interval (5 seconds) used in their study due to the efficiency of the sampling device. As a result, the mean particle residence time reported is

based on interpolation using all the measurements (Figure 5.1). While in the method used in this thesis, the time between each measurement is 0.1 seconds, which is significantly shorter than the mean particle residence time, and thus interpolation is not compulsory. In addition to the lower sampling frequency, the tracer concentration is measured based on the sample collected at the bottom of the cyclone. In contrast, in this thesis, the tracer concentration is measured at the outlet of the main drying chamber (prior to the cyclone). Last but not least, the infant model system used in their study has a higher sugar-to-protein ratio (5:1) than the fresh skim milk (~1:1) used in this thesis. Lactose is an amorphous material whose physical properties change with moisture and temperature. Lactose enters a rubbery-like state when its temperature is above the glass transition temperature, and this will contribute to more wall depositions and may extend the particle residence time. Combining all the factors mentioned above, the mean particle residence time measured in this thesis is expected to be slightly shorter than the reported value. A shorter mean particle residence time was indeed observed here. In conclusion, it is reasonable to suggest that the method used in this thesis is at least an equivalent alternative to the "reference method".

#### 5.2.2. Difference between the automated injection system and manual dye injection

At the earlier stage of the experimental design, dye injections were carried out manually to investigate the feasibility of the method developed. The detailed method is described in Chapter 3. The fitted particle residence time distribution parameters for experiments with different injection methods, manual or automatic, are shown in Table 5.1. The mean particle residence times for experiments with manual injection were slightly longer than those with automatic injection systems. This difference is likely to be caused by human reflection time and the difference in the length of tubing for dye delivery. For safety reasons, the tubing used for manual injection is significantly longer (approximately 50 mm longer) than the automated injection system. In addition to human reflection time and extended tubing, manually opening the valve is also required when performing a manual injection. Considering all the factors mentioned above, it is reasonable to suggest that manual injection would cause at least a

one-second delay in dye delivery by manual injection. Based on the results, it is reasonable to suggest that the automated injection system is equivalent to, if not superior, manual injection.

Table 5.1 CSTR fitting results for RTD measurement using different injection volumes and methods.

|                  | $\tau$ (s)  | $n$        | Injection Volume (mL) |
|------------------|-------------|------------|-----------------------|
| Manual injection | 11.9        | 15         | 1                     |
|                  | 11.4        | 10         | 1.5                   |
|                  | 11.5        | 15         | 2                     |
| Auto injection   | $9.3 \pm 1$ | $13 \pm 4$ | 2                     |

### 5.2.3. Effect of different dye injection volumes

The effect of different dye quantities has also been investigated using manual injection prior to switching to an auto-injection system. Injection volumes ranging from 1 mL, 1.5 mL, and 2 mL (over the same period of time) have been tested using Design 3 at a gas flow rate of 257 m<sup>3</sup>/hr. It was found that different dye injection volumes mainly affect the signal-to-noise (SNR) ratio. With smaller injection volumes, the signals measured were difficult to separate from the baseline (i.e., poor signal-to-noise ratio). In terms of the particle residence time distribution, the difference between fitted parameters for experiments with different injections was small (Table 5.1). This observation suggested that the injection volume mainly affects the signal-to-noise ratio and has limited effect on the RTD measured. As a result, the injection volume of 2 mL has been chosen for all experiments carried out using the auto-injection system.

## 5.3. Particle residence time distribution for pilot-scale spray dryer

The main focus of this thesis is the particle residence time distribution (RTD) of the pilot-scale spray dryer. RTD in pilot-scale spray dryers is used to evaluate the performance of different dryer designs and investigate factors affecting the particle residence time. Similar to the laboratory-scale spray dryer, measured signals have been fitted with the CSTR-TIS model for a quantitative comparison between different pilot-scale spray dryer designs.

### 5.3.1. Mean particle residence time – $\tau$

The mean particle residence time determines the duration of thermal exposure for the particle, which is an important factor that affects the quality of the spray-dried products. In

general, the shorter the mean particle residence, the better the performance of the dryer, provided that the desired final moisture content is achieved.

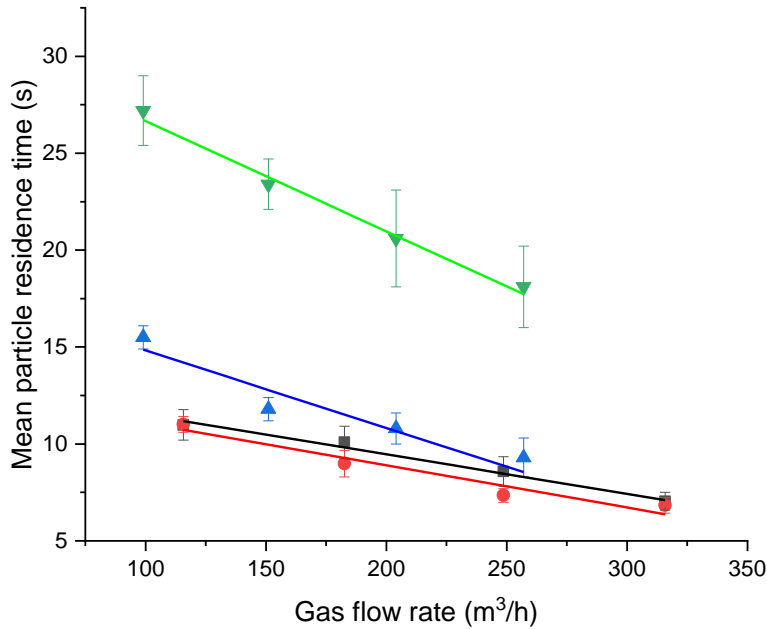


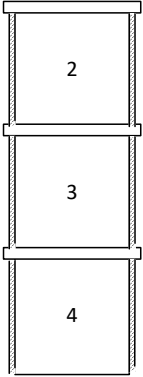
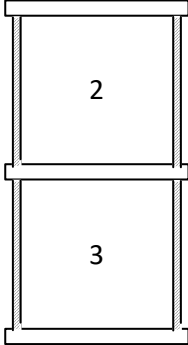
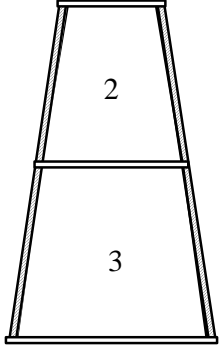
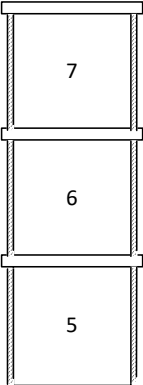
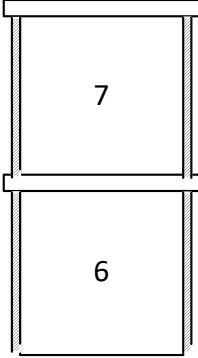
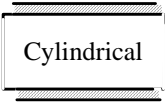
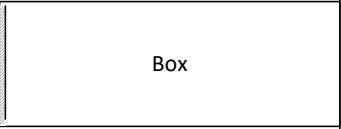
Figure 5.3 Mean particle residence time ( $\tau$ ) ■: Design 1: 4-inch connection ●: Design 2: 6-inch connection ▲: Design 3: Box connection ▼ Design 4: Conical drying chamber.

As shown in Figure 5.3, the mean particle residence time increased as the gas flow rate decreased. This observation is related to the fact that the particle residence time is mainly affected by the gas residence time and the gas flow rate. During the spray drying process, high-velocity droplets from the atomiser rapidly approach the drying gas velocity (Langrish, 2009). Thus, the particles are expected to have a similar residence time to the gas if there are no particle-wall interactions, and the gas residence time would normally be expected to be inversely proportional to the gas flow rate. Due to the differences in the designs, mainly their different dimensions (Table 5.2), the mean gas residence time for each design is different at any given gas flow rate. The difference in the internal volumes of Designs 1 and 2 is negligible compared with the differences between the other designs. Therefore, similar gas and particle residence times should be expected for the first two designs, which are consistent with the



observed values. The internal volume of Designs 3 and 4 are significantly larger than the first two designs, and thus longer mean gas and particle residence times are expected.

Table 5.2 Key difference between designs and internal volume of different designs.

| Parts of the spray dryer                  | Designs   |          |   |   |
|---|---|----------|---|---|
|   | Design 1  | Design 2 | Design 3  | Design 4  |
| Drying column 1                           |    |          |    |  |
| Drying column 2                           |   |          |   |   |
| Type of Connection between drying columns |  |          |  |   |
| Internal volume (m <sup>3</sup> )         | 0.228   | 0.230    | 0.262   | 0.765   |

### 5.3.1. The ratios between mean particle residence times and gas residence times

As discussed previously, the particle residence time is mainly affected by the gas residence time; it is undesirable to evaluate the performance of different designs solely on the basis of the absolute particle residence time. In practice, the particle residence time is expected to be significantly longer than the gas residence time due to particle-wall interactions. In addition to the operating conditions and the properties of the feed, the design of the spray dryer also plays an important role in determining the particle residence time. In this thesis, the feed and inlet gas temperatures are the same for all the designs. The difference between the mean particle and gas residence time ratios mainly depends on the dryer designs. Therefore, the ratio between the particle residence time and the estimated residence time of the gas has been used here to evaluate the performance of different designs. In other studies, the particle-to-gas residence time ratio is also called the chamber coefficient ( $\epsilon$ ) and was found to be related to the design of the spray dryer (Oakley, 2004). The gas residence times for different designs were estimated based on the gas flow rate and the internal volume of each design.

$$\tau_{gas} = \frac{Q}{V_{internal}} \quad 5.1$$

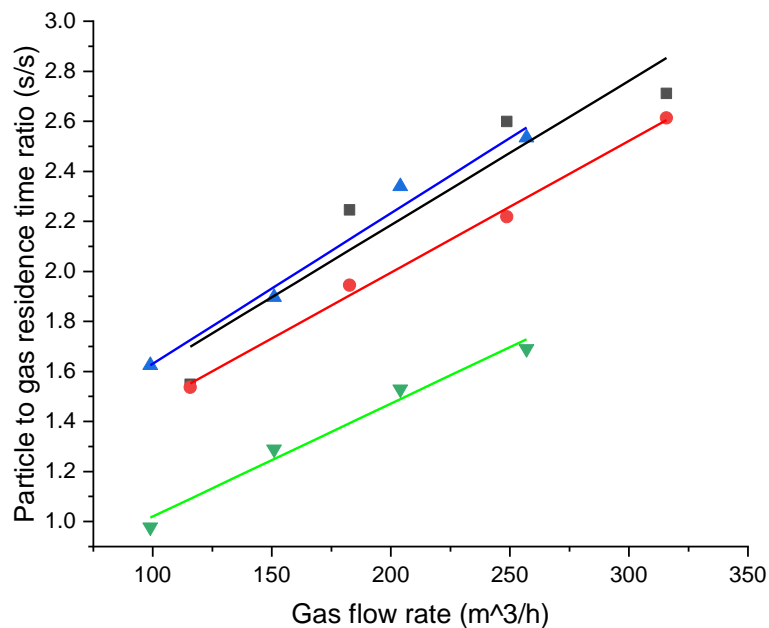


Figure 5.4 Ratios between particle and gas residence time for different configurations and gas flow rates ■: Design 1: 4-inch connection ●: Design 2: 6-inch connection ▲: Design 3: Box connection ▼: Design 4: Conical drying chamber.

### 5.3.1.1. Cylindrical connection designs (Design 1&2)

As shown in Figure 5.4, Design 1 has the second highest particle-to-gas residence time ratio of all the designs for most gas flow rates. This observation is related to the suboptimal connection design between the two drying columns. The CFD simulation result for designs 1 and 2 from an earlier study by Langrish et al. (2020) is shown in Figure 5.5.

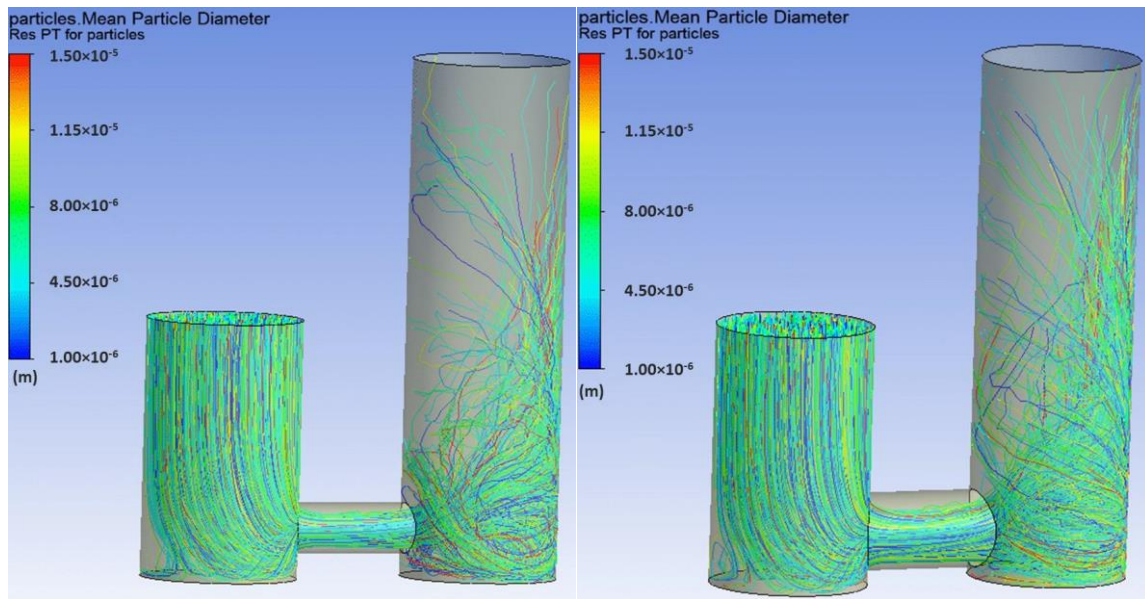


Figure 5.5 CFD simulation results for the first two designs. Left: Design 1 Right: Design 2 (Langrish et al., 2020).

As shown in Figure 5.5, the four-inch connection between the two drying columns created a particle recirculation zone at the entrance and the exit of the connection due to sudden contraction and expansion (Langrish et al., 2020). The increased diameter (6 inches) of the connection in Design 2 has somewhat reduced the particle recirculation behaviour, and a small decrease in the particle-to-gas residence time ratio was observed for Design 2. The reduction in particle recirculation is likely to be due to the smoother flow pattern across the broader connection.

### 5.3.1.2. Box connections and cylindrical drying chambers (Design 3)

Inspired by the difference between the CFD simulation results for Designs 1 and 2, the connection between two drying chambers has been further widened to a "box" connection. In Design 3, two drying chambers have been unified via a box connection to avoid sudden gas velocity changes due to the sudden contraction and expansion. As shown in the CFD simulation

result (Figure 5.6), the box connection between two drying chambers has resulted in a smoother gas flow pattern. It may be beneficial in terms of less wall deposition and recirculation in the air flow pattern.

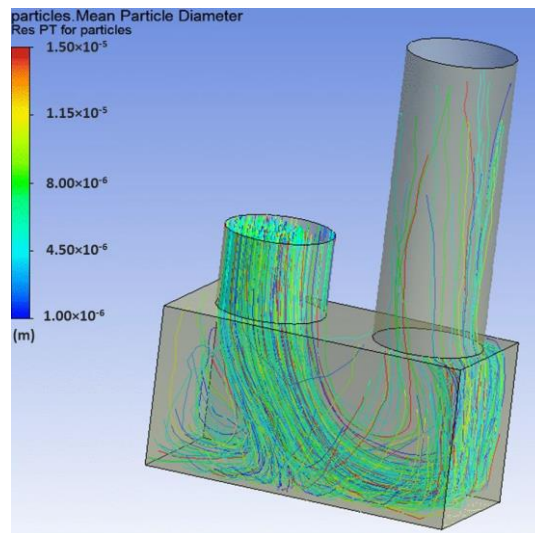


Figure 5.6 CFD simulation results for Design 3 (Langrish et al., 2020).

However, the observed mean particle-to-gas residence time ratio for Design 3 is slightly higher than the first two designs at the same gas flow rate. This result is likely to be related to the recirculation zone observed at the bottom left of the box in previous CFD simulations by Langrish et al. (2020). The recirculation zone may extend the mean particle residence time and widen the spread of the particle residence time distribution. In addition to the bottom-left corner, the particles are likely to hit the top plate of the box near the bottom of the second drying column and the right inner wall. Similar behaviour has also been observed in other CFD simulation studies (Huang and Mujumdar, 2005). Despite having a slightly higher particle-to-gas residence time ratio, the box design is still promising due to its smoother gas flow pattern (Langrish et al., 2020).

#### 5.3.1.1. Box connections and cylindrical drying chambers (Design 4)

As discussed in a previous study by Langrish et al. (2020), most wall depositions were found within the first two drying chambers, except the bottom of the box chamber. This phenomenon is likely to be due to spray from the atomiser hitting the inner wall of the dryer

directly, which is caused by the mismatch between the spray pattern (conical) and the geometry of the drying chamber (cylindrical) (Figure 5.7).

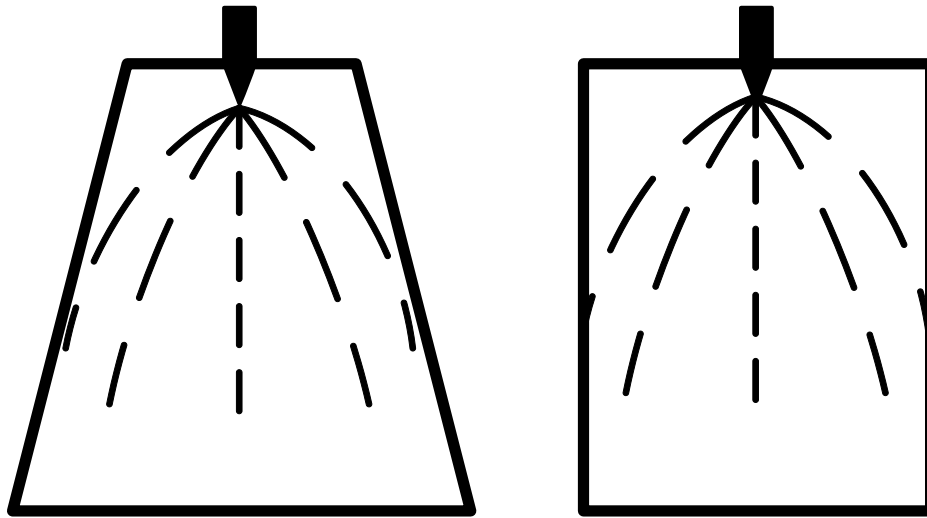


Figure 5.7 Difference between cylindrical and conical drying chambers.

To address this issue, the shapes of drying chambers 2 and 3 have been changed from cylindrical to conical in Design 4. As demonstrated in Figure 5.7, Changing the shape of drying chambers 2 and 3 from cylindrical to conical may reduce particle-wall interactions as a conical shape can better fit the spray pattern produced by the atomiser. This expectation has been confirmed as the observed particle-to-gas residence time ratio for Design 4 is significantly closer to unity than the previous designs at all gas flow rates ( $P < 0.05$ ). It is also worth mentioning that at the lowest gas flow rate, the average particle-to-gas residence time ratio for Design 4 is slightly less than unity. This observation is likely due to the high initial velocity of the droplets coming out of the atomiser. Similar behaviour has also been reported in other studies (Anandharamakrishnan et al., 2010; Zbicinski et al., 2002).

#### 5.4. Spread of particle residence time – $n$

Other than the average length of time for the particles to stay in the dryer, the spread of the particle residence time is another important performance indicator. A broader spread in particle residence time distribution means a larger portion of the spray-dried products will stay longer than the mean particle residence time. A portion of spray-dried products having a longer residence time than others can affect the quality of the final product adversely. Therefore, the

tighter the distribution, the better the performance. The spread of the particle residence time distribution (RTD) is described by the number of equivalent continuous-stirred-tank reactors (CSTR) in series ( $n$ ). A higher value for  $n$  corresponds with a tighter spread in the residence time (i.e., closer to the behaviour of a plug-flow reactor, PFR) and vice versa.

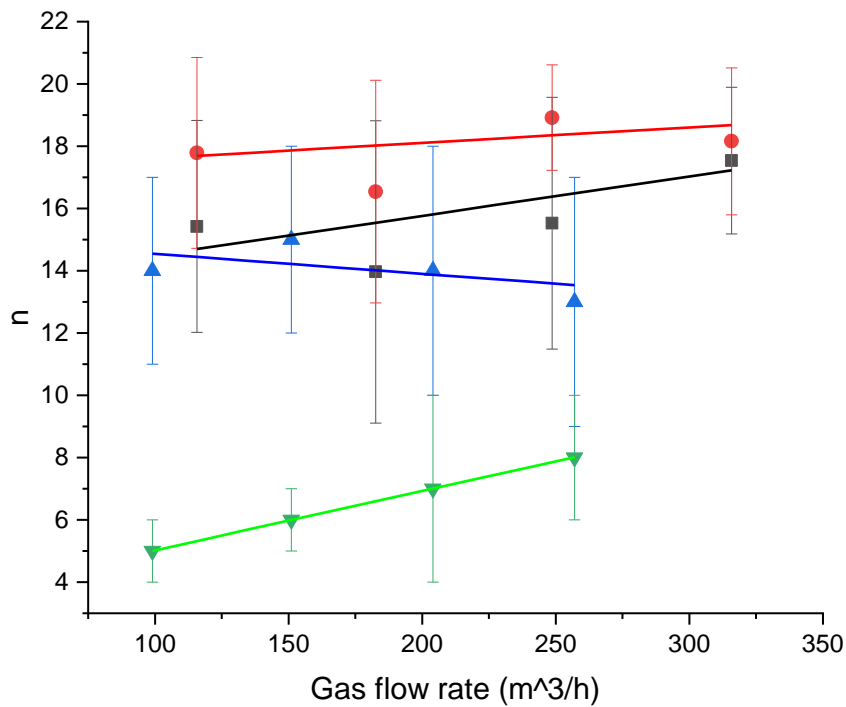


Figure 5.8 Number of equivalent CSTR in series ( $n$ ) for different configurations and gas flow rates. ■: Design 1: 4-inch connection ●: Design 2: 6-inch connection ▲: Design 3: Box connection ▼: Design 4: Conical drying chamber.

As shown in Figure 5.8, different gas flow rates have a limited impact on the spread of particle residence time for a given chamber design ( $P > 0.05$ ). The difference in the spread of particle residence times for the first three designs is also small ( $P > 0.05$ ). This observation is likely to be due to the similarities in their designs (i.e., chambers 1, 2, 3, 6 and 7 are shared for the first three designs). The spread of the RTD in Design 4 is significantly greater than in the first three designs ( $P < 0.05$ ). The broader spread of the RTD in Design 4 may be partly due to the recirculation zone near the bottom left of the box connection mentioned in previous studies (Langrish et al., 2020). The recirculation zone at the bottom-left section of the box connection will be the next point of development for improved designs. The conical chamber design may

also cause extra re-circulation and widen the spread of the RTD in Design 4. However, this hypothesis does require confirmation from CFD simulations for Design 4, and it will be the focus of future studies. Last but not least, the spread of the RTD for Design 4 showed a promising trend (i.e., increasing  $n$ ) as the gas flow rate increased despite having the widest spread.

### 5.5. Fluctuations in measured signals

As shown in Figure 5.9, negative values at the initial part of the measurement were observed. They are likely caused by the short disruption in the feed to the atomiser due to the introduction of the red dye solution, and this has a limited impact on the RTD measurement.

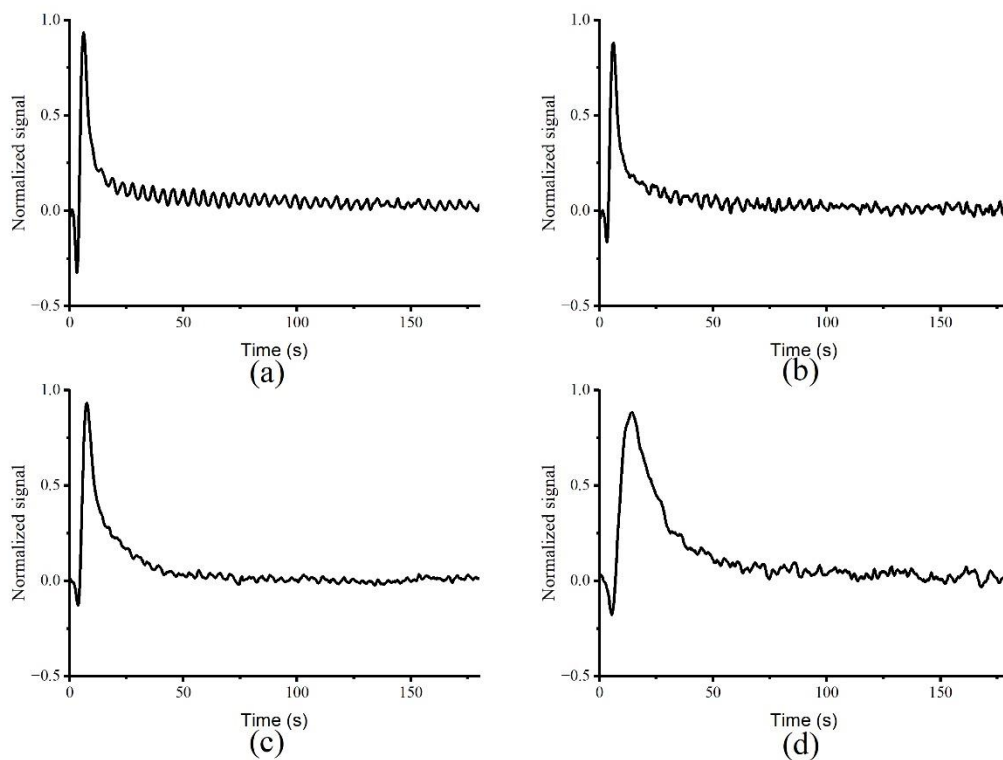


Figure 5.9 Averaged normalised signals for all designs at the maximum gas flow rate ( $257\text{-}315\text{ m}^3/\text{hr}$ ) (a): Design 1: 4-inch connection (b): Design 2: 6-inch connection (c): Design 3: Box connection (d): Design 4: Conical drying chamber.

Fluctuations were also observed in all measured particle residence time distribution (RTD) signals. The noise from the photomultiplier itself was sampled at an early stage of the experimental design. The relative magnitude of the noise from the photomultiplier is



approximately 1% of the baseline values, while the fluctuations observed are around 5% of the baseline values. Furthermore, fluctuations in measured signals were also observed in other studies that used scattered light methods (Ruprecht and Kohlus, 2018). As a result, it is not likely that the fluctuations are inherent to the measurement system, and it is more likely to be linked to physical processes occurring within the dryer, including flow-stability issues or wall-deposition-related issues. Wall deposition and their re-entrainment process is a well-known physical process that occurs during spray drying processes (Francia et al., 2015; Keshani et al., 2015). Wall deposits that are re-entrained may be different in size and shape due to aggregation (Kousaka et al., 1980). In addition to the shape and size, re-entrained wall deposits may also contain tracers. As a result, wall depositions refracted the laser differently and caused fluctuations in the measured RTD signal.

Fourier transforms for the last 60 seconds of all the measured signals were performed using fast Fourier Transform (FFT) using MATLAB. Since the sampling duration is 60 seconds, any signals with a frequency lower than  $1/60$  Hz cannot be properly measured. According to the Nyquist-Shannon sampling theorem, to accurately characterize any waveform from a time series of data, the sampling frequency must be twice the signal frequency (Shannon, 1949). Therefore, any signals with a frequency higher than 5 Hz were ignored since the sampling frequency is 10 Hz. The frequency with the highest amplitude in each measurement has been defined as the dominant frequency in the signals. The averaged values of the dominant peaks for all combinations of gas flow rates and configurations are shown in Figure 5.10.

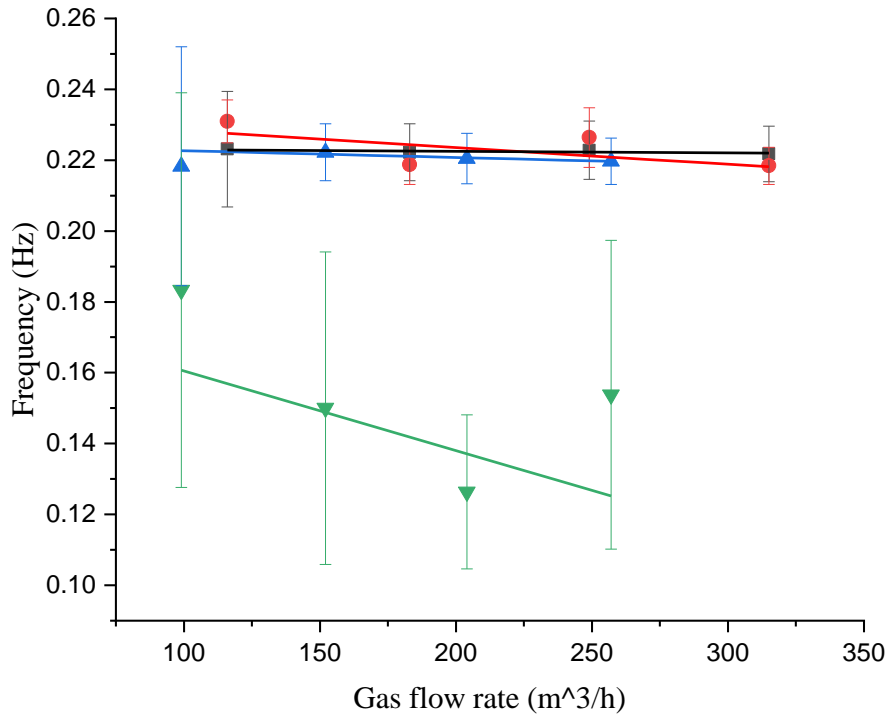


Figure 5.10 Dominant frequencies for different configurations and gas flow rates ■: Design 1: 4-inch connection ●: Design 2: 6-inch connection ▲: Design 3: Box connection ▼ Design 4: Conical drying chamber.

### 5.5.1. Flow related factors

It is unclear whether the fluctuation is caused by flow-stability related issues. If the flow is time-dependent or transient, the fluctuations observed in signals may be related to the oscillation in the flow. A dimensionless parameter can describe the oscillation behaviour of the flow, called the Strouhal number ( $Sr$ ), which can be expressed as a function of the Reynolds number (Guo et al., 2001; Katopodes, 2018; Roshko, 1954).

A summary of gas velocity,  $Re$ ,  $Sr$  for different parts of the spray dryer at different drying gas flow rates are shown in Table 5.3. Reynolds numbers in different parts of the spray dryer in this thesis are within a range ( $10^3 < Re < 10^5$ ) where the Strouhal number is approximately constant ( $Sr \approx 0.2$ ) (Guo et al., 2001; Katopodes, 2018). The  $Sr$  calculated based on the frequency measured is within a range of 0.02 to 0.71, which is different from the  $Sr$  for flow oscillation estimated based on the Reynolds number of around 0.2. Furthermore, when the Strouhal number is constant, the oscillation frequency of the vortex shedding is proportional to

the gas velocity for a given characteristic length. In this thesis, the frequency of the fluctuations is independent of the gas flow rate and, thus the gas velocity for the same configuration (Figure 5.10). These observations suggested that the fluctuations in the signals are not simply related to any oscillations in the flow patterns.

Table 5.3 Summary of gas velocity,  $Re$ ,  $Sr$  for different parts of the spray dryer at different drying gas flow rates.

| Gas flow rate<br>(m <sup>3</sup> /hr) | Design 1         |                | Design 2         |                | Design 3       |                 |                | Design 4         |                |                  |
|---------------------------------------|------------------|----------------|------------------|----------------|----------------|-----------------|----------------|------------------|----------------|------------------|
|                                       | $D = 0.101$<br>m | $D = 0.3$<br>m | $D = 0.152$<br>m | $D = 0.3$<br>m | $D = 0.3$<br>m | $D = 0.35$<br>m | $D = 0.3$<br>m | $D = 0.485$<br>m | $D = 0.6$<br>m | $D = 0.624$<br>m |
| <b>Dominant frequency (Hz)</b>        |                  |                |                  |                |                |                 |                |                  |                |                  |
| 257 - 315                             | 0.222            |                | 0.218            |                | 0.220          |                 |                | 0.154            |                |                  |
| 204 - 250                             | 0.223            |                | 0.226            |                | 0.220          |                 |                | 0.126            |                |                  |
| 152 - 180                             | 0.222            |                | 0.219            |                | 0.222          |                 |                | 0.150            |                |                  |
| 99 - 116                              | 0.223            |                | 0.238            |                | 0.218          |                 |                | 0.183            |                |                  |
| <b>Gas velocity (m/s)</b>             |                  |                |                  |                |                |                 |                |                  |                |                  |
| 257 - 315                             | 11               | 1.24           | 4.86             | 1.25           | 1.01           | 0.74            | 1.01           | 0.39             | 0.25           | 0.23             |
| 204 - 250                             | 8.62             | 0.98           | 3.83             | 0.98           | 0.8            | 0.59            | 0.8            | 0.31             | 0.2            | 0.19             |
| 152 - 180                             | 6.33             | 0.72           | 2.75             | 0.71           | 0.6            | 0.44            | 0.6            | 0.23             | 0.15           | 0.14             |
| 99 - 116                              | 4.01             | 0.45           | 1.77             | 0.45           | 0.39           | 0.29            | 0.39           | 0.15             | 0.1            | 0.09             |
| <b><math>Re</math></b>                |                  |                |                  |                |                |                 |                |                  |                |                  |
| 257 - 315                             | 58188            | 19590          | 38830            | 19590          | 15945          | 13668           | 15945          | 9863             | 7973           | 7666             |
| 204 - 250                             | 45817            | 15425          | 30654            | 15425          | 12675          | 10865           | 12675          | 7840             | 6338           | 6094             |
| 152 - 180                             | 33643            | 11326          | 21969            | 11326          | 9405           | 8062            | 9405           | 5818             | 4703           | 4522             |
| 99 - 116                              | 21323            | 7179           | 14169            | 7179           | 6135           | 5258            | 6135           | 3795             | 3067           | 2949             |
| <b><math>Sr</math></b>                |                  |                |                  |                |                |                 |                |                  |                |                  |
| 257 - 315                             | 0.002            | 0.05           | 0.01             | 0.06           | 0.05           | 0.11            | 0.04           | 0.16             | 0.27           | 0.3              |
| 204 - 250                             | 0.003            | 0.08           | 0.01             | 0.08           | 0.07           | 0.15            | 0.04           | 0.21             | 0.35           | 0.35             |
| 152 - 180                             | 0.003            | 0.08           | 0.01             | 0.09           | 0.09           | 0.17            | 0.02           | 0.29             | 0.47           | 0.47             |
| 99 - 116                              | 0.005            | 0.14           | 0.02             | 0.15           | 0.15           | 0.28            | 0.18           | 0.44             | 0.72           | 0.71             |

### 5.5.2. Wall deposition and wall deposit re-entrainment related factors

Another plausible explanation for the fluctuations observed is that the fluctuations are related to wall deposition and re-entrainment processes. There is no significant difference between the dominant frequencies in the first three designs ( $P > 0.05$ ). This observation may be related to the fact that drying chambers 1, 2, 3, 6 and 7 are shared between these three designs. The dominant frequencies for Design 4 are slightly lower than those for the first three designs ( $P < 0.25$ ). Like the fitted parameters (i.e.,  $\tau$  and  $n$ ) for the CSTR-TIS model, larger variations in the dominant frequencies in Design 4 were observed, which may be related to the geometry of the drying chambers. This result suggests that the difference in fluctuation frequencies is likely linked to drying chambers 2 and 3, which are also the chambers where most wall deposition occurs (Langrish et al., 2020). The high wall-deposition fluxes observed in chambers 2 and 3 are probably due to the high-velocity droplets from the atomiser directly contacting the inner wall of the spray dryer. In addition to the comparison between the spray pattern and the shape of the drying chamber, chambers 2 and 3 are also the chambers with the highest gas temperatures, and the inlet gas temperatures are well above the sticky-point temperatures of the particles. Although the gas and particle temperatures are different in the initial stage of drying, this situation may also lead to a greater extent of wall deposition (Ozmen and Langrish, 2002). The conical shape design in Design 4 aims to fit better the spray pattern produced by the atomiser and thus reduce the chance of droplets depositing onto the inner wall.

Factors affecting the wall deposition and the re-entrainment process are summarised and shown in Figure 5.11 (Hanus and Langrish, 2007b).

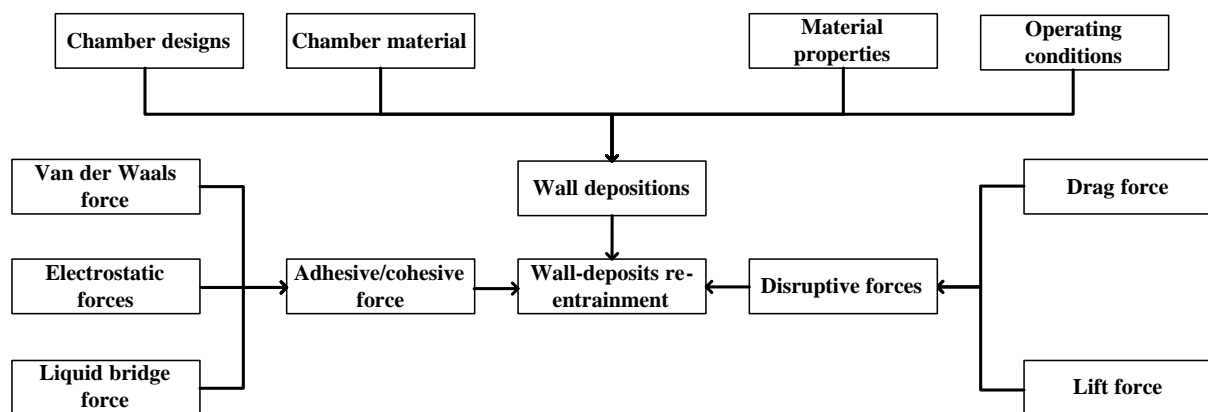


Figure 5.11 Factors affecting the wall deposition and wall deposit re-entrainment.

Other than the gravitational forces, one of the main disruptive forces (i.e., forces that remove wall deposits from the inner wall of the spray dryer) for the re-entrainment of wall deposits is the force from turbulent flow fluctuations inside the spray dryer. Within the

boundary layer of turbulent flows, approximately 50% of the turbulence energy production occurs at the inner layer for the boundary layer in the form of turbulent bursts (Kline et al., 1967). Therefore, it is important to estimate the turbulent burst frequency inside the spray dryer and compare it with the observed fluctuation frequencies. Here, in this thesis, turbulent burst frequencies have been estimated based on the data available in the literature since measuring the turbulent burst frequency is complicated and beyond the scope of this thesis. A few studies have proposed different methods for estimating the scaling behaviour of the turbulent burst frequency, including inner/outer variable scaling, mixed scaling, mixed modelling (inner and outer variables) and scaling based on the Taylor microscale (Blackwelder and Haritonidis, 1983; Lu and Willmarth, 1973; Metzger et al., 2010). Only the outer variable and inner variable scaling methods were used in this thesis. Although the later methods may be better in estimating the mean turbulent burst frequency in the drying chamber, they were not implemented in this thesis because some of the variables required for implementing the latest estimation methods were not measured due to practical issues and are beyond the scope of this thesis. Last but not least, this thesis did not estimate the mean turbulent burst frequencies in the conical drying chambers due to their more complicated geometry. Additionally, it appears that no work in the literature has investigated the mean turbulent burst frequency in a similar geometry (i.e., a conical chamber).

#### 5.5.2.1. *Turbulent burst frequency estimation – Outer variable*

The outer variable normalised turbulent burst frequency can be described by equation 5.2 (Lu and Willmarth, 1973):

$$f = \frac{1}{C * \left(\frac{\delta}{U_{\infty}}\right)} \quad 5.2$$

Here  $C$  is a constant depending on the Reynolds number,  $\delta$  is the thickness of the boundary layer, and  $U_{\infty}$  is the freestream velocity of the fluid.

The Reynolds number ( $Re$ ) at each flow rate is calculated using equation 5.3, a well-known engineering formula:

$$Re = \frac{\rho U_{\infty} L}{\mu} \quad 5.3$$

Here  $\rho$  is the density of the fluid,  $L$  is a characteristic dimension of the pipe, and  $\mu$  is the kinematic viscosity of the fluid.

As discussed previously, the turbulent frequency of the first two drying chambers is the main focus of this thesis. Thus the characteristics dimension used in the calculation for the Reynolds number is the diameter of these chambers (i.e.  $L = D = 0.3\text{m}$ ).

The boundary layer thickness can be estimated using equation 5.4.

$$\delta(x) = 0.37 * \frac{x}{Re_x^{\frac{1}{5}}} \quad 5.4$$

Where  $x$  is the distance from the start of the boundary layer.

### Sample calculation for outer variable methods:

A sample calculation is given for Design 1 at the maximum gas flow rate ( $315 \text{ m}^3/\text{hr}$ ).

For the purposes of simplifying the calculation, the following assumptions were made:

- The flow is assumed to be a fully developed turbulent flow as soon as the gas flow enters the drying chamber.
- The drying medium is assumed to be dry air at  $100^\circ\text{C}$ , and the gas properties do not change within the chamber.

Using the diameter of the drying chamber ( $D = 0.3 \text{ m}$ ) and the density ( $\rho$ ) and dynamic viscosity ( $\mu$ ) of dry air at  $100^\circ\text{C}$ , which are  $0.9458 \text{ kg m}^{-3}$  and  $2.18 \times 10^{-5} \text{ kg m}^{-1}\text{s}^{-1}$ , respectively.

$$Re = \frac{\rho U_\infty L}{\mu} = \frac{0.9458 * \frac{315}{3600} * 0.3}{\frac{1}{4} * 0.3^2 * \pi} = \frac{2.18 * 10^{-5}}{2.18 * 10^{-5}} = 16104$$

Based on the Reynolds number ( $Re$ ), the boundary layer thickness ( $\delta$ ) at  $0.1 \text{ m}$  from the top of the drying chamber ( $x = 0.1 \text{ m}$ ) can be estimated using equation 5.4.

$$\delta(0.1) = 0.37 * \frac{x}{Re_x^{\frac{1}{5}}} = 0.37 * \frac{0.1}{16104^{\frac{1}{5}}} = 0.00533 \text{ (m)}$$

The values of  $C$  vary significantly dependent on the methods for quantifying the turbulent burst within the range of the Reynolds number applicable to this thesis. As a result, maximum and minimum  $C$  values at each corresponding Reynolds number were used for the calculations.  $C_{max}$  and  $C_{min}$  values used for estimating turbulent burst frequency are shown in Table 5.4.

Table 5.4  $C_{max}$  and  $C_{min}$  were used for estimating outer normalised turbulent burst frequencies at different Re (Values of C are from Metzger et al. (2010)).

| Gas flowrate (m <sup>3</sup> /hr) | Re    | Cmin | Cmax |
|-----------------------------------|-------|------|------|
| 315                               | 16104 | 5    | 7    |
| 257                               | 13139 | 3    | 7    |
| 249                               | 12730 | 4.2  | 7.5  |
| 204                               | 10429 | 3    | 6.5  |
| 183                               | 9356  | 3    | 7    |
| 152                               | 7771  | 3.5  | 6.5  |
| 116                               | 5930  | 2.4  | 6.5  |
| 99                                | 5061  | 1    | 7    |

The turbulent burst frequency at a distance of 0.1 m from the top of the drying chambers can be estimated by substituting  $C_{max}$  and the estimated boundary layer thickness ( $\delta$ ) into equation 5.2.

$$f = \frac{1}{C * (\frac{\delta}{U_{\infty}})} = \frac{1}{7 * (\frac{0.00533}{\frac{315}{3600}})} = 33.2 \text{ Hz}$$

$$\frac{1}{\frac{1}{4} * 0.3^2 * \pi}$$

The calculations above were also performed for other conditions and different points in the drying chambers, and the results are shown in Tables 5.5 - 5.6.



Table 5.5 Estimated turbulent burst frequency based on outer variables for Design 1&2 (diameter = 0.3 m).

| <b>Gas flow rate<br/>(m<sup>3</sup>/hr)</b> | <b><i>Re</i></b> | <b><i>f<sub>min</sub></i> at <i>x</i> = 0.1 m</b> | <b><i>f<sub>max</sub></i> at <i>x</i> = 0.1 m</b> | <b><i>f<sub>min</sub></i> at <i>x</i> = 0.5 m</b> | <b><i>f<sub>max</sub></i> at <i>x</i> = 0.5 m</b> | <b><i>f<sub>min</sub></i> at <i>x</i> = 1 m</b> | <b><i>f<sub>max</sub></i> at <i>x</i> = 1 m</b> |
|---|------------------|---|---|---|---|---|---|
| 315   | 16104            | 33.2  | 46.4  | 6.6   | 9.3   | 3.3   | 4.6   |
| 249   | 12730            | 23.3  | 41.7  | 4.7   | 8.3   | 2.3   | 4.2   |
| 183   | 9356             | 17.3  | 40.3  | 3.5   | 8.1   | 1.7   | 4.0   |
| 116   | 5930             | 10.8  | 29.2  | 2.2   | 5.8   | 1.1   | 2.9   |

Table 5.6 Estimated turbulent burst frequency based on outer variables for Design 3 (diameter = 0.3 m).

| <b>Gas flow rate<br/>(m<sup>3</sup>/hr)</b> | <b><i>Re</i></b> | <b><i>f<sub>min</sub></i> at <i>x</i> = 0.1 m</b> | <b><i>f<sub>max</sub></i> at <i>x</i> = 0.1 m</b> | <b><i>f<sub>min</sub></i> at <i>x</i> = 0.5 m</b> | <b><i>f<sub>max</sub></i> at <i>x</i> = 0.5 m</b> | <b><i>f<sub>min</sub></i> at <i>x</i> = 1 m</b> | <b><i>f<sub>max</sub></i> at <i>x</i> = 1 m</b> |
|---|------------------|---|---|---|---|---|---|
| 257   | 13139            | 33.2  | 77.4  | 6.6   | 15.5  | 3.3   | 7.7   |
| 204   | 10429            | 26.9  | 58.4  | 5.4   | 11.7  | 2.7   | 5.8   |
| 152   | 7771             | 18.6  | 34.6  | 3.7   | 6.9   | 1.9   | 3.5   |
| 99  | 5061             | 10.0  | 70.0  | 2.0   | 14.0  | 1.0   | 7.0   |

### 5.5.2.2. Turbulent burst frequency estimation – inner variables

In a later study by Blackwelder and Haritonidis (1983), inner variables were found to be more appropriate for describing the scaling of the turbulent burst frequency. The inner variable normalised turbulent burst frequency can be described by equation 5.5:

$$f^+ = \frac{f}{\left(\frac{u_\tau^2}{\nu}\right)} \quad 5.5$$

Here,  $f^+$  is the outer variable normalised frequency,  $\nu$  is the kinematic viscosity of the gas, and  $u_\tau$  is the friction or shear velocity.

Re-arranging equation 5.5 gives the following equation:

$$f = \frac{u_\tau^2}{\nu} * f^+ \quad 5.6$$

The shear velocity is defined by equation 5.7 (Schlichting and Gersten, 2018):

$$u_\tau = \sqrt{\left(\frac{\tau_w}{\rho}\right)} \quad 5.7$$

Here,  $\tau_w$  is the wall shear stress, which can be estimated based on a force balance, as shown in equation 5.8 (Potter and Wiggert, 2009):

$$\tau_w = \frac{D}{4} * \frac{\Delta P}{L} \quad 5.8$$

Here,  $D$  is the pipe diameter,  $\Delta P$  is the pressure drop due to friction, and  $L$  is the length of the pipe. Drying chambers were treated as straight pipes to estimate the pressure drop along the drying chambers. For a straight pipe,  $\Delta P/L$  can be estimated using equation 5.9 (Potter and Wiggert, 2009):

$$\frac{\Delta P}{L} = \frac{4f_f}{D} * \rho * \frac{u^2}{2} \quad 5.9$$

Here,  $f_f$  is the Fanning friction factor. The Fanning friction factor can be estimated using the correlation developed by Haaland (1983):

$$f_f = \left( -3.6 * \log_{10} \left( \frac{6.9}{Re} + \left( \frac{\varepsilon}{3.7D} \right)^{\frac{10}{9}} \right) \right)^{-2} \quad 5.10$$

Here  $\varepsilon$  is the roughness of the surface.

Blackwelder and Haritonidis (1983) found that the normalised turbulent burst frequency is approximately 1/300 Hz when the Reynolds number ( $Re$ ) is within the range of 1000 to 10000.

### Sample calculation for inner variable method:

A sample calculation is given for Design 1 at the maximum gas flow rate (315 m<sup>3</sup>/hr).

For the purposes of simplifying the calculation, the following assumptions were made:

- The flow is assumed to be a fully developed turbulent flow as soon as the gas flow enters than drying chamber.
- The drying medium is assumed to be dry air at 100°C, and the gas properties do not change within the chamber.
- The surface roughness ( $\varepsilon$ ) of the inner wall of the drying chamber is 0.015 mm, and it does not change due to wall depositions.

Using the diameter of the drying chamber ( $D = 0.3$  m), and the density ( $\rho$ ) and dynamic viscosity ( $\mu$ ) of dry air at 100°C, which are 0.9458 kg m<sup>-3</sup> and 2.18 × 10<sup>-5</sup> kg m<sup>-1</sup>s<sup>-1</sup>, respectively.

$$Re = \frac{\rho U_{\infty} L}{\mu} = \frac{0.9458 * \frac{315}{3600} * 0.3}{\frac{1}{4} * 0.3^2 * \pi * 2.18 * 10^{-5}} = 16104$$

Based on the Reynolds number ( $Re$ ), the diameter of the drying chamber and the surface roughness ( $\varepsilon$ ) of the drying chamber, the fanning friction factor can be calculated using equation 5.9:

$$f_f = \left( -3.6 * \log_{10} \left( \frac{6.9}{Re} + \left( \frac{\frac{\varepsilon}{D}}{3.7} \right)^{\frac{10}{9}} \right) \right)^{-2} = \left( -3.6 * \log_{10} \left( \frac{6.9}{16104} + \left( \frac{\frac{0.0015}{1000}}{0.3} \right)^{\frac{10}{9}} \right) \right)^{-2}$$

$$= 0.007$$

Substituting equation 5.9 into equation 5.10 gives the equation:

$$\tau_w = \frac{D}{4} * \frac{\Delta P}{L} = f_f * \rho * \frac{u^2}{2} \quad 5.11$$

From the Fanning friction factor, the shear stress ( $\tau_w$ ) can be calculated using equation 5.11:

$$\tau_w = f_f * \rho * \frac{u^2}{2} = 0.007 * 0.9458 * \frac{\left( \frac{\frac{315}{3600}}{\frac{1}{4} * 0.3^2 * \pi} \right)^2}{2} = 0.00494 \text{ Pa}$$

From the shear stress ( $\tau_w$ ), the shear velocity ( $u_\tau$ ) can be estimated using equation 5.7:

$$u_\tau = \sqrt{\frac{\tau_w}{\rho}} = \sqrt{\frac{0.00494}{0.9458}} = 0.0723 \text{ m s}^{-1}$$

From the shear velocity ( $u_\tau$ ), and  $f^+ = 1/300$  from the literature (Blackwelder and Haritonidis, 1983), the mean turbulent burst frequency can be estimated using equation 5.6:

$$f = \frac{u_\tau^2}{\nu} * f^+ = \frac{0.0723^2}{\frac{2.18 * 10^{-5}}{0.9458}} * \frac{1}{300} = 0.76 \text{ Hz}$$

The calculations above were also performed for other conditions, and the results are shown in Table 5.7.

Table 5.7 Estimated turbulent burst frequency based on inner variables for Designs 1 - 3 (diameter = 0.3 m)

| <b>Gas flow rate (m<sup>3</sup>/hr)</b> | <b>Re</b> | <b>f (Hz)</b> | <b>Dominant frequency range (Hz)</b> |
|---|-----------|---------------|--------------------------------------|
| 315                                     | 16104     | 0.76          | 0.218 – 0.222                        |
| 257                                     | 13139     | 0.58          | 0.220                                |
| 249                                     | 12730     | 0.50          | 0.223 – 0.226                        |
| 204                                     | 10429     | 0.38          | 0.220                                |
| 183                                     | 9356      | 0.29          | 0.219 – 0.222                        |
| 152                                     | 7771      | 0.23          | 0.222                                |
| 116                                     | 5930      | 0.13          | 0.223 – 0.238                        |
| 99                                      | 5061      | 0.11          | 0.219                                |

As shown in Table 5.7, the estimated turbulent burst frequencies are higher than those observed, except for those at the lowest gas flow rate. Considering that the wall deposition occurred during the operation of the dryer, the roughness of the inner wall surface may be higher than the values assumed here. Thus, the actual turbulent burst frequencies are likely to be higher than the estimated values based on the inner variables.

Although the estimated turbulent burst frequencies are greater than the frequencies observed, they are still within the same order of magnitude. The two frequencies are not identical because the re-entrainment process is likely to be hindered by the material being spray dried. Given this hypothesis about the turbulent bursts acting as driving forces for the re-entrainment process, it would be expected that the frequencies of the bursts should be greater than the frequencies for the re-entrainment process because the material would be expected to dampen the frequency for the re-entrainment of the deposits. This hypothesised trend has indeed been observed here. In conclusion, it is reasonable to suggest that the fluctuations observed are most likely to be related to the wall deposition and re-entrainment process. The lowest wall-deposition re-entrainment frequency observed in Design 4 suggests that the conical chamber design has successfully reduced the chances of wall deposition occurring in the first two chambers (i.e., chambers 2&3).

### 5.6. Effect of feed stickiness

To investigate the effect of different feeds on the particle residence time distribution and the observed frequencies, a salt solution (NaCl, 8.8 wt%) was used as the feed instead of fresh

skim milk. Compared with skim milk, which generally gives amorphous lactose components in the spray-dried powders, salt gives crystalline powders, and it is less likely to deposit on the inner walls of the dryer (Flowers et al., 2019; Langrish et al., 2018). Other than stickiness, salt solution and skim milk have many physical properties that may also affect the particle residence time distribution. These differences in physical properties may not significantly impact the particle residence time distribution. For example, salt solutions are expected to have smaller initial droplet diameters under the same atomisation conditions due to their lower viscosity. The difference in initial droplet diameter may lead to a small difference in the relaxation time (i.e., the time for the droplets to slow down to the gas velocity). The relaxation times estimated by Stokes law for the droplet sizes relevant to this thesis ranges from 0.0003 to 0.001 seconds. The difference in relaxation time due to the difference in initial droplet size is insignificant compared with the overall particle residence time. Therefore, the effect of variation in the initial droplet size caused by different feed properties on the overall particle residence time may be ignored.

The salt solution experiments were only performed for the two latter designs (Design 3 and 4) at the maximum gas flow rate since they represent the effects of different drying chamber designs on the particle residence time distribution (Design 3 has cylindrical drying chambers, Design 4 has conical drying chambers).

Table 5.8 RTD measurement result summary for experiments with salt solution.

| Gas flow rate<br>(m <sup>3</sup> /hr) | Measurements   | Design 4 | Design 3 |
|---------------------------------------|--|----------|----------|
| 257                                   | Mean particle residence time ( $\tau$ , s)             | 14.9     | 8.3      |
|                                       | Mean gas time (s)                                      | 10.7     | 3.7      |
|                                       | Ratio between particle and air residence time<br>(s/s) | 1.4      | 2.2      |
|                                       | Number of equivalent CSTR in series (n)                | 9        | 15       |
|                                       | Fluctuation frequency (Hz)                             | 0.063    | 0.206    |
|                                       | $Re_{min}$   | 7359     | 15945    |

As shown in Table 5.8, the mean particle residence time is shorter, when salt solution is used as feed, compared with fresh skim milk ( $P < 0.05$ ). These results suggest that the mean particle residence time may be affected by the physical properties of the feed, which mainly

affects the wall deposition and re-entrainment behaviour. Experiments using salt solutions as the feed also show a tighter spread than skim milk, but the difference may not be significant (Design 3:  $P = 0.07$ , Design 4:  $P = 0.21$ ). The similar spread of the particle residence time distribution suggests that the spread is more dependent on the design of the drying chambers and recirculation and is less dependent on the material properties. The fluctuation frequencies observed when salt solution is used as the feed are slightly lower than those with skim milk (Design 3:  $P < 0.01$ , Design 4:  $P < 0.3$ ). This observation further supports the hypothesis that the fluctuations in the signals are indeed linked to the wall deposition and re-entrainment process, since the fluctuations are different for the different feed materials.

## 5.7. Other performance parameters

### 5.7.1. Solid recovery rates

The solid recovery rate is an important indicator of the performance of different designs of spray dryers because it is related to the throughput of the equipment. The recovery rate for Design 4 is slightly higher than other designs at most gas flow rates, but the difference may not be significant ( $P > 0.05$ ). The solid recovery rates decreased with the gas flow rate observed for all the designs. This behaviour may be related to the design of the spray dryer. Unlike traditional tall-form spray dryers, the spray dryer used in this thesis has two vertical drying columns connected by a cylindrical or box connection to reduce the height of the dryer while providing sufficient residence time for the drying of the particles. Lower gas flow rates may not be sufficient for carrying larger particles from the bottom of the spray dryer to the outlet. This hypothesis is supported by the decreasing trend in mean particle diameters ( $D_{x50}$  and  $D_{x90}$ ) with the decrease in gas flow rates. In addition to the small particle diameter, this hypothesis is also supported by observations in previous studies, where the highest wall deposition fluxes occur at the bottom of the drying chambers (Table 5.9) (Huang et al., 2018; Langrish et al., 2020).

Table 5.9 Physical properties of spray-dried powder collected from different designs and gas flow rates.

| Gas flow rate                   | Measurements         | 4-inch cylindrical connection | 6-inch cylindrical connection | Box connection | Conical drying chamber |
|---------------------------------|----------------------|-------------------------------|-------------------------------|----------------|------------------------|
| 257 - 315<br>m <sup>3</sup> /hr | Moisture content     | 3%                            | 2%                            | 3%             | 3%                     |
|                                 | Solids recovery rate | 43%                           | 51%                           | 48%            | 51%                    |
|                                 | $Dx_{10}$ (μm)       | 4.2                           | 4.7                           | 5.2            | 4.9                    |
|                                 | $Dx_{50}$ (μm)       | 8.4                           | 8.9                           | 11.8           | 10.0                   |
|                                 | $Dx_{90}$ (μm)       | 16.2                          | 13.2                          | 19.8           | 25.2                   |
| 204 - 250<br>m <sup>3</sup> /hr | Moisture content     | 3%                            | 2%                            | 4%             | 3%                     |
|                                 | Solids recovery rate | 33%                           | 37%                           | 41%            | 41%                    |
|                                 | $Dx_{10}$ (μm)       | 3.9                           | 4.2                           | 5.2            | 5.0                    |
|                                 | $Dx_{50}$ (μm)       | 7.0                           | 7.3                           | 11.5           | 9.6                    |
|                                 | $Dx_{90}$ (μm)       | 13.2                          | 12.0                          | 19.2           | 17.9                   |
| 152 - 180<br>m <sup>3</sup> /hr | Moisture content     | 3%                            | 3%                            | 5%             | 4%                     |
|                                 | Solids recovery rate | 14%                           | 13%                           | 17%            | 23%                    |
|                                 | $Dx_{10}$ (μm)       | 3.7                           | 4.0                           | 4.7            | 5.0                    |
|                                 | $Dx_{50}$ (μm)       | 6.6                           | 6.4                           | 9.1            | 9.2                    |
|                                 | $Dx_{90}$ (μm)       | 8.9                           | 13.2                          | 17.2           | 17.0                   |
| 99 - 116<br>m <sup>3</sup> /hr  | Moisture content     | 6%                            | 4%                            | 7%             | 7%                     |
|                                 | Solids recovery rate | 7%                            | 11%                           | 8%             | 6%                     |
|                                 | $Dx_{10}$ (μm)       | 4.4                           | 3.8                           | 4.8            | 5.1                    |
|                                 | $Dx_{50}$ (μm)       | 6.3                           | 6.2                           | 8.3            | 8.0                    |
|                                 | $Dx_{90}$ (μm)       | 10.3                          | 8.9                           | 14.5           | 12.5                   |



### 5.7.2. Morphology of the particles

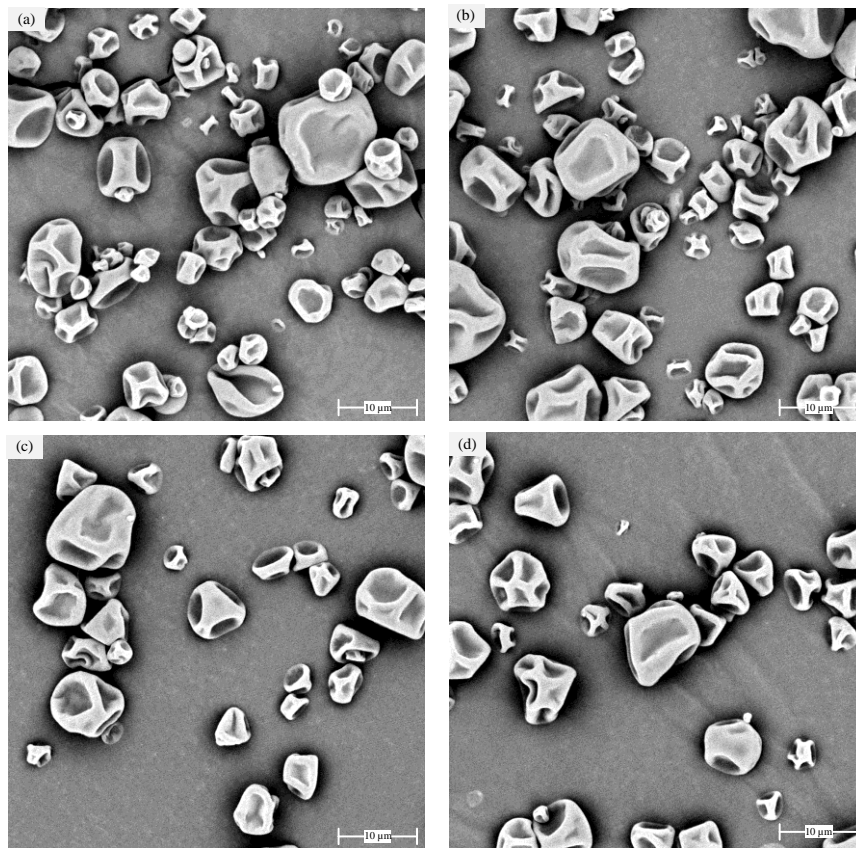


Figure 5.12 SEM image of particle collected from different gas flow from maximum gas flow rate (a): Design 1: 4-inch connection (b): Design 2: 6-inch connection (c): Design 3: Box connection (d): Design 4: Conical drying chamber.

The morphology of the particles may play an important role in the functionality (e.g., wettability and dispersibility) of the spray-dried products (Kim et al., 2002). SEM images of the particles collected from different designs are shown in Figure 5.12. Shrinkage in the particles was observed for most of the particles collected, which is related to the low drying temperature (inlet gas temperature: 100°C). The surfaces of particles dried at lower temperatures tend to stay moist for a longer period than the surfaces of the particles dried at higher temperatures. The moist surface of the particle allows shrinkage to occur during the spray-drying process (Hassan and Mumford, 1993; Hecht and King, 2000; Nijdam and Langrish, 2006; Walton, 2000). Other than the shrinkage in the observed particles, powders collected from Designs 1 and 2 have more small particles than those collected from Designs 3 and 4. This observation is also confirmed by the smaller particle diameter ( $D_{x10}$ ) for the particles collected from the first two designs. Since the same atomiser and atomising conditions

were used across all designs and operating conditions, the difference in particle size distribution depends more on the design of the spray dryer rather than the atomiser. Smaller particles in the collected samples are probably caused by the collisions between the particles and the inner wall of the spray dryer. Smaller particle diameters were observed for the first two designs compared with the later designs, which is likely to be linked to the smaller connection between the two drying columns.

## 5.8. Conclusion

In this chapter, the performances of four different designs of a pilot-scale spray dryer have been evaluated mainly based on the particle residence time distributions (RTD), solid recovery rates, and physical properties of the spray-dried products. The mean particle residence times increased as the gas flow rate decreased. The ratios between the particle and gas residence time varied significantly depending on the designs of the drying chambers and gas flow rates (Design 1: 1.5 – 2.7 s/s, Design 2: 1.5 – 2.6 s/s, Design 3: 1.5 – 2.5 s/s, and Design 4: 1.0 – 1.7 s/s). Later designs have a wider spread in the particle residence time distribution compared with the first two designs, and the spread is likely to be related to recirculation within the dryers. Fluctuations were observed in all measured signals and were probably linked to wall deposition and re-entrainment processes. In conclusion, the results have suggested that the shape of the first two drying chambers plays an important role in both the particle residence time distribution and the wall deposit re-entrainment process. The conical chamber design appears to be superior to the cylindrical design. Optimising the design of the connecting chamber (i.e., the bottom chamber) to reduce recirculation could be a focus of future studies. As discussed previously in Chapter 2, the mean particle residence time plays an important role in the study of reactions that occur within the spray dryers, including Maillard reactions. The study of RTD of different configurations of the spray dryer is an important part of studying Maillard reactions in spray dryers.

## Chapter 6. Modelling Maillard reactions under different spray drying conditions

This chapter mainly focused on developing a mathematical model for simulating the Maillard reactions kinetics during spray drying under different conditions and validating this model by comparison with experimental studies on the pilot-scale spray dryer described in Chapter 4.

| <b>Symbols</b> |   |
|----------------|---|
| $\mu$          | Viscosity                                       |
| $A$            | Surface area                                    |
| $C$            | Concentration                                   |
| $C_D$          | Drag coefficient                                |
| $C_p$          | Specific heat                                   |
| $d$            | Diameter  |
| $D$            | Diffusivity                                     |
| $E_a$          | Apparent activation energy                      |
| $G$            | Mass flow rate                                  |
| $h$            | Distance from the atomiser                      |
| $H_{evap}$     | Heat of evaporation                             |
| $H_h$          | Enthalpy  |
| $J$            | Mass transfer flux                              |
| $K$            | Mass-transfer coefficient                       |
| $k$            | Thermal conductivity/ reaction kinetic constant |
| $K_B$          | Boltzmann's constant                            |
| $L$            | Characteristic dimension                        |
| $M$            | Molar mass                                      |
| $n_{droplets}$ | Number of droplets                              |
| $Nu$           | Nusselt number                                  |
| $P$            | Pressure  |
| $p$            | Partial pressure                                |
| $Pr$           | Prandtl number                                  |
| $q$            | Heat transfer flux                              |
| $R$            | Radius  |
| $R$            | Ideal gas constant                              |
| $Re$           | Reynolds number                                 |
| $Sc$           | Schmidt number                                  |
| $Sh$           | Sherwood number                                 |
| $T$            | Temperature                                     |
| $U$            | Velocity  |
| $UA$           | Overall heat loss coefficient                   |
| $X$            | Moisture content                                |
| $Y$            | Humidity  |
| $\xi$          | Relative drying rate                            |
| $\rho$         | Density   |
| $\psi$         | Volume fraction                                 |

## 6.1. Introduction

Developing a mathematical simulation model for Maillard reactions kinetics during spray drying is highly desirable. Simulation models can provide a better understanding of how the quality of the spray-dried products can be affected by different factors. Additionally, a well-developed simulation model can also significantly reduce the difficulty and cost of the optimisation process. Other than the common factors such as temperature and reaction time, the kinetics of Maillard reactions can be affected by both the moisture content and the ratio between the reactants. A few studies have investigated the kinetic Maillard reactions that occur during the spray-drying process or under conditions that are applicable to spray drying (Gómez-Narváez et al., 2022, 2019; Miao and Roos, 2004; Park et al., 2016). However, the effects of the segregation process that occurs during spray drying do not appear to have been studied yet. The detailed mechanisms and the importance of the segregation process have been discussed in Chapter 2. In short, the segregation process is a process whereby different components separate from each other. The segregation process occurs during the spray drying process of a mixture (e.g., milk) and leads to a heterogenous distribution of the components, which may play an important role in the kinetics of Maillard reactions as it is a multi-reactant reaction (Baklouti et al., 1998; Kim et al., 2003; Nursten, 2005). As demonstrated in Chapter 4 and many other studies (Nursten, 2005), the ratio between the two primary reactants (i.e., sugars and proteins) is an important factor affecting the kinetics of Maillard reactions. Therefore, the potential impact of the component segregation process needs to be addressed to better understand the kinetics of Maillard reactions that occur during spray drying. The main focus of this chapter is to develop a model for Maillard reactions that occur during the spray-drying processes with the segregation process in mind.

The modelling process for predicting the Maillard reactions kinetic in spray dryers mainly involves two parts, one for the drying kinetics and the other one for the reaction kinetics. The drying kinetic model accounts for the physical part of the overall model, including temperature, moisture contents and distribution of components. Then, the reaction kinetic model estimates

the chemical reaction kinetics of Maillard reactions based on the conditions predicted by the drying kinetics model.

## 6.2. Modelling the drying kinetics

The main focus of this thesis is the kinetics of Maillard reactions in spray dryers, while the component segregation and the drying process are not the main focus of this thesis. Developing a new model for the drying kinetic and segregation process is beyond the scope of this thesis. There are mainly two types of approaches when modelling spray drying processes: the lumped-parameter approach and the distributed-parameter approach. Briefly, the lumped-parameter approach treats the droplets/particles inside the dryer as a whole, while in the distributed-parameter approach, particles are divided into many sublayers, and each layer can have different compositions and properties. The segregation and drying kinetic part of the distributed-parameter model used in this thesis have been adapted from a previous study by Wang and Langrish (2009b). For both lumped and distributed-parameter approaches, the changes in the external conditions outside the particles have been based on a parallel-flow model for the gas and particle conditions in the dryer (Langrish, 2009). This parallel-flow approach assumes that the gas and the solid particles flow in parallel to each other through the dryer and allows for changes in solid particle and gas properties as functions of distance through the dryer (Langrish, 2009). This approach is different to the approach used in a similar study by Gómez-Narváez et al. (2022), where *"The temperature and humidity of air in the drying chamber are"* assumed to be *"homogeneous and equal to the temperature and humidity in the outlet."* Their approach to the drying kinetic has some drawbacks compared with the parallel-flow modelling method. The well-mixed approach of Gómez-Narváez et al. (2022) only predicts the outlet temperature of the gas and the solids, and this approach assumes that the temperatures are *"homogeneous and equal"* throughout the chamber. This situation may result in differences between the actual and predicted temperatures in the dryer, particularly since peak particle temperatures have been reported inside co-current spray dryers that are higher than the outlet temperatures (Chiou et al., 2008). As shown in this thesis and many other studies, the particle temperature is an important factor for the kinetics of Maillard reactions in

spray dryers (Gómez-Narváez et al., 2019; Miao and Roos, 2004; Nursten, 2005; Park et al., 2016). Additionally, the effect of moisture content has not been considered in their model for heat damage simulation, although relevant data were measured and reported in their study.

### 6.2.1. Lumped-parameter modelling approach

For the purpose of comparison, a simulation model based on the lumped-parameter modelling approach has been developed. In this thesis, the parallel-follow modelling approach described in the study of Langrish (2009) is adapted here to describe the drying kinetics. This drying kinetic model is the same model used for modelling the particle temperature and moisture content history within the dryer in Chapter 4. Equations of this model are shown below:

#### Equations for droplet momentum:

The movement of the particles within the spray dryer is predicted based on momentum balances:

$$\frac{dU_{px}}{dh} = \left( \left( 1 - \frac{\rho_a}{\rho_p} \right) g - \frac{3 \rho_a C_D U_R (U_{px} - U_{airx})}{4 \rho_p d_p} \right) \frac{1}{U_{px}} \quad 6.1$$

$$\frac{dU_{pr}}{dh} = \left( -\frac{3 \rho_a C_D U_R (U_{pr} - U_{airr})}{4 \rho_p d_p} \right) \frac{1}{U_{px}} \quad 6.2$$

$$\frac{dU_{pt}}{dh} = \left( -\frac{3 \rho_a C_D U_R (U_{pt} - U_{airt})}{4 \rho_p d_p} \right) \frac{1}{U_{px}} \quad 6.3$$

Where  $\rho$  is density,  $C_D$  is the drag coefficient,  $U$  is the velocity,  $d$  is the diameter,  $h$  is the distance from the atomiser. The suffix  $R$  represents the relative difference between the air and the particle, the suffixes  $x$ ,  $r$ , and  $t$  represent the axial, radial and tangential velocity component, respectively, and suffixes  $p$  and  $air$  refer to the particle and the drying air, respectively.

The drag coefficient ( $C_D$ ) and overall relative velocity of the particle to gas ( $U_r$ ) can be calculated using equations 6.4 - 6.5 (Rhodes, 1998):

$$U_R = \sqrt{(U_{px} - U_{airx})^2 + (U_{pt} - U_{airt})^2 + (U_{pr} - U_{airr})^2} \quad 6.4$$

$$C_D = \frac{24}{Re_p} (1 + 0.15Re_p^{0.687}) \quad 6.5$$

Where  $Re$  is the Reynolds number.

The Reynolds number ( $Re$ ) can be calculated using a well-known engineering formula:

$$Re = \frac{\rho_{air} U_R L}{\mu_{air}} \quad 6.6$$

Here  $\rho$  is the density of the air ( $\text{kg m}^{-3}$ ),  $L$  is a characteristic dimension of the particle (i.e., the diameter of the particle, m), and  $\mu_{air}$  is the kinematic viscosity of the air (Pa.s).

### Mass transfer equations for droplets:

The rate of interfacial mass transfer between particle and drying gas is estimated based on the concept of a characteristics drying curve (CDC) (Keey, 1978):

$$\frac{dm_p}{dh} = -\xi \frac{A_p K_p}{U_{px}} (p_{vs} - p_{vp}) \quad 6.7$$

Where  $A$  is the surface area of the particle,  $K_p$  is the mass-transfer coefficient,  $p$  is the partial pressure,  $\xi$  is the relative drying rate. Suffixes  $vs$  and  $vp$  represent the vapour pressure on the surface of the particle and the vapour pressure in the bulk air, respectively.

Here, in this thesis, the drying rate is assumed to be only limited by the moisture content of the particles (i.e., a linear characteristic drying curve,  $\xi = X/X_i$ ). The linear CDC produces comparable results with more comprehensive approaches (e.g., non-linear CDC, REA) while being less computationally demanding (Langrish and Kockel, 2001).

The droplet diameter ( $d_p$ ), which is required for estimating the surface area of the droplets, can be calculated using equations 6.8 - 6.9:

$$d_p = d_{pi} \left( \frac{\rho_{pi} - 1000}{\rho_p - 1000} \right)^{\frac{1}{3}} \quad 6.8$$

$$\rho_p = \frac{1 + X}{1 + X \frac{\rho_s}{\rho_w}} \rho_s \quad 6.9$$



Here,  $X$  is the moisture content (dry basis, kg/kg). The suffix  $i$  represents the initial moisture content, and the suffixes  $s$  and  $w$  represent the solute and the solvent, respectively.

For the mass transfer between the gas and droplet, the mass-transfer coefficients can be estimated using equations 6.10 - 6.11:

$$K_p = \frac{M_w K_m}{M_a P} \quad 6.10$$

$$K_m = \frac{\rho_a D_v Sh}{d_p} \quad 6.11$$

Here,  $K_m$  is the mass transfer coefficient,  $M$  is the molar mass,  $P$  is the pressure inside the dryer ( $P = 101325 \text{ Pa}$ ),  $D_v$  is the diffusivity of water in air,  $Sh$  is the Sherwood number.

The water diffusivity of water in the air can be estimated using equation 6.12 (Perry et al., 1997):

$$D_v = \frac{1.117564 * 10^{-9} * T_p^{1.75} * 101325}{P} \quad 6.12$$

The Sherwood number can be calculated using the Frossling equation (Frossling, 1938):

$$Sh = 2.0 + 0.6 Re^{\frac{1}{2}} Sc^{\frac{1}{3}} \quad 6.13$$

Here,  $Sc$  is the Schmidt number.

The kinematic viscosity of the air can be estimated using equation 6.14:

$$\mu_{air} = (-0.0003 * T_{air_{abs}}^2 + 0.0687 * T_{air_{abs}} + 0.885) * 10^{-6} \quad 6.14$$

The Schmidt number can be calculated using equation 6.15:

$$Sc = \frac{\mu_{air}}{\rho_{air} D_v} \quad 6.15$$

### Heat transfer equations for droplets:

The heat transfer between particles and drying gas is mainly through convection and cooling due to water evaporation:

$$\frac{dT_p}{dh} = \frac{\pi d_p k_a Nu (T_{air} - T_p) + \frac{dm_p}{dh} U_{px} H_{evap}}{m_s (C_{ps} + X C_{pw}) U_{px}} \quad 6.16$$

Here,  $k_a$  is the thermal conductivity of air,  $Nu$  is the Nusselt number,  $H_{evap}$  is the heat of evaporation for water, and  $C_p$  is the specific heat capacity.

The thermal conductivity of air can be estimated using empirical correlation (Kannuluik and Carman, 1951):

$$k_a = 1.5207 * 10^{-11} * T_{air_{abs}}^3 - 4.8574 * 10^{-8} * T_{air_{abs}}^2 + 1.0184 * 10^{-4} * T_{air_{abs}} - 0.00039333 \quad 6.17$$

The Nusselt number ( $Nu$ ) for particles in the air can be estimated using empirical correlation (McAllister et al., 2013):

$$Nu = 2 + 0.6Re^{\frac{1}{2}}Pr^{\frac{1}{3}} \quad 6.18$$

Here,  $Pr$  is the Prandtl number for air.

The Prandtl number ( $Pr$ ) is defined as the ratio between momentum diffusivity and thermal diffusivity:

$$Pr = \frac{C_{p_{air}}\mu_{air}}{k_{air}} \quad 6.19$$

Here,  $C_{p_{air}}$  is the specific heat of air ( $J\ kg^{-1}\ K^{-1}$ ).

The specific heat of air ( $C_{p_{air}}$ ) can be calculated based on empirical correlation (Patanwar and Shukla, 2012):

$$C_{p_{air}} = 1.9327 * 10^{-10}T_{air_{abs}}^4 - 7.9999 * 10^{-7}T_{air_{abs}}^3 + 1.1407 * 10^{-3}T_{air_{abs}}^2 - 0.4489 * T_{air_{abs}} + 1057.3 \quad 6.20$$

The latent heat of evaporation of water  $\Delta H_{evap}$  at temperature  $T$  ( $^{\circ}C$ ) can be estimated using empirical correlation (Stanish et al., 1986):

$$\Delta H_{evap} = 2.792 * 10^6 - 160T_{air_{abs}} - 3.43T_{air_{abs}}^2 \quad 6.21$$

### **For the gas side heat and mass transfer:**

The heat and mass transfer for the drying gas can be estimated based on the heat and mass transfer occurring around the particles:

$$\frac{dY_b}{dh} = \frac{1}{G} \left( -\frac{dm_p}{dh} \right) n_{droplets} \quad 6.22$$

$$\frac{dH_h}{dh} = -\frac{1}{G} \left( \left( m_s (C_{ps} + X C_{pw}) \frac{dT_p}{dh} \right) n_{droplets} - UA * \frac{(T_{air} - T_{amb})}{L} \right) \quad 6.23$$

Here,  $Y_b$  is the humidity of the bulk air,  $n_{droplets}$  is the number of droplets,  $H_h$  is the enthalpy of humid air,  $G$  is the mass flow rate of air,  $UA$  is the overall heat loss coefficient from the dryer to the surroundings,  $T_{amb}$  is the ambient temperature, and  $L$  is the total length of the drying chamber.

### 6.2.2. Distributed-parameter modelling approach

The second modelling approach for the drying kinetic is the distributed-parameter modelling one. The distributed-parameter modelling approach has several advantages over the lumped-parameter modelling approach. For example, it is the inherently better approach to simulate the segregation process that occurs during the spray-drying process, indeed, the only real way to do this, given that the lumped-parameter approach assumed spatial homogeneity within particles. In addition to modelling the segregation process, the distributed-parameter modelling approach allows temperature and moisture content gradients across the particle, which are also critical factors for Maillard reaction kinetics.

The distributed-parameter modelling approach is mainly based on the finite volume method (FVM). FVM is a well-developed method that has been widely used in the field of simulations, including computational fluid dynamics (CFD). To apply FVM in this thesis, particles (integral volume) are divided into many sublayers (surface integral), and the changes in the composition are evaluated based on the fluxes across the different layers. The advantage of choosing FVM is that the heat and mass fluxes into/leaving the sub-layer are the same as the fluxes across the adjacent cells. Therefore, it is inherently conservative for both heat and mass. A schematic diagram demonstrating the FVM approach is shown in Figure 6.1.

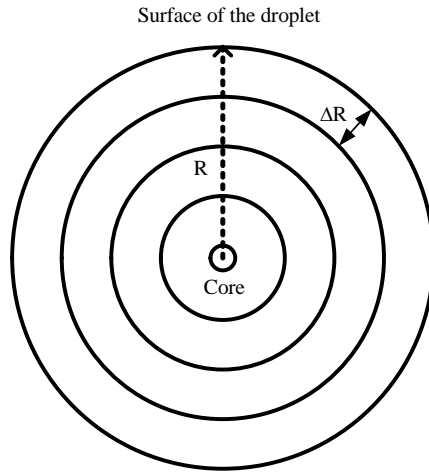


Figure 6.1 Schematic diagram for finite volume method (FVM) applied in this thesis.  $R$ : Radius of the droplet  $\Delta R$ : thickness of the sub-layer.

Three types of control volumes need to be considered, namely the core, intermediate and outermost layer. In the innermost layer (core), heat and mass are only transferred between the core layer and its adjacent layer. Slightly different to the core layer, the intermediate layers have heat and mass transfer from the two of its adjacent layers. For the outermost layer, heat and mass transfer occur between the inner layer adjacent to it and the drying gas.

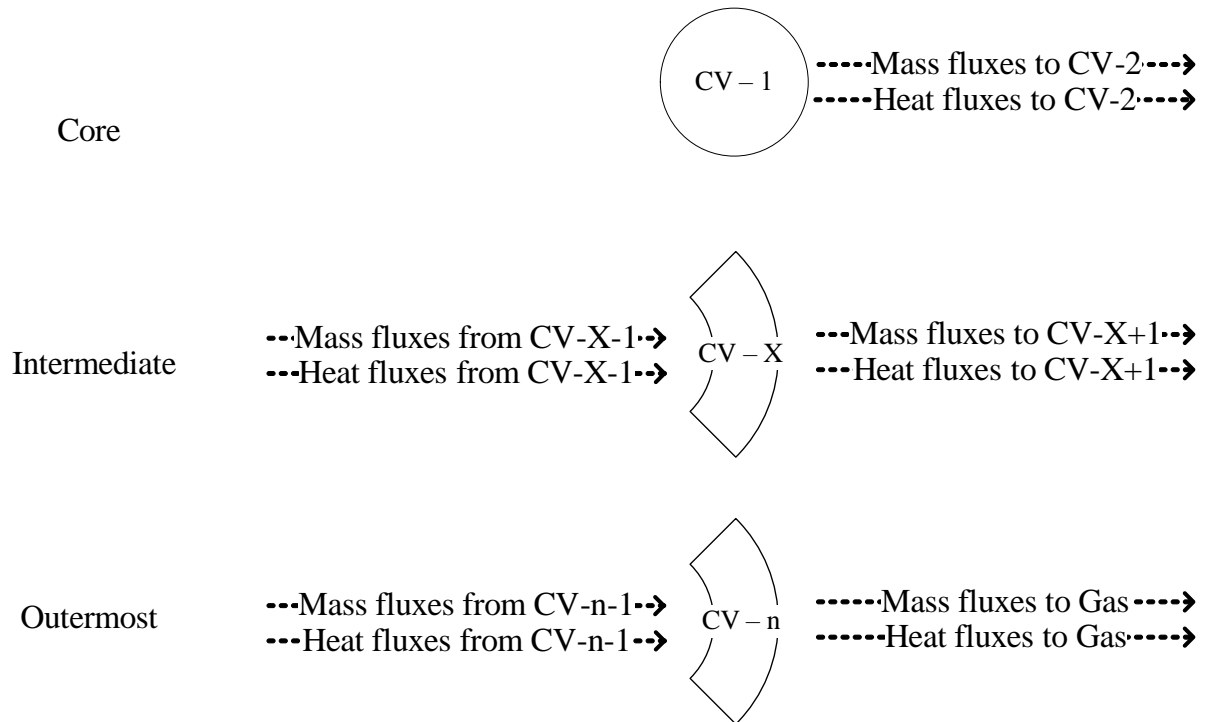


Figure 6.2 Schematic diagram of different cells used in this thesis. CV-1: Core control volume CV-X: intermediate control volume CV-n: outermost control volume.

Components and water transfer through different layers of the particles mainly through diffusion, and the mass transfer between the outermost layer and the drying medium (usually air) is mainly through convection and water evaporation. Similar to mass transfer, heat transfer for the intermediate and core layers is through conduction. While for the outermost layer, heat transfer occurs in the form of conductive heat transfer to its adjacent inner layer and convective heat transfer to the drying gas. In addition to conduction and convection, heat removal via water evaporation also needs to be considered for the outermost layer.

The distributed-parameter model used in this thesis is essentially a further refinement of the existing lumped-parameter model (parallel-flow model) within the particles. Some equations are shared between two approaches (e.g., equations for physical properties, heat and mass transfer between particles and gas, and gas-side heat and mass transfer), at the particle surfaces and outside the particle.

#### 6.2.2.1. Mass transfer

##### **Mass transfer between the outermost layer and drying gas**

In the outermost layer, water leaves the surface of the particle to the drying gas via evaporation. The rate of water evaporation at the outmost layer of the particle is adapted from the equation used for the lumped-parameter models (equation 6.7).

$$\frac{dm_{evap}}{dt} = \xi A_p K_p (p_{vs} - p_{vp}) \quad 6.24$$

Unlike the lumped-parameter model, the relative drying rate is estimated based on the moisture content of the outermost layer ( $X_n$ ) instead of the overall moisture content ( $X$ ) (i.e.  $\xi = X_n / X_i$ ).

The changes in the humidity of drying air can be described as:

$$\frac{dYb}{dt} = \frac{1}{G} \frac{dm_{evap}}{dt} n_{particles} \quad 6.25$$

### Mass transfer between the outermost layer and its adjacent inner layer

During spray drying, the moisture content of the outermost layer decreases, and the concentration of different components increases as water is evaporated from the surface of the particles to drying gas. Due to the concentration gradient between the outermost layer ( $n^{\text{th}}$  layer) and its adjacent inner layer ( $(n-1)^{\text{th}}$  layer), water diffuses from the  $(n-1)^{\text{th}}$  layer to the  $n^{\text{th}}$  layer, while other components diffuse toward the inner layers.

The mass transfer between layers can be described using the Fickian diffusion model:

$$J_i = -D_i * \frac{dC_i}{dR} \quad 6.26$$

Here  $J_i$  is the mass transfer flux across the surface ( $\text{kg m}^{-2}\text{s}^{-1}$ ),  $D_i$  is the diffusion coefficient of component  $i$ , and  $dC_i/dR$  is the concentration gradient of component  $i$  across distance  $dR$ .

The rate of mass transfer between two layers can be derived from the Fickian diffusion model:

$$\frac{dm_{i,j}}{dt} = J_{i,j} * A_j = \left( -D_{i,j} * \frac{(C_{i,j} - C_{i,j+1})}{R_j - R_{j+1}} \right) * 4\pi R_j^2 \quad 6.27$$

Here  $dm_{i,j}/dt$  is the mass flow ( $\text{kg/s}$ ),  $J_{i,j}$  is the mass transfer flux ( $\text{m}^2 \text{s}^{-1}$ ),  $A_j$  is the surface area ( $\text{m}^2$ ),  $D_{i,j}$  the diffusion coefficient ( $\text{kg m}^{-2}\text{s}^{-1}$ ),  $C_{i,j}$  is the mass concentration ( $\text{kg/m}^3$ ), and  $R_j$  is the radius (m). The subscript  $i$  and  $j$  denote component  $i$  and the  $j^{\text{th}}$  layer of the particles, respectively.

For the outermost layer:

$$\frac{dm_{i,n}}{dt} = \left( -D_{i,n} * \frac{(C_{i,n} - C_{i,n-1})}{R_n - R_{n-1}} \right) * 4\pi R_{n-1}^2 \quad 6.28$$

$$\frac{dm_{w,n}}{dt} = \left( -D_w * \frac{(C_{w,n} - C_{w,n-1})}{R_n - R_{n-1}} \right) * 4\pi R_{n-1}^2 \quad 6.29$$

### The overall water transfer in the outermost layer

The overall water transfer in the outermost layer can be described using equation 6.30:

$$\frac{dm_{w,n}}{dt} = \left( -D_w * \frac{(C_{w,n} - C_{w,n-1})}{R_n - R_{n-1}} \right) * 4\pi R_{n-1}^2 - \xi K_p (p_{vs} - p_{vp}) 4\pi R_n^2 \quad 6.30$$

### Mass transfer between intermediate layers

Similar to the mass transfer between the outermost layer and its adjacent inner layer, water and other components also transfer between the intermediate layers of the particle due to the concentration gradient. The mass transfer between the intermediate layers can be described using equations 6.31 - 6.32.

$$\frac{dm_{i,j}}{dt} = \left( -D_{i,j} * \frac{(C_{i,j} - C_{i,j-1})}{R_j - R_{j-1}} \right) * 4\pi R_{j-1}^2 + \left( -D_{i,j+1} * \frac{(C_{i,j+1} - C_{i,j})}{R_{j+1} - R_j} \right) * 4\pi R_j^2 \quad 6.31$$

$$\frac{dm_{w,j}}{dt} = \left( -D_w * \frac{(C_{w,j} - C_{w,j-1})}{R_j - R_{j-1}} \right) * 4\pi R_{j-1}^2 + \left( -D_w * \frac{(C_{w,j+1} - C_{w,j})}{R_{j+1} - R_j} \right) * 4\pi R_j^2 \quad 6.32$$

### Mass transfer in the core layer

In the core layer (the 1<sup>st</sup> layer), water and other components of particles are transferred between the core layer and its adjacent layer (i.e., the 2<sup>nd</sup> layer). The mass transfer between the core layer and the second layer can be described using equations 6.33 - 6.34:

$$\frac{dm_{i,1}}{dt} = \left( -D_{i,2} * \frac{(C_{i,2} - C_{i,1})}{R_2 - R_1} \right) * 4\pi R_1^2 \quad 6.33$$

$$\frac{dm_{w,1}}{dt} = \left( -D_w * \frac{(C_{w,2} - C_{w,1})}{R_2 - R_1} \right) * 4\pi R_1^2 \quad 6.34$$

### Diffusion coefficient of different components in the particles

During the drying process, water in the outermost layer evaporates, and water in the inner layers of the particle diffuses to the outer layers due to concentration differences. The diffusion coefficient of water within the particles can be described using equation 6.35 (Wang and Langrish, 2009b):

$$D_w = 2.5 * 10^{-9} * \left( \frac{T_{j,abs} + T_{avg,abs}}{2} \right)^{1.625} \quad 6.35$$

Here,  $D_w$  is the diffusivity of the water,  $T_{j,abs}$  is the absolute temperature (K) in the  $j^{th}$  layer of the particle and  $T_{avg,abs}$  is the average temperature (K) of the particles.

The diffusion coefficient of other components can be estimated based on the Stokes-Einstein equation:

$$D_i = \frac{K_B T}{6 * \pi \mu R_i} \quad 6.36$$

Here  $D_i$  is the diffusion coefficient ( $\text{m}^2 \text{s}^{-1}$ ) of component  $i$  at absolute temperature  $T$  (K).  $K_B$  is the Boltzmann's constant ( $1.38 * 10^{-23} \text{ J K}^{-1}$ ),  $\mu$  is the viscosity of the solvent (Pa.s), and  $R_i$  is the approximate radius of component  $i$ .

The viscosity of water over the temperature range of  $-8 \text{ }^\circ\text{C}$  to  $150 \text{ }^\circ\text{C}$  is estimated using the model proposed by Kestin et al. (1978):

$$\log_{10} \frac{\mu(T)}{\mu(20)} = \frac{20 - T}{T + 96} (1.2378 - 1.303 * 10^{-3}(20 - T) + 3.06 * 10^{-6}(20 - T)^2 + 2.55 * 10^{-8} * (20 - T)^3) \quad 6.37$$

$$\mu(T) = \mu(20) * 10^{\frac{20-T}{T+96}(1.2378-1.303*10^{-3}(20-T)+3.06*10^{-6}(20-T)^2+2.55*10^{-8}*(20-T)^3)} \quad 6.38$$

Here,  $\mu(T)$  is the viscosity (Pa s) of water at  $T \text{ }^\circ\text{C}$ , and  $\mu(20)$  is the viscosity of water at  $20 \text{ }^\circ\text{C}$  ( $0.001002 \text{ Pa s}$ ).

Estimated diffusion coefficients for the main components of milk in water based on the Stokes-Einstein equation are shown in Table 6.1.

Table 6.1 Estimated binary diffusion coefficients of main components of milk at infinity dilution (Foerster et al., 2016).

|                 | <b>Radius<br/>(nm)</b> | <b>Diffusivity at 25 °C<br/>(<math>\text{m}^2 \text{s}^{-1}</math>)</b> | <b>Diffusivity at 100 °C<br/>(<math>\text{m}^2 \text{s}^{-1}</math>)</b> |
|-----------------|------------------------|---|--|
| Protein micelle | 75                     | $2.91 * 10^{-12}$   | $1.30 * 10^{-11}$  |
| Lactose         | 0.5                    | $4.36 * 10^{-10}$   | $1.95 * 10^{-09}$  |

### **Diffusion of protein to the surface of particles**

Many studies have reported that protein molecules tend to move toward the air-water interface due to high surface activity (Graham and Phillips, 1979). The diffusion of protein to the outer surface of the particles can be described as follows:



$$\frac{dm_{protein,surf}}{dt} = \frac{4 * D_{protein,n} C_{protein,n-1} * A_p}{\pi * C_{protein,n-1} (R_n - R_{n-1})} \quad 6.39$$

Here,  $dm_{protein,surf}/dt$  is the mass transfer rate of proteins moving toward the surface of the particles.

### Formation of solids

During the spray drying process, the moisture content of the particles reduces, and solids are formed. The rate of solid formation can be described as follow:

$$\frac{dm_{solids,i,j}}{dt} = m_{w,j} * (C_{i,j} - S_{i,j}) \quad 6.40$$

Here,  $dm_{solids,i,j}/dt$  is the solid formation rate of component  $i$  in the  $j^{th}$  layer and  $S_{i,j}$  is the solubility of component  $i$  in the  $j^{th}$  layer. The solid formation rate in the simulation model has been constrained to be a non-negative value to prevent unrealistic results.

#### 6.2.2.2. Heat transfer

##### Heat transfer for the outermost layer

The heat transfer between the outermost layer of the particles and the drying gas is mainly in the form of convective heat transfer and cooling due to water evaporation. The heat transfer between the outermost layer and the gas can also be described by adapting equations from the lumped-parameter models (equations 6.16 and 6.23). In addition to the heat transfer with drying gas, the conductive heat transfer with its adjacent inner layer also needs to be considered.

The overall heat transfer for the outermost layer can be described as:

$$\frac{dH_n}{dt} = \pi d_p k_{air} Nu (T_{air} - T_n) - \frac{dmevap}{dt} H_{evap} - \frac{dcond_{n-1}}{dt} \quad 6.41$$

##### Heat transfer within particles

During spray-drying processes, the heat transfer within the particle is mainly in the form of conductive heat transfer. The convective heat transfer within the particle due to the movement

of different components is negligible as the convective fluxes are low (Wang and Langrish, 2009b). The flux of conductive heat transfer can be estimated using Fourier's law, a well-known engineering formula:

$$q = -k * \Delta T \quad 6.42$$

Here,  $q$  is the conductive heat transfer flux ( $\text{W m}^{-2}$ ),  $k$  is the conductivity of the component ( $\text{W m}^{-1}\text{K}^{-1}$ ), and  $\Delta T$  is the temperature difference (K).

The thermal conductivity of each component is estimated using empirical equations for estimating the thermal conductivity of common food components developed by Choi (1986):

$$k_{water} = 0.57109 + 1.7625 * 10^{-3} T_j - 6.7036 * 10^{-6} T_j^2 \quad 6.43$$

$$k_{lactose} = k_{carbohydrate} = 0.20141 + 1.387 * 10^{-3} T_j - 4.3312 * 10^{-6} T_j^2 \quad 6.44$$

$$k_{protein} = 0.17881 + 1.1958 * 10^{-3} T_j - 2.7178 * 10^{-6} T_j^2 \quad 6.45$$

The overall thermal conductivity of a particle layer can be estimated using the parallel model, where components are assumed to be parallel to the direction of heat flow (Sahin and Sumnu, 2006).

$$k_{overall,j} = \sum_{i=1}^3 k_{i,j} \psi_{i,j} \quad 6.46$$

The volume fraction of component  $i$  in the  $j^{\text{th}}$  layer of the particle can be calculated based on their mass fraction and density (Sahin and Sumnu, 2006).

$$\psi_{i,j} = \frac{V_{i,j}}{V_{total}} = \frac{\frac{C_{i,j}}{\rho_{i,j}}}{\sum_{i=1}^4 \left( \frac{C_{i,j}}{\rho_{i,j}} \right)} \quad 6.47$$

Here,  $\rho_{i,j}$  is the densities ( $\text{kg m}^{-3}$ ) of component  $i$  in the  $j^{\text{th}}$  layer of the particle, and they can be estimated using empirical correlations (Choi, 1986):

$$\rho_{water} = 997.18 + 3.1439 * 10^{-3} T_{abs} \quad 6.48$$

$$\rho_{lactose} = 1599.1 - 0.31046 T_{abs} \quad 6.49$$

$$\rho_{protein} = 1329.9 - 0.31046 T_{abs} \quad 6.50$$

Summarising the equations above, the heat transfer for the core layer and intermediate layers can be described using the following equations:

$$\frac{dh_1}{dt} = (k_{overall,1} * T_2 - T_1) * 4\pi R_1^2 \quad 6.51$$

$$\frac{dH_j}{dt} = (k_{overall,j} * (T_j - T_{j-1}) * 4\pi R_{j-1}^2 + (k_{overall,j+1} * (T_{j+1} - T_j) * 4\pi R_{j+1}^2) \quad 6.52$$

### 6.3. Kinetic model for Maillard reactions in spray drying

The second part of the simulation model is the model for the kinetics of Maillard reactions. Three factors need to be considered in the kinetic model, 1. temperature, 2. moisture content, and 3. ratios between the reactants. The combined effect of the above factors has been investigated using the methods described in Chapter 3 as part of the modelling process.

### 6.3.1. Effect of temperature on the kinetics of Maillard reactions

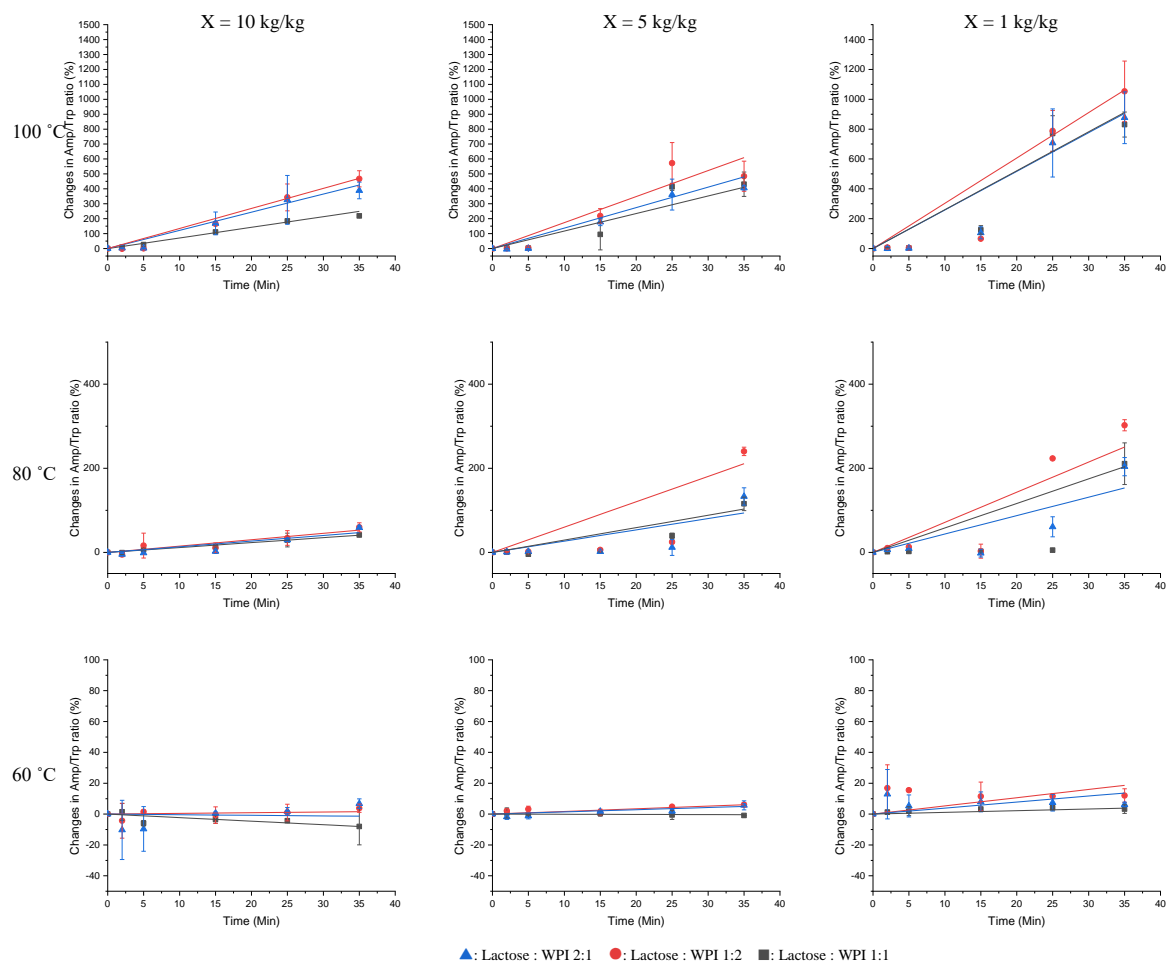


Figure 6.3 Experimentally measured changes in AMP/Trp ratios under different temperatures as functions of heating time for model systems with different reactant ratios and moisture contents.

As shown in Figure 6.3, the reaction rate increases as the heating temperature increases, which is common for many reactions. In the study by Gómez-Narváez et al. (2022), an increase in the rate of HMF formation has also been observed for the system (lactose:WPI 7:1) as the temperature increases. Similar to the AMP/Trp ratio used as an experimental indicator in this thesis, HMF is another indicator for Maillard reactions (Morales and Boekel, 1998). The reaction rate at 60°C is low regardless of the moisture content and the reactant ratio. When the temperature increased from 80°C to 100°C, a significant increase in the reaction rate was observed for all conditions. These observations are similar to those in Chapter 4, where the reaction rate also increased significantly when the temperature rose above a certain value. The

significant increase in reaction rate is likely to be linked to protein denaturation. During protein denaturation, the special structure of proteins changes, exposing more reactive functional groups. As a result of having more exposed reactive sites, the reaction rate increases. Other studies have also reported that the rate of protein denaturation increases when the temperature rises above 80°C (Jaskulski et al., 2017).

#### 6.3.1. Effect of moisture content on the kinetics of Maillard reactions

It is clear that the reaction rates for model systems with lower moisture contents are much higher than those with higher moisture contents. The higher reactant concentrations in the samples with lower moisture contents are a key cause of these observations. As discussed in Chapter 2, the moisture content plays an important role in the reaction kinetics of Maillard reactions. When the moisture contents are high, the reaction rate is decreased due to the dilution effect, and the reaction rates are higher at low moisture contents due to higher reactant concentrations. In a relevant study by Carabasa-Giribet and Ibarz-Ribas (2000), glucose solutions with moisture contents ranging from  $X = 5.7$  kg/kg to  $X = 1.2$  kg/kg and a fixed sugar-to-protein ratio of (5000:1) were heated at temperatures from 85°C to 100°C for up to 80 hours. The highest reaction rate was also observed for the model systems with the lowest moisture content. The relationship between moisture content and the reaction rate is complicated for systems with lower moisture contents. In the study of Gómez-Narváez et al. (2022), model systems with lower moisture contents ( $X$  ranging from 0.0291 to 0.0974 kg/kg) were used. The rate of protein denaturation (measured as loss in available lysine) increases as the moisture content increases, probably due to higher reactant concentrations. While for the Maillard reactions indicators (i.e., Furosine and browning index (BI)), the rate of formation of these markers was found to be reduced as the moisture content decreased. This observation is probably due to the mobility of molecules being limited at lower moisture contents, and thus the reaction rate is decreased (Schmitz-Schug et al., 2014).

#### 6.3.2. Effect of reactant ratio on the kinetics of Maillard reactions

A higher Maillard reaction rate for model systems with higher protein-to-lactose ratios at all moisture contents and heating temperatures has been observed. The highest reaction rate

has been observed in the model systems with the lowest lactose-to-WPI ratio (1:2). This trend is consistent with the findings in Chapter 4, where the model system with a lower lactose-to-WPI ratio (1:2) was found to be more sensitive to Maillard reactions under the same spray-drying conditions compared with model systems having lower WPI contents. Again, this observation is likely to be due to protein concentrations being the rate-limiting factor in the kinetics of Maillard reactions that occur during spray drying. It is also worth mentioning that for the samples with the lowest moisture content ( $X = 1$  kg/kg), the Maillard reaction rates in those samples were similar, especially at higher temperatures. This observation suggests that, at lower moisture contents and higher temperatures, the actual ratios of the components may be different to those in the initial solution due to reduced protein solubility. Unlike lactose, whose solubility increases with temperature (Table 6.2), the solubility of whey protein decreases when the temperature increases, mainly due to denaturation (Table 6.3). Protein unfolding (denaturation) exposes more reaction sites, which may increase the reaction rate. At the same time, the exposed hydrophobic functional groups reduce the solubility of proteins in water and thus limit the mobility of the molecules (Pelerine and Gomes, 2008).

Table 6.2 Lactose solubility in water (Hudson, 1904).

| Temperature (°C) | Solubility (wt%) |
|------------------|------------------|
| 0                | 10.6             |
| 15               | 14.5             |
| 25               | 17.8             |
| 39               | 24.0             |
| 49               | 29.8             |
| 64               | 39.7             |
| 73               | 46.3             |
| 89               | 58.2             |

Table 6.3 Whey protein isolate solubility in water (Pelerine and Gomes, 2008).

| Temperature (°C) | Solubility (wt%) |
|------------------|------------------|
| 40               | 100              |
| 50               | 85               |
| 60               | 68               |
| 70               | 78               |
| 80               | 73               |
| 90               | 32               |

In summary, temperature, moisture content, and component ratios play a complex and important role in the kinetics of Maillard reactions that occur during spray-drying processes. At higher moisture contents, temperatures and component ratios are the dominant factors for the kinetics of Maillard reactions, while at lower moisture contents, the component ratio becomes less critical, likely due to lower solubilities and limited mobility of the molecules.

### 6.3.3. Fitting of the kinetic parameters

The experimental results have been fitted with different kinetic models to quantitatively represent and evaluate the reaction rate for each combination of factors.

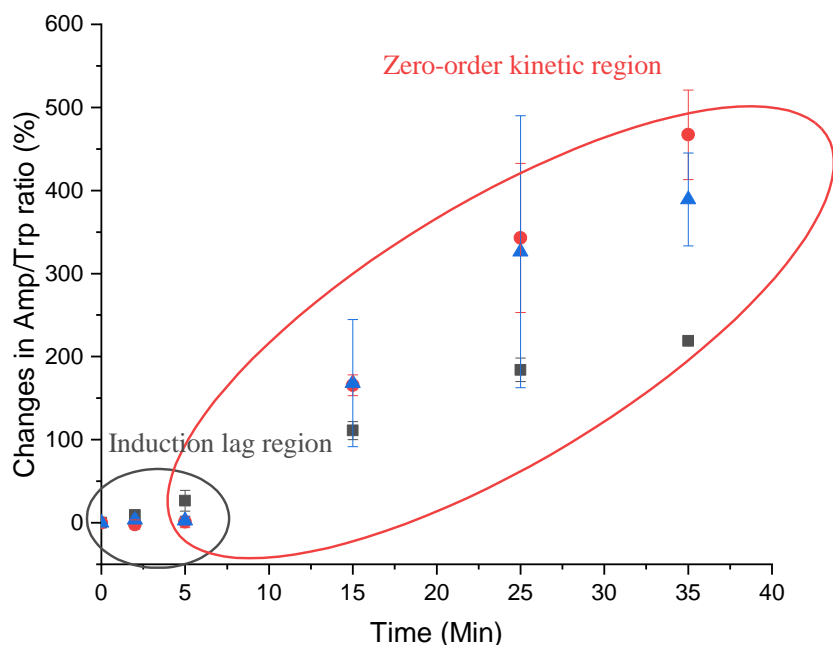


Figure 6.4 Experimentally measured changes in AMP/Trp ratios for model systems with different reactant ratios with  $X=10$  kg/kg heated at  $100^{\circ}\text{C}$ .

As shown in Figure 6.4, there is clearly an induction lag in the changes in Amp/Trp ratios during the initial stages of the experiment. During the induction period, the changes in the extent of Maillard reactions were not significant. Such an induction period could also be found in samples collected from other experimental conditions. Miao and Roos (2004) have also reported similar behaviour in changes in optical density (OD) at both 280 nm and 420 nm. Optical density at 420 nm is a marker commonly used for measuring the degree of browning in samples, and it is sometimes used as an indicator for the extent of Maillard reactions. In their study, an induction period was also found for the changes in OD. The rate of changes in OD during the first 15 minutes of heating time is low, and beyond the induction lag period, the change in OD appeared to be following zero-order kinetics (Miao and Roos, 2004). In both their study and this thesis, samples were initially at room temperature prior to heating. Thus,



the actual temperature of the samples at the start of the experiments is lower than the desired reaction temperature. However, it is not reasonable to preheat the samples to the desired temperature before experiments, as thermal degradation does occur during the preheating process. This disagreement between the actual and experimental temperatures is likely to be the main cause of the induction lag observed in the experimental results (Miao and Roos, 2004). As a result, the reaction kinetics constant fitted in this thesis is based on the changes in AMP/Trp ratios at steady state (i.e., after the induction period).

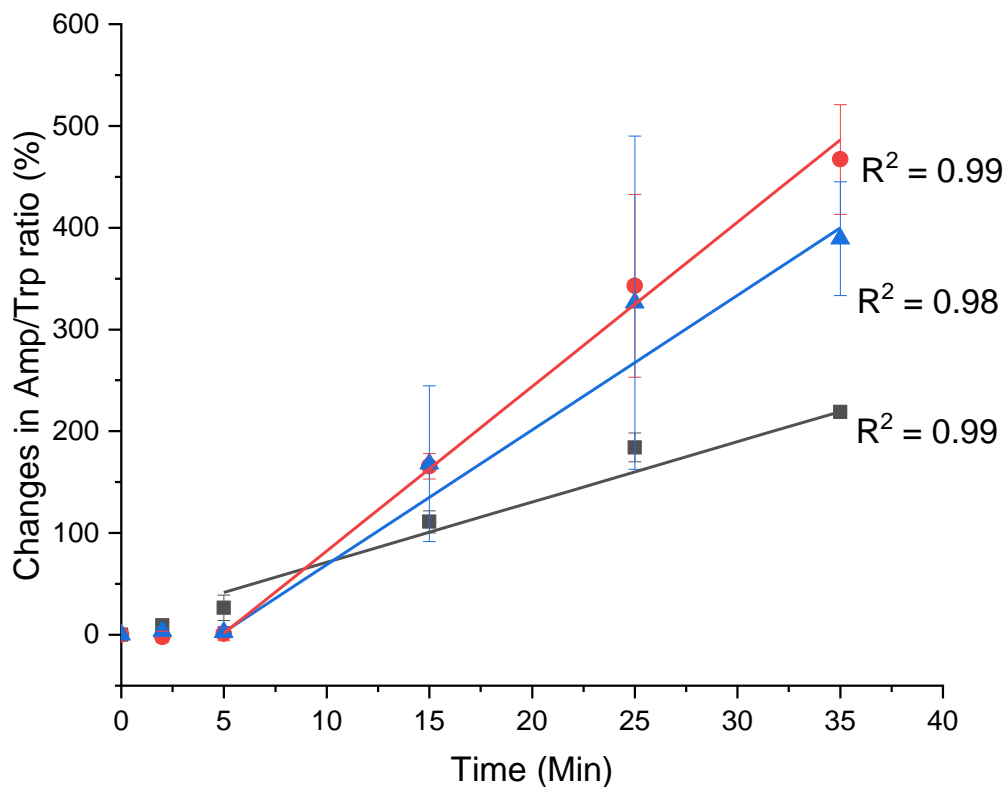


Figure 6.5 Example of the kinetic constant fitting process ( $X=10$  kg/kg heated at  $100^{\circ}\text{C}$  with different reactant ratios).

As shown in Figure 6.5, the AMP/Trp ratio increased linearly with time after the induction period, suggesting that changes in AMP/Trp ratio probably follow zero-order reaction kinetics. Similar behaviour is observed in experiments with different heating temperatures and reactant ratios, except for experiments with a heating temperature of  $60^{\circ}\text{C}$ . No clear induction lag period was observed in experiments with a heating temperature of  $60^{\circ}\text{C}$ , probably related to a very

small overall change in the AMP/Trp changes over time. Therefore, for experiments with a heating temperature of 60°C, the reaction rate constants have been estimated based on all the data points that are available.

For zero-order kinetics, the reaction kinetics can be described using equation 3.7:

$$\frac{dAMP/Trp}{dt} = k \quad 6.53$$

The zero-order kinetic constant,  $k$ , of experimental data after the induction lag period has been fitted using MATLAB 2022b with the least-squares method, and the fitted results are summarised in Table 6.4.

Table 6.4 Fitted kinetics parameters ( $k$  in cps/cps/S \*10<sup>-5</sup>) of experimental data (Zero-order).

| <b>100 °C</b>  |                |                |                |
|----------------|----------------|----------------|----------------|
| Lactose : WPI  | 1 : 2          | 2 : 1          | 1 : 1          |
| $X = 10$ kg/kg | $6.6 \pm 0.8$  | $15.0 \pm 1.7$ | $9.6 \pm 1.0$  |
| $X = 5$ kg/kg  | $12.3 \pm 0.7$ | $18.9 \pm 2.0$ | $13.9 \pm 4.2$ |
| $X = 1$ kg/kg  | $31.4 \pm 1.7$ | $37.8 \pm 0.2$ | $34.1 \pm 3.5$ |
| <b>80 °C</b>   |                |                |                |
| Lactose : WPI  | 1 : 2          | 2 : 1          | 1 : 1          |
| $X = 10$ kg/kg | $0.8 \pm 0.0$  | $1.8 \pm 0.2$  | $1.5 \pm 0.2$  |
| $X = 5$ kg/kg  | $2.8 \pm 0.4$  | $4.3 \pm 0.1$  | $2.5 \pm 0.6$  |
| $X = 1$ kg/kg  | $4.1 \pm 0.9$  | $9.2 \pm 0.4$  | $4.5 \pm 0.5$  |
| <b>60 °C</b>   |                |                |                |
| Lactose : WPI  | 1 : 2          | 2 : 1          | 1 : 1          |
| $X = 10$ kg/kg | $-0.4 \pm 0.4$ | $0 \pm 0.1$    | $0.1 \pm 0.0$  |
| $X = 5$ kg/kg  | $0 \pm 0.0$    | $0 \pm 0.0$    | $0.2 \pm 0.0$  |
| $X = 1$ kg/kg  | $0.2 \pm 0$    | $0.1 \pm 0.1$  | $0.2 \pm 0.1$  |

#### 6.3.4. Sensitivity analysis for different factors

To determine the relative importance of the various factors on the reaction kinetic constant for Maillard reactions, analysis of variance (ANOVA) was performed for all the fitted kinetic constants. The probability ( $P$ ) of retaining the null hypothesis (i.e., there is no significant difference between the sets of data being compared, or in other words, the factor has no significant impact on the reaction kinetics) is shown in Tables 6.5 - 6.7. Here, in this thesis, the interpolation of the ANOVA results is based on a 95% confidence level (i.e., the threshold value for  $P$  is 0.05, reject the null hypothesis if  $P > 0.05$ ). The ANOVA results show that

different heating temperatures significantly impact the fitted reaction rate constants ( $P < 0.05$  for all conditions). The effect of moisture contents on the fitted reaction rate constants is significant except for the experiments with a heating temperature of 60°C, probably linked to the larger variance for those experiments due to the low extent of Maillard reactions in the heated samples. The component ratios appear to have the least impact on the fitted reaction constant, especially for experiments with a high heating temperature and low moisture contents ( $P > 0.05$ ). This observation agrees well with the previous hypothesis for the effect of solubilities for different components on the actual reactant ratio. In conclusion, out of the three factors, the component ratios have the least impact on the reaction kinetics.

Table 6.5  $P$  values for the impact heating temperature on the fitted reaction kinetic constants at the same moisture content and reactant ratio.

| <b>Lactose : WPI</b> | <b>1 : 2</b> | <b>2 : 1</b> | <b>1 : 1</b> |
|----------------------|--------------|--------------|--------------|
| $X = 10$ kg/kg       | 0.00         | 0.00         | 0.00         |
| $X = 5$ kg/kg        | 0.00         | 0.00         | 0.02         |
| $X = 1$ kg/kg        | 0.00         | 0.00         | 0.00         |

Table 6.6  $P$  values for the impact moisture content on the fitted reaction kinetic constants at the same heating temperature and reactant ratio.

| <b>Lactose : WPI</b> | <b>1 : 2</b> | <b>2 : 1</b> | <b>1 : 1</b> |
|----------------------|--------------|--------------|--------------|
| 100 °C               | 0.00         | 0.00         | 0.01         |
| 80 °C                | 0.02         | 0.00         | 0.02         |
| 60 °C                | 0.27         | 0.02         | 0.11         |

Table 6.7  $P$  values for the impact reactant ratios on the fitted reaction kinetic constants at the same heating temperature and moisture content.

|        | <b><math>X = 10</math> kg/kg</b> | <b><math>X = 5</math> kg/kg</b> | <b><math>X = 1</math> kg/kg</b> |
|--------|----------------------------------|---------------------------------|---------------------------------|
| 100 °C | 0.01                             | 0.18                            | 0.14                            |
| 80 °C  | 0.02                             | 0.04                            | 0.01                            |
| 60 °C  | 0.30                             | 0.07                            | 0.03                            |

#### 6.4. Prediction model for kinetics constants

In this thesis, three different factors that can affect the Maillard reaction kinetics have been considered: 1. heating temperatures, 2. moisture contents of the samples, and 3. ratios between two different reactants. There are three independent variables and one dependent variable, making the rate constant prediction model effectively a 4D ( $x, y, z, w$ ) mathematical model. Fitting a 4D mathematical model is possible but difficult, especially considering the fact that

three independent variables may not be truly independent of each other. For example, the temperature and the moisture content can affect the actual reactant ratios by affecting the solubility of the reactants. Therefore, in this thesis, the kinetic constant prediction model has been reduced to a 3D ( $x, y, z$ ) mathematical model, and the effect of the third factor has been included as "switches" in the overall simulation model. In other words, 3D models have been developed separately based on the two independent variables that have the most impact on the reaction kinetics for each corresponding value of the third independent variable. In the sensitivity analysis of the factors investigated in this thesis, the changes in reactant ratios were found to be having the least impact on the reaction kinetics. As a result, a prediction mode for the kinetic constants has been developed based on the temperature and moisture content for each reactant ratio.

#### 6.4.1. Temperature dependency of the kinetics constant

The temperature dependence of the reaction rate can be described using the well-known Arrhenius equation (Arrhenius, 1889):

$$k = A * \exp \frac{-E_a}{RT} \quad 6.54$$

Here,  $k$  is the rate constant,  $A$  is a constant,  $E_a$  is the activation energy of the reaction (J/mol),  $R$  is the ideal gas constant (J/K/mol), and  $T$  is the absolute temperature (K).

The Arrhenius equation has been widely used in many studies to study reactions during food processing. An alternative form of the Arrhenius equation is more often used for predicting the changes in reaction constants with the temperature (Peleg et al., 2012):

$$k(T) = k_{ref} * \exp \left( c * (T - T_{ref}) \right) \quad 6.55$$

Here,  $k(T)$  is the rate constant at temperature  $T$  (K),  $k_{ref}$  is the rate constant at the reference temperature  $T_{ref}$  (K), and  $c$  is a constant ( $K^{-1}$ ).

The temperature dependence of the reaction rate constants obtained from fitting zero-order kinetic models has been fitted using the modified Arrhenius equation (equation 6.55). The fitting processes were carried out using the non-linear curve fit function in OriginPro 2022.

80 °C has been chosen as the reference temperature ( $T_{ref}$ ) as it is the average heating temperature used in this thesis, and its corresponding average rate constants are regarded as reference rate constants ( $K_{ref}$ ).

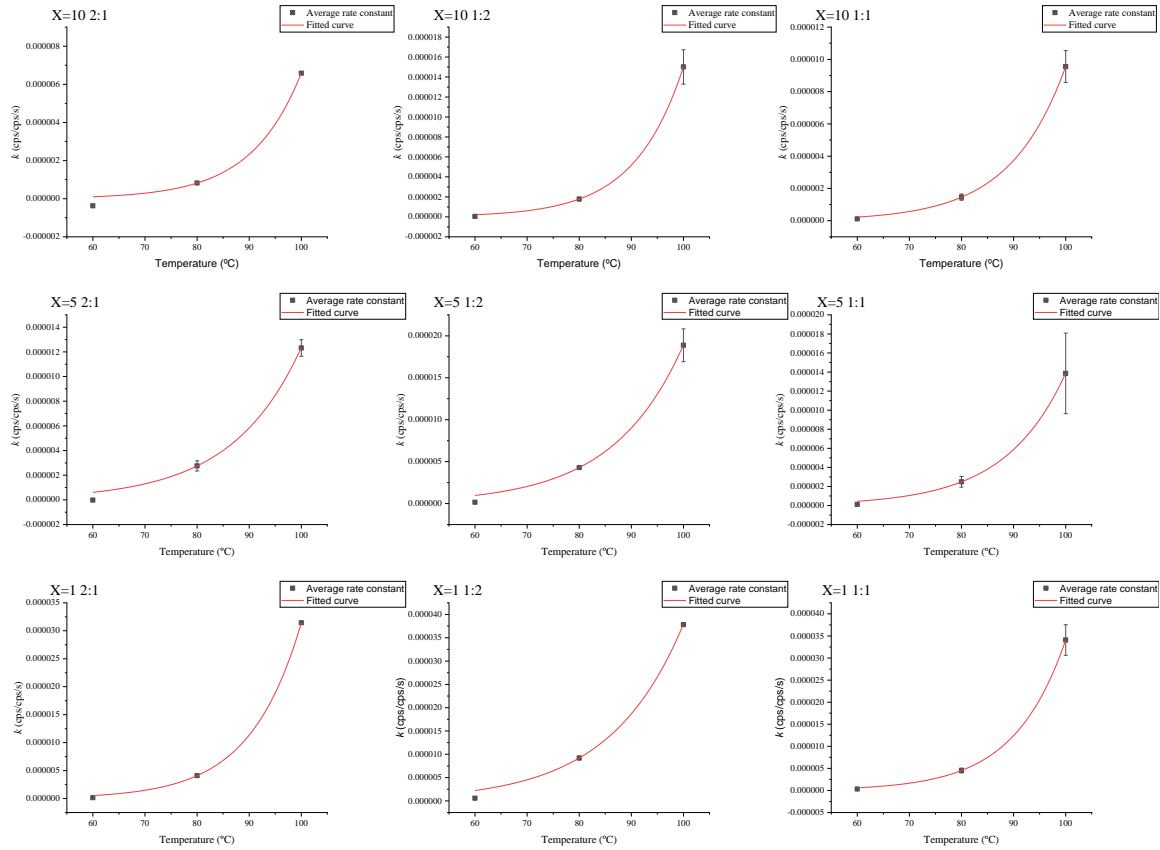


Figure 6.6 Fitting result of the Arrhenius equation for the rate constant.

Table 6.8 P values for the impact reactant ratios on the fitted reaction kinetic constants under the same heating temperature and reactant ratio.

| Lactose : WPI | Moisture contents | $c$               | $R^2$ |
|---------------|-------------------|-------------------|-------|
| 2 : 1         | $X= 10$ kg/kg     | $0.104 \pm 0.003$ | 0.98  |
|               | $X= 5$ kg/kg      | $0.075 \pm 0.002$ | 0.99  |
|               | $X= 1$ kg/kg      | $0.102 \pm 0.001$ | 0.99  |
| 1 : 2         | $X= 10$ kg/kg     | $0.107 \pm 0.002$ | 0.98  |
|               | $X= 5$ kg/kg      | $0.074 \pm 0.002$ | 0.99  |
|               | $X= 1$ kg/kg      | $0.071 \pm 0.001$ | 0.99  |
| 1 : 1         | $X= 10$ kg/kg     | $0.094 \pm 0.002$ | 0.99  |
|               | $X= 5$ kg/kg      | $0.086 \pm 0.005$ | 0.92  |
|               | $X= 1$ kg/kg      | $0.101 \pm 0.002$ | 0.99  |

As shown in Figure 6.6 and Table 6.8, the modified Arrhenius equation fitted the behaviour of the rate constant changes with changing temperatures well. Therefore, the Arrhenius type of

equations has been chosen for modelling the temperature dependence of the rate constant in this thesis.

#### 6.4.2. Combined effects of temperature and moisture content

During the spray-drying process, the moisture content of the particles changes rapidly, and changes in moisture contents also play an important role in the reaction kinetics. Therefore, the effect of moisture content on the reaction kinetics also needs to be considered in the modelling. Unlike the temperature dependency of reaction rates, which usually can be described using the Arrhenius equation or Arrhenius-type equations, modelling the effect of both the moisture content and temperature is more complicated. In most studies concerning reactions that occur during drying processes, different models were used to account for the effect of moisture content as the existing model does not fit well with experimental data (Di Scala and Crapiste, 2008; Qiu et al., 2018; Schmitz-Schug et al., 2014). The general approach used in those studies is making the constants in the modified Arrhenius equation (i.e.,  $k_{ref}$  and  $c$ ) moisture content dependent. Here, in this thesis, a similar approach has also been used for modelling the temperature and moisture content dependency of the rate constants.

In the Arrhenius-type equations, there are usually two parameters,  $k_{ref}$ , the frequency factor or the pre-exponential factor and  $c$ , proportional to the energy required for initiating the chemical reactions (i.e., apparent activation energy,  $E_a$ ). The changes in these two factors,  $k_{ref}$  and  $c$ , with different moisture contents have been plotted against the changes in moisture contents and shown in Figures 6.7 – 6.8.

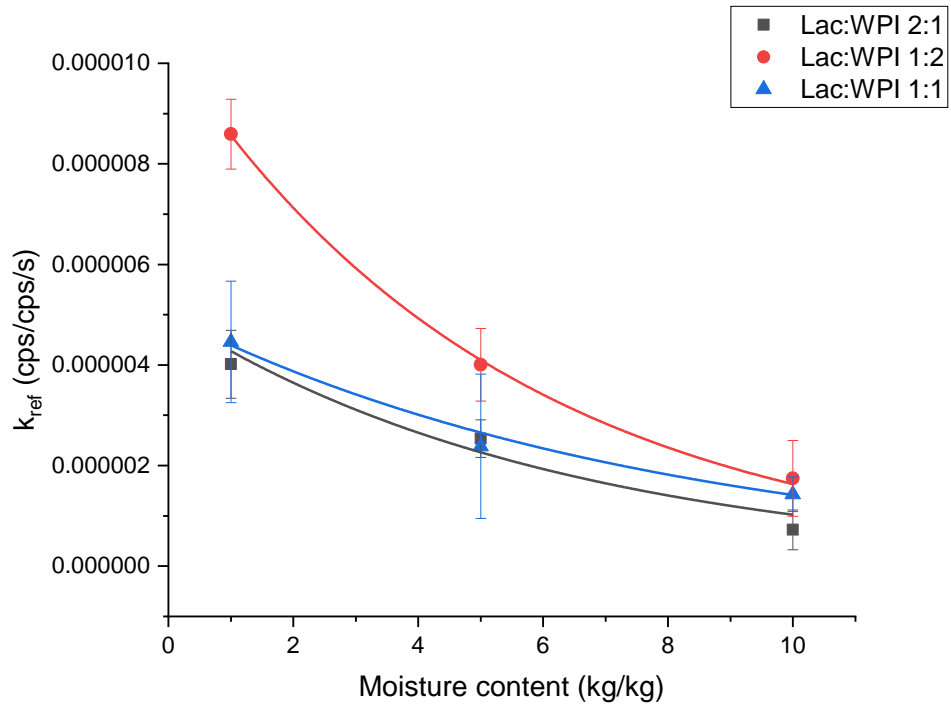


Figure 6.7 Moisture content dependency of the constant  $k_{ref}$  in the Arrhenius equation.

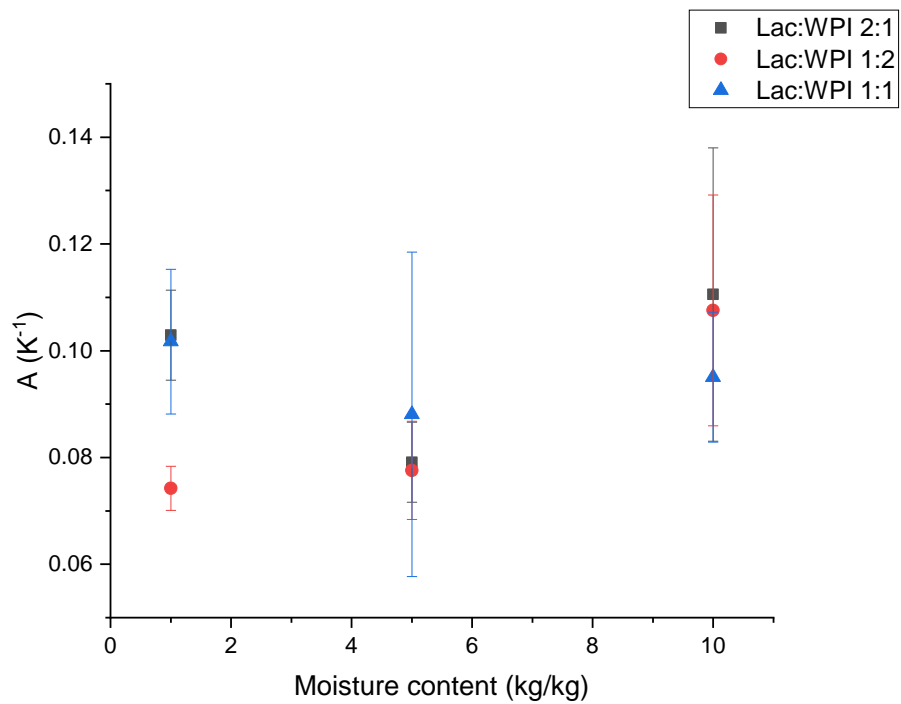


Figure 6.8 Moisture content dependency of the constant  $c$  in the Arrhenius equation.

As shown in Figure 6.7, the moisture dependency of the frequency factor ( $k_{ref}$ ) can also be fitted well with an exponential model (i.e., Arrhenius-type equations). Therefore, the moisture dependency of the  $k_{ref}$  is described using equation 6.56:

$$k_{ref}(X) = c_1 * \exp\left(c_2 * (X - X_{ref})\right) \quad 6.56$$

Here,  $c_1$  and  $c_2$  are constants, and  $X_{ref}$  is the reference moisture content.

The constant  $c$  in the equation 6.56 appears to be relatively constant regardless of the changes in moisture contents compared with  $k_{ref}$ . This observation arises because the constant  $c$  in the Arrhenius-type equations relates to the apparent activation energy ( $E_a$ ) of the modelled reaction. The apparent activation energies are specified for each reaction and can be considered constant regardless of the conditions. Another study has reported that the apparent activation energy for lysine loss in model dairy formulations varies significantly at lower moisture constants ( $X < 0.1$  kg/kg), which is probably linked to changes in the physical state of lactose (e.g., glass transition) (Schmitz-Schug et al., 2014). Their findings may not be applicable here, as for all the conditions used in this thesis, the heating temperatures are all above the glass transition temperature of the model system ( $T_g < 0$  °C). Therefore, the constant  $c$  in the equation 6.56 will be included as a constant in the model for describing the temperature and moisture content dependency of the reaction constant. Combining equations 6.55 and 6.56 gives:

$$K(T, X) = k_{ref} * \exp\left(c_1 * (X - X_{ref})\right) * \exp\left(c_2 * (T - T_{ref})\right) \quad 6.57$$

Here, again, the average moisture content ( $X = 5$  kg/kg) and temperature ( $T = 80$ °C) are chosen as the reference moisture content ( $X_{ref}$ ) and the reference temperature ( $T_{ref}$ ).

The 3D fitting of equation 6.57 was performed using Matlab 2022b based on the trust region algorithm, and the result are summarised in Table 6.9. The initial guesses for the fitting process were specified in the following way:  $c_1$  and  $c_2$  were the average values obtained from fitting data points with equation 6.56.  $k_{ref}$  was the average rate constant at the reference temperature ( $T_{ref} = 80$ °C) and moisture constant ( $X_{ref} = 5$  kg/kg). The fitted parameters were also limited to



be within the same magnitude as the initial guesses (e.g., the fitted  $K_{ref}$  was limited to the range of  $10^{-6}$  to  $10^{-5}$ ).

Table 6.9 Fitted parameters for a model describing the temperature and moisture content dependency of Maillard reaction rate constants.

| Lactose : WPI | $k_{ref}(cps/cps*10^{-6})$ | $c_1$                | $c_2$                | $R^2$ |
|---------------|----------------------------|----------------------|----------------------|-------|
| 1:2           | $4.064 \pm 2.499$          | $-0.108 \pm 0.0367$  | $0.0900 \pm 0.03091$ | 0.97  |
| 1:1           | $2.465 \pm 1.710$          | $-0.1947 \pm 0.0561$ | $0.092 \pm 0.0600$   | 0.98  |
| 2:1           | $2.1898 \pm 1.043$         | $-0.2134 \pm 0.0431$ | $0.0901 \pm 0.0231$  | 0.98  |

Note: Fitted parameters are expressed as the estimated mean  $\pm$  95% confidence interval range.

### 6.4.3. Modelling Maillard reactions kinetics with different drying kinetic models

#### 6.4.3.1. Modelling Maillard reaction kinetic with lumped-parameter models

To model the Maillard reactions occurring during the spray-drying process, the following equation was added to the existing parallel flow model:

$$\frac{dMR}{dh} = \frac{k_{ref} * \exp(c_1 * (X - X_{ref})) * \exp(c_2 * (T_p - T_{ref}))}{U_{px}} \quad 6.58$$

Here,  $dMR/dh$  is the change in the AMP/Trp ratios as a function of the axial distance travelled by the particles within the dryer. The constants in the reaction kinetic model were selected based on the lactose-to-WPI in the feed solutions.

#### 6.4.3.2. Modelling Maillard reactions kinetics with distributed-parameter models

Similar to the drying kinetic model, most equations are shared between the lumped and distributed models. The kinetics of the Maillard reaction for each sub-layer can be described as follows:

$$\frac{dMR_j}{dt} = k_{ref} * \exp(c_1 * (X_j - X_{ref})) * \exp(c_2 * (T_j - T_{ref})) \quad 6.59$$

Unlike the lumped-parameter modelling approach, in the distributed-parameter modelling approach, each sublayer of the particles has different component ratios. The effect of different component ratios in the samples is introduced into the simulation as switches to reduce the complexity of the kinetic reaction model, as discussed earlier in this chapter. For example, when the lactose-to-WPI ratio is not greater than 0.5 in a sub-layer, the reaction rate constants

will be estimated based on the kinetic model fitted based on data from heating model systems with a lactose-to-WPI ratio 1:2.

Since a zero-order reaction kinetic is used in this thesis, the reaction rate is independent of the reactant concentration. In the distributed parameter model, the overall changes in the extent of Maillard reactions for each particle were estimated by the weighted sum based on the mass fraction of protein in each individual sublayer:

$$\frac{dMR_{overall}}{dt} = \sum_{j=1}^n \frac{dMR_j}{dt} * \frac{m_{protein_j}}{\sum_{j=1}^n m_{protein_j}} \quad 6.60$$

## 6.5. Simulation results from different modelling approaches

### 6.5.1. Drying kinetics predicted by different modelling approaches

To compare the drying kinetics simulated using different modelling approaches, the temperature and moisture contents of the particle predicted by a base case simulation are shown in Figure 6.9 and Figure 6.11. Here, the overall average particle temperature and moisture content are reported instead of the values of each sublayer for the distributed-parameter model. The initial inputs for the base-case simulation are listed in Table 6.10.

Table 6.10 Initial conditions of the base case simulation.

| Conditions  | Lumped-parameter | Distributed-parameter |
|---|------------------|-----------------------|
| Particle moisture content (kg/kg)                   |                  | 10.37                 |
| Inlet gas temperature (°C)                          |                  | 190                   |
| Droplet temperature (°C)                            |                  | 20                    |
| Inlet gas humidity (kg/kg)                          |                  | 0.005                 |
| Overall heat loss coefficient (W/m <sup>2</sup> /K) |                  | 5                     |
| Feed flow rate (mL/min)                             |                  | 27                    |
| Drying gas flow rate (m <sup>3</sup> /hr)           |                  | 257                   |
| Particle diameter (m)                               |                  | 20 * 10 <sup>-6</sup> |
| AMP/Trp of the feed (cps/cps)                       |                  | 0.0055                |
| Lactose-to-WPI ratio                                |                  | 2                     |
| Particle velocity (axial) (m/s)                     |                  | 19.3                  |
| Particle velocity (radial)(m/s)                     |                  | 5.18                  |
| Particle velocity (tangential)(m/s)                 |                  | 0                     |
| ODE solver  |                  | ODE 23s               |
| Number of sub-layers                                | N/A              | 5                     |
| Span of the simulation                              | [0,3.5 m]        | [0,3.336s]            |
| Step size   | Variable         | 0.001 s               |

Note: The durations of the simulations were determined by the shortest distance travelled by the particles within the dryer (i.e., the shortest distance between the atomiser and the outlet of the dryer). For the distributed-parameter model, the simulation stops when the axial distance

travelled by particles is equal to the shortest distance between the atomiser and the outlet of the dryer, which is approximately 3.336 seconds.

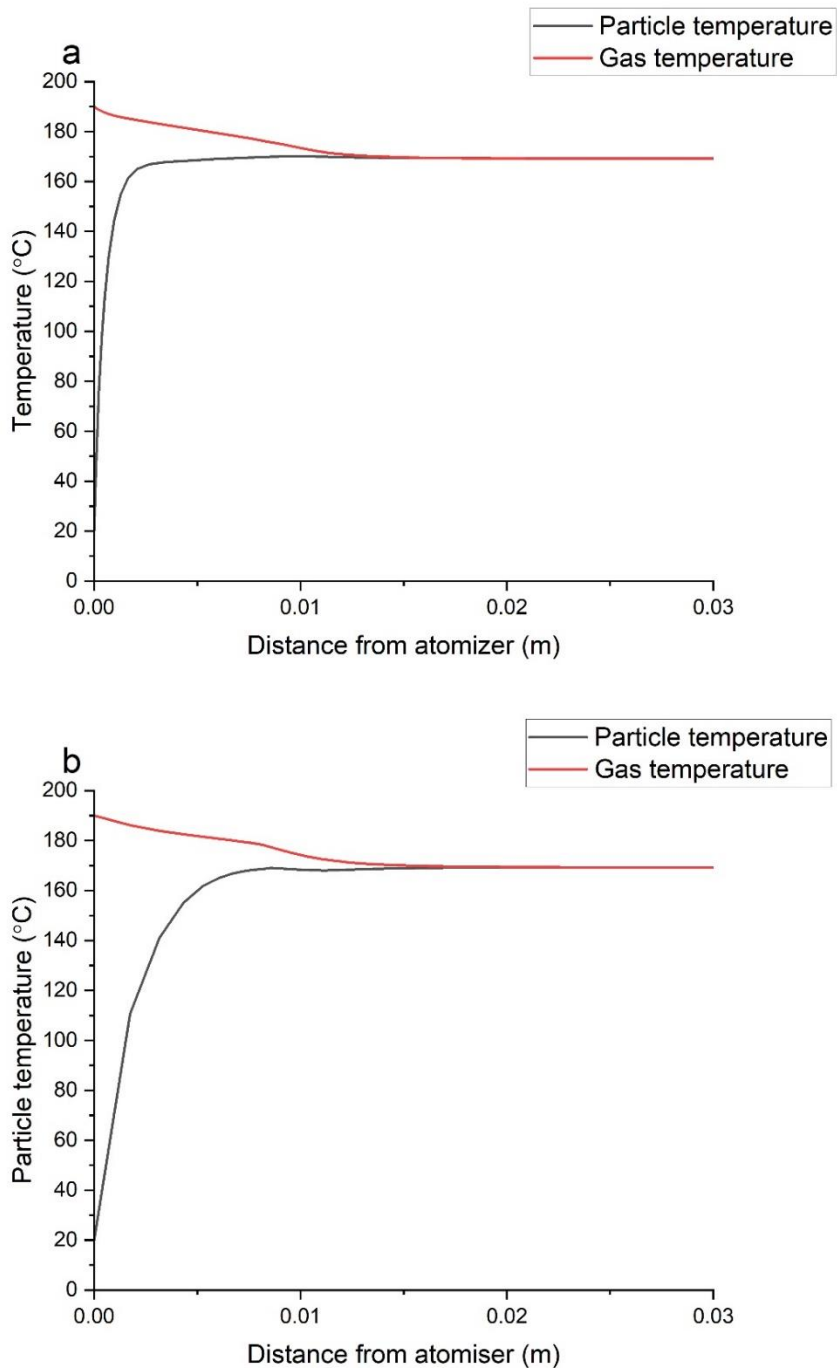


Figure 6.9 Temperature history of drying gas and particles (average) predicted by different modelling approaches (initial stage). (a) Lumped-parameter model (b) distributed-parameter model.

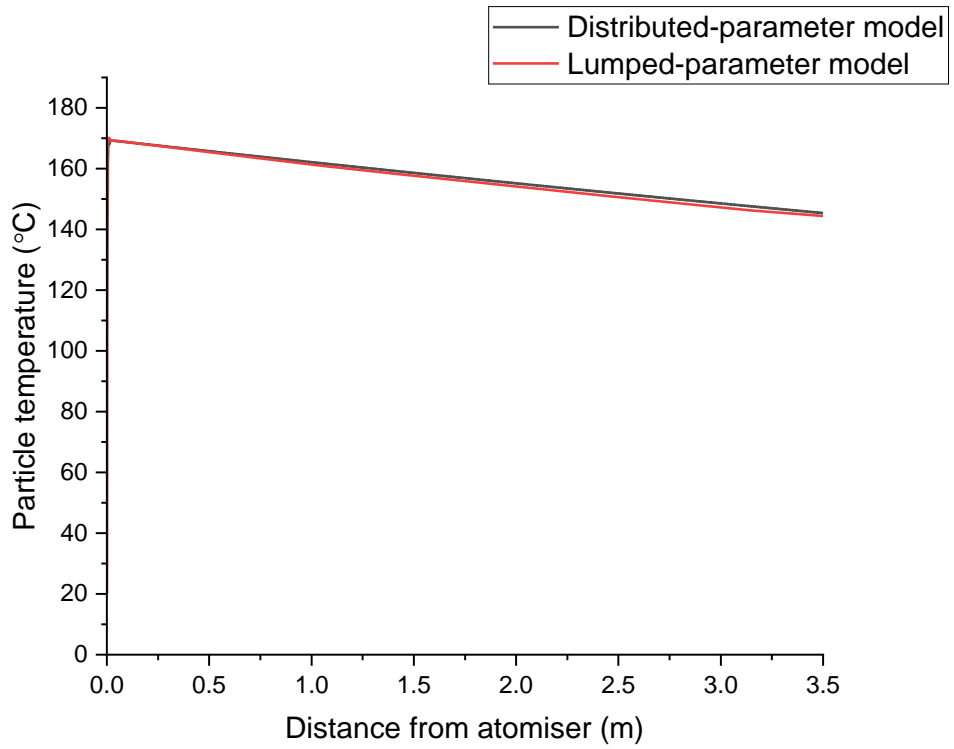


Figure 6.10 Particle (average) temperature history predicted by different modelling approaches (whole dryer).

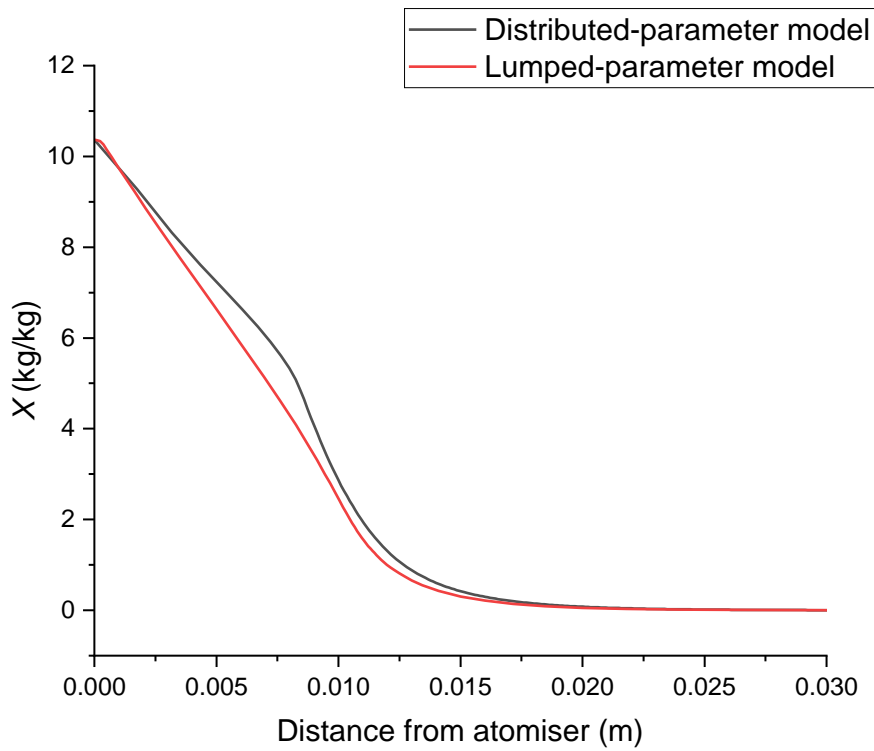


Figure 6.11 Particle moisture content history predicted by different modelling approaches (initial stage).

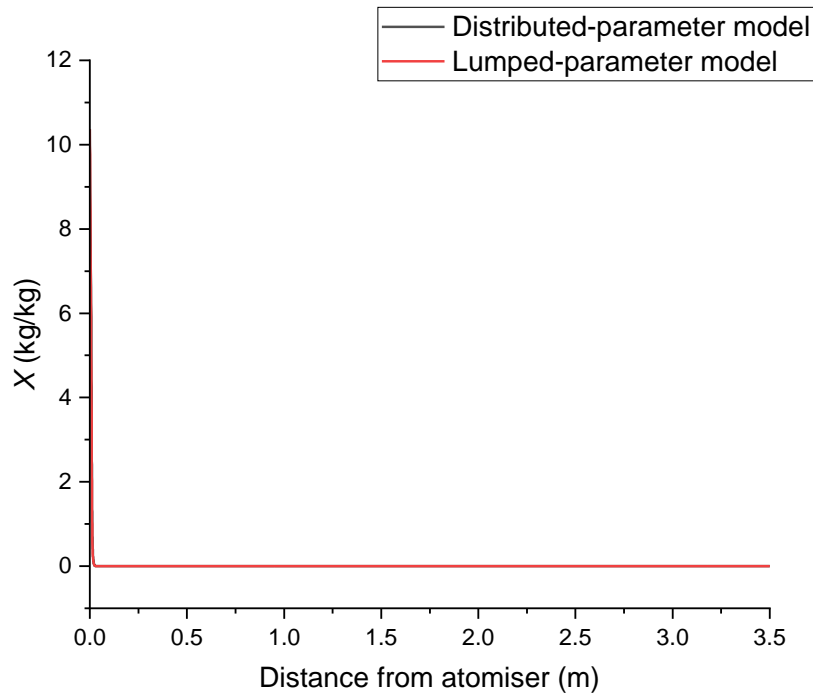


Figure 6.12 Particle moisture content history predicted by different modelling approaches (whole dryer).

As shown in Figures 6.9 - 6.12, the drying kinetics predicted by different approaches are similar and become effectively the same once the moisture content of the particle is sufficiently low (the differences in the final prediction values are less than 0.5%). During the initial drying stage, the overall drying rate of the particle predicted by the distributed-parameter model is slightly lower than those predicted by the lumped-parameter model. The predicted particle temperature also rises more slowly compared with the lumped-parameter model. The difference in the drying kinetics predicted by the different modelling approaches is partly due to the difference in the driving forces for the particle-gas interfacial mass transfer.

Both models used a linear CDC approach to estimating the interfacial mass transfer rate. The only difference is how the relative drying rate is calculated ( $\zeta$ ). The relative drying rate is determined based on the moisture content of the outermost layer in the case of the distributed-parameter model. In contrast, the overall moisture content of the particle is used in the lumped-parameter model. The outermost layer of the particle has a much smaller mass compared to the whole particle. For the same evaporation rate (which is true at the start of the spray-drying process), the moisture content of the outermost layer drops more rapidly

compared to the whole particle, as demonstrated in Figure 6.13. As a result, the relative drying rates in the distributed-parameter model decreased more rapidly compared with those calculated in the lumped-parameter model. Due to smaller driving forces for interfacial mass transfer, the overall drying rate predicted by the distributed-parameter model is lower than the values predicted by the lumped-parameter model.

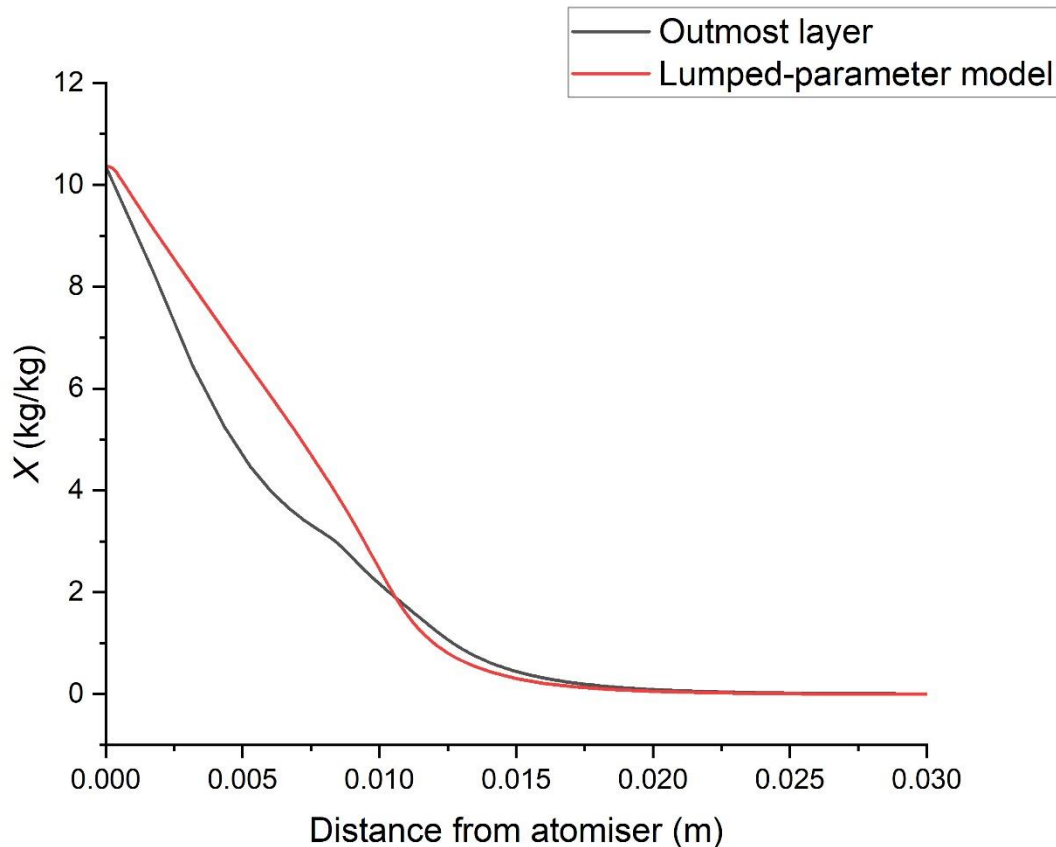


Figure 6.13 Moisture content history of the outermost layer of the particle (from the distributed-parameter model) and the value predicted by the lumped-parameter model.

The difference in the overall particle temperature is due to the overall heat transfer rate in the distributed-parameter model being limited by the conductive heat transfer within the particle. The conductive heat transfer coefficient within the particle is approximately one-tenth of the convective heat transfer coefficient, which occurs at the surface of the particles. In lumped-parameter approaches, particles are treated as a whole; thus, the overall heat transfer rate is not limited by the internal conductive heat transfer rate. As a result, the lump-parameter

approach predicts a faster overall heating rate during the early stage of the drying process. For the same reason, particle temperature decreases more slowly at the later stages of the drying process, resulting in slightly higher overall particle temperatures than the lumped-parameter model (Figure 6.10).

### 6.5.2. Predicted internal particle temperature, moisture content and component distribution

In the lumped-parameter approach, the particle is treated as a whole. Thus, the internal temperature, moisture content and component distribution are the same as those for the overall particles. In contrast, the distributed-parameter modelling approach allows different temperatures, moisture contents and component distribution across the inside of the particles. The particle temperatures, moisture contents and component distributions predicted by the distributed-parameter model using base case conditions are shown in Figure 6.15 d-f.

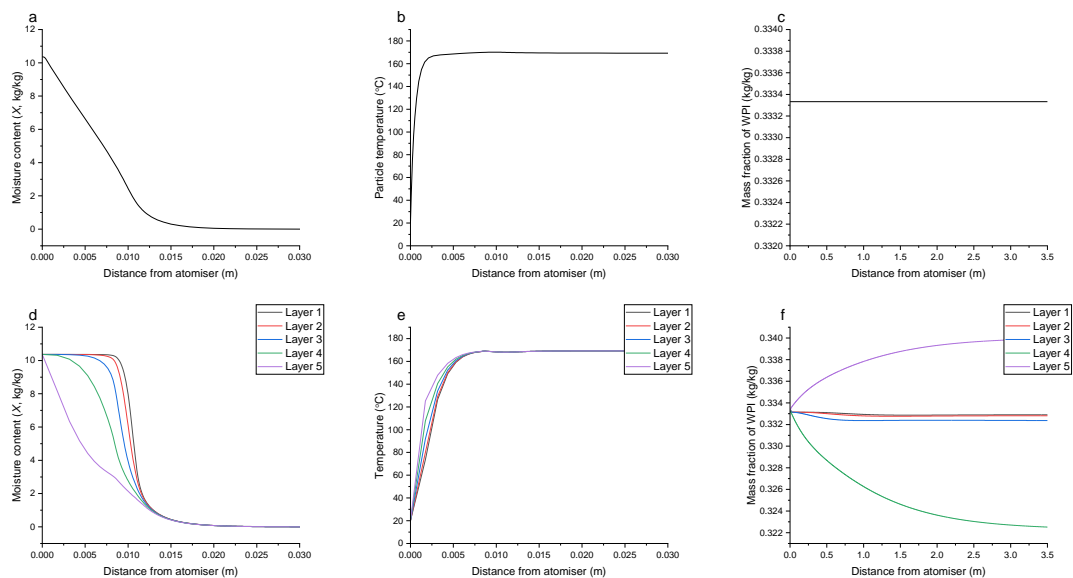


Figure 6.14 Prediction result from the lumped- and distributed-parameter approaches. a – c: lumped-parameter model d – f: distributed-parameter model

As shown in Figure 6.15 d-f, the distributed-parameter model has successfully predicted the heterogeneous temperature, moisture content and component distribution within the particles. The highest temperature, WPI-to-lactose ratio, and lowest moisture content were observed at the outermost layer (Layer 5) and gradually decreased (or increased in the case of

moisture contents) throughout the particle. The predicted internal behaviours are potentially more realistic than the lumped-parameter model. The distributed model has successfully predicted the overall trend of component segregation during spray drying (i.e., proteins move toward the surface of the particles while lactose moves in the opposite direction.). However, the prediction result of the protein coverage at the surface of the particles is less than ideal. The predicted protein mass fraction at the outermost layer (surface of the particle) is significantly lower than those measured experimentally via XPS (approximately 20% lower) (Putranto et al., 2017). The difference in predicted and experimental values is probably linked to the prediction methods for protein movement and the thickness of the sublayers used in the simulation model. The effect of the thickness of sublayers will be discussed later in this chapter. Although the predicted values are different to those measured experimentally, the current model is sufficient to reflect the potential impact of component segregation on the Maillard reaction kinetics during spray drying. The impact of component ratios on the kinetics of Maillard reactions is introduced as switches in the current model. In other words, as long as the predicted changes in component ratios are sufficient to trigger the "switches" for the reaction kinetic constants, the impact of component segregation will be reflected in the predicted extent of Maillard reactions in the spray-dried product. Nevertheless, this statement does not apply to more comprehensive reaction kinetics models (e.g., 4D, multi-response, or higher-order kinetics models) where the component ratios are not introduced as "switches", or the rate constants are based on the reactant concentration(s). Refining the segregation prediction model can be the focus of future studies.

### 6.5.3. Effect of the number of sublayers on prediction results

One of the most critical parameters for the distributed-parameters models, which is also the biggest difference between the two different modelling approaches, is the number of sublayers. A "distributed-parameter" model with one sublayer is no different to a lumped-parameter model. In theory, for any distributed-parameter models, the higher the number of sublayers, the more realistic the prediction result will be until the thickness of each sublayer is smaller than the molecules. The theoretical maximum number of sublayers that can be used for the



base case simulation is 128 layers (calculated based on the initial diameter of the droplet and hydraulic diameter of proteins) when shrinkage of the particle is not considered. The effect of different numbers of sublayers was investigated by running simulations with 3, 5, and 10 sublayers while keeping other conditions the same as the base case simulation.

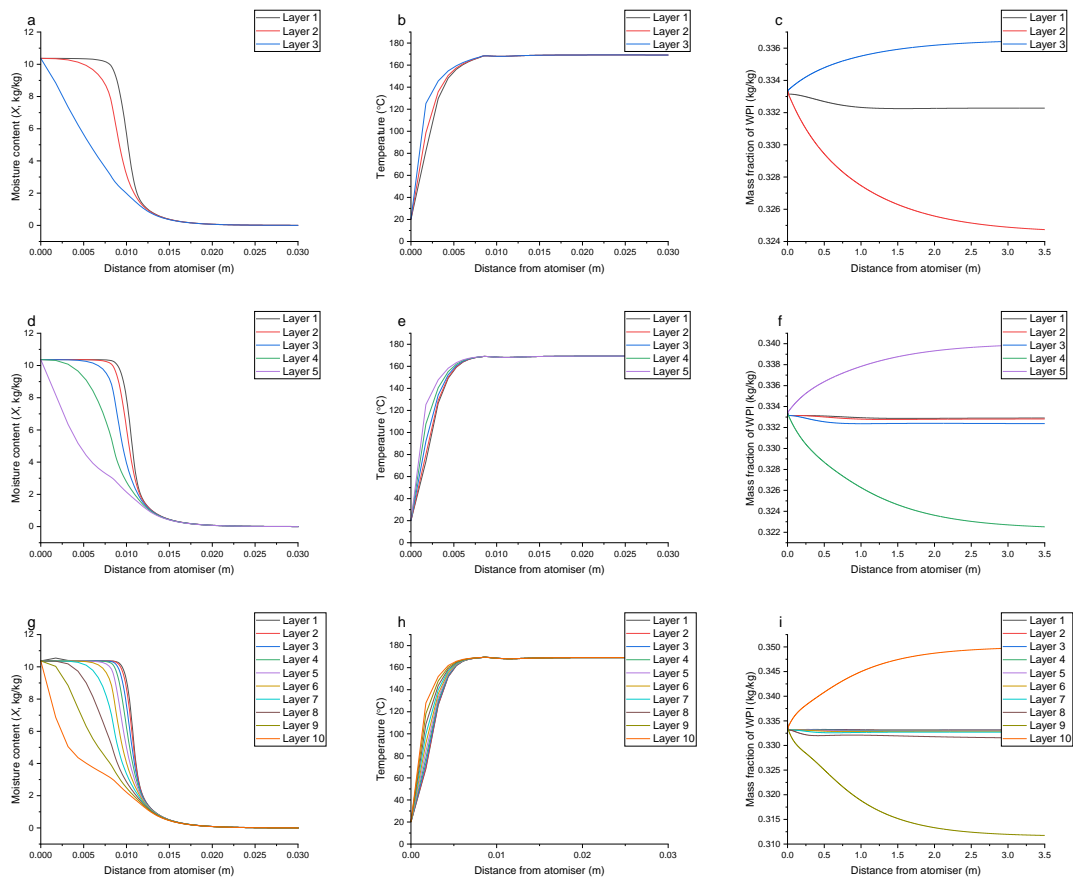


Figure 6.15 Prediction result from the distributed-parameter model with a different number of sub-layers. a – c: 3 layers d – f: 5 layers g – i: 10 layers.

As shown in Figure 6.15, the number of sublayers has no significant impact on the temperature and moisture profile predicted by the model. Improvement in the predicted particle surface composition was observed, but the improvement is not substantial. Running a simulation model with a higher number of sublayers is also computationally demanding. The computational time for the model increased from 65 seconds to 739 seconds when the number of sublayers increased from 5 to 10. Additionally, the solution also becomes unstable due to the reduced layer thickness. The reduced layer thickness increases the differences between the

heat and mass transfer rate and the heat and mass "capacity" within a sublayer and thus reduces the stability of the model. Solution stability can be improved by reducing the step size used in the ODE solver at the cost of further increasing the computational complexity. A combination of 5 sublayers and a step size of 0.0001s were used in this thesis, as it provided a reasonable balance between accuracy and computational cost.

#### 6.5.4. Prediction results from the lumped-parameter model

The simulation results from the lumped-parameter model were compared with the experimentally measured results from Chapter 4 (Figure 6.16). Most of the inputs for the simulations were the same as the base case, except the inlet gas temperatures and feed compositions were changed to match experimental conditions. Here, for consistency, the predicted extent of Maillard reactions in the spray-dried products was also converted to percentage changes in AMP/Trp ratios compared with the feed (average AMP/Trp in feed is 0.0055 cps/cps).

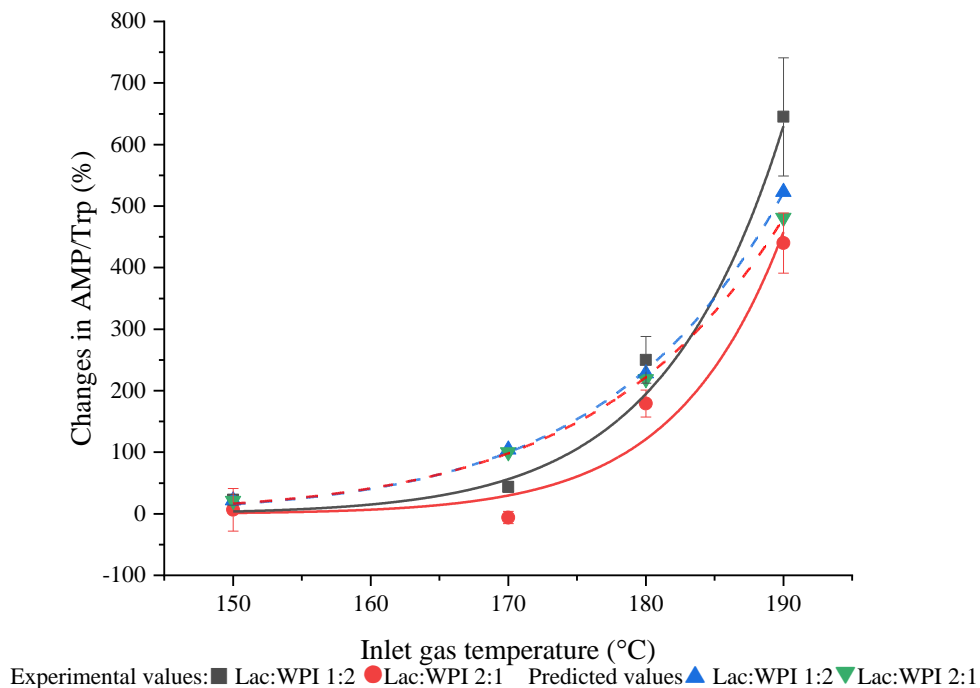


Figure 6.16 Predicted result from lumped parameter model and experimental data.

As shown in Figure 6.16, the predicted values from the lumped-parameter models are similar to the experimentally measured values for all the conditions ( $R^2$  ranging from 0.88 - 0.92). The difference between the predicted and actual values is likely to be because reaction kinetics are modelled based on data obtained via heat at temperatures lower than the particle temperatures within the dryer. Temperatures up to 100 °C were used in the isothermal heating experiments, while the outlet temperatures of spray drying experiments were up to 145 °C; Thus, the temperature difference was up to 45 K. Other than the temperature difference, the difference in moisture content could also contribute to the difference between the predicted and the actual values. In this thesis, the lowest moisture content used for the heating experiments was 1 kg/kg, as most segregation occurs when the moisture content is above 0.1 kg/kg. During the spray drying process, the moisture content of the particles falls significantly below 1 kg/kg, and the diffusion process limits the reaction rate at lower moisture contents (Gómez-Narváez et al., 2022, 2019; Miao and Roos, 2004; Schmitz-Schug et al., 2014). In terms of the overall trends in predicted and experimentally measured values, the prediction model has underestimated the temperature dependency of the Maillard reactions during spray drying. In other words, it overestimated the extent of Maillard reactions at lower temperatures and underestimated them at higher temperatures. Parameter  $c_2$  describes the temperature dependency of the reactions in the model developed. As mentioned previously,  $c_2$  is proportional to the apparent activation energy ( $E_a$ ) of the reaction in Arrhenius-type equations. An increase in the apparent activation energy in the samples at lower moisture contents was reported in an earlier study by Schmitz-Schug et al. (2014). This finding further emphasised the importance of investigating the reactions kinetics at lower moisture contents. In summary, the kinetics of Maillard reactions for model systems with lower moisture contents need to be addressed to obtain a better estimation of the kinetics for Maillard reactions in spray dryers, which can be a focus of future studies.

#### 6.5.1. Prediction results from the distributed-parameter model

In the distributed-parameter model, the reaction kinetics in each sublayer were calculated separately based on the temperature, moisture contents and component ratios for each sublayer.

Different reaction rates were predicted for each individual sublayer due to different conditions for each individual sublayer. As shown in Figure 6.17, the outermost layer was predicted to have the highest reaction rate compared with the inner layers. This observation is due to the outermost layer of the particle having the highest temperature and protein-to-lactose ratio and the lowest moisture content.

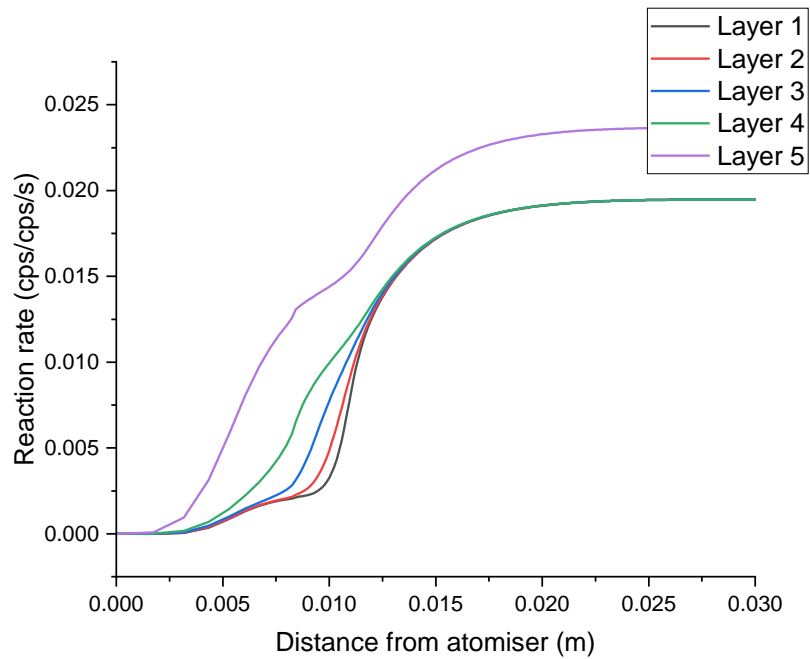


Figure 6.17 Predicted reaction rate for each sublayer from the distributed-parameter model.

The simulation results from the distributed-parameter model were compared with the experimentally measured results from Chapter 4 (Figure 6.18). The same input parameters and reaction kinetic constants were used. The predicted values were also converted to percentage changes.

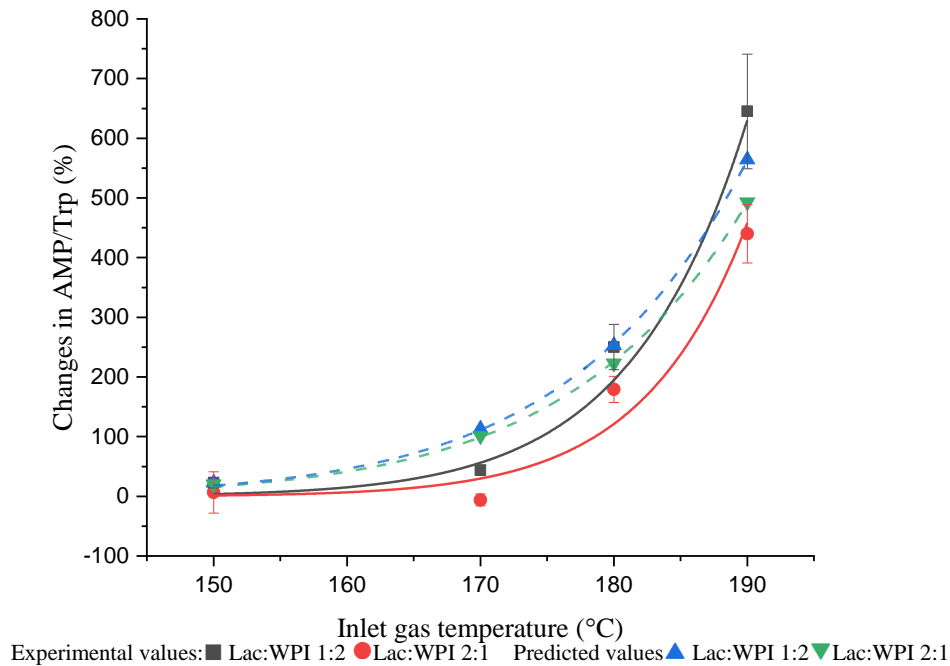


Figure 6.18 Predicted result from distributed-parameter model and experimental data.

As shown in Figure 6.18, the overall trend in the predicted values from the distributed-parameter model is the same as those predicted by the lumped-parameter model ( $R^2$  ranging from 0.87 - 0.95). This observation is probably due to the overall drying kinetics predicted by the models used here being largely the same. The predicted values from the distributed-parameter model are slightly higher at higher inlet gas temperatures than the lumped-parameter model. The performance of the models was evaluated based on the total sum of square errors of (SSE) compared with the average experimental values under the same conditions. The SSE for the distributed-parameter model is 17.7% less than that for the lumped-parameter model. This result suggested that the distributed-parameter model better predicted Maillard reaction kinetics during spray drying. The better performance of the distributed-parameter model is probably linked to the more realistic temperature, moisture content and component distribution profile within the particles compared with the lumped-parameter model. In summary, the distributed-parameter modelling approach showed a clear advantage over the traditional lump-parameter approach.

## 6.6. Limitations of the simulation models developed

### 6.6.1. Particle residence time

In the simulation models, the particle movement within the dryer is estimated based on the momentum equations (equations 6.1 - 6.3). The momentum equations did not consider the particle-wall interactions, recirculations, and other factors that could affect the particle residence time. For both simulation models, the particle residence time is estimated to be approximately 3.4 seconds. The estimated particle residence time in the simulation model is closer to the gas residence time estimated in Chapter 5 (3.5 seconds) compared with the experimentally measured mean particle residence time, which is nearly three times the estimated gas residence time ( $9.9 \pm 1.0$  seconds). The underestimated particle residence time leads to underestimating the extent of Maillard reactions that occur during the spray drying process. In order to have a more accurate description of the particle movement and the particle temperature and moisture content history, computational fluid dynamics (CFD) or other more comprehensive modelling methods are required.

### 6.6.2. Moisture content of the particles

As mentioned earlier in the discussion, the reaction kinetics model developed in this model is based on model systems with a moisture content of no less than 1 kg/kg. Therefore, the effects of lower moisture contents on reaction kinetics are extrapolated based on the trends in the measured results. In this thesis, the reaction rate constants were found to increase as the moisture content decreased, likely due to the concentrating effect. However, as shown in other studies, the reaction rate decreases at lower moisture contents due to limited particle mobility (Schmitz-Schug et al., 2014). This difference between the predicted and actual correlation between the reaction rate constants may lead to an overestimation of the extent of the Maillard reaction in the final product. In order to address this issue, the reaction kinetics at lower moisture contents should also be investigated, even though the segregation process is close to being completed at lower moisture contents (Putranto et al., 2017). Additionally, for reaction kinetics at lower moisture contents, the physical state of the particles also needs to be considered. Lactose is an amorphous material whose physical properties depend on moisture

content and temperature. The mobility of the lactose molecules is affected by their physical state, and molecule mobility is higher when the temperature is above the glass transition temperature of the particles. The effect of glass transition is not considered in this thesis as the glass transition temperatures of the model systems (less than 0°C) are significantly lower than the heating temperatures (60°C - 100°C) due to their relatively high moisture contents.

### 6.6.3. Markers for Maillard reactions

Last but not least, a single indicator of Maillard reactions was measured here in this thesis. As discussed in Chapter 2, the Maillard reactions scheme involves a series of reactions and can be divided into three stages. Ideally, at least one marker for each stage of Maillard reactions needs to be investigated to properly model the Maillard reaction kinetics. This issue needs to be addressed in later studies.

## 6.7. Conclusions

In this chapter, the effect of different moisture content ( $X = 1, 5, 10$  kg/kg), heating temperatures (60, 80, 100°C) and different lactose-to-WPI ratios (1:2, 1:1, and 2:1) on the kinetic of Maillard reactions in model systems were investigated. Results have shown that the reaction rate increases exponentially with the temperature and fits well with Arrhenius-type equations. The reaction rate was found to increase with the decrease in moisture contents within the range of moisture contents tested. The component ratios do impact the reaction kinetics, but they were less significant compared with the other two factors, especially at higher temperatures and lower moisture contents, probably related to the different solubilities of the two main reactants. The reaction kinetic models were then coupled with both lumped and distributed-parameter drying kinetic models to simulate the impact of different inlet gas temperatures and feed compositions on the extent of the spray-dried products. The simulation results were then compared with the experimental results from Chapter 4. Both the lumped and distributed-parameter models have reasonably predicted the extent of Maillard reactions. The difference between the predicted and actual values is probably due to the overestimated rate constants estimated based on heating model systems with relatively high moisture contents and the approximation for the effect of the reactant ratios. Overall, the simulation results still

produce promising results compared with previous studies (i.e., significantly closer to the experimental values), likely due to a more comprehensive modelling approach for the drying kinetics and careful reaction rate studies. last but not least, the distributed-parameter modelling approach has shown a clear advantage over the traditional lumped-parameter modelling approach.



## Chapter 7. Conclusion and further consideration

In this chapter, the findings in earlier chapters are summarised. Considerations for future studies based on the findings or issues that have not been addressed in earlier chapters were also discussed in this chapter.

## 7.1. Overview of the thesis

Spray drying has been widely used to extend the shelf life of perishable goods and reduce the cost of transportation, and one of the typical applications of spray drying processes is milk powder production or the production of other spray-dried dairy products. As a good source of proteins, milk and its related products have relatively high protein content. Besides proteins, they also contain significant amounts of reducing sugars (e.g., lactose). The combination of high protein and reducing sugars makes milk and its related products particularly subject to Maillard reactions during thermal processing, including spray drying. Given the importance of food safety and the complex nature of Maillard reactions, it is important to study the kinetics of Maillard reactions that occur during the spray-drying processes.

A few studies have investigated the Maillard reactions that occur during spray drying processes. Existing studies mainly focus on how operating conditions may affect the kinetics of Maillard reactions for a specific feed. In contrast, the characteristics of the spray dryer, properties of the feeds, and physical processes that occur during spray drying were often not considered. In other words, current studies mainly focus on optimising a specific spray-drying process while lacking a more systematic approach and investigation from an engineering point of view.

The first part of this thesis aimed to investigate the kinetics of Maillard reactions in spray dryers with different feed compositions under different operating conditions. Model systems with different sugar-to-protein ratios, fresh skim milk and reconstituted skim milk were spray dried with different inlet gas temperatures. The extent of Maillard reactions in the spray-dried products was measured using a fluorometric method and colourimetry analysis. Results have shown that different feed compositions significantly impact the reaction kinetics under the same spray-drying conditions. A strong correlation between the colour formation and the extent of Maillard reactions was also observed. Additionally, the experimental measurements in this chapter provided a foundation for the later chapters.

The second part of this thesis aimed to study the impact of the design and dimensions of spray dryers on the particle residence time distribution in these dryers. Although a few studies have studied particle residence time distributions in spray dryers, the effects of different designs and dimensions of spray dryers have not been studied yet. A non-intrusive laser-based measurement method was developed for the needs of this study. Measurement results have shown that different designs and dimensions significantly impact the particle residence time distribution, which can be critical to the Maillard reactions kinetics in spray dryers. Furthermore, the measurement methods developed here showed a clear advantage over intrusive methods used in previous studies.

The last part of this thesis was aimed at developing a preliminary mathematical model for simulating the kinetics of Maillard reactions in spray dryers. The potential impact of component segregation on the kinetics of Maillard reactions in the spray dryer was considered for the first time. The more comprehensive distributed-parameter modelling approach has significantly improved the prediction results compared with previous studies using a more traditional lumped-parameter modelling approach.

## 7.2. Maillard reactions under different spray drying conditions

Chapter 4 investigates the extent of Maillard reactions of the spray-dried milk and milk-like model systems under different spray-drying conditions. Experimental results from the pilot-scale spray dryer showed that the extent of Maillard reactions in the spray-dried products increases with the inlet gas temperatures. The reaction rate increased significantly when the inlet gas temperature specifically increased from 180°C to 190°C ( $T_{out} = 136 - 146^\circ\text{C}$ ), regardless of the composition of the feed. This observation is probably linked to the protein unfolding. For different types of feed, different trends were observed. For real food systems, the differences between the responses of reconstituted milk and fresh milk to the spray-drying processes were minor. This observation reinforces the point in the previous study that the reconstituted milk is similar to fresh milk except for having additional thermal degradation. The model systems were found to be more sensitive to Maillard reactions than real food systems, probably due to lower lactose-WPI ratios compared with real food systems (2:1 or 1:2

vs. ~5:1). Additionally, model systems with lower lactose-to-WPI ratios were found to be more sensitive to Maillard reactions under the same spray-drying conditions. Based on this finding, it is reasonable to suggest that the WPI (proteins) may be the rate-limiting reactant for Maillard reactions in spray dryers. No significant changes in the extent of Maillard reactions was observed for samples collected from spray drying experiments using the laboratory-scale spray dryer. This observation is likely due to the relatively short particle residence time in the laboratory-scale spray dryer compared with the pilot-scale spray dryer. This observation further emphasised the importance of particle residence time distribution for reactions that occur in spray dryers. Last but not least, a strong correlation between the colour formation and the content of Advanced Maillard reaction products was observed. This correlation can be further developed into a rapid quality evaluation method for thermal degradation in materials sensitive to Maillard reactions and milk and milk-like systems.

### 7.3. Effect of different designs of the spray dryer on the particle residence time distribution and the quality of the final product

The findings in Chapter 4 suggested that the particle residence time may play an important role in the reactions kinetics of Maillard reactions in spray dryers. As a result, a laser-based non-intrusive system for particle residence time measurement was developed in Chapter 5. The method developed was validated against the findings from other studies and found to be no worse than those used in previous studies in any respect. The particle residence time distributions were recorded for four different designs of the pilot-scale spray dryers at a different gas flow rates, ranged from 99 m<sup>3</sup>/hr to 315 m<sup>3</sup>/hr. Measured response curves were then fitted with a continuous-stirred-tank-reactor tank-in-series (CSTR-TIS) model for quantitative comparison. The mean particle residence times for the different designs of pilot-scale spray dryers were found to be significantly longer than those for the laboratory-scale spray dryer (3.3 seconds, laboratory scale, vs. 6.8 - 27.2 seconds, pilot scale). The difference between the particle residence times is mainly due to the differences in the dimensions of the spray dryers. This observation also confirmed the hypothesis for the null result in the laboratory-scale spray dryer in the earlier chapter. The ratios between the particle and gas

residence time were used to evaluate the performance differences between different designs as they are different in dimensions. In general, the closer the ratio is to unity, the better is the performance of the dryer. The ratios between the particle and gas residence time were found to vary significantly depending on the designs of the drying chambers and gas flow rates (Design 1: 1.5 – 2.7 s/s, Design 2: 1.5 – 2.6 s/s, Design 3: 1.5 – 2.5 s/s, and Design 4: 1.0 – 1.7 s/s). The smallest ratio between the particle and gas residence time was observed for Design 4, which has a conical design for the first two drying chambers and a box connection between two drying columns. Other than the mean particle residence time, the spread of the particle residence time is also an important performance indicator. A tighter spread of the particle residence time is more desirable, as it suggests a smaller difference between the longest particle residence time and the means particle residence time (i.e., less tailing). The spreads of particle residence time distributions for the first three designs were similar ( $n = 13 - 18$ ), and the widest spread was observed for Design 4 ( $n = 5 - 8$ ). The wider spread of residence time distribution is probably linked to recirculation zones within the dryer. Fluctuations were observed in all measured signals and were probably linked to wall deposition and re-entrainment processes. These fluctuations were also observed in other studies but have not been investigated. The frequencies of the fluctuations were analysed using Fourier transforms. Results have shown that Design 4 has the lowest fluctuation frequency ( $f = 0.015$  Hz vs.  $f = 0.22$  Hz), which suggests that it should have the least amount of wall deposition. This hypothesis is supported by the highest solid recovery rate observed in Design 4 along all four designs for most flow rates (up to 51%). Measuring the wall deposition rate in different designs of the pilot-scale spray dryer could be the focus of future studies. Based on the findings above, it is reasonable to suggest that the shape of the first two drying chambers plays an important role in both the particle residence time distribution and the wall deposit re-entrainment processes. The conical chamber design (Design 4) appears to be superior to the cylindrical design (Designs 1 - 3) due to the gas and particle residence times being most similar and due to having the lowest wall deposition rate, despite having the widest spread of particle residence times.

#### 7.4. Modelling Maillard reactions under different spray drying conditions

Developing a mathematical model that simulates the kinetics of Maillard reactions in spray dryers is an excellent complement to experimentally investigating the effect of different factors (Chapter 4). The mathematical model may also provide a deeper insight into the kinetics of Maillard reactions in spray dryers. In Chapter 6, Maillard reactions kinetics in spray dryer were simulated by developing mathematical models with different modelling approaches. The drying kinetics were modelled using lumped-parameter and distributed-parameter models. The distributed-parameter model is essentially a further refinement of the lumped-parameter model where the insides of the particles are not assumed to be homogenous. Reaction kinetic models were developed based on a heated model system under isothermal conditions. Model systems with different compositions (Lac:WPI 1:2, 1:1, and 2:1) and moisture contents ( $X = 1, 5, 10$  kg/kg) were heated isothermally at different temperatures (60, 80, 100°C) for up to 35 minutes. Experimental results have shown that the temperature and moisture content dependency were fitted well with Arrhenius-type equations, and compositions have a less significant impact on the Maillard reaction kinetics. As a result, the effect of different feed compositions was included as “switches” in the reaction kinetics model to reduce the complexity of the reaction kinetic model. The reaction kinetic model has then been coupled with both drying kinetic models, and the simulation results showed good agreement with the experimental results obtained in Chapter 4 ( $R^2$  ranging from 0.87 to 0.95). The distributed parameter model was found to be 17.7% better than the lumped parameter one in terms of the overall predictions. The more comprehensive modelling approaches used in this thesis also showed a better agreement with experimental data than models developed in earlier studies.

#### 7.5. Recommendations and future works

This thesis investigated the effects of different spray drying conditions on the kinetics of Maillard reactions and the effect of different spray dryer designs on the particle residence time distribution. A mathematical model for Maillard reactions in spray dryers has also been successfully developed. Despite the fruitful outcomes of this thesis that have addressed some

of the research gaps identified in Chapter 2, some findings still need to be refined or further investigated.

#### 7.5.1. Additional markers for thermal degradations

In this thesis, the extent of Maillard reactions in the samples was measured using the fluorescence method and colour analysis. These two methods are mainly used to measure the markers of the advanced and final stages of Maillard reactions, and they are less sensitive in mild conditions. In Chapter 5, the inlet gas temperature used for the measurement of particle residence time distribution was limited to 100°C due to the operating temperature limits of the photomultiplier. To investigate the potential impact of designs of spray dryers on the Maillard reactions, the extent of Maillard reactions in samples spray dried at the same temperature as the residence time distribution was measured. However, based on findings in Chapter 4, the two markers used in this thesis were expected to be not sensitive enough to produce meaningful results due to the lower inlet gas temperature and relatively small differences in the mean particle residence time. To address this issue, Maillard reactions indicators that are more sensitive to thermal exposure should be considered in later studies.

Other than using more sensitive markers indicators for Maillard reactions, measuring markers from multiple stages of Maillard reactions are also desirable. As discussed in Chapters 2 and 6, Maillard reactions have a complex reaction scheme, which can be divided into three stages: early, advanced, and final. Ideally, at least one marker for each stage of the Maillard reactions should be measured. With multiple markers for Maillard reactions, a more comprehensive modelling approach, such as the multi-response model, can be used to understand the Maillard reactions kinetics better. A better understanding of the kinetics of Maillard reactions would be beneficial for controlling the extent of Maillard reactions in the spray-dried products or applying Maillard reaction conjugates in spray-drying processes as additives.

### 7.5.2. Maillard reactions kinetics at lower moisture contents

As highlighted in Chapter 6, the temperature dependency of the Maillard reaction is underestimated in current models. The reaction kinetic model used in this thesis is developed based on isothermally heating samples with relatively high moisture contents ( $X = 1 - 10$  kg/kg, where most segregation processes occur). Some studies have reported an increase in the apparent activation energy at lower moisture contents due to changes in the physical state of sugars. A higher apparent activation energy suggests that the reaction rate is more sensitive to temperature changes. The difference in kinetics for Maillard reactions at different moisture contents is probably the main cause of underestimation in current models. To better understand the Maillard reaction products, the kinetics for Maillard reactions should continue to be investigated in future studies at lower moisture contents.

### 7.5.3. Effect of component segregations

As discussed throughout this thesis, the ratio between two reactants, WPI and lactose, plays an important role in the Maillard reaction kinetics. One of the critical physical processes that occurs during the spray-drying process is component segregation. Components segregation leads to a heterogenous distribution of component ratios within the particles and affects the kinetics of Maillard reactions. In Chapter 6, a distributed-parameter simulation model was developed with the inclusion of a component segregation process. Even though the approach used in this study is only a first approximation for the effects of component segregation, the prediction result was a significant improvement over a prediction model that did not include the effect of segregation (i.e., lumped-parameter model). This promising result suggested that the effect of component segregation on Maillard reactions kinetics should be investigated further with a more careful modelling approach.

### 7.5.4. Computational fluid dynamics (CFD) simulations for different designs of the spray dryer

In Chapter 5, the effect of different spray dryer designs on the particle residence time distribution was investigated. The conical drying chamber and box connection designs (Design 4) have shown promising results compared with earlier designs. The smaller particle-to-gas



residence time ratio in Design 4 was expected to be linked with the steadier flow pattern within the dryer. However, without confirmation from Computational fluid dynamics (CFD) simulations, it is not possible to come to a definitive conclusion. CFD simulations are also required to investigate the recirculation zones within the dryer, which could be the cause for the wider spread of particle residence time distributions observed in later designs. In addition to investigating the recirculation zones within the dryer, CFD simulations can be used to estimate some of the driving forces for wall-deposition re-entrainment processes (e.g., turbulent burst frequency). Last but not least, CFD simulations could assist with improving the design of the spray dryers and by reducing the spread of particle residence times, thus, the amount of thermal exposure to the product may be reduced.

Besides assisting with the redesign process for the spray dryer, CFD simulations can also improve the accuracy of the mathematical model developed in Chapter 6. As highlighted in Chapter 6, the particle residence times predicted by the model developed are significantly shorter than those measured experimentally, due to the limitations of the developed plug-flow/parallel-flow model. CFD simulations are more likely to produce more realistic particle trajectories within the dryer compared with those estimated solely based on plug flow of gas. CFD predictions of the residence time distributions should also be compared with the measured particle residence time distributions in Chapter 5. In addition, together with the reaction kinetics from Chapter 6, better predictions (with CFD) of the observed extents of Maillard reaction from Chapter 4 may be achieved.

#### 7.5.5. Effects of other spray drying conditions

Exploring the effects of other spray drying conditions could also be the focus of further research. For example, the humidity of the inlet gas could be an important factor that needs to be considered. In a study by Samborska et al. (2019), a “dry” (low-humidity) drying gas was found to be beneficial in spray drying for thermal-sensitive products. Their results may also be applicable to the topic of this thesis, Maillard reactions in spray dryers. In addition to inlet gas humidity, other factors such as initial droplet size distribution, addition of different drying aids,

and different types of feed could also be topics for future research on Maillard reactions in spray dryers.

## Chapter 8. Impact of COVID-19 on the scope of this thesis

In this chapter, the impact of COVID-19-related government-imposed restrictions on the scope is highlighted here, as per the requirement of thesis examination under emergency conditions.

## 8.1. Overview of the COVID-19 impacts

During the period of candidature, there were two severe disruptions in the research progress due to government-imposed lockdowns between 18<sup>th</sup> March 2020 – 1<sup>st</sup> July 2020 and from 26<sup>th</sup> June 2021 until 11<sup>th</sup> October 2021. During these two periods, the university campus and essential equipment were not accessible. As the research projects in this thesis have been heavily experimental-based, losing access to the university campus has adversely affected the research progress. The University of Sydney policies allow working from home (WFH), given work health safety (WHS) requirements are met. These policies did not apply to the research projects in this thesis as the instruments required are pilot-scale or chemicals have toxicities that are not suitable for WFH. In addition to the direct impact of lockdowns, the uncertainties in both the timing and durations of lockdowns also limited experiments that required constant measurement or could not be unattended for a long period. In summary, the progress of research progress has been adversely affected despite the strongest efforts having been put into minimising the negative impacts.

## 8.2. Potential research projects and outcomes without COVID-19 restrictions

As discussed previously, the scope of this thesis has been limited by COVID-19 restrictions. Potential research projects and outcomes that represent six months' worth of work are discussed here.

### 8.2.1. Measuring kinetic of Maillard reactions at lower moisture contents

In chapter 6, the kinetics of Maillard reactions were only studied at relatively high moisture contents ( $X = 1 - 10$  kg/kg), while the kinetics at lower moisture contents were not studied. Measuring the kinetics of Maillard reactions at lower moisture contents was included in the early planning stage of this thesis, and relevant equipment had been set up. The processes of measuring Maillard reactions at lower moisture contents are largely the same as those at higher moisture contents except for additional steps in sample preparation. Samples with different compositions were freeze-dried and then conditioned to different moisture contents. Sample conditioning is achieved by placing samples in sealed containers filled with different saturated

salt solutions. Different saturated salt solutions can give a relative humidity ranging from 11% RH (LiCl) to 77% RH (NaCl), and the moisture content of the samples inside the container changes until equilibrium is reached. Based on preliminary testing, 5 to 6 days are required for samples conditioned at low relative humidities to reach equilibrium. During this period and storage, weighing the samples daily, if not more often, is required. Given the uncertainties in both the timing and durations of lockdowns, experiments that required conditioning samples using saturated salt solution were revised. Additionally, some of the salts used in this thesis are toxic and do not have safer alternatives (e.g., LiCl); thus, working from home was not possible for this type of experiments.

As discussed in chapter 6, the kinetics of Maillard reactions at lower moisture content may differ from those at higher moisture contents. The difference in reaction kinetics could be the main cause of underestimating the temperature dependency of Maillard reactions in the current model. A better prediction model is expected with the additional kinetics data at lower moisture contents.

#### 8.2.2. Measuring furosine content in samples

Other than investigating the kinetics of Maillard reactions at lower moisture contents, measuring furosine content in the samples was also considered at the early stage of the thesis (prior to COVID-19). In fact, similar to measurements for kinetics at low moisture contents, the equipment required for measuring furosine has also been set up. Furosine is a marker for the early stage of Maillard reactions and has lower detection limits than markers for later stages of Maillard reactions. In other words, furosine is more sensitive than other markers, which is particularly suitable for investigating the effect of different spray dryer designs (different particle residence time distribution) on Maillard reactions, where the differences are expected to be small. In the measurement method for furosine in milk and other dairy products, acid hydrolysis is required for hydrolysing proteins and converting Amadori products into furosine. Acid hydrolysis is performed by heating the samples at 110°C in concentrated hydrochloric acid (37% HCL) for 23 hours, and there is no safer alternative to acid hydrolysis. Given the uncertainties in both the timing and durations of lockdowns, measurement for furosine content

in samples was not possible due to safety reasons. Without measuring furosine or other more sensitive markers for Maillard reactions, a more conclusive summary of the potential impact of spray dryers' designs on the kinetics of Maillard reactions is not possible.

### 8.3. Conclusion

In summary, due to COVID-19 relation restrictions, experiments or measurements that required constant monitoring could not be performed. Thus, the overall scope of this thesis was limited by approximately six months' work, and a request has been made to examine the thesis under emergency conditions.

## References

- Aalaei, K., Sjöholm, I., Rayner, M., Teixeira, C., Tareke, E., 2019. Early and advanced stages of Maillard reaction in infant formulas: analysis of available lysine and carboxymethyl-lysine. *PLoS One* 14. <https://doi.org/10.1371/journal.pone.0220138>
- Adachi, S., 1958. Formation of lactulose and tagatose from lactose in strongly heated milk. *Nature* 181, 840–841. <https://doi.org/10.1038/181840a0>
- Ahmed, M.U., Thorpe, S.R., Baynes, J.W., 1986. Identification of N( $\epsilon$ )-carboxymethyllysine as a degradation product of fructoselysine in glycated protein. *Journal of Biological Chemistry* 261, 4889–4894.
- Ahmed, N., Argirov, O.K., Minhas, H.S., Cordeiro, C.A.A., Thornalley, P.J., 2002. Assay of advanced glycation endproducts (AGEs): surveying AGEs by chromatographic assay with derivatization by 6-aminoquinolyl-N-hydroxysuccinimidyl-carbamate and application to N $\epsilon$ -carboxymethyl-lysine- and N $\epsilon$ -(1-carboxyethyl)lysine-modified albumin. *Biochemical Journal* 364, 1–14. <https://doi.org/10.1042/bj3640001>
- Akagawa, M., Miura, T., Suyama, K., 2002. Factors influencing the early stage of the Maillard reaction. *Int. Congr. Ser.* 1245, 395–396. [https://doi.org/10.1016/S0531-5131\(02\)00896-8](https://doi.org/10.1016/S0531-5131(02)00896-8)
- Ali, M., Mahmud, T., Heggs, P., Ghadiri, M., Bayly, A., Crosby, M., Ahmadian, H., Martindejuan, L., Alam, Z., 2017. Residence time distribution of glass ballotini in isothermal swirling flows in a counter-current spray drying tower. *Powder Technol.* 305, 809–815. <https://doi.org/10.1016/j.powtec.2016.10.023>
- Ames, J.M., Cämmerer, B., Velisek, J., Cejpek, K., Obretenov, C., Cioroi, M., 2000. The nature of melanoidins and their investigation. *Melanoidins in Food and Health* 1, 13–29.
- Anandharamakrishnan, C., Gimbut, J., Stapley, A.G.F., Rielly, C.D., 2010. A study of particle histories during spray drying using computational fluid dynamic simulations. *Drying Technol.* 28, 566–576. <https://doi.org/10.1080/07373931003787918>
- Anese, M., Manzocco, L., Maltini, E., 2001. Determination of the glass transition temperatures of "solution A" and HMW melanoidins and estimation of viscosities by the WLF equation: a preliminary study, in *Melanoidins in Food and Health* 2, 137–141.
- Arrhenius, S., 1889. Über die dissociationswärme und den einfluss der temperatur auf den dissociationsgrad der elektrolyte. *Z. Phys. Chem. (N F)* 4U, 96–116. <https://doi.org/10.1515/zpch-1889-0408>
- Australia New Zealand Food Standards, 2006. A risk profile of dairy products in Australia. Patent.
- Baklouti, S., Chartier, T., Baumard, J.F., 1998. Binder distribution in spray-dried alumina agglomerates. *J. Eur. Ceram. Soc.* 18, 2117–2121. [https://doi.org/10.1016/S0955-2219\(98\)00107-1](https://doi.org/10.1016/S0955-2219(98)00107-1)
- Bertrand, E., Meyer, X.M., Machado-Maturana, E., Berdagué, J.L., Kondjoyan, A., 2015. Modelling the Maillard reaction during the cooking of a model cheese. *Food Chem.* 184, 229–237. <https://doi.org/10.1016/j.foodchem.2015.03.097>

- Birchal, V.S., Passos, M.L., 2005. Modeling and simulation of milk emulsion drying in spray dryers. *Brazilian Journal of Chemical Engineering* 22, 293–302. <https://doi.org/10.1590/S0104-66322005000200018>
- Birlouez-Aragon, I., Nicolas, M., Metais, A., Marchond, N., Grenier, J., Calvo, D., 1998. A rapid fluorimetric method to estimate the heat treatment of liquid milk. *Int. Dairy J.* 8, 771–777. [https://doi.org/10.1016/S0958-6946\(98\)00119-8](https://doi.org/10.1016/S0958-6946(98)00119-8)
- Birlouez-Aragon, I., Pischetsrieder, M., Leclère, J., Morales, F.J., Hasenkopf, K., Kientsch-Engel, R., Ducauze, C.J., Rutledge, D., 2004. Assessment of protein glycation markers in infant formulas. *Food Chem.* 87, 253–259. <https://doi.org/10.1016/j.foodchem.2003.11.019>
- Blackwelder, R.F., Haritonidis, J.H., 1983. Scaling of the bursting frequency in turbulent boundary layers. *J. Fluid Mech.* 132, 87–103. <https://doi.org/10.1017/s0022112083001494>
- Bosch, L., Alegría, A., Farré, R., Clemente, G., 2007. Fluorescence and color as markers for the Maillard reaction in milk–cereal based infant foods during storage. *Food Chem.* 105, 1135–1143. <https://doi.org/10.1016/j.foodchem.2007.02.016>
- Brands, C.M., Alink, G.M., Boekel, M.A., Jongen, W.M., 2000. Mutagenicity of heated sugar-casein systems: effect of the Maillard reaction. *J. Agric. Food Chem.* 48, 2271–2275. <https://doi.org/10.1021/jf9907586>
- Bylund, G., Svensson, C., 1995. Dairy processing handbook: the chemistry of milk, in: *Dairy Processing Handbook*.
- Carabasa-Giribet, M., Ibarz-Ribas, A., 2000. Kinetics of colour development in aqueous glucose systems at high temperatures. *J. Food Eng.* 44, 181–189. [https://doi.org/10.1016/S0260-8774\(00\)00027-3](https://doi.org/10.1016/S0260-8774(00)00027-3)
- Caric, M., Kalab, M., 1987. Effects of drying techniques on milk powders quality and microstructure : a review. *Food Microstructure* 6, 171–180.
- Carter, B., Patel, H., Barbano, D.M., Drake, M.A., 2018. The effect of spray drying on the difference in flavor and functional properties of liquid and dried whey proteins, milk proteins, and micellar casein concentrates. *J. Dairy Sci.* 101, 3900–3909. <https://doi.org/10.3168/jds.2017-13780>
- Ceylan Sahin, C., Erbay, Z., Koca, N., 2018. The physical, microstructural, chemical and sensorial properties of spray dried full-fat white cheese powders stored in different multilayer packages. *J. Food Eng.* 229, 57–64. <https://doi.org/10.1016/j.jfoodeng.2017.11.022>
- Chansataporn, W., Tangduangdee, C., Nopharatana, M., Siriwattanayotin, S., 2019. Kinetics of Maillard reaction in a chicken meat model system using a multiresponses modeling approach. <https://doi.org/10.1002/kin.21224>
- Charlesworth, D.H., Marshall, W.R., Jr, 1960. Evaporation from drops containing dissolved solids. *AIChE J.* 6, 9–23. <https://doi.org/10.1002/aic.690060104>
- Chegini, G.R., Khazaei, J., Ghobadian, B., Goudarzi, A.M., 2008. Prediction of process and product parameters in an orange juice spray dryer using artificial neural networks. *J. Food Eng.* 84, 534–543. <https://doi.org/10.1016/j.jfoodeng.2007.06.007>



- Chen, H., Diep, E., Langrish, T.A.G., Glasser, B.J., 2020. Continuous fluidized bed drying: Residence time distribution characterization and effluent moisture content prediction. *AIChE J.* 66. <https://doi.org/10.1002/aic.16902>
- Chen, X.D., Lin, S.X.Q., 2005. Air drying of milk droplet under constant and time-dependent conditions. *AIChE J.* 51, 1790–1799. <https://doi.org/10.1002/aic.10449>
- Chiou, D., Langrish, T.A.G., Braham, R., 2008. Partial crystallization behavior during spray drying: Simulations and experiments. *Drying Technol.* 26, 27–38. <https://doi.org/10.1080/07373930701781181>
- Choi, Y.H., 1986. Effects of temperature and composition on the thermal conductivity and thermal diffusivity of some food components. *Korean J. Food Sci. Technol.* 18, 357–363.
- Claeys, W.L., Van Loey, A.M., Hendrickx, M.E., 2003. Kinetics of hydroxymethylfurfural, lactulose and furosine formation in milk with different fat content. *Journal of Dairy Research* 70, 85–90. <https://doi.org/10.1017/S0022029902005897>
- Copado, C.N., Diehl, B.W.K., Ixtaina, V.Y., Tomás, M.C., 2017. Application of Maillard reaction products on chia seed oil microcapsules with different core/wall ratios. *LWT - Food Science and Technology* 86, 408–417. <https://doi.org/10.1016/j.lwt.2017.08.010>
- Davidek, T., Clety, N., Aubin, S., Blank, I., 2002. Degradation of the Amadori compound N-(1-deoxy-d-fructos-1-yl) glycine in aqueous model systems. *Journal of Agricultural and Food Chemistry* 50, 5472–5479. <https://doi.org/10.1021/jf025561j>
- Di Scala, K., Crapiste, G., 2008. Drying kinetics and quality changes during drying of red pepper. *Lebenson. Wiss. Technol.* 41, 789–795. <https://doi.org/10.1016/j.lwt.2007.06.007>
- Edrisi Sormoli, M., 2016. Scale-up of the spray-drying process for bioactive fruit extracts. University of Sydney.
- Einarsson, H., 1987. The effect of pH and temperature on the antibacterial effect of Maillard reaction products. *Lwt* 20, 56–58.
- Einarsson, H., Eklund, T., Nes, I.F., 1988. Inhibitory mechanisms of Maillard reaction products. *Microbios* 53, 27–36.
- Einarsson, H., Snygg, B.G., Eriksson, C., 1983. Inhibition of bacterial growth by Maillard reaction products. *Journal of Agricultural and Food Chemistry* 31, 1043–1047. <https://doi.org/10.1021/jf00119a031>
- Fäldt, P., Bergenståhl, B., 1994. The surface composition of spray-dried protein-lactose powders. *Colloids and Surfaces A: Physicochemical and Engineering Aspects* 90, 183–190. [https://doi.org/10.1016/0927-7757\(94\)02914-8](https://doi.org/10.1016/0927-7757(94)02914-8)
- Fang, Z., Wang, R., Bhandari, B., 2013. Effects of type and concentration of proteins on the recovery of spray-dried sucrose powder. *Drying Technol.* 31, 1643–1652. <https://doi.org/10.1080/07373937.2013.770011>
- Fathi, F., N. Ebrahimi, S., Matos, L.C., P. P. Oliveira, M.B., Alves, R.C., 2022. Emerging drying techniques for food safety and quality: A review. *Compr. Rev. Food Sci. Food Saf.* 21, 1125–1160. <https://doi.org/10.1111/1541-4337.12898>

- Fialho, T.L., Martins, E., Silva, C.R. de J., Stephani, R., Tavares, G.M., Silveira, A.C.P., Perrone, Í.T., Schuck, P., De Oliveira, L.F.C., De Carvalho, A.F., 2018. Lactose-hydrolyzed milk powder: Physicochemical and technofunctional characterization. *Drying Technol.* 36, 1688–1695. <https://doi.org/10.1080/07373937.2017.1421551>
- Finot, P.A., Deutsch, R., Bujard, E., 1981. The extent of the Maillard reaction during the processing of milk. *Prog. Food Nutr. Sci.* 5, 345–355.
- Flowers, P., Langley, R., Robinson, W.R., Theopold, K.H., 2019. *Chemistry 2e*. OpenStax.
- Foerster, M., Gengenbach, T., Woo, M.W., Selomulya, C., 2016. The impact of atomization on the surface composition of spray-dried milk droplets. *Colloids Surf. B Biointerfaces* 140, 460–471. <https://doi.org/10.1016/j.colsurfb.2016.01.012>
- Fox, P., 2002. Significance of indigenous enzymes in milk and dairy products. *Handbook of food enzymology*. <https://doi.org/10.1201/9780203910450.ch19>
- Fox, P.F., Kelly, A.L., 2006. Indigenous enzymes in milk: overview and historical aspects—Part 1. *Int. Dairy J.* 16, 500–516. <https://doi.org/10.1016/j.idairyj.2005.09.013>
- Francia, Martin, L., Bayly, A.E., Simmons, M.J.H., 2015. The role of wall deposition and re-entrainment in swirl spray dryers. *AIChE Journal* 61, 1804–1821. <https://doi.org/10.1002/aic.14767>
- Friedman, M., 1996. Food browning and its prevention: an overview. *J. Agric. Food Chem.* 44, 631–653. <https://doi.org/10.1021/jf950394r>
- Frossling, N., 1938. *Über die Verdunstung fallender Tropfen*. *Mater. Sci.*
- Gac, J.M., Gradoń, L., 2013. A distributed parameter model for the spray drying of multicomponent droplets with a crust formation. *Adv. Powder Technol.* 24, 324–330. <https://doi.org/10.1016/j.appt.2012.08.004>
- Ge, S.J., Lee, T.C., 1997. Kinetic significance of the Schiff base reversion in the early-stage Maillard reaction of a phenylalanine-glucose aqueous model system. *Journal of Agricultural and Food Chemistry* 45, 1619–1623. <https://doi.org/10.1021/jf960458d>
- Gianfrancesco, A., 2009. *Spray Drying Engineering : Particle Stickiness in Relation With Agglomeration*.
- Gökmen, V., Şenyuva, H.Z., 2007. Effects of some cations on the formation of acrylamide and furfurals in glucose-asparagine model system. *Eur. Food Res. Technol.* 225, 815–820. <https://doi.org/10.1007/s00217-006-0486-7>
- Gómez-Narváez, F., Contreras-Calderón, J., Pérez-Martínez, L., 2019. Usefulness of some Maillard reaction indicators for monitoring the heat damage of whey powder under conditions applicable to spray drying. *Int. Dairy J.* 99. <https://doi.org/10.1016/j.idairyj.2019.104553>
- Gómez-Narváez, F., Díaz-Osorio, A., Gómez-Narváez, S., Simpson, R., Contreras-Calderón, J., 2022. Modeling the impact of spray drying conditions on some Maillard reaction indicators in nano - filtered whey. *J. Food Process Eng.* <https://doi.org/10.1111/jfpe.14212>
- Graham, D.E., Phillips, M.C., 1979. Proteins at liquid interfaces: I. Kinetics of adsorption and surface denaturation. *J. Colloid Interface Sci.* 70, 403–414. [https://doi.org/10.1016/0021-9797\(79\)90048-1](https://doi.org/10.1016/0021-9797(79)90048-1)

- Grigioni, G., Biolatto, A., Irurueta, M., Sancho, A.M., Páez, R., Pensel, N., 2007. Color changes of milk powder due to heat treatments and season of manufacture. *Ciencia y Tecnología Alimentaria* 5, 335–339. <https://doi.org/10.1080/11358120709487709>
- Guo, B., Langrish, T.A.G., Fletcher, D.F., 2001. Numerical simulation of unsteady turbulent flow in axisymmetric sudden expansions. *J. Fluids Eng.* 123, 574–587. <https://doi.org/10.1115/1.1374441>
- Haaland, S.E., 1983. Simple and explicit formulas for the friction factor in turbulent pipe flow. *J. Fluids Eng.* 105, 89–90. <https://doi.org/10.1115/1.3240948>
- Hanus, M.J., Langrish, T.A.G., 2007a. Re-entrainment of wall deposits from a laboratory-scale spray dryer. *Asia-Pac. J. Chem. Eng.* 2, 90–107. <https://doi.org/10.1002/apj.47>
- Hanus, M.J., Langrish, T.A.G., 2007b. Resuspension of wall deposits in spray dryers. *J. Zhejiang Univ. - Sci. A* 8, 1762–1774. <https://doi.org/10.1631/jzus.2007.a1762>
- Harvie, D.J.E., Langrish, T.A.G., Fletcher, D.F., 2002. A computational fluid dynamics study of a tall-form spray dryer. *Food and Bioproducts Processing: Transactions of the Institution of Chemical Engineers, Part C* 80, 163–175. [https://doi.org/10.1016/S0960-3085\(02\)70316-7](https://doi.org/10.1016/S0960-3085(02)70316-7)
- Haseley, P., Oetjen, G.-W., 2018. *Freeze-Drying*, 3rd ed. Wiley-VCH Verlag GmbH & Co. KGaA, Weinheim, Germany. <https://doi.org/10.1002/9783527808946>
- Hassan, H.M., Mumford, C.J., 1993. Mechanisms of drying of skin-forming materials.III. Droplets of natural products. *Drying Technol.* 11, 1765–1782. <https://doi.org/10.1080/07373939308916927>
- Hecht, J.P., King, C.J., 2000. Spray drying: Influence of developing drop morphology on drying rates and retention of volatile substances. 1. Single-drop experiments. *Ind. Eng. Chem. Res.* 39, 1756–1765. <https://doi.org/10.1021/ie9904652>
- Hodge, J.E., 1953. Dehydrated foods, chemistry of browning reactions in model systems. *J. Agric. Food Chem.* 1, 928–943. <https://doi.org/10.1021/jf60015a004>
- Huang, G.Q., Wang, H.O., Wang, F.W., Du, Y.L., Xiao, J.X., 2020. Maillard reaction in protein – polysaccharide coacervated microcapsules and its effects on microcapsule properties. *Int. J. Biol. Macromol.* 155, 1194–1201. <https://doi.org/10.1016/j.ijbiomac.2019.11.087>
- Huang, K., Zhang, P.J., Hu, B., Yu, S.J., 2016. The effect of spray drying on sucrose-glycine caramel powder preparation. *J. Sci. Food Agric.* 96, 2319–2327. <https://doi.org/10.1002/jsfa.7347>
- Huang, L., Kumar, K., Mujumdar, A.S., 2003. Use of computational fluid dynamics to evaluate alternative spray dryer chamber configurations. *Drying Technol.* 21, 385–412. <https://doi.org/10.1081/DRT-120018454>
- Huang, L., Mujumdar, A.S., 2006. Numerical study of two-stage horizontal spray dryers using computational fluid dynamics. *Drying Technol.* 24, 727–733. <https://doi.org/10.1080/07373930600685046>
- Huang, L., Mujumdar, A.S., 2005. Development of a new innovative conceptual design for horizontal spray dryer via mathematical modeling. *Drying Technol.* 23, 1169–1187. <https://doi.org/10.1081/DRT-200059328>

- Huang, X., Sormoli, M.E., Langrish, T.A.G., 2018. Review of some common commercial and noncommercial lab-scale spray dryers and preliminary tests for a prototype new spray dryer. *Drying Technol.* 36, 1900–1912. <https://doi.org/10.1080/07373937.2018.1459679>
- Hudson, C.S., 1904. The hydration of milk-sugar in solution. *J. Am. Chem. Soc.* 26, 1065–1082. <https://doi.org/10.1021/ja01999a002>
- Hurrell, R.F., Finot, P.A., Ford, J.E., 1983. Storage of milk powders under adverse conditions. *Br. J. Nutr.* 49, 343–354. <https://doi.org/10.1079/bjn19830043>
- Jaskulski, M., Atuonwu, J.C., Tran, T.T.H., Stapley, A.G.F., Tsotsas, E., 2017. Predictive CFD modeling of whey protein denaturation in skim milk spray drying powder production. *Adv. Powder Technol.* 28, 3140–3147. <https://doi.org/10.1016/j.apt.2017.09.026>
- Jeantet, R., Ducept, F., Dolivet, A., Méjean, S., Schuck, P., 2008. Residence time distribution: a tool to improve spray-drying control. *Dairy Sci. Technol.* 88, 31–43. <https://doi.org/10.1051/dst:2007006>
- Jousse, F., Jongen, T., Agterof, W., Russell, S., Braat, P., 2002. Simplified kinetic scheme of flavor formation by the Maillard reaction. *J. Food Sci.* 67, 2534–2542. <https://doi.org/10.1111/j.1365-2621.2002.tb08772.x>
- Karmas, R., Pilar Buera, M., Karel, M., 1992. Effect of glass transition on rates of nonenzymic browning in food systems. *J. Agric. Food Chem.* 40, 873–879. <https://doi.org/10.1021/jf00017a035>
- Katekhong, W., Charoenrein, S., 2018. Influence of spray drying temperatures and storage conditions on physical and functional properties of dried egg white. *Drying Technol.* 36, 169–177. <https://doi.org/10.1080/07373937.2017.1307218>
- Kato, H., Van Chuyen, N., Lee, I.E., Kim, S.B., Hayase, F., 1987. Inhibition of nitrosamine formation by nondialyzable melanoidins. *Agricultural and Biological Chemistry* 51, 1333–1338. <https://doi.org/10.1271/bbb1961.51.1333>
- Katopodes, N.D., 2018. Free-surface flow: environmental fluid mechanics. Butterworth-Heinemann.
- Keeney, M., Bassette, R., 1959. Detection of intermediate compounds in the early stages of browning reaction in milk products. *Journal of Dairy Science* 42, 945–960. [https://doi.org/10.3168/jds.S0022-0302\(59\)90678-2](https://doi.org/10.3168/jds.S0022-0302(59)90678-2)
- Key, R.B., 1978. Introduction to industrial drying operations. Pergamon, Oxford ; New York.
- Keshani, S., Daud, W.R.W., Nourouzi, M.M., Namvar, F., Ghasemi, M., 2015. Spray drying: an overview on wall deposition, process and modeling. *J. Food Eng.* 146, 152–162. <https://doi.org/10.1016/j.jfoodeng.2014.09.004>
- Keshani, S., Daud, W.R.W., Woo, M.W., Nourouzi, M.M., Talib, M.Z.M., Chuah, A.L., Russly, A.R., 2013. Reducing the deposition of fat and protein covered particles with low energy surfaces. *J. Food Eng.* 116, 737–748. <https://doi.org/10.1016/j.jfoodeng.2013.01.003>
- Keshani, S., Daud, W.R.W., Woo, M.W., Talib, M.Z.M., Chuah, A.L., Russly, A.R., 2012. Artificial neural network modeling of the deposition rate of lactose powder in spray dryers. *Drying Technol.* 30, 386–397. <https://doi.org/10.1080/07373937.2011.638228>

- Kestin, J., Sokolov, M., Wakeham, W.A., 1978. Viscosity of liquid water in the range  $-8^{\circ}\text{C}$  to  $150^{\circ}\text{C}$ . *J. Phys. Chem. Ref. Data* 7, 941–948. <https://doi.org/10.1063/1.555581>
- Kieviet, F., Kerkhof, P.J.A.M., 1995. Measurements of particle residence time distributions in A co-current spray dryer. *Drying Technol.* 13, 1241–1248. <https://doi.org/10.1080/07373939508917019>
- Kieviet, F.G., 1997. Modelling quality in spray drying. Ph.D. Dissertation. <https://doi.org/10.6100/IR477431>
- Killie, S., Hafskjold, B., Borgen, O., Ratkje, S.K., Hovde, E., 1991. High-pressure diffusion measurements by Mach - Zehnder interferometry. *AIChE Journal* 37, 142 – 146. <https://doi.org/10.1002/aic.690370113>
- Kim, E., Chen, X.D., Pearce, D., 2003. On the mechanisms of surface formation and the surface compositions of industrial milk powders. *Drying Technology* 21, 265–278. <https://doi.org/10.1081/DRT-120017747>
- Kim, E.H.-J., Chen, X.D., Pearce, D., 2002. Surface characterization of four industrial spray-dried dairy powders in relation to chemical composition, structure and wetting property. *Colloids Surf. B Biointerfaces* 26, 197–212. [https://doi.org/10.1016/s0927-7765\(01\)00334-4](https://doi.org/10.1016/s0927-7765(01)00334-4)
- Kline, S.J., Reynolds, W.C., Schraub, F.A., Runstadler, P.W., 1967. The structure of turbulent boundary layers. *J. Fluid Mech.* 30, 741–773. <https://doi.org/10.1017/S0022112067001740>
- Koca, N., Erbay, Z., Kaymak-Ertekin, F., 2015. Effects of spray-drying conditions on the chemical, physical, and sensory properties of cheese powder. *J. Dairy Sci.* 98, 2934–2943. <https://doi.org/10.3168/jds.2014-9111>
- Kocadağlı, T., Gökmen, V., 2016. Multiresponse kinetic modelling of Maillard reaction and caramelisation in a heated glucose/wheat flour system. *Food Chem.* 211, 892–902. <https://doi.org/10.1016/j.foodchem.2016.05.150>
- Kousaka, Y., Okuyama, K., Endo, Y., 1980. Re-entrainment of small aggregate particles from a plane surface by air stream. *J. Chem. Eng. Jpn.* 13, 143–147. <https://doi.org/10.1252/jcej.13.143>
- Lakni, W., Jayasinghe-Mudalige, U.K., 2010. Customer-defined quality of food: an empirical investigation based on kano analytical methods for milk powder. *Jiangsu nong ye xue bao* 4, 45. <https://doi.org/10.4038/jas.v4i2.1644>
- Langrish, T., Huang, X., Zhong, C., 2018. Wall deposition experiments in a new spray dryer. Presented at the 21th International Drying Symposium. <https://doi.org/10.4995/IDS2018.2018.8270>
- Langrish, T.A.G., 2009. Multi-scale mathematical modelling of spray dryers. *J. Food Eng.* 93, 218–228. <https://doi.org/10.1016/j.jfoodeng.2009.01.019>
- Langrish, T.A.G., Harrington, J., Huang, X., Zhong, C., 2020. Using CFD simulations to guide the development of a new spray dryer design. *Processes* 8. <https://doi.org/10.3390/PR8080932>

- Langrish, T.A.G., Kockel, T.K., 2001. The assessment of a characteristic drying curve for milk powder for use in computational fluid dynamics modelling. *Chem. Eng. J.* 84, 69–74. [https://doi.org/10.1016/S1385-8947\(00\)00384-3](https://doi.org/10.1016/S1385-8947(00)00384-3)
- Lea, C.H., Hannan, R.S., 1949. Studies of the reaction between proteins and reducing sugars in the "dry" state. *Biochim. Biophys. Acta* 3, 313–325. [https://doi.org/10.1016/0006-3002\(49\)90100-6](https://doi.org/10.1016/0006-3002(49)90100-6)
- Lee, K.G., Shibamoto, T., 2002. Toxicology and antioxidant activities of non-enzymatic browning reaction products: Review. *Food Reviews International* 18, 151–175. <https://doi.org/10.1081/FRI-120014356>
- Lee, Y.Y., Tang, T.K., Phuah, E.T., Alitheen, N.B.M., Tan, C.P., Lai, O.M., 2017. New functionalities of Maillard reaction products as emulsifiers and encapsulating agents, and the processing parameters: a brief review. *J. Sci. Food Agric.* 97, 1379–1385. <https://doi.org/10.1002/jsfa.8124>
- Lee, Y.Y., Tang, T.K., Tan, C.P., Alitheen, N.B.M., Phuah, E.T., Karim, N.A.A., Lai, O.M., 2015. Entrapment of palm-based medium- and long-chain triacylglycerol via Maillard reaction products. *Food Bioprocess Technol.* 8, 1571–1582. <https://doi.org/10.1007/s11947-015-1520-1>
- Lorenzen, P.C., Martin, D., Clawin-Rädecker, I., Barth, K., Knappstein, K., 2010. Activities of alkaline phosphatase,  $\gamma$ -glutamyltransferase and lactoperoxidase in cow, sheep and goat's milk in relation to heat treatment. *Small Rumin. Res.* 89, 18–23. <https://doi.org/10.1016/j.smallrumres.2009.11.013>
- Lu, S.S., Willmarth, W.W., 1973. Measurements of the structure of the Reynolds stress in a turbulent boundary layer. *J. Fluid Mech.* 60, 481–511. <https://doi.org/10.1017/S0022112073000315>
- Lucey, J.A., 2002. ADSA Foundation Scholar Award. Formation and physical properties of milk protein gels. *J. Dairy Sci.* 85, 281–294. [https://doi.org/10.3168/jds.s0022-0302\(02\)74078-2](https://doi.org/10.3168/jds.s0022-0302(02)74078-2)
- Maillard, L.C., 1912. Action des acides aminés sur les sucres: Formation des mélanoidines par voie méthodique. Réaction de Maillard. *C. R. Acad. Sci.* 154, 66–68.
- Martins, S.I.F.S., Jongen, W.M.F., Boekel, M.A.J.S., 2000. A review of Maillard reaction in food and implications to kinetic modelling. *Trends Food Sci. Technol.* 11, 364–373. [https://doi.org/10.1016/S0924-2244\(01\)00022-X](https://doi.org/10.1016/S0924-2244(01)00022-X)
- Martins, S.I.F.S., Boekel, M.A.J.S., 2005. A kinetic model for the glucose/glycine Maillard reaction pathways. *Food Chem.* 90, 257–269. <https://doi.org/10.1016/j.foodchem.2004.04.006>
- Martins, S.I.F.S., Boekel, M.A.J.S., 2002. Key intermediates in early stage Maillard reaction: kinetic analysis. *Int. Congr. Ser.* 1245, 469–470. [https://doi.org/10.1016/S0531-5131\(02\)00904-4](https://doi.org/10.1016/S0531-5131(02)00904-4)
- Masters, K., 1979. *Spray Drying Handbook*, 3d ed. ed. G. Godwin, London. <https://doi.org/10.1080/07373938908916598>
- Masters, K., 1972. *Spray drying: An introduction to principles, operational practice, and applications*. Cleveland, CRC Press.

- Matiacevich, S.B., Santagapita, P.R., Buera, M.P., 2005. Fluorescence from the maillard reaction and its potential applications in food science. *Crit. Rev. Food Sci. Nutr.* 45, 483–495. <https://doi.org/10.1080/10408390591034472>
- Mazza, M.G.G., Brandão, L.E.B., Wildhagen, G.S., 2003. Characterization of the residence time distribution in spray dryers. *Drying Technol.* 21, 525–538. <https://doi.org/10.1081/DRT-120018460>
- McAllister, S., Chen, J.-Y., Fernandez-Pello, A.C., 2013. *Fundamentals of combustion processes*, 2011th ed, Mechanical Engineering Series. Springer, New York, NY.
- McSweeney, P.L.H., Fox, P.F., 2009. *Advanced dairy chemistry*. <https://doi.org/10.1007/978-0-387-84865-5>
- Meerdink, G., 1994. Drying of liquid food droplets enzyme inactivation and multicomponent diffusion. <https://doi.org/10.1080/07373939408960007>
- Meshram, B.D., Asgar, S., Ranvir, S., Adil, S., 2018. Chemical markers for monitoring heat damage of processed milk: review. *International Journal of Chemical Studies* 6, 2073–2081.
- Metzger, M., McKeon, B., Arce-Larreta, E., 2010. Scaling the characteristic time of the bursting process in the turbulent boundary layer. *Physica D* 239, 1296–1304. <https://doi.org/10.1016/j.physd.2009.09.004>
- Miao, S., Roos, Y.H., 2004. Nonenzymatic browning kinetics of a carbohydrate-based low-moisture food system at temperatures applicable to spray drying. *J. Agric. Food Chem.* 52, 5250–5257. <https://doi.org/10.1021/jf049706t>
- Michalska, A., Wojdyło, A., Brzezowska, J., Majerska, J., Ciska, E., 2019. The influence of inulin on the retention of polyphenolic compounds during the drying of blackcurrant juice. *Molecules* 24. <https://doi.org/10.3390/molecules24224167>
- Morales, F.J., Romero, C., Jiménez-Pérez, S., 1997. Chromatographic determination of bound hydroxymethylfurfural as an index of milk protein glycosylation. *Journal of Agricultural and Food Chemistry* 45, 1570–1573. <https://doi.org/10.1021/jf960930v>
- Morales, F.J., Boekel, M.A.J.S., 1998. A study on advanced Maillard reaction in heated casein/sugar solutions: colour formation. *Int. Dairy J.* 8, 907–915. [https://doi.org/10.1016/S0958-6946\(99\)00014-X](https://doi.org/10.1016/S0958-6946(99)00014-X)
- Morales, F.J., Boekel, M.A.J.S., 1997. A study on advanced maillard reaction in heated casein/sugar solutions: Fluorescence accumulation. *Int. Dairy J.* 7, 675–683. [https://doi.org/10.1016/S0958-6946\(97\)00071-X](https://doi.org/10.1016/S0958-6946(97)00071-X)
- Mundt, S., Wedzicha, B.L., Boekel, M.A.J.S., 2002. A kinetic model for the maltose–glycine reaction. *Int. Congr. Ser.* 1245, 465–467. [https://doi.org/10.1016/S0531-5131\(02\)00914-7](https://doi.org/10.1016/S0531-5131(02)00914-7)
- Nijdam, J.J., Langrish, T.A.G., 2006. The effect of surface composition on the functional properties of milk powders. *J. Food Eng.* 77, 919–925. <https://doi.org/10.1016/j.jfoodeng.2005.08.020>
- Nijdam, J.J., Langrish, T.A.G., 2005. An investigation of milk powders produced by a laboratory-scale spray dryer. *Drying Technol.* 23, 1043–1056. <https://doi.org/10.1081/DRT-200060208>

- Nishanthi, M., Chandrapala, J., Vasiljevic, T., 2018. Physical properties of selected spray dried whey protein concentrate powders during storage. *J. Food Eng.* 219, 111–120. <https://doi.org/10.1016/j.jfoodeng.2017.09.021>
- Nunes, L., Martins, E., Tuler Perrone, Í., Fernandes de Carvalho, A., 2019. The Maillard reaction in powdered infant formula. *Journal of Food and Nutrition Research* 7, 33–40. <https://doi.org/10.12691/jfnr-7-1-5>
- Nursten, H., 2005. *The Maillard reaction: chemistry, biochemistry, and implications*. Royal Society of Chemistry.
- Nursten, H.E., 1986. *Maillard Browning Reaction in Dried Foods*.
- Oakley, D.E., 2004. Spray dryer modeling in theory and practice. *Dry. technol.* 22, 1371–1402. <https://doi.org/10.1081/drt-120038734>
- Oakley, D.E., 1994. Scale-up of spray dryers with the aid of computational fluid dynamics. *Drying Technol.* 12, 217–233. <https://doi.org/10.1080/07373939408959954>
- Ozmen, L., Langrish, T.A.G., 2003. An Experimental Investigation of the Wall deposition of milk powder in a pilot-scale spray dryer. *Drying Technol.* 21, 1253–1272. <https://doi.org/10.1081/DRT-120023179>
- Ozmen, L., Langrish, T.A.G., 2002. Comparison of glass transition temperature and sticky point temperature for skim milk powder. *Drying Technol.* 20, 1177–1192. <https://doi.org/10.1081/DRT-120004046>
- Park, C.W., Stout, M.A., Drake, M., 2016. The effect of spray-drying parameters on the flavor of nonfat dry milk and milk protein concentrate 70. *J. Dairy Sci.* 99, 9598–9610. <https://doi.org/10.3168/jds.2016-11692>
- Patanwar, P., Shukla, S.K., 2012. Parametric studies of a hybrid desiccant cooling system. *Nucl. Eng. Des./Fusion* 2, 253–258. <https://doi.org/10.5923/j.ijee.20120205.09>
- Peleg, M., Normand, M.D., Corradini, M.G., 2012. The Arrhenius equation revisited. *Crit. Rev. Food Sci. Nutr.* 52, 830–851. <https://doi.org/10.1080/10408398.2012.667460>
- Pelerine, D.H.G., Gomes, M.T. de M.S., 2008. Whey proteins solubility curves at several temperatures values. *Ciência e Natura* 30, 17–25.
- Pereyra Gonzales, A.S., Naranjo, G.B., Leiva, G.E., Malec, L.S., 2010. Maillard reaction kinetics in milk powder: Effect of water activity at mild temperatures. *Int. Dairy J.* 20, 40–45. <https://doi.org/10.1016/j.idairyj.2009.07.007>
- Perry, R.H., Chilton, C.H., Green, D.W., 1997. *Perry's chemical engineers' handbook*, 7th ed, Handbook. McGraw-Hill Publishing, London, England.
- Pisecký, J., 1997. *Handbook of milk powder manufacture*. Niro. <https://doi.org/10.1007/978-1-908517-43-2>
- Pokorný, J., Pilková, L., Davídek, J., Valentová, H., 1988. Effect of Amadori rearrangement products on the non-enzymic browning in model systems. *Food / Nahrung* 32, 767–776. <https://doi.org/10.1002/food.19880320814>
- Potter, M.C., Wiggert, D.C., 2009. *Mechanics of fluids*. Nelson Engineering, Florence, KY.
- Putranto, A., Foerster, M., Woo, M.W., Selomulya, C., Chen, X.D., 2017. A continuum-approach modeling of surface composition and ternary component distribution inside



- low fat milk emulsions during single droplet drying. *AIChE J.* 63, 2535–2545. <https://doi.org/10.1002/aic.15657>
- Qian, F., Sun, J., Cao, D., Tuo, Y., Jiang, S., Mu, G., 2017. Experimental and modelling study of the denaturation of milk protein by heat treatment. *Korean J Food Sci Anim Resour* 37, 44–51. <https://doi.org/10.5851/kosfa.2017.37.1.44>
- Qiu, J., Vuist, J.-E., Boom, R.M., Schutyser, M.A.I., 2018. Formation and degradation kinetics of organic acids during heating and drying of concentrated tomato juice. *Lebenson. Wiss. Technol.* 87, 112–121. <https://doi.org/10.1016/j.lwt.2017.08.081>
- Reid, D.S., Levine, H., 1991. Beyond water activity: recent advances based on an alternative approach to the assessment of food quality and safety. *Critical Reviews in Food Science and Nutrition* 30, 115–360. <https://doi.org/10.1080/10408399109527543>
- Reineccius, G.A., 1999. Kinetics of flavor formation during Maillard browning. *Flavor Chemistry* 345–352. [https://doi.org/10.1007/978-1-4615-4693-1\\_29](https://doi.org/10.1007/978-1-4615-4693-1_29)
- Ren, G.R., Zhao, L.J., Sun, Q., Xie, H.J., Lei, Q.F., Fang, W.J., 2015. Explore the reaction mechanism of the Maillard reaction: a density functional theory study. *J. Mol. Model.* 21, 1–17. <https://doi.org/10.1007/s00894-015-2674-5>
- Rhim, J.W., Jones, V.A., Swartzel, K.R., 1988. Kinetics studies in the colour changes of skim milk. *LWT - Food Science and Technology* 21, 334–338.
- Rhodes, M., 1998. *Introduction to particle technology.* John Wiley & Sons, Chichester, England.
- Ritota, M., Di Costanzo, M.G., Mattera, M., Manzi, P., 2017. New trends for the evaluation of heat treatments of milk. *J. Anal. Methods Chem.* 2017, 1864832. <https://doi.org/10.1155/2017/1864832>
- Rongsirikul, N., Hongsprabhas, P., 2016. Brown pigment formation in heated sugar–protein mixed suspensions containing unmodified and peptically modified whey protein concentrates. *J. Food Sci. Technol.* 53, 800–807. <https://doi.org/10.1007/s13197-015-1955-4>
- Roos, Y.H., 2016. Phase Transitions in Foods. <https://doi.org/10.1016/c2012-0-06577-5>
- Roos, Y.H., 2009. Solid and Liquid States of Lactose. *Advanced Dairy Chemistry* 3, 1–778. <https://doi.org/10.1007/978-0-387-84865-5>
- Roos, Y.H., 2002. Importance of glass transition and water activity to spray drying and stability of dairy powders. *Lait* 82, 475–484.
- Roos, Y.H., Jouppila, K., Zielasko, B., 1996. Non-enzymatic browning-induced water plasticization. *J. Therm. Anal. Calorim.* 47, 1437–1450. <https://doi.org/10.1007/bf01992838>
- Roser, B., 1991. Trehalose, a new approach to premium dried foods. *Trends in Food Science and Technology* 2, 166–169. [https://doi.org/10.1016/0924-2244\(91\)90671-5](https://doi.org/10.1016/0924-2244(91)90671-5)
- Roshko, A., 1954. On the Development of Turbulent Wakes from Vortex Streets. [ntrs.nasa.gov](http://ntrs.nasa.gov).
- Ruprecht, N.A., Kohlus, R., 2018. Determination and modelling of the particle size dependent residence time distribution in a pilot plant spray dryer. Presented at the 21st International Drying Symposium Proceedings. <https://doi.org/10.4995/ids2018.2018.7740>

- Sahin, S., Sumnu, S.G., 2006. Thermal properties of foods, in: Sahin, S., Sumnu, S.G. (Eds.), *Physical Properties of Foods*. Springer New York, New York, NY, pp. 107–155. [https://doi.org/10.1007/0-387-30808-3\\_3](https://doi.org/10.1007/0-387-30808-3_3)
- Saltzman, W.M., Radomsky, M.L., Whaley, K.J., Cone, R.A., 1994. Antibody diffusion in human cervical mucus. *Biophysical Journal* 66, 508–515. [https://doi.org/10.1016/S0006-3495\(94\)80802-1](https://doi.org/10.1016/S0006-3495(94)80802-1)
- Samborska, K., Jedlińska, A., Wiktor, A., Derewiaka, D., Wołosiak, R., Matwijczuk, A., Jamróz, W., Skwarczyńska-Maj, K., Kielczewski, D., Błażowski, Ł., Tułodziecki, M., Witrowa-Rajchert, D., 2019. The effect of low-temperature spray drying with dehumidified air on phenolic compounds, antioxidant activity, and aroma compounds of rapeseed honey powders. *Food Bioprocess Technol.* <https://doi.org/10.1007/s11947-019-02260-8>
- Santivarangkna, C., Kulozik, U., Foerst, P., 2007. Alternative drying processes for the industrial preservation of lactic acid starter cultures. *Biotechnology Progress* 23, 302–315. <https://doi.org/10.1021/bp060268f>
- Schlichting, H., Gersten, K., 2018. *Boundary-Layer Theory*. Springer, Berlin, Germany.
- Schmitz, I., Gianfrancesco, A., Kulozik, U., Foerst, P., 2011. Kinetics of lysine loss in an infant formula model system at conditions applicable to spray drying. *Drying Technol.* 29, 1876–1883. <https://doi.org/10.1080/07373937.2011.589553>
- Schmitz-Schug, I., Foerst, P., Kulozik, U., 2013. Impact of the spray drying conditions and residence time distribution on lysine loss in spray dried infant formula. *Dairy Sci. Technol.* 93, 443–462. <https://doi.org/10.1007/s13594-013-0115-8>
- Schmitz-Schug, I., Kulozik, U., Foerst, P., 2016. Modeling spray drying of dairy products – Impact of drying kinetics, reaction kinetics and spray drying conditions on lysine loss. *Chem. Eng. Sci.* 141, 315–329. <https://doi.org/10.1016/j.ces.2015.11.008>
- Schmitz-Schug, I., Kulozik, U., Foerst, P., 2014. Reaction kinetics of lysine loss in a model dairy formulation as related to the physical state. *Food Bioproc. Tech.* 7, 877–886. <https://doi.org/10.1007/s11947-013-1119-3>
- Schuck, P., 2006. Spray drying of dairy products: a review. *New Food* 1, 14–20.
- Shannon, C.E., 1949. Communication in the Presence of Noise. *Proceedings of the IRE* 37, 10–21. <https://doi.org/10.1109/JRPROC.1949.232969>
- Sherrington, D.C., 1993. Introduction to physical polymer science. *React. Polym.* 20, 217–218. [https://doi.org/10.1016/0923-1137\(93\)90096-x](https://doi.org/10.1016/0923-1137(93)90096-x)
- Shishir, M.R.I., Chen, W., 2017. Trends of spray drying: A critical review on drying of fruit and vegetable juices. *Trends Food Sci. Technol.* 65, 49–67. <https://doi.org/10.1016/j.tifs.2017.05.006>
- Singh, M.J., Chandrapala, J., Udabage, P., McKinnon, I., Augustin, M.A., 2015. Heat-induced changes in the properties of modified skim milks with different casein to whey protein ratios. *J. Dairy Res.* 82, 135–142. <https://doi.org/10.1017/S0022029914000739>
- Stanish, M.A., Schajer, G.S., Kayihan, F., 1986. A mathematical model of drying for hygroscopic porous media. *AIChE J.* 32, 1301–1311. <https://doi.org/10.1002/aic.690320808>

- Straatsma, J., Van Houwelingen, G., Steenbergen, A.E., De Jong, P., 1999. Spray drying of food products: 1. Simulation model. *J. Food Eng.* 42, 67–72. [https://doi.org/10.1016/S0260-8774\(99\)00107-7](https://doi.org/10.1016/S0260-8774(99)00107-7)
- Thijssen, H.A.C., Coumans, W.J., 1985. Short-cut calculation for non-isothermal drying of shrinking and non-shrinking particles and of hollow spheres containing an expanding central gas core. pp. 11–20. [https://doi.org/10.1007/978-3-662-21830-3\\_2](https://doi.org/10.1007/978-3-662-21830-3_2)
- Tomlinson, A.J., Mlotkiewicz, J.A., Lewis, I.A.S., 1993. An investigation of the compounds produced by spray-drying an aqueous solution of glucose and glycine. *Food Chem.* 48, 373–379. [https://doi.org/10.1016/0308-8146\(93\)90320-F](https://doi.org/10.1016/0308-8146(93)90320-F)
- Tran, T.T.H., Jaskulski, M., Tsotsas, E., 2017. Reduction of a model for single droplet drying and application to CFD of skim milk spray drying. *Drying Technol.* 35, 1571–1583. <https://doi.org/10.1080/07373937.2016.1263204>
- Uribarri, J., Woodruff, S., Goodman, S., Cai, W., Chen, X., Pyzik, R., Yong, A., Striker, G.E., Vlassara, H., 2010. Advanced glycation end products in foods and a practical guide to their reduction in the diet. *Journal of the American Dietetic Association* 110. <https://doi.org/10.1016/j.jada.2010.03.018>
- Boekel, M.A., 2001. Kinetic aspects of the Maillard reaction: a critical review. *Nahrung* 45, 150–159. [https://doi.org/10.1002/1521-3803\(20010601\)45:3<150::AID-FOOD150>3.0.CO;2-9](https://doi.org/10.1002/1521-3803(20010601)45:3<150::AID-FOOD150>3.0.CO;2-9)
- Boekel, M.A.J.S., 1998. Effect of heating on Maillard reactions in milk. *Food Chem.* 62, 403–414. [https://doi.org/10.1016/S0308-8146\(98\)00075-2](https://doi.org/10.1016/S0308-8146(98)00075-2)
- Boekel, M.A.J.S., 1998. Effect of heating on Maillard reactions in milk. *Food Chemistry* 62, 403–414. [https://doi.org/10.1016/S0308-8146\(98\)00075-2](https://doi.org/10.1016/S0308-8146(98)00075-2)
- Boekel, M.A.J.S., Martins, S.I.F.S., 2002. Fate of glycine in the glucose–glycine reaction: a kinetic analysis. *Int. Congr. Ser.* 1245, 289–293. [https://doi.org/10.1016/S0531-5131\(02\)00893-2](https://doi.org/10.1016/S0531-5131(02)00893-2)
- Vasbinder, A.J., Alting, A.C., De Kruif, K.G., 2003. Quantification of heat-induced casein–whey protein interactions in milk and its relation to gelation kinetics. *Colloids Surf. B Biointerfaces* 31, 115–123. [https://doi.org/10.1016/S0927-7765\(03\)00048-1](https://doi.org/10.1016/S0927-7765(03)00048-1)
- Vasbinder, A.J., de Kruif, C.G., 2003. Casein–whey protein interactions in heated milk: the influence of pH. *Int. Dairy J.* 13, 669–677. [https://doi.org/10.1016/S0958-6946\(03\)00120-1](https://doi.org/10.1016/S0958-6946(03)00120-1)
- Verardo, V., Riciputi, Y., Messia, M.C., Marconi, E., Caboni, M.F., 2017. Influence of drying temperatures on the quality of pasta formulated with different egg products. *Eur. Food Res. Technol.* 243, 817–825. <https://doi.org/10.1007/s00217-016-2795-9>
- Walton, D.E., 2000. The morphology of spray-dried particles a qualitative view. *Drying Technol.* 18, 1943–1986. <https://doi.org/10.1080/07373930008917822>
- Wang, S., Langrish, T., 2009a. A review of process simulations and the use of additives in spray drying. *Food Research International.* <https://doi.org/10.1016/j.foodres.2008.09.006>

- Wang, S., Langrish, T., Adhikari, B., 2013. A multicomponent distributed parameter model for spray drying: model development and validation with experiments. *Drying Technol.* 31, 1513–1524. <https://doi.org/10.1080/07373937.2013.813533>
- Wang, S., Langrish, T.A.G., 2009b. A distributed parameter model for particles in the spray drying process. *Adv. Powder Technol.* 20, 220–226. <https://doi.org/10.1016/j.appt.2009.03.004>
- Wijlhuizen, A.E., Kerkhof, P.J.A.M., Bruin, S., 1979. Theoretical study of the inactivation of phosphatase during spray-drying of skim-milk. *Chem. Eng. Sci.* 34, 651–660.
- Yaylayan, V.A., Ismail, A.A., Mandeville, S., 1993. Quantitative determination of the effect of pH and temperature on the keto form of d-fructose by FT IR spectroscopy. *Carbohydr. Res.* 248, 355–360. [https://doi.org/10.1016/0008-6215\(93\)84141-R](https://doi.org/10.1016/0008-6215(93)84141-R)
- Yen, G.C., Hsieh, P.P., 1994. Possible mechanisms of antimutagenic effect of Maillard reaction products prepared from xylose and lysine. *Journal of Agricultural and Food Chemistry* 42, 133–137. <https://doi.org/10.1021/jf00037a023>
- Zbicinski, I., Strumillo, C., Delag, A., 2002. Drying kinetics and particle residence time in spray drying. *Drying Technol.* 20, 1751–1768. <https://doi.org/10.1081/DRT-120015412>
- Zhong, C., Tan, S., Langrish, T., 2019. Redness generation via Maillard reactions of whey protein isolate (WPI) and ascorbic acid (vitamin C) in spray-dried powders. *J. Food Eng.* 244, 11–20. <https://doi.org/10.1016/j.jfoodeng.2018.09.020>

## Appendix:

### A.1. Codes for controlling automated dye injection system

```
#coding:utf-8

#Dye injection system
#Jacky Zhou
#21 01 2021

#Import functions
import RPi.GPIO as GPIO
import time

#set GPIO mode
GPIO.setmode(GPIO.BCM)

#setting output mode
GPIO.setup(17,GPIO.OUT)
GPIO.setup(27,GPIO.OUT)

#loop control
for x in range(1,3):
    GPIO.output(17,GPIO.HIGH)
    GPIO.output(27,GPIO.HIGH)
    time.sleep(0.5)
    GPIO.output(17,GPIO.LOW)
    GPIO.output(27,GPIO.LOW)
    time.sleep(179.5)

GPIO.cleanup()
```

## A.2. Codes for colour analysis

### Main file:

```
%Cleaning
clc,clear all,close all

%Number of images
n=6;

%Calculate L,a,b,E,Chroma values
for i=1:n

    %Load image
    imageName=[num2str(i),'.jpg'];

    %Calculate averaged L,a,b,E,Chroma values
    output=getAverage(imread(imageName));
    L(i)=output(1);
    a(i)=output(2);
    b(i)=output(3);
    E(i)=sqrt(L(i)^2+a(i)^2+b(i)^2);
    C(i)=sqrt(a(i)^2+b(i)^2);
end

%Display the averaged L,a,b,E,Chroma values
disp(L);
disp(a);
disp(b);
disp(E);
disp(C);

%Export results as matrix
result=[L;a;b;E;C];
```

## Function file 1: getAverage.m

```
function output=getAverage(image)

%Get size of the image
[row,col,color]=size(image);

%Initiate counters
sumr=0;
sumg=0;
sumb=0;

%Set range for sampling windows
ri=round(0.5*row-25);
re=round(0.5*row+25);
ci=round(0.5*col-25);
ce=round(0.5*col+25);

%Extract r,g,b values from sampling windows
r=image((ri:re),(ci:ce),1);
g=image((ri:re),(ci:ce),2);
b=image((ri:re),(ci:ce),3);

%Calculate averaged r,g,b values within the sampling window
avgr=averageMatrix(r);
avgg=averageMatrix(g);
avgb=averageMatrix(b);

%Regenerate colour values
matrix(1,1,1)=uint8(avgr);
matrix(1,1,2)=uint8(avgg);
matrix(1,1,3)=uint8(avgb);

%Convert and return colour values in CIElab colour space
output=rgb2lab(matrix);
end
```

## Function file 2: averageMatrix.m

```
function average=averageMatrix(matrix)

%get size of the matrix
[r,c]=size(matrix);

%initiate counter
sum=0;

%Change values to type double, and calculate sum of all values in the matrix
for i=1:r
    for j=1:c
        sum=sum+double(matrix(i,j));
    end
end

%Calculate average of all values in the matrix, and return
average=sum/r/c;
end
```



### A.3. Codes for CSTR-TIS model fitting

#### Main file

```
%Cleaning
clc,clear all,close all

%Globalising parameters
global n tau

%Loop though all measured signals
for colcounter=1:12

%Initiate the reset counter 1
counter=1;

%Load processed data
data=xlsread('100% 100C.xlsx');

%Set sampling region for signals
dlength=1800;
dstart=1;

%Change number last number for the different peaks
data=data(dstart:dlength,colcounter)';

% Normalised the data
data=data/max(data);

%Initiate the reset counter 2
counter3=1;

%Try out different n and tau, stored in the difference matrix
for n=1:20
    counter2=1;
    for tau=0.1:0.1:30
        counter=1;
        %Calculate RTD based on current n and tau
        for t=0.1*dstart:0.1:0.1*dlength
            rtd(counter)=csrtmodel(t);
            counter=counter+1;
        end
    end
end
```

```

        % Normalised the estimated RTD
        rtd=rtd/max(rtd);

        %Calculated the square root of the sum of squared error (SSE) and
        stored in a matrix
        difference(counter2,counter3)=sqrt(sum((data-rtd).^2));
        counter2=counter2+1;
    end
    counter3=counter3+1;
end

%Calculate size of the matrix storing SSE
[r,c]=size(difference);

%Reset counters
rmin=1;
cmin=1;

%Find minimum difference from the matrix storing SSE
for i=1:c
    for j=1:r
        if difference(rmin,cmin)>difference(j,i)
            rmin=j;
            cmin=i;
        end
    end
end

%Export the minimum tau and n
result(colcounter,1)=rmin/10;
result(colcounter,2)=cmin;

end

```

### Function file 1: cstrmodel.m

```
function output=cstrmodel(t)

%Globalising tau and n
global tau n

%Calculate RTD based on tau and n
output=n/factorial(n-1)*exp(-n*t/tau)*(n*t/tau)^(n-1);
end
```

#### A.4. Code for Fourier transform of measured signals

```
%Cleaning
clc,clear all,close all

%Load data
data=xlsread("80%.xlsx");

[rr,cc]=size(data);

%Data length
L=600;

%Sampling frequency Hz
fs=10;

%Sampling period(s)
T=1/fs;

%Time domain (s)
t=(0:(L-1))*T;

for i=1:cc
    %FFT of the signal
    figure(1)
    result=fft(data(1200:1800,i));
    f = fs*(0:(L/2))/L;
    P2 = abs(result/L);
    P1 = P2(1:L/2+1);
    P1(2:end-1) = 2*P1(2:end-1);

    %Find peaks of signal in frequency domain, and sorted peak frequency in
    %a descending order
    [result,locs]=findpeaks(P1, 'SortStr', 'descend');

    %Loop though peaks found
    if length(result')>=1
        counter=1;
        for j=1:length(result')

            %Ignore all peaks if peak frequency is lower than 1/60 Hz,
            %and report the peak frequency with highest amplitude
        end
    end
end
```

```
    if f(locs(counter))>=1/60
        peakfrequency(i)=f(locs(counter));
        peakheight(i)=P1(locs(counter));
    else
        counter=counter+1;
    end
end
end
end
```